UNIVERSITAT POLITÈCNICA
DE CATALUNYA

Ph.D. Dissertation

Bayesian Signal Processing Techniques for GNSS Receivers:

from multipath mitigation to positioning

Author: Pau Closas Gómez

Thesis advisors: Prof. Juan A. Fernández Rubio
Dr. Carles Fernández Prades

Signal Processing and Communications Group
Department of Signal Theory and Communications
Universitat Politècnica de Catalunya

Barcelona, June 2009

Annuntio vobis gaudium magnum;
Habemus Thesis.

A la Míriam,

Abstract

This dissertation deals with the design of satellite-based navigation receivers. The term Global Navigation Satellite Systems (GNSS) refers to those navigation systems based on a constellation of satellites, which emit ranging signals useful for positioning. Although the american GPS is probably the most popular, the european contribution (Galileo) will be operative soon. Other global and regional systems exist, all with the same objective: aid user's positioning. Initially, the thesis provides the state-of-the-art in GNSS: navigation signals structure and receiver architecture. The design of a GNSS receiver consists of a number of functional blocks. From the antenna to the final position calculation, the design poses challenges in many research areas. Although the Radio Frequency chain of the receiver is commented in the thesis, the main objective of the dissertation is on the signal processing algorithms applied after signal digitation. These algorithms can be divided into two: synchronization and positioning. This classification corresponds to the two main processes typically performed by a GNSS receiver. First, the relative distance between the receiver and the set of visible satellites is estimated. These distances are calculated after estimating the delay suffered by the signal traveling from its emission at the corresponding satellite to its reception at the receiver's antenna. Estimation and tracking of these parameters is performed by the synchronization algorithm. After the relative distances to the satellites are estimated, the positioning algorithm starts its operation. Positioning is typically performed by a process referred to as trilateration: intersection of a set of spheres centered at the visible satellites and with radii the corresponding relative distances. Therefore, synchronization and positioning are processes performed sequentially and in parallel. The thesis contributes to both topics, as expressed by the subtitle of the dissertation.

On the one hand, the thesis delves into the use of Bayesian filtering for the tracking of synchronization parameters (time-delays, Doppler-shifts and carrier-phases) of the received signal. One of the main sources of error in high precision GNSS receivers is the presence of multipath replicas apart from the line-of-sight signal (LOSS). Wherefore the algorithms proposed in this part of the thesis aim at mitigating the multipath effect on synchronization estimates. The dissertation provides an introduction to the basics of Bayesian filtering, including a compendium of the most popular algorithms. Particularly, Particle Filters (PF) are studied as one of the promising alternatives to deal with nonlinear/nonGaussian systems. PF are a set of simulation-based algorithms, based on Monte-Carlo methods. PF provide a discrete characterization of the posterior distribution of the system. Conversely to other simulation-based methods, PF are supported by convergence results which make them attractive in cases where the optimal solution cannot be analytically found. In that vein, a PF that incorporates a set of features to enhance its performance and robustness with a reduced number of particles is proposed. First, the linear part of the system is optimally handled by a Kalman Filter (KF), procedure

referred to as Rao-Blackwellization. The latter causes a reduction on the variance of the particles and, thus, a reduction on the number of required particles to attain a given accuracy when characterizing the posterior distribution. A second feature is the design of an importance density function (from which particles are generated) close to the optimal, not available in general. The selection of this function is typically a key issue in PF designs. The dissertation proposes an approximation of the optimal importance function using Laplace's method. In parallel, Extended Kalman Filter (EKF) and Unscented Kalman Filter (UKF) algorithms are considered, comparing these algorithms with the proposed PF by computer simulations.

On the other hand, a novel point of view in the positioning problem constitutes one of the original contributions of the thesis. Whereas conventional receivers operate in a two-steps procedure (synchronization and positioning), the proposal of the thesis is a Direct Position Estimation (DPE) from the digitized signal. Considering the novelty of the approach, the dissertation provides both qualitative and quantitative motivations for the use of DPE instead of the conventional two-steps approach. DPE is studied following the Maximum Likelihood (ML) principle and an algorithm based on the Accelerated Random Search (ARS) is considered for a practical implementation of the derived estimator. Computer simulation results carried show the robustness of DPE in scenarios where the conventional approach fails, for instance in multipath-rich scenarios. One of the conclusions of the thesis is that joint processing of satellite's signals provides enhance positioning performances, due to the independent propagation channels between satellite links. The dissertation also presents the extension of DPE to the Bayesian framework: Bayesian DPE (BDPE). BDPE maintains DPE's philosophy, including the possibility of accounting for sources of side/prior information. Some examples are given, such as the use of Inertial Measurement Systems and atmospheric models. Nevertheless, we have to keep in mind that the list is only limited by imagination and the particular applications were BDPE is implemented.

Finally, the dissertation studied the theoretical lower bounds of accuracy of GNSS receivers. Some of those limits were already known, others see the light as a result of the research reported in the dissertation. The Cramér-Rao Bound (CRB) is the theoretical lower bound of accuracy of any unbiased estimator of a parameter. The dissertation recalls the CRB of synchronization parameters, result already known. A novel contribution of the thesis is the derivation of the CRB of the position estimator for either conventional and DPE approaches. These results provide an asymptotical comparison of both GNSS positioning approaches. Similarly, the CRB of synchronization parameters for the Bayesian case (Posterior Cramér-Rao Bound, PCRB) is given, used as a fundamental limit of the Bayesian filters proposed in the thesis.

Resum

Aquesta tesi gira al voltant del disseny de receptors per a sistemes globals de navegació per satèl·lit (Global Navigation Satellite Systems, GNSS). El terme GNSS fa referència a tots aquells sistemes de navegació basats en una constel·lació de satèl·lits que emeten senyals de navegació útils per a posicionament. El més popular és l'americà GPS. Els esforços d'Europa per a tenir un sistema similar veuran el seu fruït en un futur proper, el sistema s'anomena Galileo. Altres sistemes globals i regionals existeixen dissenyats per al mateix objectiu: calcular la posició dels receptors. Inicialment la tesi presenta l'estat de l'art en GNSS: estructura dels actuals senyals de navegació i arquitectura dels receptors. El disseny d'un receptor per a GNSS consta d'un seguit de blocs funcionals. Començant per l'antena receptora fins al càlcul final de la posició del receptor, el disseny proporciona una gran motivació per a la recerca en diversos àmbits. Tot i que la cadena de Radiofreqüència del receptor també és comentada a la tesis, l'objectiu principal de la recerca realitzada recau en els algorismes de processament de senyal emprats un cop realitzada la digitalització del senyal rebut. En un receptor per a GNSS, aquests algorismes es poden dividir en 2 classes: els de sincronisme i els de posicionament. Aquesta classificació correspon als dos grans processos que típicament realitza el receptor. Primer, s'estima la distància relativa entre el receptor i el conjunt de satèl·lits visibles. Aquestes distàncies es calculen estimant el retard patit pel senyal des que es emès pel corresponent satèl·lit fins que es rebut pel receptor. De l'estimació i seguiment del retard se n'encarrega l'algorisme de sincronisme. Un cop calculades la distàncies relatives als satèl·lits, multiplicant per la velocitat de la llum el retards estimats, l'algorisme de posicionament pot operar. El posicionament es realitza típicament pel procés de trilateralització: intersecció del conjunt d'esferes centrades als satèl·lits visibles i de radi les distàncies estimades, relatives al receptor GNSS. Així doncs, sincronització i posicionament es realitzen de forma seqencial i ininterrompudament. La tesi fa contribucions a ambdós parts, com explicíta el subtitol del document.

Per una banda, la tesi investiga l'ús del filtrat Bayesià en el seguiment dels paràmetres de sincronisme (retards, desviaments Doppler i fases de portadora) del senyal rebut. Una de les fonts de degradació de la precisió en receptors GNSS és la presència de repliques del senyal directe, degudes a rebots en obstacles propers. És per això que els algorismes proposats en aquesta part de la tesi tenen com a objectiu la mitigació de l'efecte multicamí. La dissertació realitza una introducció dels fonaments teòrics del filtrat Bayesià, incloent un recull dels algorismes més populars. En particular, el Filtrat de Partícules (Particle Filter, PF) s'estudia com a una de les alternatives més interessants actualment per a enfrontar-se a sistemes no-lineals y/o no-Gaussians. Els PF són mètodes basats en el mètode de Monte Carlo que realitzen una caracterització discreta de la funció de probabilitat a posteriori del sistema. Al contrari d'altres mètodes basats en simulacions, els PF tenen resultats de convergència que els fan especialment atractius en casos on la solució òptima no es pot trobar. En aquest sentit es proposa un PF que incorpora un seguit de característiques

que el fan assolir millors prestacions i robustesa que altres algorismes, amb un nombre de partícules reduït. Per una banda, es fa un seguiment dels estats lineals del sistema mitjanant un Filtre de Kalman (KF), procediment conegut com a Rao-Blackwellization. Aquest fet provoca que la variància de les partícules decreixi i que un menor nombre d'elles siguin necessàries per a assolir una certa precisió en l'estimació de la distribució a posteriori. D'altre banda, un dels punts crítics en el disseny de PF és la selecció d'una funció d'importància (emprada per a generar les partícules) similar a l'òptima. Aquesta funció òptima no està disponible en general. En aquesta tesi, es proposa una aproximació de la funció d'importància òptima basada en el mètode de Laplace. Paral·lelament es proposen algorismes com l'Extended Kalman Filter (EKF) i l'Unscented Kalman Filter (UKF), comparant-los amb el PF proposat mitjançant simulacions numèriques.

Per altra banda, la presentació d'un nou enfocament al problema del posicionament és una de les aportacions originals de la tesi. Si habitualment els receptors operen en dos passos (sincronització i posicionament), la proposta de la tesi rau en l'Estimació Directa de la Posició (Direct Position Estimation, DPE) a partir del senyal digital. Tenint en compte la novetat del mètode, es proporcionen motivacions qualitatives i quantitatives per a l'ús de DPE enfront al mètode convencional de posicionament. Se n'ha estudiat l'estimador de màxima versemblana (Maximum Likelihood, ML) i un algorisme per a la seva implementació pràctica basat en el l'algorisme Accelerated Random Search (ARS). Els resultats de les simulacions numèriques mostren la robustesa de DPE a escenaris on el mètode convencional es veu degradat, com per exemple el cas d'escenaris rics en multicamí. Una de les reflexions fruït dels resultats és que l'ús conjunt dels senyals provinents dels satèl·lits visibles proporciona millores en l'estimació de la posició, doncs cada senyal està afectada per un canal de propagació independent. La tesi també presenta l'extensió de DPE dins el marc Bayesià: Bayesian DPE (BDPE). BDPE manté la filosofía de DPE, tot incloent-hi possibles fonts d'informació a priori referents al moviment del receptor. Es comenten algunes de les opcions com l'ús de sistemes de navegació inercials o la inclusió d'informació atmosfèrica. Tot i així, cal tenir en compte que la llista només està limitada per la imaginació i l'aplicació concreta on el marc BDPE s'implementi.

Finalment, la tesi estudia els límits teòrics en la precisió dels receptors GNSS. Alguns d'aquests límits teòrics eren ja coneguts, d'altres veuen ara la llum. El límit de Cramér-Rao (Cramér-Rao Bound, CRB) ens prediu la mínima variància que es pot obtenir en estimar un paràmetre mitjançant un estimador no esbiaixat. La tesi recorda el CRB dels paràmetres de sincronisme, resultat ja conegut. Una de les aportacions és la derivació del CRB de l'estimador de la posició pel cas convencional i seguint la metodologia DPE. Aquests resultats proporcionen una comparativa asimptòtica dels dos procediments pel posicionament de receptors GNSS. Similarment, el CRB de sincronisme pel cas Bayesià (Posterior Cramér-Rao Bound, PCRB) es presenta, com a límit teòric dels filtres Bayesians proposats en la tesi.

Contents

List of Figures

Notation

Boldface upper-case letters denote matrices and boldface lower-case letters denote column vectors.

$\mathbb{R}$, $\mathbb{C}$	The set of real and complex numbers, respectively.
$\mathbb{R}^{N\times M}$, $\mathbb{C}^{N\times M}$	The set of $N \times M$ matrices with real- and complex-valued entries, respectively.
$\hat{x}$	Estimation and true value of parameter x.
$f(x)\|_{x=a}$	Function $f(x)$ evaluated at $x = a$.
$\|x\|$	Absolute value (modulus) of scalar x.
$\|\mathbf{x}\|$	ℓ^2-norm of vector $\mathbf{x}$, defined as $\|\mathbf{x}\| = \left(\mathbf{x}^H\mathbf{x}\right)^{\frac{1}{2}}$.
$\dim\{\mathbf{x}\}$	Dimension of vector $\mathbf{x}$.
$[\mathbf{x}]_r$	The r-th vector element.
$[\mathbf{X}]_{r,c}$	The matrix element located in row r and column c.
$[\mathbf{X}]_{r,:}$	The r-th row of matrix $\mathbf{X}$.
$[\mathbf{X}]_{:,c}$	The c-th column of matrix $\mathbf{X}$.
$\mathrm{Tr}\{\mathbf{X}\}$	Trace of matrix $\mathbf{X}$. $\mathrm{Tr}\{\mathbf{X}\} = \sum_{n=1}^{N}[\mathbf{X}]_{nn}$.
$\det(\mathbf{X})$	Determinant of matrix $\mathbf{X}$.
$\mathrm{diag}(\mathbf{x})$	A diagonal matrix whose diagonal entries are given by $\mathbf{x}$.
$\|\mathbf{X}\|_F$	Frobenius norm of matrix $\mathbf{X}$. If $\mathbf{X}$ is $N \times N$, $\|\mathbf{X}\|_F = \left(\sum_{u=1}^{N}\sum_{v=1}^{N}\|x_{uv}\|^2\right)^{\frac{1}{2}} = \left(\mathrm{Tr}\left\{\mathbf{X}^H\mathbf{X}\right\}\right)^{\frac{1}{2}}$
$\mathbf{I}$	Identity matrix. A subscript can be used to indicate the dimension.

$\mathbf{X}^*$	Complex conjugate of matrix $\mathbf{X}$ (also applied to scalars).
$\mathbf{X}^T$	Transpose of matrix $\mathbf{X}$.
$\mathbf{X}^H$	Complex conjugate and transpose (Hermitian) of matrix $\mathbf{X}$.
$\mathbf{X}^\dagger$	Moore-Penrose pseudoinverse of matrix $\mathbf{X}$. If $\mathbf{X}$ is $M \times N$, $\mathbf{X}^\dagger = \mathbf{X}^H \left(\mathbf{X}\mathbf{X}^H\right)^{-1}$ if $M \leq N$, $\mathbf{X}^\dagger = \mathbf{X}^{-1}$ if $M = N$, and $\mathbf{X}^\dagger = \left(\mathbf{X}^H\mathbf{X}\right)^{-1}\mathbf{X}^H$ if $M \geq N$.
$\odot$	Schur-Hadamard (elementwise) product of matrices. If $\mathbf{A}$ and $\mathbf{B}$ are two $N \times M$ matrices: $\mathbf{A} \odot \mathbf{B} = \begin{pmatrix} a_{11}b_{11} & a_{12}b_{12} & \cdots & a_{1M}b_{1M} \\ a_{21}b_{21} & a_{22}b_{22} & \ddots & a_{2M}b_{2M} \\ \vdots & \vdots & \cdots & \vdots \\ a_{N1}b_{N1} & a_{N2}b_{N2} & \cdots & a_{NM}b_{NM} \end{pmatrix}$
$\otimes$	The Kronecker or tensor product. If $\mathbf{A}$ is $m \times n$, then $\mathbf{A} \otimes \mathbf{B} = \begin{pmatrix} [\mathbf{A}]_{11}\mathbf{B} & \cdots & [\mathbf{A}]_{1m}\mathbf{B} \\ \vdots & & \vdots \\ [\mathbf{A}]_{n1}\mathbf{B} & \cdots & [\mathbf{A}]_{nm}\mathbf{B} \end{pmatrix}$
$\mathbf{P}_\mathbf{X}$	Orthogonal projector onto the subspace spanned by the columns of $\mathbf{X}$. $\mathbf{P}_\mathbf{X} = \mathbf{X}\left(\mathbf{X}^H\mathbf{X}\right)^{-1}\mathbf{X}^H$.
$\mathbf{P}_\mathbf{X}^\perp$	$\mathbf{I} - \mathbf{P}_\mathbf{X}$, orthogonal projector onto the orthogonal complement to the columns of $\mathbf{X}$.
$\mathcal{N}(\boldsymbol{\mu}, \boldsymbol{\Sigma})$	Multivariate Gaussian distribution with mean $\boldsymbol{\mu}$ and covariance matrix $\boldsymbol{\Sigma}$.
$\mathcal{U}(a, b)$	Uniform distribution in the interval $[a, b]$.
$\mathbb{E}\{\cdot\}$	Statistical expectation. When used with a subindex, it specifies the distribution over which the expectation is taken, e.g., $\mathbb{E}_x\{\cdot\}$ over the distribution of a random variable x; $\mathbb{E}_{x,y}\{\cdot\}$ over the joint distribution of x and y, $p(x, y)$; $\mathbb{E}_{x\|y}\{\cdot\}$ over the distribution of x conditioned to y, $p(x\|y)$.
$\ln(\cdot)$	Natural logarithm (base e).
$\delta(n-m)$	Kronecker's delta function, defined as: $\delta(n-m) = \delta_{n,m} \triangleq \begin{cases} 1, & \text{if } n = m \\ 0, & \text{if } n \neq m \end{cases}$
$\Re\{\cdot\}$, $\Im\{\cdot\}$	Real and imaginary parts, respectively.

$o_p(f_N)$	A sequence of random variables X_N is $X_N = o_p(f_N)$, for $f_N > 0 \ \ \forall N$, when $\frac{X_N}{f_N}$ converges to zero in probability, i.e., $\lim_{N\to\infty} P\left\{\left\lvert\frac{X_N}{f_N}\right\rvert > \delta\right\} = 0 \ \ \forall \delta > 0$
$f(t) * g(t)$	Convolution between $f(t)$ and $g(t)$.
$\arg\max_x f(x)$	Value of x that maximizes $f(x)$.
$\arg\min_x f(x)$	Value of x that minimizes $f(x)$.
$\frac{\partial f(\mathbf{x})}{\partial x_i}$	Partial derivative of function $f(\mathbf{x})$ with respect to the variable x_i.
$\frac{\partial f(\mathbf{x})}{\partial \mathbf{x}}$	Gradient of function $f(\mathbf{x})$ with respect to vector $\mathbf{x}$.
$\frac{\partial^2 f(\mathbf{x})}{\partial \mathbf{x}^2}$	Hessian matrix of function $f(\mathbf{x})$ with respect to vector $\mathbf{x}$.
$\nabla_{\mathbf{x}} f(\mathbf{x})$	Gradient of function $f(\mathbf{x})$ with respect to vector $\mathbf{x}$.
$\mathcal{H}_{\mathbf{x}} f(\mathbf{x})$	Hessian matrix of function $f(\mathbf{x})$ with respect to vector $\mathbf{x}$.
$\triangle_{\mathbf{x}_1}^{\mathbf{x}_2} f(\mathbf{x})$	second-order partial derivatives operator of function $f(\mathbf{x})$ with respect to vectors $\mathbf{x}_1$ and $\mathbf{x}_2$. Notice that $\mathcal{H}_{\mathbf{x}} f(\mathbf{x}) \triangleq \triangle_{\mathbf{x}}^{\mathbf{x}} f(\mathbf{x})$ and $\triangle_{\mathbf{x}_1}^{\mathbf{x}_2} = \nabla_{\mathbf{x}_1}\left[\nabla_{\mathbf{x}_2}^T\right]$.
$\dot{f}(t), \ddot{f}(t)$	*d*erivatives *o*f *t*ime of function $f(t)$, equivalent to $\frac{\partial f(\mathbf{t})}{\partial t}$ and $\frac{\partial^2 f(\mathbf{t})}{\partial t^2}$ respectively.
a.s.	almost surely convergence.
i.i.d.	independent identically distributed.
q.e.d.	quod erat demonstrandum.
r.v.	random variable.
*w.p.*1.	convergence with probability one.

Acronyms

ADC Analog-to-Digital Converter.

AGC Automatic Gain Control.

AGN Additive Gaussian Noise.

AIC Akaike's Information Criteria.

ARS Accelerated Random Search.

AS Anti Spoofing.

ASIC Application-Specific Integrated Circuit.

AWGN Additive White Gaussian Noise.

BDPE Bayesian Direct Position Estimation.

BF Bootstrap Filter.

BIM Bayesian Information Matrix.

BLUE Best Linear Unbiased Estimator.

BPSK Binary Phase Shift Keying.

BOC Binary Offset Carrier.

CDMA Code Division Multiple Access.

CN0 Carrier to Noise density Ratio, C/N_0.

COTS Commercial Off-The-Shelf.

CPLD Complex Programmable Logic Device.

CRB Cramér Rao Bound.

CRC Cyclic Redundancy Check.

CRPF Cost Reference Particle Filter.

DBF Digital Beamforming.

DGNSS Differential GNSS.

DLL Delay Lock Loop.

DOA Direction Of Arrival.

DPE Direct Position Estimation.

DS-SS Direct-Sequence Spread-Spectrum.

DSP Digital Signal Processor.

DSS Discrete State-Space model.

ECEF Earth-Centered Earth-Fixed coordinate system.

EGNOS European Geostationary Navigation Overlay System.

EIRP Effective Isotropic Radiated Power.

EKF Extended Kalman Filter.

ELS Early/Late Slope algorithm.

EM Expectation Maximization algorithm.

EML Early Minus Late algorithm.

ENU East-North-Up coordinate system.

FDOA Frequency Difference Of Arrival.

FFT Fast Fourier Transform.

FIM Fisher Information Matrix.

FLL Frequency Lock Loop.

FPGA Field Programmable Gate Array.

GBAS Ground-Based Augmentation Systems.

GDOP Geometric Dilution Of Precision.

GLONASS GLObalnaya Navigasionnay Sputnikovaya Sistema.

GLRT Generalized Likelihood Ratio Tests.

GNSS Global Navigation Satellite System.

GPS Global Positioning System.

HMM Hidden Markov Model.

HRC High Resolution Correlator.

IF Intermediate Frequency.

IMU Inertial Measurement Unit.

INS Inertial Navigation System.

IRNSS Indian Regional Navigation Satellite System.

IS Importance Sampling.

ITU International Telecommunication Union.

KF Kalman Filter.

LAAS Local-Area Augmentation System.

LFSR Linear Feedback Shift Register.

LHCP Left Hand Circularly Polarized.

LLPF Local Linearization Particle Filter.

LNA Low Noise Amplifier.

LO Local Oscillator.

LS Least Squares.

LOSS Line Of Sight Signal.

MAI Multiple Access Interference.

MAP Maximum a posteriori.

MDL Minimum Description Length.

MEDLL Multipath Estimating Delay Lock Loop.

MEMS Micro Electro Mechanical System.

MEO Medium Earth Orbit.

MET Multipath Elimination Technology.

MIMO Multiple Input Multiple Output.

ML Maximum Likelihood.

MLE Maximum Likelihood Estimator.

MMSE Minimum Mean Square Error.

MSE Mean Square Error.

NCO Numerical Controlled Oscillator.

MVB Minimum Variance Beamforming.

PAC Pulse Amplitude Correlator.

PCRB Posterior Cramér Rao Bound.

PDF Probability Density Function.

PF Particle Filter.

PLL Phase Lock Loop.

PMC Population Monte Carlo.

PPP Precise Point Positioning.

PRN Pseudorandom Noise.

PVT Position, Velocity and Time.

QPSK Quadrature Phase Shift Keying.

QZSS Quasi-Zenith Satellite System.

RF Radio Frequency.

RHCP Right Hand Circularly Polarized.

RMSE Root Mean Squared Error.

RPF Regularized Particle Filter.

SAGE Space-Alternating Generalized Expectation-Maximization algorithm.

SAR Search And Rescue.

SBAS Space-Based Augmentation Systems.

SDCM System for Differential Correction and Monitoring.

SDR Software Defined Radio.

SIR Sampling Importance Resampling.

SIS Sequential Importance Sampling.

SISA Signal In Space Accuracy.

SINR Signal to Interference plus Noise Ratio.

SMC Sequential Monte Carlo.

SMI Sample Matrix Inversion.

SMR Signal to Multipath Ratio.

SNAS Satellite Navigation Augmentation System.

SNR Signal to Noise Ratio.

SS State Space.

SV Space Vehicle.

TDOA Time Difference Of Arrival.

TOA Time Of Arrival.

TTFF Time To First Fix.

TTL Transistor-Transistor Logic.

UKF Unscented Kalman Filter.

UTC Universal Time Coordinated.

VDLL Vector Delay Locked Loop.

VHDL Very high speed integrated circuit Hardware Description Language.

WAAS Wide-Area Augmentation System.

WGS84 World Geodetic System 1984.

WLS Weighted Least Squares.

WSSUS Wide Sense Stationary with Uncorrelated Scattering.

1 Introduction

THIS thesis deals with the design of advanced receivers for its use in navigation systems. The focus is on the algorithms required to synchronize the receiver with the emitters of navigation signals and the procedures performed to compute its position. We restrict ourselves to the case of satellite-based navigation systems, that is to say, those systems which are based on a constellation of satellites to aid positioning of a receiver by emitting ranging signals. Particularly, we take a Bayesian approach to affront some of the problems that a receiver has to deal with. Therefore, the inclusion of prior information is one of the main concerns of this dissertation, along with the proposal of algorithms to effectively account for it.

1.1 Motivation and Objectives of the Thesis

Satellite navigation systems have undergone a remarkable development since their apparition. These systems are generally referred to as GNSS, a short for Global Navigation Satellite Systems. First, the american Global Positioning System (GPS) opened the application to the mass-market and, nowadays, the forthcoming european Galileo renewed the research interest on this topic. Although many contributions can be found in the literature related to any of the aspects concerning GNSS, most of the problems remain

unsolved, at least with the degree of coverage, reliability and accuracy that applications (and imagination) demand. Therefore, and fortunately, there are stimulating open fields for further research in many directions.

A GNSS receiver, after signal sampling and downconversion, executes two sequential signal processing operations: synchronization and positioning. The former tries to keep track of the synchronization parameters (i.e., time-delay, carrier-phase and Doppler deviation) of the visible satellites. Synchronization is typically performed independently for each satellite by a bank of identical channels (possibly using DLL-based algorithms). These parameters provide information of the relative distance between the receiver and the corresponding satellite, ranging information which is used by the positioning algorithm. Thus, GNSS receivers consist of a two-steps procedure, where the performance of the synchronization procedure plays an essential role. One of the most critical issues in the design of GNSS receivers is the robustness of the synchronization algorithm against multipath propagation. This effect induces a bias in time-delay estimates that is propagated to the computation of receiver's position. The presence of direct signal's replicas might be caused by reflections on surrounding buildings or trees, for instance. Therefore, it is reasonable to assume that *real-world* scenarios are multipath-rich environments. Many algorithms have been proposed in the literature to overcome this effect, consult Chapter 2 for a survey.

One of the objectives of the thesis is to propose an algorithm to track the synchronization parameters of a satellite, which additionally mitigates the multipath effect. The proposed algorithm is based on the Bayesian nonlinear filtering theory and, particularly, on Sequential Monte Carlo (SMC) methods. These simulation-based methods have recently attracted the interest of many researchers of distinct topics, all of them being haunted by their ability to deal with nonlinear/nonGaussian systems. We can encounter these methods under several names, with Particle Filters (PFs) being the one we adopt hereinafter. The proposed PF has a number of enhanced features, such as employing a variance reduction technique known as Rao-Blackwellization. Rao-Blackwellization helps circumventing the curse of dimensionality in SMC methods by tackling the linear part of the system by the optimal algorithm in those cases: the Kalman Filter (KF). Another attribute designed to improve the performance of the PF is the use of a nearly optimal importance density function, from which particles are generated. Furthermore, a procedure to extract Doppler-shifts from complex amplitudes estimates is proposed. The performance of the PF is compared to other Bayesian filtering alternatives – namely, the Extended Kalman Filter (EKF) and the Unscented Kalman Filter (UKF) –, as well as to its lowest accuracy bound, given by the Posterior Cramér-Rao Bound (PCRB). The research related to the use of Bayesian filters for multipath mitigation purposes is divulged in Chapter 3.

Is there an alternative to the conventional two-steps positioning approach? this is the question we tried to answer during the research reported in Chapter 4. The response is

the Direct Position Estimation (DPE) approach, a novel framework for positioning GNSS receivers. Basically, the idea is to merge synchronization and position computation operations into a single estimation step. Then, the input to an algorithm implementing DPE's approach is the stream of sampled signal and its output should be the estimated receiver's position itself. This philosophy has important consequences in the receiver. Firstly, we notice that signals from different satellites are no longer processed independently, thus improving the rejection to multiple access interference. Besides, joint processing of signals propagating through independent links enhances the robustness of the receiver in certain scenarios, such as multipath environments. The interest in DPE's approach came after evaluating the drawbacks of the conventional approach, listed in Chapter 4. Now it suffices to understand the versatility of DPE to incorporate prior information in the computation of user's position, as compared to the conventional approach to positioning. In the two-steps approach, side information can be considered whether in the synchronization algorithm or in the positioning procedure. We will realize in Chapter 3 that the former is possible, despite few intuitive models exist to that aim. The most conventional way to include prior information in GNSS receivers is, thus, in the computation of position. Unfortunately, if synchronization parameters appear to be corrupted, the positioning solution will be likely to be also unreliable, in spite of the fact of using a priori information for its calculation. Conversely, DPE provides a natural framework for the inclusion of prior information, while ensuring its efficient usage, because the parameters of interest in the estimation problem are the user coordinates. It will be seen that the use of prior data for those unknowns is, by far, easier than considering prior information in the estimation of synchronization parameters.

So far the thesis proposes algorithms, approaches or alternatives to solve common problems faced by GNSS receivers. Notwithstanding, we are also interested in realizing how close the proposed algorithms are from their theoretical accuracy bounds. Work can be found in the literature studying the lower bounds of synchronization algorithms. For instance, it can be proved that any unbiased time-delay estimator based on a single antenna has a variance that approaches to infinity when the relative delay between the direct signal and a multipath replica approaches to zero. However, the impact of this effect – or more generally, the performance of a time-delay estimator – in the final position estimate has not yet been evaluated. In previous works, the computed variance bounds for the estimation of synchronization parameters have been typically transformed to compute the bounds of ranging parameters. The latter bounds constitute a rule of thumb to approximate the degradation of the final position estimate. It is apparent that this approach does not yield to accurate positioning bounds, useful for benchmarking, as it does not account for the joint processing of synchronization estimates in the positioning procedure. Therefore, this approach cannot be used to effectively assess the influence of synchronization algorithms in position estimates. Chapter 5 addresses this issue, studying the theoretical variance bounds of position estimates, analyzing both conventional and DPE positioning

approaches. In addition, the error bounds for the tracking problem studied in Chapter 3 are also accounted.

To sum up, this thesis proposes:

- A review of Bayesian filtering, that is to say, fundamentals and discussion of optimal/sub-optimal algorithms, with a special emphasis on particle filtering.
- A framework for tracking the synchronization parameters of a satellite relying on Bayesian filtering algorithms. Thus, allowing the use of a priori information of these parameters.
- An efficient PF algorithm for tracking time-delays and complex amplitudes of the direct signal and its replicas. In addition, a methodology to extract Doppler-shifts is also suggested.
- A framework for Direct Position Estimation (DPE) in software-defined radio receivers, with a comparison to the conventional positioning approach.
- A framework for the inclusion of prior information in GNSS receivers following DPE's philosophy, termed as Bayesian Direct Position Estimation (BDPE) approach.
- An analysis of the Maximum Likelihood Estimator of position under DPE's approach and proposal of a practical algorithm to implement it.
- A establishment of fundamental bounds in GNSS positioning algorithms, as given by the Cramér-Rao Bound. Namely, variance bounds for position estimation under conventional and DPE's approaches are derived. Furthermore, the Posterior Cramér-Rao Bound is used for the problem of on-line tracking of synchronization parameters.
- An extensive simulation study of the algorithms proposed.

1.2 Thesis Outline and Reading Directions

The dissertation consists of six chapters, where review material and novel contributions are presented. The thesis might be of interest to two groups of people: those working in the satellite-navigation field and to signal-processing oriented researchers. The document is organized according to this premise, providing the basics of each topic. In this section, we glance at the structure of the document, serving as a guide to the reader. For the sake of clarity, the mathematical notation and the acronyms used along the dissertation can be consulted at the beginning of the document.

The dissertation has begun with **Chapter 1**, presenting the motivations and scope of the thesis. The objectives were highlighted and the structure of the thesis is being presented, guiding the reader before starting the journey across the research reported in the forthcoming pages. **Chapter 2** provides the reader with the basics of satellite navigation systems, concepts which are a requisite to correctly follow subsequent chapters. Indeed, this chapter could be skipped if deemed necessary. Namely, the chapter presents the general signal structure and propagation channel of most satellite-based navigation systems. Specifically, GPS and Galileo systems are discussed in more detail due to their paramount significance in nowadays' research in the topic. Nevertheless, the aim of the chapter is not to perform an exhaustive exposition of those systems, since it would have required many space in the thesis without adding new material not already published in the literature. Thus, the reader is referred to the references therein for further details. Chapter 2 also sketches the architecture of a navigation receiver, providing a better understanding of the problems treated along the dissertation and their impact in the receiver's chain. The considered receiver is flavored by the Software Defined Radio paradigm, which consists in digitizing as close to the antenna as possible. Thus, signal processing typically performed by dedicated analog devices can be handled by versatile software platforms.

The use of Bayesian filters to track the synchronization parameters of visible satellites is investigated in **Chapter 3**. The chapter can be divided into two differentiated parts. On the one hand, an overview of Bayesian nonlinear filtering is presented. Therein a reader can find an explanation of the conceptual solution, followed by a discussion on a number of optimal and sub-optimal algorithms to implement the Bayesian recursion. Although PFs fall under the latter category of algorithms, an extended overview is provided in Chapter 3 due to its significance and usage along the dissertation. On the other hand, the chapter presents the original contribution by the author to the multipath mitigation problem using Bayesian filters. Assuming a system model which considers a fixed number of multipath replicas per satellite and independent processing of satellites' signals, a number of filters are considered. The most remarkable work is on the use of PFs, though EKF and UKF are also explored. These algorithms are simulated, compared and plotted against the theoretical lower bound provided by the PCRB.

Chapter 4 proposes a novel framework for positioning a receiver in satellite-based navigation systems, termed as Direct Position Estimation or DPE for short. DPE merges the two-steps that a conventional state-of-the-art receiver performs to compute its position into a single optimization problem. The chapter starts highlighting the drawbacks of two-steps based positioning and proving that, indeed, DPE cannot be outperformed by the conventional approach. The estimators of both synchronization parameters and position coordinates are derived using the ML principle. This allows a fair comparison of both positioning alternatives. The estimator derived under DPE's philosophy turns to be a multivariate non-convex optimization problem. A practical algorithm is proposed

based on the Accelerated Random Search (ARS) algorithm, whose performance is shown in a number of realistic scenarios. Furthermore, the inclusion of side information in GNSS receivers is discussed and Bayesian DPE framework introduced. For the sake of completeness, examples of practical interest where prior information can be easily used are commented.

Chapter 5 delves into the derivation of performance bounds for the estimation problems encountered in GNSS receivers. Actually, it is an important point of this dissertation, as these results are used in preceding chapters. Namely, the two main problems of navigation systems are treated: synchronization and positioning. On the one hand, variance bounds for the estimation of synchronization parameters are obtained in the case of ML-like estimation and in on-line tracking, given by the CRB and PCRB respectively. On the other hand, the error bounds of either positioning approaches (two-steps and DPE) are likewise documented in Chapter 5 along with a comparison under realistic scenarios. Finally, a summary of the contributions, conclusions and guides for future research arising from this work can be consulted in **Chapter 6**. At the end of the document, the reader can find the list of publications by the author during the pursue of the PhD degree. Additionally, at the end of each chapter one can find the publications related to the particular topics discussed there.

2

Fundamentals of Global Navigation Satellite Systems

GLOBAL Navigation Satellite System (GNSS) is the general concept used to identify those systems that allow user positioning based on a constellation of satellites. Specific GNSS are the well-known american GPS or the forthcoming european Galileo. Both systems rely on the same principle: the user computes its position by means of measured distances between the receiver and the set of visible satellites. These distances are calculated estimating the propagation time that transmitted signals take from each satellite to the receiver. Therefore, the conventional approach to GNSS positioning is based on a two-steps procedure. First, the receiver estimates the distance between the receiver and the satellites. Then, these distances are used to obtain user position by means of a procedure referred to as trilateration. Useful GNSS textbook references can be found in the literature, for instance [Par96, Kap96, Str97, Gre01, Bor07].

This chapter provides an overview to GNSS basics. The emphasis is on the concepts which are required to follow the rest of the dissertation. Section 2.1 presents the structure and particularities of GNSS signals. The generic architecture of a GNSS receiver is sketched in Section 2.2. Then the two-steps positioning approach, i.e., synchronization and trilateration, is discussed in Sections 2.2.2 and 2.2.3, respectively.

2.1 GNSS Signal Structure

A general signal model for most navigation systems consists of a direct-sequence spread-spectrum (DS-SS) signal [HW08], synchronously transmitted by all the satellites in the constellation. This type of signals enable Code Division Multiple Access (CDMA) transmissions, i.e., satellite signals are distinguished by orthogonal (or quasi-orthogonal) codes. At a glance, these signals consists of two main components: a ranging code (the PRN spreading sequence) and a low rate data-link (broadcasting necessary information for positioning such as satellites orbital parameters and corrections). The complex baseband model of the signal transmitted by the i-th satellite reads as

$$s_{T,i}(t) = s_{I,i}(t) + j s_{Q,i}(t) \ , \tag{2.1}$$

where its phase and quadrature components are defined as

$$\begin{aligned} s_{I,i}(t) &= \sqrt{2P_I}\ q_{I,i}(t) \qquad (2.2)\\ &= \sqrt{2P_I} \sum_{m_I=-\infty}^{\infty} b_{I,i}(m_I) \sum_{u_I=1}^{N_{c_I}} \sum_{k_I=1}^{L_{c_I}} c_{I,i}\left(k_I\right) g_I\left(t - m_I T_{b_I} - u_I T_{\mathrm{PRN}_I} - k_I T_{c_I}\right) \\ s_{Q,i}(t) &= \sqrt{2P_Q}\ q_{Q,i}(t) \qquad (2.3)\\ &= \sqrt{2P_Q} \sum_{m_Q=-\infty}^{\infty} b_{Q,i}(m_Q) \sum_{u_Q=1}^{N_{c_Q}} \sum_{k_Q=1}^{L_{c_Q}} c_{Q,i}\left(k_Q\right) g_Q\left(t - m_Q T_{b_Q} - u_Q T_{\mathrm{PRN}_Q} - k_Q T_{c_Q}\right) \ , \end{aligned}$$

with the following definitions for the in-phase component – analogous for the quadrature signal – holding:

- P_I is the transmitted power, considered equal for all satellites and elevation-dependant [Tsu00].
- $b_{I,i}(t) \in \{-1, 1\}$ is the sequence of low-rate data bits, with T_{b_I} being the bit period.
- $c_{I,i}(t) \in \{-1, 1\}$ is the PRN spreading sequence. The chip length of the codeword and the chip period are denoted by L_{c_I} and T_{c_I}, respectively. Therefore, $T_{\mathrm{PRN}_I} = L_{c_I} T_{c_I}$ is the codeword period. N_{c_I} are the number of code epochs per data bit. Figure 2.1 aims at clarifying the relation between these bits/chips parameters.
- The energy-normalized chip shaping pulse is denoted by $g_I(t)$.

Notice that several carrier frequencies can be used at a time, with the presented baseband structure being thus replicated. When transmitted, satellite's signals travel through a

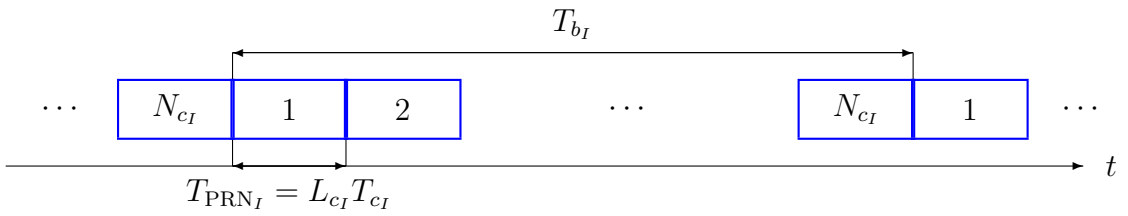

Figure 2.1: Relation among the parameters defining bits and spreading sequences in a generic navigation signal (in-phase component).

propagation channel which modifies its amplitude, phase and delay. Indeed, many replicas of the same transmitted signal can reach the receiver's antenna due to multipath propagation. In general, these replicas are caused by reflections of the direct signal (or line-of-sight signal, LOSS) in surrounding obstacles (e.g. buildings, trees, ground, etc). Such propagation channel is generically modeled by a linear time-varying impulse response with M propagation paths [Rap96, Fon01a]:

$$h_i(t) = \sum_{m=0}^{M-1} \alpha_{i,m}(t) e^{j\phi_{i,m}(t)} \delta(t - \tau_{i,m}(t)) \ , \tag{2.4}$$

where $\alpha_{i,m}(t)$, $\phi_{i,m}(t)$ and $\tau_{i,m}(t)$ stand for the amplitude, phase and delay of the m-th propagation path for the i-th satellite. Notice that subindex $m = 0$ denotes LOSS parameters. These time-varying parameters have been statistically modeled, thus each being assumed as realizations of a $r.v.$ with known distribution. Typically, the assumptions are that amplitudes are Rice or Rayleigh (when shadowed) distributed [Pro95, Irs05], phases are uniformly generated [Jak74] and time-delays are assumed piecewise constant in the observation interval [Van94]. In general, we consider that paths are independent, which is referred to as the Wide Sense Stationary with Uncorrelated Scattering (WSSUS) channel model. Thus, M can be different between satellite channels. A huge effort is being carried at the German Aerospace Center (DLR) to characterize the GNSS propagation channel model, see for instance the results reported in [Ste03, Ste04].

Therefore, considering M_s visible satellites, the received signal is the superposition of the transmitted signals, as propagated through the corresponding channel, and corrupted by additive noise, $n(t)$. This reads as

$$\begin{aligned} x(t) &= \sum_{i=0}^{M_s-1} s_{R,i}(t) + n(t) = \sum_{i=0}^{M_s-1} s_{T,i}(t) * h_i(t) + n(t) \\ &= \sum_{i=0}^{M_s-1} \sum_{m=0}^{M-1} \alpha_{i,m}(t) e^{j\phi_{i,m}(t)} s_{T,i}(t - \tau_{i,m}(t)) + n(t) \ . \end{aligned} \tag{2.5}$$

Yet another effect modifies the transmitted signal when captured at the receiver's antenna manifold: the *Doppler spread*. It is well known that a relative motion between transmitter and receiver causes a frequency shift in the received signal, with respect to the one emitted. This frequency broadening was discovered in mid 19^{th} century by C. Doppler, as reported in his original manuscript [Dop42]. The equations governing such frequency deviation can be readily found in the literature. Hence, we provide here another interpretation/derivation of the effect. We will see that the Doppler deviation is included in the general model (2.4) as the linear component of the phase. For the sake of simplicity let us consider the propagation channel of a single satellite, dropping subindex i from (2.4). This assumption is valid due to the independent nature of satellite links. In addition, we contemplate the case of $M = 1$, i.e., only LOSS results from channel propagation, and neglect the noise term. With this setup, the analytic representation of the RF signal emitted by the satellite under study is $s_T(t)e^{j2\pi f_c t}$, where f_c is the carrier frequency of the navigation signal. Then, the received analytical signal is of the form

$$\begin{aligned}\left(s_T(t)e^{j2\pi f_c t}\right) * h(t) &= \alpha_0(t)s_T(t-\tau_0(t))e^{j2\pi f_c(t-\tau_0(t))} \\ &= s_R(t)e^{j2\pi f_c t} \end{aligned} \tag{2.6}$$

with

$$s_R(t) = \alpha_0(t)s_T(t-\tau_0(t))e^{-j2\pi f_c \tau_0(t)} \tag{2.7}$$

being the received complex baseband signal. Notice that we omit the term $e^{j\phi_0(t)}$ because it will be seen here how to obtain its explicit expression. Let us focus on the last term in (2.7), where the carrier frequency is modified by the time-varying channel delay. If we approximate this delay by its first-order Taylor expansion in the neighborhood of an arbitrary instant t_0

$$\begin{aligned}\tau_0(t) &\approx \tau_0(t_0) + \left.\frac{\partial\tau_0(t)}{\partial t}\right|_{t=t_0}(t-t_0) \\ &= \tau_0(t_0) - \left.\frac{\partial\tau_0(t)}{\partial t}\right|_{t=t_0} t_0 + \left.\frac{\partial\tau_0(t)}{\partial t}\right|_{t=t_0} t \ , \end{aligned} \tag{2.8}$$

then we can write

$$\begin{aligned} e^{-j2\pi f_c\tau_0(t)} &\approx e^{-j2\pi f_c \left.\frac{\partial\tau_0(t)}{\partial t}\right|_{t=t_0} t - j2\pi f_c\left(\tau_0(t_0) - \left.\frac{\partial\tau_0(t)}{\partial t}\right|_{t=t_0} t_0\right)} \\ &= e^{j2\pi f_d t + \phi_0} \ , \end{aligned} \tag{2.9}$$

where

$$\begin{aligned} f_d &= -f_c \left.\frac{\partial\tau_0(t)}{\partial t}\right|_{t=t_0} \\ \phi_0 &= -j2\pi f_c\left(\tau_0(t_0) - \left.\frac{\partial\tau_0(t)}{\partial t}\right|_{t=t_0} t_0\right) \end{aligned} \tag{2.10}$$

are the Doppler-deviation and constant phase variation of the received signal due to the travel time. Hence, we can write

$$s_R(t) \approx \alpha_0(t) e^{j2\pi f_d(t)t+\phi_0} s_T(t-\tau_0(t)) \tag{2.11}$$

as the received LOSS for a given satellite.

Therefore, for the i-th satellite, the m-th phase of the channel model in (2.4) can be explicitly expressed as

$$\phi_{i,m}(t) = 2\pi f_{d_{i,m}}(t)t + \phi_{i,m,0} \ , \tag{2.12}$$

which is linear in time and with $f_{d_{i,m}}(t)$ and $\phi_{i,m,0}$ being obtained using the corresponding time-delay $\tau_{i,m}(t)$ in definitions (2.10).

When dealing with the Doppler deviation of the LOSS coming from the i-th satellite, it is common to use a vector formulation. This is derived from (2.10):

$$\begin{aligned}
f_{d_{i,0}} &= -\frac{f_c}{c}\frac{\partial \parallel \mathbf{p}_i(t_{\text{tx}}) - \mathbf{p}(t_{\text{rx}}) \parallel}{\partial t} \\
&= -\frac{f_c}{c}\frac{1}{2 \parallel \mathbf{p}_i(t_{\text{tx}}) - \mathbf{p}(t_{\text{rx}}) \parallel}\frac{\partial \left(\mathbf{p}_i(t_{\text{tx}}) - \mathbf{p}(t_{\text{rx}})\right)^T \left(\mathbf{p}_i(t_{\text{tx}}) - \mathbf{p}(t_{\text{rx}})\right)}{\partial t} \\
&= -\frac{f_c}{c}\frac{1}{2 \parallel \mathbf{p}_i(t_{\text{tx}}) - \mathbf{p}(t_{\text{rx}}) \parallel}\Big(\left(\mathbf{p}_i(t_{\text{tx}}) - \mathbf{p}(t_{\text{rx}})\right)^T \left(\mathbf{v}_i(t_{\text{tx}}) - \mathbf{v}(t_{\text{rx}})\right) \\
&+ \left(\mathbf{p}_i(t_{\text{tx}}) - \mathbf{p}(t_{\text{rx}})\right)^T \left(\mathbf{v}_i(t_{\text{tx}}) - \mathbf{v}(t_{\text{rx}})\right)\Big) \\
&= -\frac{f_c}{c}\frac{\left(\mathbf{p}_i(t_{\text{tx}}) - \mathbf{p}(t_{\text{rx}})\right)^T}{\parallel \mathbf{p}_i(t_{\text{tx}}) - \mathbf{p}(t_{\text{rx}}) \parallel}\left(\mathbf{v}_i(t_{\text{tx}}) - \mathbf{v}(t_{\text{rx}})\right) \\
&= -\frac{f_c}{c}\left(\mathbf{v}_i(t_{\text{tx}}) - \mathbf{v}(t_{\text{rx}})\right)^T \frac{\left(\mathbf{p}_i(t_{\text{tx}}) - \mathbf{p}(t_{\text{rx}})\right)}{\parallel \mathbf{p}_i(t_{\text{tx}}) - \mathbf{p}(t_{\text{rx}}) \parallel} \ ,
\end{aligned} \tag{2.13}$$

where t_{tx} and t_{rx} refer to transmission and reception times, respectively. Notice that the travel time of the signal emitted by the satellite to reach the receiver can be written as the distance between them, divided by the speed of light c:

$$\tau_{i,0}(t_{\text{rx}}) = \frac{1}{c} \parallel \mathbf{p}_i(t_{\text{tx}}) - \mathbf{p}(t_{\text{rx}}) \parallel \ . \tag{2.14}$$

Also we define $\mathbf{p}$ and $\mathbf{v}$ as the position and velocity vectors of the receiver, respectively. Similarly, $\mathbf{p}_i$ and $\mathbf{v}_i$ are defined for the i-th satellite. In navigation applications, the Doppler-shift ranges in ± 12 kHz. When acquiring this frequency deviation, the receiver is accounting for satellite/user relative motions and local oscillator drift.

The signal transmitted by a specific navigation system can be obtained particularizing (2.2) and (2.3) according to the designed parameters of the system. Hereinafter this section, we discuss the main characteristics of current GNSS standards.

2.1.1 GPS signals

Global Positioning System (commonly known by its acronym, GPS) is the american satellite navigation system, which provides timing and ranging since 1993. The constellation consists of 24 operational Medium Earth Orbit (MEO) satellites deployed in 6 evenly spaced planes with an inclination of 55^o. It was designed to provide global coverage with, as a rule of thumb, 4 to 8 (elevation mask of 15^o), 10 (elevation mask of 10^o) or 12 (elevation mask of 5^o) visible satellites at any time of day. These satellites have a period of approximately 12 sidereal days with an altitude of about 20200 km above the Earth.

GPS navigation signals are emitted using 3 frequency bands, in the L-band of the electromagnetic spectrum. The links are commonly referred to as L1, L2 and L5. These bands are obtained from the fundamental frequency $f_o = 10.23$ MHz, being their corresponding carrier frequencies multiples of it:

$$\begin{aligned} f_c\,(\mathrm{L1}) &= 154 \cdot f_o = 1575.42 \text{ MHz} \\ f_c\,(\mathrm{L2}) &= 120 \cdot f_o = 1227.60 \text{ MHz} \\ f_c\,(\mathrm{L5}) &= 115 \cdot f_o = 1176.45 \text{ MHz} \,, \end{aligned} \tag{2.15}$$

having all an allocated ITU bandwidth of 24 MHz. Notice that L3 (1381.05 MHz) and L4 (1379.913 MHz) bands have been used only for military services and are not discussed hereinafter. Each satellite link transmits its own set of ranging signals, which are distinguished by their corresponding spreading codes. At a glance:

L1 link. In the current configuration, it consists of two components: P code (in-phase) and C/A code (quadrature). The C/A code (short for coarse/acquisition code) is a nonclassified PRN sequence for civilian use, having 3 dB more power than the P code. C/A code is the ranging signal typically used by mass market devices. The P code refers to the precision code, being much longer than the C/A code. It is an encrypted nonclassified code used for enhanced performance in GPS receivers due to its higher code rate. For details of P and C/A codes refer to the interface specification document [Ser06a]. In addition, the L1 link provides the military M code, with codewords orthogonal to those used in P and C/A codes. M code is not allowed for civilian use, being therefore encrypted and unknown.

The modernization of GPS includes a new set of signals in the L1 link, aimed at civilian ranging. Although its design is still an issue, preliminary reports [Ser06b] showed that it will likely be composed of a data channel (L1CD) and a pilot channel (L1CP). This modernized civilian signal is to be added to the existing C/A and not to replace it, for backward compatibility reasons.

L2 link. Initially, this link only transmitted precision and military codes. Another civil signal was designed in a first modernization of the system, referred to as L2C code

Link	PRN code	L_c	Code rate $(1/T_c)$	Modulation	Bandwidth
L1	C/A	1023	$f_o/10$	BPSK(1)	$f_o/5$
	P	~ 7 days	f_o	BPSK(10)	$2f_o$
	M	–	$f_o/2$	BOCs(10,5)	$3f_o$
	L1CD	10230	$f_o/10$	BOCs(1,1)	$2f_o/5$
	L1CP	$10230 \cdot 1800$	$f_o/10$	BOCs(1,1)	$2f_o/5$
L2	P	~ 7 days	f_o	BPSK(10)	$2f_o$
	M	–	$f_o/2$	BOCs(10,5)	$3f_o$
	L2CM	10230	$f_o/10$	BPSK(1)	$f_o/5$
	L2CL	$10230 \cdot 75$	$f_o/10$	BPSK(1)	$f_o/5$
L5	L5I	$10230 \cdot 10$	f_o	BPSK(10)	$2f_o$
	L5Q	$10230 \cdot 20$	f_o	BPSK(10)	$2f_o$

Table 2.1: Summary of GPS codes.

and aimed for particular commercial needs [Fon01b]. This code is composed of two components: the L2CM code is modulated by a navigation message and the L2CL code is used as a pilot channel, with the latter being 75 times longer than the former. Specifications to generate L2C codes can be found in [Ser06a]. Since 2005, satellites are being replaced to L2C capable satellites and the full operative constellation is expected by 2012.

L5 link. The latest modernization of GPS signals includes the emission of ranging signals using a third carrier frequency, the L5 link. These civil signals are generally referred to as the L5C signal and were designed to meet the requirements of safety-of-life applications. Basically, this code has two components: L5I and L5Q, in-phase and quadrature respectively. Whereas L5I is modulated with a navigation message, the L5Q code is modulated onto the carrier frequency. Details can be found in the specifications [Ser05]. Nonetheless, the transmission of L5C signals will presumable not be a reality before 2015 [Sha05].

Table 2.1 summarizes the main characteristics of the codes transmitted by the GPS constellation of satellites. Notice that the parameters defining modernized GPS signals are in accordance to the latest reports, see [HW08] and the references therein.

As commented earlier, the current navigation message is a low-rate bit stream broadcasting essential information for positioning, e.g., satellite orbit, satellite health status, correction data, and other data. This digital signal has a bit duration of $T_b = 20$ ms, thus it is transmitted with a data rate of 50 bps. This low rate is required in order to guarantee a low Bit Error Rate (BER) due to the low SNR values typically dealt by GPS receivers. Refer to [Ser06a] or [Par96] for a detailed description of the structure of such navigation message. GPS modernization will incorporate new navigation message

structures and formats. For instance, a bit error correction strategy will be considered to decrease the BER.

2.1.2 Galileo signals

The european contribution to satellite navigation was termed Galileo. The system is named after the scientist and astronomer Galileo Galilei (1564–1642) who, among other achievements, discovered the first four satellites of the planet Jupiter and proposed a procedure to calculate the longitude of a point on Earth by observing the orbits of those satellites.

The Galileo constellation foresees $27 + 3$ satellites in three MEOs, inclined 56^o with respect to the equatorial plane [Fal06]. The constellation is designed to provide a minimum of 6 visible satellites worldwide with an elevation mask of 10^o. Nowadays, two experimental satellites were launched, named as GIOVE-A and GIOVE-B. These satellites emit Galileo-like signals aiming at testing several aspects of the project such as environmental effects or expected orbit perturbations. Currently, the deployment of fully operational satellites is scheduled by 2013.

Signals to be emitted by Galileo satellites will be allocated in the L-band, as in the GPS case. Five carrier frequencies define the five foreseen frequency bands: E1, E6, E5, E5a and E5b. Again, the carrier frequencies are obtained from the fundamental frequency $f_o = 10.23$ MHz:

$$\begin{aligned} f_c\,(\text{E1}) &= 154 \cdot f_o &&= 1575.420 \text{ MHz} \\ f_c\,(\text{E6}) &= 125 \cdot f_o &&= 1278.750 \text{ MHz} \\ f_c\,(\text{E5}) &= 116.5 \cdot f_o &&= 1191.795 \text{ MHz} \\ f_c\,(\text{E5a}) &= 115 \cdot f_o &&= 1176.450 \text{ MHz} \\ f_c\,(\text{E5b}) &= 118 \cdot f_o &&= 1207.140 \text{ MHz} \,, \end{aligned} \tag{2.16}$$

with allocated ITU bandwidths of 32, 40.9, 51.2, 24 and 24 MHz respectively. Notice that E1 corresponds to L1 in the GPS nomenclature and that E5a is equivalent to the L5 band. The E5 band is typically denoted as E5a+E5b band, as it can be seen as the union of those two bands. In addition, Galileo satellites incorporate Search and Rescue (SAR) payload to detect emergency signals, forward them to the SAR ground segment and provide a return link to acknowledge the emergency beacon. Frequency bands allocated for SAR purposes are $1544.05 - 1545.15$ MHz (downlink) and $406.0 - 406.1$ MHz (uplink) [Cos04].

Galileo also considers spread-spectrum signals to multiplex signals from satellites and from different services. Basically, ranging codes can be grouped in three categories: open-access, commercial and governmental. The first group of codes are not encrypted and

Link	PRN code	Channel	L_c	Code rate $(1/T_c)$	Modulation
E1	E1A	data	~ 7 days	f_o	BOCc(15,2.5)
	E1B	data	–	$f_o/2$	MBOC(6,1,1/11)
	E1C	pilot	10230	$f_o/10$	MBOC(6,1,1/11)
E6	E6A	data	~ 7 days	f_o	BOCc(10,5)
	E6B	data	–	$f_o/2$	BPSK(5)
	E6C	pilot	10230	$f_o/10$	BPSK(5)
E5	E5aI	data	$10230 \cdot 10$	f_o	BPSK(10)
	E5aQ	pilot	$10230 \cdot 20$	f_o	BPSK(10)
	E5bI	data	$10230 \cdot 20$	f_o	BPSK(10)
	E5bQ	pilot	$10230 \cdot 20$	f_o	BPSK(10)

Table 2.2: Summary of Galileo codes.

publicly known; the rest are encrypted. See Table 2.2 for an overview of those signals. One of the features of Galileo signals is that some of them are modulated by navigation messages (referred to as data channels), while others are left unmodulated (pilot channels). Data and pilot channels are placed in pairs in each band, except for E1A and E6A. These signal pairs are transmitted with equal power. The aim of pilot channels is to improve tracking performance, coping with hazardous scenarios and weak signal conditions. Briefly, we present the main characteristics of the signals in each of the three main frequency links:

E1 link. The transmitted stream in the E1 band includes three navigation signals: E1A, E1B and E1C. The E1A component is an encrypted and classified signal. Conversely, the ranging sequences E1B and E1C are unencrypted and accessible to all users. Whereas the former is a data channel, the latter is designed to modulate a pilot signal. The PRN sequences for the primary codes of E1B and E1C were published in [ESA06]. The modulation of each signal was designed to reduce narrowband interferences with other existing navigation systems, e.g., GPS. The three signals are modulated onto the carrier frequency using the hexaphase modulation defined in [Kre06].

E6 link. This link is analogous to the E1 link in the sense that it carries three signals: E6A, E6B and E6C. The first component is a public regulated service data and the other two signals are commercial ranging codes, providing a data rate of 500 bps. Signals use the same hexaphase modulation as in the E1 link.

E5 link. Two pairs of data/pilot open-access signals are transmitted in this link. E5a band carries an unencrypted ranging code and a nonclassified navigation message with a bit rate of 25 bps. This low data rate is useful when dealing with weak signals. Data channel E5bI carries both open-access and commercial signals. An

AltBOC(15,10) modulation is used to multiplex E5a and E5b signals. The frequency spectrum of an AltBOC modulation is similar to that of a BOC modulation, with the particularity that each of the two sidelobes are due to different signals. In this case, one sidelobe corresponds to the E5a set of signals and the other to the E5b band.

2.1.3 Other Navigation Systems

The Russian satellite navigation system is referred to as GLONASS, a short for *GLObalnaya Navigasionnay Sputnikovaya Sistema*. The system consists of 21+3 satellites with an altitude on the order of 19100 Km and distributed in 3 orbital planes, inclined 64.8^o with respect to the equator. GLONASS transmits two types of signals: high-accuracy (military use) and standard-accuracy (civilian use) ranging code. These signals are transmitted using 3 frequency bands (G1, G2 and G3), centered at carrier frequencies 1602.000 MHz, 1246.000 MHz and 1204.704 MHz respectively. The main difference between GLONASS and other navigation systems is that it considers Frequency Division Multiple Access (FDMA) to transmit signals from satellites. Notice, however, that ranging codes are still based on PRN sequences. Thus, this system provides a low crosscorrelation between different signals [GLO02]. Many work has been devoted in the literature to the study and design of GLONASS receivers, combining its capabilities to other navigation systems such as GPS or Galileo [Fea06].

China's first attempt to own a navigation system was termed Beidou, named after Ursa Major constellation. Beidou is a regional system based on a constellation of geostationary satellites. Currently, the system will be extended to provide global coverage. The modernized navigation system is named Beidou-2 or Compass, indistinctly. So far, the system will consist of 24+3 MEO, 5 geostationary and 3 geosynchronous satellites [Bei06, Fea06]. The MEO satellites are distributed in 3 orbits, inclined 55^o. Again, three frequencies are used to transmit navigation signals. Other regional systems are the Japanese QZSS (Quasi-Zenith Satellite System), covering East Asia and Oceania; and IRNSS (Indian Regional Navigation Satellite System), with coverage of the Indian subcontinent.

Improving the performance of GNSS receivers is usually done considering Differential GNSS (DGNSS) techniques, which are based on differential corrections broadcasted by reference stations. Additionally one can consider Augmentation systems to enhance both position accuracy and integrity. Augmentation systems provide local information (as DGNSS) with the advantage of delivering integrity information. Augmentation systems can be divided into Space-Based Augmentation Systems (SBAS) and Ground-Based Augmentation Systems (GBAS), depending on the broadcasting network. Whereas the former transmit the information using a constellation of satellites, the latter consider

ground-based communications. Systems falling in the SBAS category are US Wide-Area Augmentation System (WAAS), the European Geostationary Navigation Overlay System (EGNOS), Japan's contribution MSAS, the Indian GAGAN, the Satellite Navigation Augmentation System (SNAS) to be deployed by China and Russian's System for Differential Correction and Monitoring (SDCM). GBAS examples are pseudolites or the Local-Area Augmentation System (LAAS). These techniques are not discussed here, being out of the scope of the dissertation.

2.2 Architecture of a GNSS Receiver

New trends following the Software Defined Radio (SDR) philosophy emerged [Mit00, Ree02, Tut02], mainly thanks to recent advances in high-speed analog-to-digital converters (ADC), that aim at simplifying the RF-chain of the receivers by digitizing as close to the antenna as possible. Thus, downconversion and other processes typically performed in the analog domain can be implemented in a digital platform. Namely, *Field Programmable Gate Array* (FPGA), *Digital Signal Processors* (DSP) or *System–On–Chip* (SOC) platforms. The use of SDR receivers has attracted the interest of the GNSS community in recent times, see for instance [Tsu00, Kru01, Ako03, Kan04, FP06] and the references therein.

In a nutshell, this section presents the basic blocks composing a SDR GNSS receiver. As illustrated in Figure 2.2, the architecture can be divided in two main parts: the RF front-end chain and the consecutive signal processing. The former is composed of analog hardware (HW) devices and the latter is fully implemented in software (SW) in some digital platform. Therefore, a SDR receiver combines specialized HW/SW architectures to maintain cost-efficiency and high flexibilities in the designs. Section 2.2.1 provides some insight to the HW part of the receiver, while Sections 2.2.2 and 2.2.3 discuss the operation of the SW blocks in Figure 2.2: Digital Signal Processing and computation of the navigation solution to obtain the PVT (i.e., position, velocity and time) solution, respectively. For the sake of clarity, this section focuses on the single antenna receiver. See Appendix 2.A for a brief discussion on antenna array approaches.

2.2.1 RF front-end

The RF front-end is composed of a Right Hand Circularly Polarized (RHCP) antenna, with RHCP being the signal polarization emitted by navigation satellites. The gain for Left Hand Circularly Polarized (LHCP) signals is typically low in antennas for GNSS applications, since it was seen that the polarization of reflected signals changes from

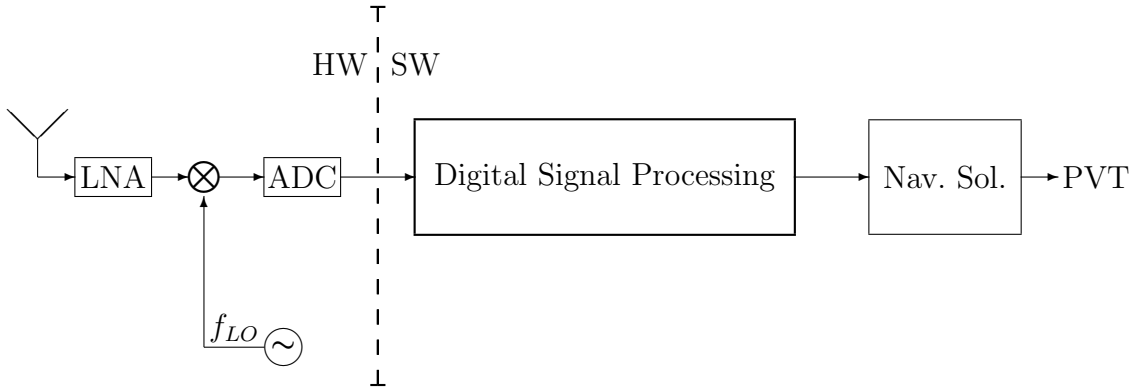

Figure 2.2: SDR GNSS receiver functional blocks.

RCHP to LHCP [Par96]. Immediately after the antenna, the signal is processed by a Low Noise Amplifier (LNA). The LNA is a fundamental block in any front-end architecture (not only in GNSS), since it constitutes the primary contribution to the overall noise figure of the receiver. The objectives of this block are twofold. On the one hand, it amplifies the received signal and, on the other hand, the LNA acts as a band-pass filter aiming at rejecting out-of-band interferences. Typically, a first downconversion to intermediate frequency (IF) is performed by a local oscillator (LO). LOs at the receivers are based on quartz crystal oscillators, whose stability cannot be compared to that of atomic clocks in the satellites. Thus, the time offset produced by internal LO perturbations is considered as an unknown parameter to be estimated by GNSS receivers, as will be seen later in this chapter. Lastly, the IF signal is digitized by an analog-to-digital converter (ADC) which discretizes the signal stream into a set of samples. Afterwards, samples are quantized by a determined number of bit levels. For GNSS purposes, one-bit quantization was seen to be enough for synchronization and positioning purposes, but higher quantization levels will provide improved SNR at the expenses of increasing the computational complexity of the receiver's implementation [Bor07].

Notice that, with the described architecture, signals entering the SW part of the receiver are still modulated at an IF. Thus, the receiver still has to demodulate the in-phase and quadrature components of the signal. A conventional I&Q demodulator will include a second LO (before ADC) to downconvert the signal to baseband [Pro94]. This process consists in splitting the received signal and multiplying each arm by a LO and its 90^o shifted version. This procedure provides I&Q components after lowpass filtering and quantization. A number of errors may appear when considering the conventional analog approach, mainly caused because the two arms must be closely matched for correct demodulation, e.g., gain balance, quadrature-phase balance or DC offsets. Following the SDR philosophy, IF sampling strategies can be considered. Thus, the I&Q demodulator can be fully implemented in the digital domain, overcoming some of the aforementioned

errors [Tsu01]. Notice that, a direct downconversion after the LNA might be unaffordable in high-speed applications [Wal99]. Nevertheless, the analog components of the RF/IF chain have to be still carefully designed.

The basics of IF sampling are here given, showing the versatility of SDR receivers. A more general study can be consulted in [Ber08a], where FPGA implementation guidelines were also given. Consider that a complex baseband signal $s(t)$, having a bandwidth of B Hz, is transmitted at RF. This signal can be regarded as the one in (2.1). We define $s_I(t)$ and $s_Q(t)$ as the in-phase and quadrature components of $s(t)$. After downconversion to an IF, expressed as f_{IF}, the signal is bandpass filtered at the receiver to avoid aliasing and to remove high-frequency components. Thus, at the output of the RF chain, the received real signal consists of the desired IF signal corrupted by noise:

$$x_{IF}(t) = a\ V(t)\cos\left(2\pi f_{IF}t + \Theta(t)\right) + n(t)\ , \tag{2.17}$$

where a is the amplitude of the signal and $n(t)$ represents additive noise. $V(t)$ and $\Theta(t)$ are the envelope and the phase of $s(t) = s_I(t) + js_Q(t)$, respectively. The IF signal feds an ADC which samples the signal at a sampling rate of $f_s = 1/T_s$ with n_b bits of quantization. Hence, the sampled version of the IF signal can be expressed as:

$$x_{IF}[n] = a\ V[n]\cos\left(2\pi f_{IF}nT_s + \Theta[n]\right) + \nu[n]\ . \tag{2.18}$$

The idea behind digital IF sampling is to undersample IF signal in order to obtain a replica of the signal at baseband, without requiring an additional downconversion. This can be accomplished by properly choosing f_{IF} and f_s. In general, the following relations

$$\begin{aligned} f_{IF} &= kf_s \pm \frac{f_s}{4} \quad ,\forall k \in \mathbb{Z} \mid k \geq 1 \\ f_s &\geq 4B \end{aligned} \tag{2.19}$$

ensure that a non-overlapped alias will appear centered at $f_s/4$. Then, one of the replicas at $\pm f_s/4$ can be downconverted to baseband using the frequency-shifting property of the Fourier transform of a signal, i.e.,

$$Z(f \pm f_o) \overset{F}{\longleftrightarrow} z[n]e^{\mp j2\pi f_o nT_s}\ . \tag{2.20}$$

With $f_o = f_s/4$, it results that we have to multiply the IF signal by $e^{-j\frac{\pi}{2}n}$ to shift the spectrum to the left. Actually, this is a straightforward operation since the sequence of cyclic values of $e^{-j\frac{\pi}{2}n}$ are $\{1, -j, -1, j\}$, where $j^2 = -1$. This process provides the I and Q components of the desired signal.

Figure 2.3 shows the spectra of the signals involved in the process. $S_{IF}(f)$ is the spectral density of the received IF signal in equation (2.17), plotted in the Figure 2.3(a).

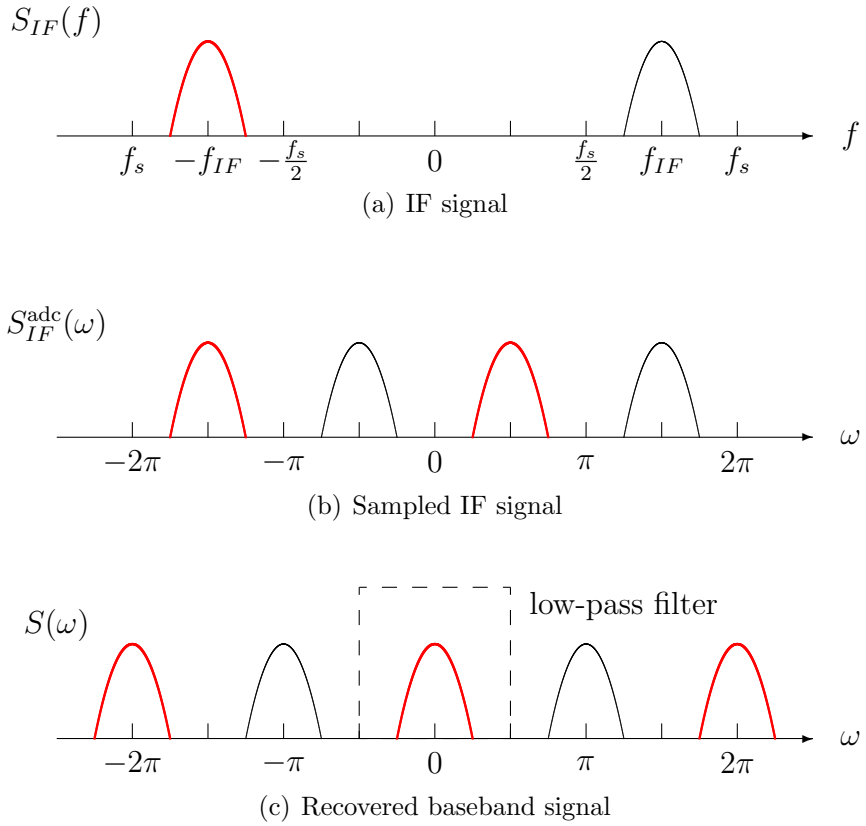

Figure 2.3: Representation of the spectral densities of when $f_{IF} = 3f_s/4$: (a) $x_{IF}(t)$, (b) $x_{IF}[n]$ and (c) $x[n] = x_{IF}[n] \cdot e^{-j\frac{\pi}{2}n}$.

Setting $f_{IF} = 3f_s/4$, i.e. $k = 1$, and sampling $x_{IF}(t)$ according to (2.19), we can observe in Figure 2.3(b) that aliasing appears without overlapping in its spectrum, denoted as $S_{IF}^{\text{adc}}(f)$. Recall that we assumed a band-limited signal $s(t)$. After frequency-shift, we obtain a baseband replica of the desired signal: $S(f) = S_{IF}^{\text{adc}}(f - f_s/4)$.

Notice that the spectral density $S_{IF}^{\text{adc}}(f)$ shown in Figure 2.3(b) is obtained for any chosen k in (2.19). Thus, the selection of k is related to implementation issues, i.e., to select a suitable f_{IF} for the application under design according to the RF front-end devices available (costs reduction criteria). The restriction on f_s to be a minimum of twice the Nyquist frequency arises in order to avoid overlapping in $S_{IF}^{\text{adc}}(f)$. After lowpass filtering $S(f)$ one can decimate the signal up to a factor that depends on the chosen sampling frequency.

2.2.2 Satellite Synchronization

The Digital Signal Processor in Figure 2.2 is in charge of a number of operations[1]. Firstly, if an IF sampling scheme is chosen, as described in Section 2.2.1, the frequency shift by $e^{-j\frac{\pi}{2}n}$ is performed for each channel independently to obtain the I&Q components of the baseband signals. Nevertheless, the main purpose of the functional block is to recover the synchronism of the received signals. In other words, time-delays, carrier-phases and Doppler-shifts are to be estimated by the receiver. As commented earlier in this chapter, these parameters provide information regarding the relative distance between the receiver and the corresponding satellite, which is used in the computation of the PVT solution (cf. Section 2.2.3).

Acquisition

Initially, the receiver has to detect which are the visible satellites and obtain a rough estimation of the synchronization parameters of those satellites. This process is referred to as *acquisition*, being typically performed by correlating the received signal and a locally generated code (corresponding to the PRN sequence of the satellite under study) [Van91, War96]. The local replica is moved in time and frequency, covering the range of all possible time-delay and Doppler-shifts, thus yielding to a two-dimensional search where the maximum provides the synchronism of the given satellite. Several alternatives exist to perform the two-dimensional search, being the most common to use an FFT-based procedure [Tsu00] due to its simplicity. Figure 2.4 illustrates the correlation output in the two possible cases: when there is a signal coming from the tested satellite and when the signal does not have enough SNR to be properly detected/acquired (or not in line-of-sight). In order to detect the satellite in Figure 2.4(a), the correlation peak has to exceed a established threshold above the noise floor. This threshold is defined according to a desired probability of false alarm [Bro00]. To further improve the quality of the acquisition process, a number of correlation outputs can be coherently averaged to increase the SNR of the peak by reducing the noise floor level (assuming zero-mean noise). The number of averages is referred to as *dwells* in the literature, with typical dwell values on the order of 10 for the GPS C/A acquisition (i.e., averaging 10 ms).

Depending on the amount of information the receiver has, the initialization of the acquisition process can be classified into: cold start (the receiver does not have any prior information), warm start (rough position estimates are available and almanac information

[1]Keep in mind that the operations performed by the Digital Signal Processor are implemented in parallel (or concurrently) in order to process the signals of all visible satellites at the same time. The number of channels is fixed in hardware receivers, but can be variable in SDR receivers.

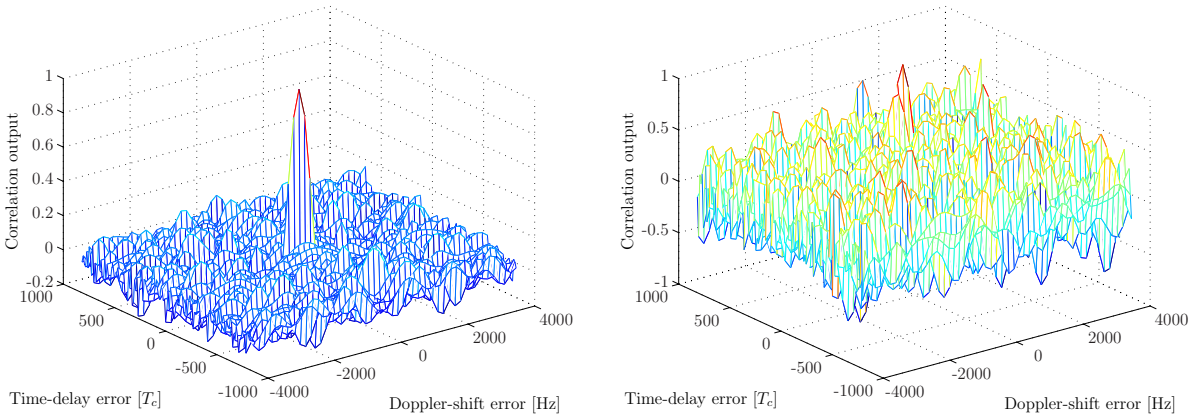

(a) (b)

Figure 2.4: Normalized correlation output versus the time-delay and Doppler shift relative error between the local code replica and the actual received signal, for a given satellite. In (a) the correlation output when there is signal from the tested satellite and in (b) the case of absence of signal (or weak signal conditions) are illustrated.

allows the estimation of visible satellites) or hot start (is the case of low-term signal blockages, where there is no need to restart ephemeris acquisition again) [FP06, p. 183].

Tracking

After acquisition is performed - that is to say, detection of visible satellites and initial coarse estimation of synchronization parameters of these satellites is available -, the receiver begins the tracking mode of operation. The objective is to keep track of synchronization parameters (i.e., time-delays, Doppler-shifts and carrier-phases) of the detected satellites and to provide accurate estimates for the computation of user's position. Furthermore, the output of this block are a set of despread bit streams, corresponding to the navigation message of each tracked satellite.

Tracking loops can be seen as a refinement of acquisition structures. Whereas the latter perform a search in a wide range of the parameters of interest, the former confines its operation to the neighborhood of a previous estimate. Thus, if correctly acquired, tracking loops are able to lock on the corresponding parameter by continuously adjusting the local code to match the received signal. Dedicated hardware structures have been used for tracking purposes before the advent of SDR receivers. Then, time-delay has been typically tracked by means of a Delay Lock Loop (DLL), which performs the same

correlation operation as done in acquisition but with lower computational complexity due to the reduced parameter space. Similarly, Phase Lock Loops (PLL) and Frequency Lock Loops (FLL) have been used for phase and Doppler tracking purposes, respectively. Even in recent implementations of SDR GNSS receivers, these structures have been mimicked and used in software-based receivers [Tsu00, Bor07] because of historical reasons.

A DLL is a practical implementation of the Maximum Likelihood Estimator (MLE) of the time-delay of a given satellite, assuming no multipath propagation [FP06]. The objective is then to locate the maximum of the correlation function between the received signal and the local code. This is done by finding the zero-crossing of the correlation's derivative. The correlation's output corresponding to the actual time-delay estimate is termed the *prompt* (P) sample. DLL-based techniques use samples adjacent to the prompt to find the zero-crossing point, i.e., to adjust the output to the next time-delay estimate. These samples are referred to as *early* (E) and *late* (L), which correspond to advanced and delayed samples with respect to the position of the prompt respectively. See Figure 2.5(a) for an illustrative representation of a correlation function and the outputs of the correlators, i.e., E/L and P samples. A number of DLL alternatives can be found in the literature [Irs03, Pro94], depending on: how EPL samples are combined to form the discriminator function, the spacing between E/L and P samples (δ-spacing), number of E/L samples considered, etc. For example, the simplest DLL that can be implemented consists of three samples from the correlator, i.e., EPL. The δ-spacing is typically set to 1 chip, for implementation simplicity. Then, the standard 1-chip wide DLL admits several alternatives depending on the construction of the discriminator function. For instance, we can consider the early-minus-late-power [Die92, Nee95], the early-minus-late-envelope or the dot product power [Fel97, Bra99] options.

Basically, DLL-based techniques proposed in the literature have been designed to mitigate the effect of multipath propagation. Recall that GNSS receivers are only interested in estimating delays of signals received directly from the satellites (the LOSSs), since they are the ones that carry information of direct propagation time. Hence, reflections distort the received signal in a way that may cause a bias in delay and carrier-phase estimations [Van93]. Actually, an important result given in [Wei95] says that any unbiased time-delay estimator based on a single antenna has a variance that approaches to infinity when the relative delay between the LOSS and its multipath replica approaches to zero. Thus, making it impossible to discriminate between LOSS and coherent multipath signals, which is seen as an unknown bias in the estimates. Multipath with relative delays lower than the chip period are referred to as coherent multipath. Therefore, multipath is probably the dominant source of error in high-precision applications since it can introduce a bias up to a hundred of meters when employing a 1-chip wide δ-spacing (standard) DLLs to track the delay, see Figure 2.5(b).

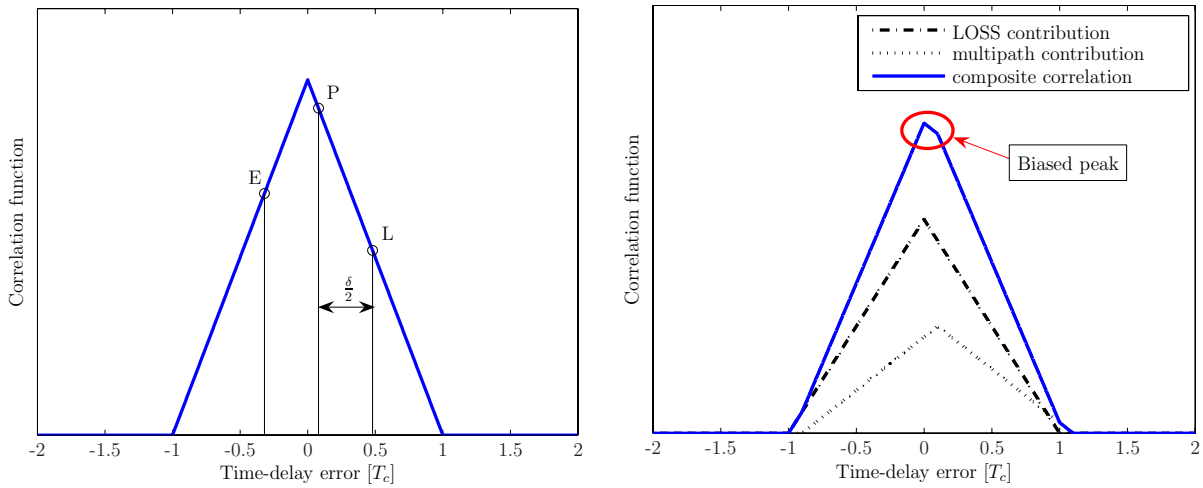

Figure 2.5: Ideal correlation function of a GPS C/A-like signal versus the relative delay offset with the local replica of the code. (a) Early/Late and Prompt samples are shown for a multipath-free scenario. In (b), the biasing effect of a multipath replica on the overall correlation function is illustrated.

Nevertheless, the versatility of the SDR paradigm allows the design and implementation of more complex and innovative approaches than those merely based on DLL structures. Many contributions to multipath mitigation can be found in the literature. Several DLL-based methods have been proposed such as the Narrow Correlator [Die92], where the δ-spacing is reduced thanks to technological advances to 0.1 or even 0.05 chips; the Pulse Aperture Correlator (PAC) [Jon04]; the Strobe Correlator [Gar96] (which is a specific implementation of the Double Delta Correlator described in [McG99], where more E/L samples are used to refine the performance); the Early1/Early2 (E1/E2) tracking technique [Die97]; or the Multipath Elimination Technology (MET) [Tow94], also referred to as Early/Late Slope technique. A robust statistical approach to the multipath problem is the Multipath Estimating Delay Lock Loop (MEDLL) developed by Van Nee [Van94, Nee95], where the Maximum Likelihood (ML) principle is applied considering the number of reflections known. Recently, [Sah06] proposed an algorithm to implement the MEDLL estimator with reduced computational complexity. Another recent approach is the Vision Correlator introduced by NovAtel [Fen05], which is an implementation of a multipath mitigation method known as the Multipath Mitigation Technique (MMT algorithm), developed by Weill [Wei02]. The use of Particle Filtering (PF) for multipath mitigation in GNSS receivers has been addressed in the literature. For example, in [Gir01] a Rao-Blackwellized PF was proposed to integrate GPS measurements and Inertial Nav-

igation Systems [Far99]. In [Gir07] a PF algorithm that operate at the observable level (i.e., pseudoranges) was presented to mitigate multipath effect in the position solution, which also considered Rao-Blackwellization of a multipath indicator process. A PF algorithm in the vein of the present paper was reported in [Clo06a], where the PF operate at the signal level in order to jointly track the LOSS and its replicas. Other PF usages can be found in the literature in the field of multisensor data fusion and switching observation models [Yan04, Car07]. Aside from these approaches, joint processing of satellite signals was seen to provide multipath mitigation capabilities in the Vector DLL (VDLL) architecture [Par96] and the Direct Position Estimation (DPE) approach, which was presented in [Clo07b] and further investigated in Chapter 4. Pioneering the use of antenna arrays in GNSS receivers we found the work by [SG00, SG05], where the MLE of synchronization parameters was explored. In addition, an hybrid beamforming technique was proposed, accounting for both temporal and spatial references. The work was followed by [FP06] with further improvements and discussions on practical aspects of antenna array systems. Efficient implementations of the MLE found in [SG05] have been recently identified, see for instance [Ant05].

2.2.3 GNSS Positioning: observables and navigation solution

The block in Figure 2.2 denoted as navigation solution is in charge of calculating the observables, demodulate the navigation message and compute user's position. Observables are a set of ranges computed from time-delay or phase-difference estimates, being the output of tracking algorithms (cf. Section 2.2.2). Since those signals are affected (biased) by satellite and receiver clock errors, the range is typically referred to as pseudorange. The demodulation of the navigation message provides the receiver with the orbital variables required to determine satellites' orbits, satellite's clock bias and other important parameters. This information and the computed pseudoranges are then processed to obtain an estimation of user's location. The time required by a receiver to provide a first position estimate, after power up, is referred to as Time To First Fix (TTFF). This parameter depends not only on the navigation solution operation, but on several issues of the receiver such as the acquisition strategy. For the sake of completeness, these processes are exposed hereinbelow.

The propagation time that a signal takes between its transmission from the i-th satellite to the user is continuously estimated by tracking algorithms. This time-delay estimate (denoted by $\hat{\tau}_i$) provides an estimation of the distance between the i-th satellite and the user, i.e., the pseudorange $\rho_i = c\hat{\tau}_i$. Thus, pseudoranges provide a nonlinear relation between user's position ($\mathbf{p} = [x, y, z]^T$) and the estimated time-delay of each satellite according to the model:

$$\rho_i = \varrho_i(\mathbf{p}) + c\,(\delta t - \delta t_i) + \epsilon_i \ , \tag{2.21}$$

where c is the speed of light, satellites are indexed by $i \in \{1, \ldots, M_s\}$ and with the following definitions:

- $\hat{\tau}_i$ is the time-delay estimate at the receiver for the LOSS emitted by the i-th satellite;
- $\varrho_i(\mathbf{p}) = \| \mathbf{p}_i - \mathbf{p} \|$ is the geometric distance between the receiver and the i-th satellite. $\mathbf{p}_i = [x_i, y_i, z_i]^T$ are the coordinates of the i-th satellite in the Earth-Centered Earth-Fixed (ECEF) coordinate system, which can be computed from the ephemeris, transmitted in the low-rate navigation message [Par96];
- δt is the bias of the receiver clock with respect to GPS time, which is unknown;
- δt_i is the clock bias of the i-th satellite with respect to GPS time, known from the navigation message; and
- the term ϵ_i includes errors from various sources such as atmospheric delays, multipath biases, ephemeris mismodeling and relativistic effects among others.

The observed carrier frequency at the receiver differs from its nominal frequency due to the Doppler effect. These frequency shifts are caused by user-satellite relative motion and by frequency errors and drifts in user and satellite clocks. Accurate Doppler-shift estimates yield to precise velocity calculations, useful in positioning and navigation applications with high user dynamics. The Doppler-shift due to the relative motion of the user and the i-th satellite is [Par96]

$$f_{d_i} = -\left(\mathbf{v}_i - \mathbf{v}\right)^T \mathbf{u}_i \, \frac{f_c}{c} \, , \tag{2.22}$$

where $\mathbf{v} = [v_x, v_y, v_z]^T$ and $\mathbf{v}_i = [v_{x_i}, v_{y_i}, v_{z_i}]^T$ are the velocity vectors of the user and the i-th satellite, respectively. $\mathbf{u}_i$ represents the unitary direction vector of the i-th satellite relative to the user, defined as

$$\mathbf{u}_i = \frac{\mathbf{p}_i - \mathbf{p}}{\| \mathbf{p}_i - \mathbf{p} \|} \tag{2.23}$$

and f_c represents the corresponding carrier frequency used in navigation systems. Recall that the derivation of (2.22) was given in (2.13), where we saw that it naturally arises due to the propagation travel time affecting the carrier frequency. Notice that we dropped the transmission and reception times for the sake of clarity. Differentiating (2.21) with respect to time, the pseudorange rate ($\dot{\rho}$) regarding the i-th satellite is related to the Doppler shift as

$$\dot{\rho}_i = \left(\mathbf{v}_i - \mathbf{v}\right)^T \mathbf{u}_i + c\left(\dot{\delta t} - \dot{\delta t}_i\right) + \epsilon_f \, , \tag{2.24}$$

with $\dot{\delta t}$ the receiver clock drift and ϵ_f noise on the phase rate measurement due to non-modeled terms.

To sum up, observables are computed for each tracked satellite from the outputs of the tracking loops. In addition, code and phase measurements can be obtained at the different frequency bands where navigation signals are emitted. This allows the receiver to combat atmospheric biases by properly combining satellite observables, since the propagation of signals through different atmosphere layers is also distinct. See for instance [Par96] for details.

Once the two observables are obtained – previous estimation of each τ_i and f_{d_i} –, the receiver computes its position. Conventional receivers are equipped with a carrier-phase loop that tracks the evolution of the carrier phase and wipes it off from the received signal before code-phase synchronization. Carrier-phase measurements can also be taken into account in the navigation solution, but it requires the estimation of the integer number of carrier cycles between the satellite and the receiver. This can be done by means of the Least-Squares AMBiguity Decorrelation Adjustment method (LAMBDA, [Teu93, Jon96]), or more sophisticated approaches based on the observation of multiple bands, such as the Three Carrier Ambiguity Resolution (TCAR, [For97]) or its generalization, the Multiple Carrier Ambiguity Resolution (MCAR, [Wer03]). In the following, we will assume that a phase locked loop is used for carrier tracking and stripping, thus mitigating the Doppler effect, but this information will not be used in the navigation solution.

Alternatives exist to compute the position of the receiver. We focus on the single point solution with code pseudoranges, that is to say, user's positioning by considering the pseudorange observable. As commented earlier, Doppler-shift estimates are used in this approach for carrier wipe off. Other alternatives include single point positioning with carrier phases or Doppler-shifts estimates and Precise Point Positioning (PPP). The latter considers accurate satellital data and dual-frequency observables [Wit00], thus achieving enhanced performances.

The single point solution with code pseudoranges used in conventional GNSS receivers is based on the linearization of a geometrical problem [Par96, Kap96, Str97, Gre01, Bor07]. The problem is to compute user's position and clock offset from a set of M_s estimated pseudoranges. Thus, from equation (2.21), we form the following system of equations,

$$\begin{aligned} \rho_i + c\delta t_i - \epsilon_i = &\parallel \mathbf{p}_i - \mathbf{p} \parallel + c\delta t \\ i = &\{1, \ldots, M_s \mid M_s \geq 4\} \ , \end{aligned} \tag{2.25}$$

which results in a nonlinear and possibly overdetermined system. The condition $M_s \geq 4$ is due to the dimensionality of the problem. The system is usually solved by linearizing each $\varrho_i(\mathbf{p})$ with respect to an initial position estimate ($\mathbf{p}^o = [x^o, y^o, z^o]^T$)

$$\varrho_i(\mathbf{p}) \simeq \varrho_i^o + \frac{x_i - x^o}{\varrho_i^o}\delta_x + \frac{y_i - y^o}{\varrho_i^o}\delta_y + \frac{z_i - z^o}{\varrho_i^o}\delta_z \ , \tag{2.26}$$

where $\delta_x = x^o - x$, $\delta_y = y^o - y$, $\delta_z = z^o - z$ and $\varrho_i^o \triangleq \varrho_i(\mathbf{p}^o) = \| \mathbf{p}_i - \mathbf{p}^o \|$. The Bancroft algorithm [Ban85] provides an initial guess on the position and the clock offset of the user receiver without any prior knowledge.

Considering (2.26), the system in (2.25) can be formulated as the following Least Squares (LS) problem,

$$\hat{\boldsymbol{\delta}} = \arg\min_{\boldsymbol{\delta}} \left\{ \| \mathbf{y} - \mathbf{T}\boldsymbol{\delta} \|^2 \right\} \ , \tag{2.27}$$

where

$$\begin{aligned} \mathbf{y} &= \begin{bmatrix} \rho_1 + c\delta t_1 - \epsilon_1 - \varrho_1^o \\ \vdots \\ \rho_{M_s} + c\delta t_{M_s} - \epsilon_{M_s} - \varrho_{M_s}^o \end{bmatrix} \\ \mathbf{T} &= \begin{bmatrix} \frac{x_1 - x^o}{\varrho_1^o} & \frac{y_1 - y^o}{\varrho_1^o} & \frac{z_1 - z^o}{\varrho_1^o} & 1 \\ \vdots & \vdots & \vdots & \vdots \\ \frac{x_{M_s} - x^o}{\varrho_{M_s}^o} & \frac{y_{M_s} - y^o}{\varrho_{M_s}^o} & \frac{z_{M_s} - z^o}{\varrho_{M_s}^o} & 1 \end{bmatrix} \\ \boldsymbol{\delta} &= \begin{bmatrix} \delta_x, \delta_y, \delta_z, \delta t \end{bmatrix}^T \ , \end{aligned} \tag{2.28}$$

and the solution

$$\hat{\boldsymbol{\delta}} = \mathbf{T}^{\dagger}\mathbf{y} \triangleq \left(\mathbf{T}^H\mathbf{T}\right)^{-1}\mathbf{T}^H\mathbf{y} \tag{2.29}$$

is straightforwardly given by the Moore-Penrose pseudoinverse ($\mathbf{T}^{\dagger}$). Therefore, we have that $\hat{\mathbf{p}} = \mathbf{p}^o + \hat{\boldsymbol{\delta}}$ is the classical position estimation provided by GNSS receivers.

The solution presented in (2.29) can be improved by using side information. As a variation, if each observation (i.e., pseudoranges) is weighted proportional to the quality of the information provided (for instance, regarding the received signal strength or the geometry of the constellation), a weighting matrix $\boldsymbol{\Omega}_w$ can be constructed and we can formulate the positioning problem in (2.25) as a Weighted LS problem:

$$\hat{\boldsymbol{\delta}} = \arg\min_{\boldsymbol{\delta}} \left\{ \left(\mathbf{y} - \mathbf{T}\boldsymbol{\delta}\right)^H \boldsymbol{\Omega}_w \left(\mathbf{y} - \mathbf{T}\boldsymbol{\delta}\right) \right\} \ , \tag{2.30}$$

whose solution is given by:

$$\hat{\boldsymbol{\delta}} = \left(\mathbf{T}^H\boldsymbol{\Omega}_w\mathbf{T}\right)^{-1}\mathbf{T}^H\boldsymbol{\Omega}_w\mathbf{y} \ . \tag{2.31}$$

Notice that since errors among satellite pseudoranges are considered uncorrelated, the weighting matrix turns to be diagonal. In general, the optimal $\boldsymbol{\Omega}_w$ is not known and it has to be constructed following a given criterion. The Gauss-Markov theorem [Pla50] shows that, when errors are uncorrelated with each other and with the independent variables and have equal variance, LS is the Best Linear Unbiased Estimator (BLUE). If measurements

are uncorrelated but have different variances, WLS is BLUE if each weight is equal to the reciprocal of the variance of the measurement. Observe that the LS solution expressed in (2.29) can be straightforwardly obtained as a particularization of the WLS for $\mathbf{\Omega}_w = \mathbf{I}$.

Finally, the computed PVT solution is forwarded to a User's interface. This interface is in charge of presenting the results in a user-friendly manner, depending on the type of GNSS receiver and the scope of the application.

Appendix 2.A Antenna array based receivers

Consider an N-element antenna array receiver with an arbitrary geometry, with the case of a single antenna receiver being a particularization of it. Antenna arrays provide interesting capabilities of automatic tracking and adaptive nulling. An array of sensors has the potential to improve the overall reception performance of the relied signals in an environment having several sources of interference, multipath propagation or weak signal reception, providing spatial diversity to enhance the desired signal reception [Wid67, Mon80, Vee88, Joh93, Tre02]. The output of an antenna array can be processed in two different ways:

Digital Beamforming. Beamforming is the combination of radio signals from a set of small non-directional antennas to simulate a large directional antenna. There are two technical approaches to steerable antennas: mechanically moved dishes and electronically steerable antenna array. In the case of dishes, the satellite tracking is performed by means of a mechanical engine, i.e., the antenna is physically moved to point the desired satellite. This solution implies high mechanical complexity. In addition, this kind of antenna does not provide any capability in spatial processing, for instance nulling the reception of other unwanted signals or adaptive processing, and they have limited jamming interference rejection.

Digital Beamforming (DBF) with antenna arrays consists of several antennas which outputs are controlled in phase and gain, i.e., multiplied by complex weights, in order to achieve a gain pattern that can be manipulated electronically. Then, all the weighted signals are combined to obtain a single output. These mentioned weights can be stacked in a complex-valued vector $\mathbf{w} = [w_0, \ldots, w_{N-1}]^T$, and the output signal of the beamformer can be computed as $y(t) = \mathbf{w}^H \mathbf{x}(t)$. Weight vector $\mathbf{w}$ can be designed following several techniques. Namely, we can consider Spatial Reference Beamforming (SRB), Temporal Reference Beamforming (TRB) and Hybrid Space-Time Beamforming (HB).

The SRB technique is based on the assumption that the receiver has the knowledge of the satellite ephemerides and a rough estimation of the receivers position. At this point, the receiver calculates the Direction of Arrival (DOA) of each visible satellite in order to feed the beamforming module with a spatial reference. With this set of information a SRB can be implemented using the well-known Minimum Variance Beamforming (MVB) algorithm also named Capon Beamformer [Wax96]. MVB consists on minimizing the total output power while forcing the beamformer to always point to the desired signal's DOA. This approach implies the prior knowledge of the steering vector. Thus, in addition to the beamformer, algorithms to estimate the DOA of the desired signals must be considered, as well as knowledge of the antenna element gain and the mutual coupling. This beamformer is array-calibration

sensitive and array-attitude dependent, which complicates its implementation, especially in a mobile receiver because the need of inertial sensors. On the other hand, the TRB approach selects all the correlated signals and attenuates the uncorrelated noise and interferences, minimizing the MSE between a reference signal and the array output. Consequently, the TRB technique does require neither a calibrated array nor attitude determination of the receiver, but a locally generated reference signal. The correlation between this reference signal and the received signal provides an estimation of the steering vector, thus, under ideal conditions both SRB and TRB behave similarly. However, when there are some errors in the knowledge of the steering vector, the MVB might attempt to cancel the desired signal because it is seen as a source of power not coming from the expected DOA. On the contrary, the TRB is not sensitive to these errors if the reference signal is properly generated. It does not need the knowledge of the steering vector (which gathers the contribution of DOAs and mutual coupling). Last but not least, HB is a hybridization of the SRB and TRB strategies, which was proposed in [SG05]. HB takes advantage of both approaches to mitigate multipath and interference contributions.

These DBF techniques can be implemented using a number of algorithms. The fastest approach is to directly compute the matrices involved in the computation of weights with a signal record of K snapshots. In the literature, this is referred to as the Sample Matrix Inversion (SMI) technique – also Direct Matrix Inversion (DMI) – and is an open-loop architecture which does not take into account the actual output of the array to compute future weights. SMI provides the optimal weights (according to one of the above criteria) and has a high adaptation rate to changing scenarios. However, its computational requirements could make its implementation too expensive for a timevarying scenario. Hence, simpler and cheaper solutions are necessary, at the expenses of lower adaptation rates. Adaptive Beamforming algorithms provide iterative solutions to compute array weights, e.g., Least Mean Square (LMS) and Recursive Least Square (RLS), which improves the convergence rate of the former.

It is out of the scope of this dissertation the study of DBF techniques and algorithms, being the interested reader referred to the provided references on the topic. To conclude, Figure 2.6 represents a block diagram of an antenna array based receiver that considers DBF. This representation is the natural extension to the single antenna architecture shown in Figure 2.2. After DBF, the resulting stream of data is equivalent to the output of an steerable antenna and, thus, it can be processed using single antenna techniques by a conventional GNSS receiver. We make the definition $\upsilon_i = [\tau_i, f_{d_i}]^T$.

Statistical Array Processing. When this approach is adopted, signal fed by each element is jointly processed. Therefore, the array is not equivalent anymore to a steer-

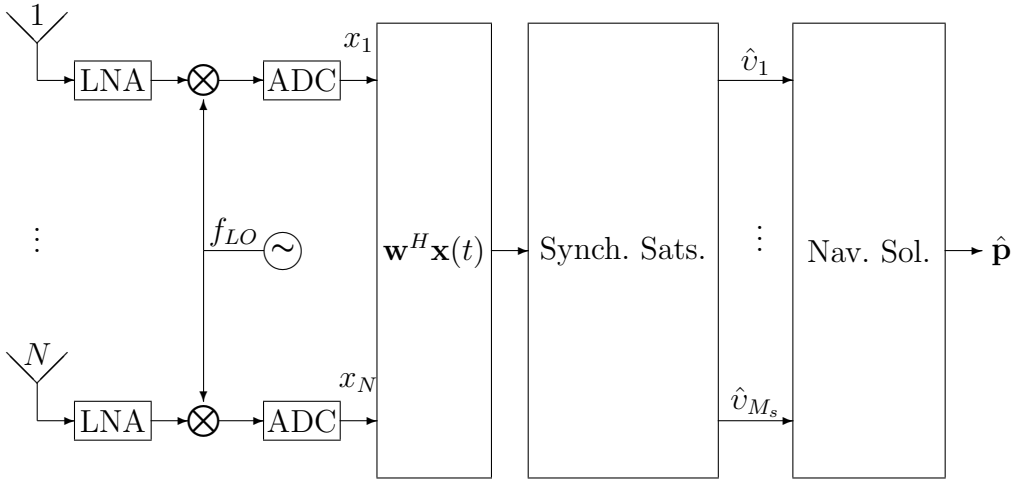

Figure 2.6: Two-steps positioning approach in a SDR GNSS receiver with DBF.

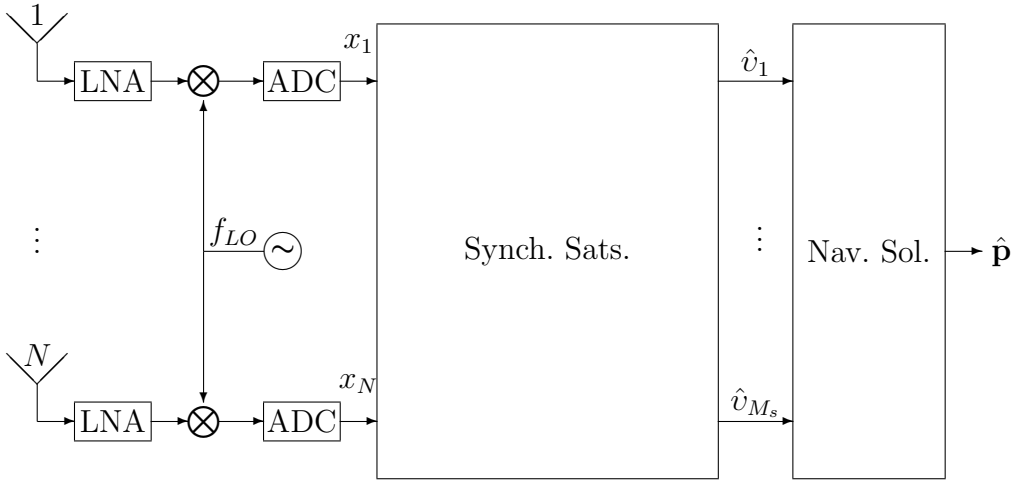

Figure 2.7: Two-steps positioning approach in a SDR GNSS receiver with an statistical array processing approach.

able antenna, with all channels being handled by a signal processing algorithm to extract the desired signal parameters. In particular, the ML estimation of GNSS synchronization parameters was studied in [SG00] and, lately, in [Sel03, FP06, Ant08]. With this setup, a GNSS receiver processes digitized signals from each channel to compute the synchronization parameters of visible satellites to, afterwards, compute user's position. This receiver's configuration is depicted in Figure 2.7.

3

Bayesian Filters for Multipath Mitigation

MANY problems involve the use of *a priori*[1] information, i.e., side information known beforehand that can be taken into account to improve the performance of a given estimation process. This is roughly the idea behind Bayesian statistics, introduced by T. Bayes in his seminal work in the 18^{th} century [Bay63], which has been reproduced in a modernized notation in [Ber58]. Anyone who ever gambled for a soccer match can readily understand the *Bayesian approach*. When someone makes a score prediction, it takes into account many prior information: table position of the two teams, statistics of past seasons, players injured, motivation, etc. The list is almost infinite in this particular case[2]. In contrast, the *classical approach* does not consider all that amount of prior data. Thus, in our example, all three possible results are treated as being equally probable ($p = 1/3$).

[1] From Latin, literally "*from the former*", meaning something presupposed. The reverse is *a posteriori*, from Latin literally "*from the latter*", meaning based on empirical knowledge.

[2] Prior information is usually the result of a subjective interpretation of reality. The soccer example is also useful to point out that a *bad* elicited prior information can lead to a losing bet, e.g. if the gambler is the supporter of one of the two teams it is evident that the subjective conditioning can play a harmful role. In general one has to be careful with the prior data considered, being one of the main criticisms to the Bayesian approach. Refer to [Rai72] for a discussion on priors.

Apart from the use of prior information, there is yet another core difference between non-Bayesian and Bayesian approaches to statistical estimation. Whereas the classical approach considers that the parameter of interest is a deterministic but unknown constant, the Bayesian approach assumes that it is a random variable (*r.v.* for short) whose a priori distribution is somehow known [Kay93]. The aim of a Bayesian estimator is to estimate the particular realization of the *r.v.* given prior data and measurements. The extension of Bayesian statistics to the case of a vector of *r.v.* is straightforward, with the underlying concept being the same.

The Bayesian approach has been widely used in many signal processing applications such as target tracking, DOA estimation, time-varying channel estimation, resource allocation, image processing, speech recognition or pattern classification. Actually, the number of applications is only limited by the imagination and the possibility/impossibility of eliciting useful prior distributions for a given problem. This chapter considers the Bayesian approach to track the synchronization parameters of a GNSS satellite under multipath environments.

The chapter is organized as follows. Section 3.1 presents the Bayesian approach in a rigorous mathematical way and a number of optimal/suboptimal algorithms are discussed. Section 3.2 is dedicated to a class of suboptimal algorithms (Particle Filters) that deserve some attention due to its paramount importance along the dissertation. The rest of the chapter is devoted to the application of those algorithms to the GNSS synchronization problem studied in this dissertation. Section 3.3 presents the modeling of the problem and Section 3.4 the algorithm proposed to mitigate the impact of multipath in the estimation of synchronization parameters. Simulation results are commented in Section 3.5 and Section 3.6 concludes the chapter.

3.1 The Bayesian approach to nonlinear filtering

In general, the natural way to account for prior information is to consider a state-space (SS) model. The SS representation provides a twofold modeling. On the one hand, *state equation* illustrates the evolution of states with time. In other words, state equation mathematically expresses the prior information that the algorithm has regarding the state[3]. On the other hand, *measurement equation* models the dependency of measurements with unknown states. In this section, we introduce the general discrete state-space (DSS) model and the Bayesian conceptual solution, which is only analytically tractable when some assumptions hold. The section discusses both optimal and state-of-the-art suboptimal algorithms to obtain the Bayesian solution. We restrict ourselves to the discrete version of

[3]We understand by *state* the evolving (vector) *r.v.* that drives measurements and which is the estimation objective.

the SS model since it is the one required along this dissertation. Although similar, the continuous SS model has its own particularities that an interested reader can explore in detail in [And79].

3.1.1 Considering Prior information: the Bayesian recursion

The DSS approach deals with the nonlinear filtering problem: recursively compute estimates of states $\mathbf{z}_k \in \mathbb{R}^{n_z}$ given measurements $\mathbf{x}_k \in \mathbb{C}^{n_x}$ at time index k based on all available measurements, $\mathbf{x}_{1:k} = \{\mathbf{x}_1, \ldots, \mathbf{x}_k\}$. State equation models the evolution in time of target states as a discrete-time stochastic model, in general

$$\mathbf{z}_k = \mathbf{f}_{k-1}(\mathbf{z}_{k-1}, \boldsymbol{\nu}_k) \ , \tag{3.1}$$

where $\mathbf{f}_{k-1}(\cdot)$ is a known, possibly nonlinear, function of the state $\mathbf{z}_k$ and $\boldsymbol{\nu}_k$ is referred to as process noise which gathers any mismodeling effect or disturbances in the state characterization. The relation between measurements and states is modeled by

$$\mathbf{x}_k = \mathbf{h}_k(\mathbf{z}_k, \mathbf{n}_k) \ , \tag{3.2}$$

where $\mathbf{h}_k(\cdot)$ is a known possibly nonlinear function and $\mathbf{n}_k$ is referred to as measurement noise. Both process and measurement noise are assumed with known statistics and mutually independent. The initial *a priori* distribution of the state vector is assumed to be known, $p(\mathbf{z}_0)$.

From equations (3.1) and (3.2) it is seen that the assumed DSS model describes a Markov process of order one, as state at time instant k depends only on the previous state. The Hidden Markov Model (HMM) is a statistical model where one Markov process, representing the underlying system, is observed through a stochastic process. Meaning that states are not directly observable, but measurements. The idea behind the HMM model is graphically shown in Figure 3.1, where it appears as evident that states are hidden and that the algorithm has access to measurements. In addition, the algorithm must have perfect knowledge of state and measurement equations, represented in Figure 3.1 by vertical and horizontal arrows respectively.

Alternatively, the DSS can be expressed in terms of states and measurement distributions, i.e., prior and likelihood distributions respectively. This interpretation is equivalent to that in (3.1) and (3.2), but is useful in some problems. In this case, state equation is written as

$$\mathbf{z}_k \sim p(\mathbf{z}_k|\mathbf{z}_{k-1}) \quad \text{for } k \geq 1 \ , \tag{3.3}$$

where $p(\mathbf{z}_k|\mathbf{z}_{k-1})$ is referred to as the transitional prior. The relationship between measurements and states is generically modeled by the probability distribution

$$\mathbf{x}_k \sim p(\mathbf{x}_k|\mathbf{z}_k) \quad \text{for } k \geq 1 \ , \tag{3.4}$$

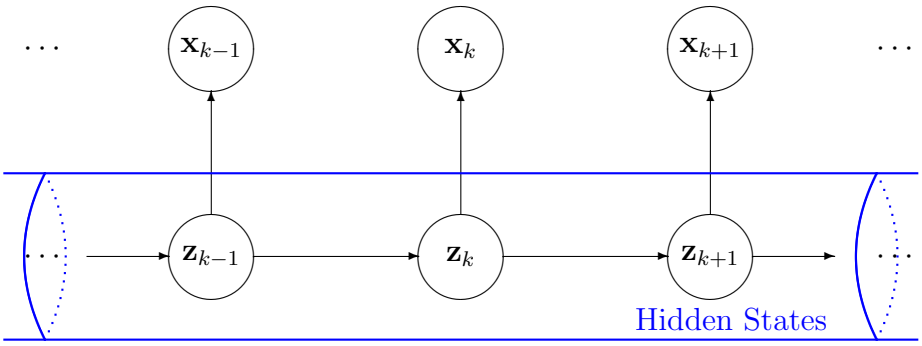

Figure 3.1: Graphical interpretation of the DSS model as a Markov process of order one

referred to as the likelihood function. Similarly as in the functional interpretation of the DSS, $p(\mathbf{z}_0)$ is assumed known.

From a Bayesian standpoint, the posterior distribution $p(\mathbf{z}_{0:k}|\mathbf{x}_{1:k})$ provides all necessary information about the state of the system $\mathbf{z}_{0:k}$, given all measurements $\mathbf{x}_{1:k}$ and the prior $p(\mathbf{z}_{0:k})$. The *Bayes' theorem* allows to express the posterior in terms of the likelihood and prior distributions:

$$p(\mathbf{z}_{0:k}|\mathbf{x}_{1:k}) = \frac{p(\mathbf{x}_{1:k}|\mathbf{z}_{0:k})p(\mathbf{z}_{0:k})}{p(\mathbf{x}_{1:k})} \ , \tag{3.5}$$

which can be written as

$$p(\mathbf{z}_{0:k}|\mathbf{x}_{1:k}) = \frac{p(\mathbf{z}_0)\prod_{t=1}^{k} p(\mathbf{x}_t|\mathbf{z}_t)p(\mathbf{z}_t|\mathbf{z}_{t-1})}{p(\mathbf{x}_{1:k})} \tag{3.6}$$

where we take into account that measurements are independent given $\mathbf{z}_{0:k}$ and consider the Markov state evolution depicted in Figure 3.1.

We are interested in the marginal distribution $p(\mathbf{z}_k|\mathbf{x}_{1:k})$ since, as will be seen later in this section, it allows the estimation of the realization of the target state vector $\mathbf{z}_k$. $p(\mathbf{z}_k|\mathbf{x}_{1:k})$ can be obtained by marginalization of (3.6), being the dimension of the integral growing with k. Alternatively the desired density[4] can be computed sequentially in two stages: prediction and update. The basic idea is to, assuming the filtering distribution known at $k-1$, first predict the new state and then incorporate the new measurement to obtain the distribution at k:

$$\cdots \longrightarrow p(\mathbf{z}_{k-1}|\mathbf{x}_{1:k-1}) \longrightarrow \underbrace{p(\mathbf{z}_k|\mathbf{x}_{1:k-1})}_{\text{prediction}} \longrightarrow \underbrace{p(\mathbf{z}_k|\mathbf{x}_{1:k})}_{\text{update}} \longrightarrow \cdots$$

[4]In the sequel, $p(\mathbf{z}_k|\mathbf{x}_{1:k})$ is referred to as the filtering distribution. In contrast to $p(\mathbf{z}_{0:k}|\mathbf{x}_{1:k})$, which is the posterior distribution.

First we notice from (3.6) that the posterior distribution can be recursively expressed as:

$$p(\mathbf{z}_{0:k}|\mathbf{x}_{1:k}) = \frac{p(\mathbf{x}_k|\mathbf{z}_k)p(\mathbf{z}_k|\mathbf{z}_{k-1})}{p(\mathbf{x}_k|\mathbf{x}_{1:k-1})} p(\mathbf{z}_{0:k-1}|\mathbf{x}_{1:k-1}) \ , \tag{3.7}$$

where the marginal $p(\mathbf{z}_k|\mathbf{x}_{1:k})$ also satisfies the recursion [Sor88]. Given that $p(\mathbf{z}_0) \triangleq p(\mathbf{z}_0|\mathbf{x}_0)$ is known, where $\mathbf{x}_0$ is the set of no measurements, we can assume that the required density at time $k-1$ is available, $p(\mathbf{z}_{k-1}|\mathbf{x}_{1:k-1})$. In the prediction stage the predicted distribution is obtained by considering that $p(\mathbf{z}_k|\mathbf{z}_{k-1}, \mathbf{x}_{1:k-1}) = p(\mathbf{z}_k|\mathbf{z}_{k-1})$, due to the first-order Markovian SS model considered. Using the Chapman-Kolmogorov equation (see Appendix 3.A) to remove $\mathbf{z}_{k-1}$ we obtain,

$$p(\mathbf{z}_k|\mathbf{x}_{1:k-1}) = \int p(\mathbf{z}_k|\mathbf{z}_{k-1}) p(\mathbf{z}_{k-1}|\mathbf{x}_{1:k-1}) d\mathbf{z}_{k-1} \ . \tag{3.8}$$

Whenever a new measurement becomes available at instant k, the predicted distribution in (3.8) is updated via the Bayes' rule (see Appendix 3.A)

$$\begin{aligned} p(\mathbf{z}_k|\mathbf{x}_{1:k}) &= p(\mathbf{z}_k|\mathbf{x}_k, \mathbf{x}_{1:k-1}) \\ &= \frac{p(\mathbf{x}_k|\mathbf{z}_k, \mathbf{x}_{1:k-1}) p(\mathbf{z}_k|\mathbf{x}_{1:k-1})}{p(\mathbf{x}_k|\mathbf{x}_{1:k-1})} \\ &= \frac{p(\mathbf{x}_k|\mathbf{z}_k) p(\mathbf{z}_k|\mathbf{x}_{1:k-1})}{p(\mathbf{x}_k|\mathbf{x}_{1:k-1})} \ , \end{aligned} \tag{3.9}$$

being the normalizing factor

$$p(\mathbf{x}_k|\mathbf{x}_{1:k-1}) = \int p(\mathbf{x}_k|\mathbf{z}_k) p(\mathbf{z}_k|\mathbf{x}_{1:k-1}) d\mathbf{z}_k \ . \tag{3.10}$$

Now the recursion is enclosed by equations (3.8) and (3.9), assuming some knowledge about the state evolution and the relation between measurements and states, described by $p(\mathbf{z}_k|\mathbf{z}_{k-1})$ and $p(\mathbf{x}_k|\mathbf{z}_k)$ respectively. This recursion form the basis of the optimal Bayesian solution.

To sum up, the interest on characterizing the filtering distribution is that it enables one to compute optimal state estimates with respect to any criterion [Kay93], conditional upon measurements up to time k'. For example, the Minimum Mean Square Error (MMSE) estimator is extensively used in engineering applications, which is the conditional mean of the state with respect to available measurements,

$$\hat{\mathbf{z}}_k^{\text{MMSE}} = \mathbb{E}\left\{\mathbf{z}_k|\mathbf{x}_{1:k'}\right\} = \int \mathbf{z}_k p(\mathbf{z}_k|\mathbf{x}_{1:k'}) d\mathbf{z}_k \ . \tag{3.11}$$

Another approach is to compute the Maximum a posteriori (MAP) estimate, which reduces to find the state value which maximizes the filtering distribution,

$$\hat{\mathbf{z}}_k^{\text{MAP}} = \arg\max_{\mathbf{z}_k} \left\{ p(\mathbf{z}_k|\mathbf{x}_{1:k'}) \right\} \ , \tag{3.12}$$

among many other criterions which can be used[5]. In general, we would like to compute any function $g(\cdot)$ of the state:

$$\widehat{g(\mathbf{z}_k)}^{\text{MMSE}} = \mathbb{E}\left\{ g(\mathbf{z}_k)|\mathbf{x}_{1:k'} \right\} = \int g(\mathbf{z}_k) p(\mathbf{z}_k|\mathbf{x}_{1:k'}) d\mathbf{z}_k \ , \tag{3.13}$$

conditional upon measurements up to time k'.

Depending on the value of k' we identify three different problems:

Smoothing. It is the case of $k' > k$, were the state $\mathbf{z}_{0:k}$ is estimated using future measurements.

Filtering. Corresponds to the case $k' = k$. It is the problem considered in the sequel and the approach that is followed along the dissertation.

Prediction. In this case, one predicts values of states with measurements of previous instants: $k' < k$.

What the reader has read so far, corresponds to the conceptual solution of Bayesian filtering (smoothing and prediction) that is endowed with the sequential equations (3.8) and (3.9). Unfortunately, in general this recursion cannot be solved analytically. There are few cases where the posterior distribution can be characterized by a sufficient statistic. This is the case of linear/Gaussian models where the Kalman Filter (KF) yields to the optimal solution [Kal60, And79]. Another interesting case is when the SS is discrete and finite, where the optimal solution exists and can be found via optimal grid based methods [Ris04]. However, there are more general SS models that can only be solved via suboptimal algorithms. For nonlinear systems, the KF can be modified in order to cope with this situation. A classical solution to deal with nonlinearities is to resort to the Extended Kalman Filter (EKF) [And79] by linearizing the model at some point of interest. Another alternative, based on the KF, is the Unscented Kalman Filter (UKF) [Jul97, Wan00, Mer00] were the model is not linearized and, instead, a Gaussian posterior is considered which is characterized by a set of deterministically chosen sample points. Basically we can conclude that there are several alternatives in the literature, being some

[5]Intuitively, the non-Bayesian counterparts to the MMSE and MAP estimators are the Least Squares (LS) and Maximum Likelihood (ML) estimators, respectively. In the latter, prior information is omitted or, equivalently, a noninformative prior is used.

of them discussed in the rest of this section. First, Section 3.1.2 discusses the special cases were optimal algorithms can be used. Then, Section 3.1.3 reviews a number of suboptimal algorithms. Notice that particle filtering [Ris04] falls in the category of suboptimal algorithms. Nevertheless, it deserves a separate section in this dissertation. In order to provide the reader with the basic concepts of particle filtering, Section 3.4 provides a brief tutorial to this powerful tool.

3.1.2 Optimal Algorithms

There are few cases where the Bayesian filtering problem can be analytically solved. This section presents two cases and their associated optimal algorithms: the Kalman Filter and Grid-based methods.

Kalman Filter

Nobody can question that the Kalman Filter (KF) has been one of the most used algorithms since its conception [Kal60]. Simple in its formulation, the KF provides an optimal Bayesian solution when the SS model is linear/Gaussian in both state and measurement equations. Thus, the model considered is

$$\begin{aligned} \mathbf{z}_k &= \mathbf{F}_{k-1}\mathbf{z}_{k-1} + \boldsymbol{\nu}_k \\ \mathbf{x}_k &= \mathbf{H}_k\mathbf{z}_k + \mathbf{n}_k \end{aligned} \tag{3.14}$$

where $\mathbf{F}_{k-1}$ and $\mathbf{H}_k$ are known matrices that represent linear functions, referred to as *transitional* and *measurement* matrices respectively. $\boldsymbol{\nu}_k$ and $\mathbf{n}_k$ are mutually independent random variables drawn from a zero-mean white Gaussian probability density function with known covariance matrices, $\boldsymbol{\Sigma}_{z,k}$ and $\boldsymbol{\Sigma}_{n,k}$ respectively.

The KF considers the posterior pdf as a Gaussian distribution, being completely characterized by its mean and covariance. Then, the prediction and update steps in equations (3.8) and (3.9) result in

$$\begin{aligned} p(\mathbf{z}_{k-1}|\mathbf{x}_{1:k-1}) &= \mathcal{N}\left(\mathbf{z}_{k-1};\ \hat{\mathbf{z}}_{k-1|k-1}, \mathbf{P}_{k-1|k-1}\right) \\ p(\mathbf{z}_k|\mathbf{x}_{1:k-1}) &= \mathcal{N}\left(\mathbf{z}_k;\ \hat{\mathbf{z}}_{k|k-1}, \mathbf{P}_{k|k-1}\right) \\ p(\mathbf{z}_k|\mathbf{x}_{1:k}) &= \mathcal{N}\left(\mathbf{z}_k;\ \hat{\mathbf{z}}_{k|k}, \mathbf{P}_{k|k}\right) \ . \end{aligned} \tag{3.15}$$

The KF provides the mean and covariance of each step in an iterative way [And79]:

$$\begin{aligned} \hat{\mathbf{z}}_{k|k-1} &= \mathbf{F}_{k-1}\hat{\mathbf{z}}_{k-1|k-1} \\ \mathbf{P}_{k|k-1} &= \mathbf{\Sigma}_{z,k} + \mathbf{F}_{k-1}\mathbf{P}_{k-1|k-1}\mathbf{F}_{k-1}^T \\ \hat{\mathbf{z}}_{k|k} &= \hat{\mathbf{z}}_{k|k-1} + \mathbf{K}_k\left(\mathbf{x}_k - \mathbf{H}_k\hat{\mathbf{z}}_{k|k-1}\right) \\ \mathbf{P}_{k|k} &= \mathbf{P}_{k|k-1} - \mathbf{K}_k\mathbf{S}_k\mathbf{K}_k^T \ , \end{aligned} \tag{3.16}$$

where it is defined the Kalman gain matrix as

$$\mathbf{K}_k = \mathbf{P}_{k|k-1}\mathbf{H}_k^T\mathbf{S}_k^{-1} \tag{3.17}$$

and the variance of the innovation term as

$$\mathbf{S}_k = \mathbb{E}\left\{\left|\mathbf{x}_k - \mathbf{H}_k\hat{\mathbf{z}}_{k|k-1}\right|^2\right\} = \mathbf{H}_k\mathbf{P}_{k|k-1}\mathbf{H}_k^T + \mathbf{\Sigma}_{n,k} \ . \tag{3.18}$$

Intuitively, a state prediction $\hat{\mathbf{z}}_{k|k-1}$ is done considering state equation in (3.14), i.e., a priori information. The state estimation at k is given by updating $\hat{\mathbf{z}}_{k|k-1}$ with a term that depends on the innovation error $\mathbf{x}_k - \mathbf{H}_k\hat{\mathbf{z}}_{k|k-1}$, which corrects the state prediction. The innovation error refers to the misadjusting between actual and predicted measurements, being controlled by the Kalman gain matrix. Initially, this matrix takes large values, since the main source of information are the measurements. Conversely, for increasing k, the updated values of $\mathbf{K}_k$ decrease since the algorithm gives more importance to prior data.

As said, the KF computes the mean and covariance matrices of the densities involved in (3.15) in a sequential way. In the case of linear/Gaussian models, the KF is the optimal solution. However, the assumptions might be too tight. They may not hold in some applications where the dependence of measurements on states is nonlinear or noises cannot be considered normally distributed or zero-biased. This is one of the main criticisms made against the use of such algorithm, which is nowadays still (widely) used.

Grid-based methods

Another case where the Bayesian recursion in equations (3.1) and (3.2) can be analytically solved is when the SS is discrete and the number of states is finite. Under these assumptions, Grid-based methods can be optimally applied [Buc71].

Consider that at time index $k-1$ the finite discrete states are $\mathbf{z}_{k-1}^i$ s.t. $i = 1, \ldots, n_z$ and that we define the conditional probability of each state given measurements up to time $k-1$ as

$$P\left\{\mathbf{z}_{k-1} = \mathbf{z}_{k-1}^i | \mathbf{x}_{1:k-1}\right\} \triangleq w_{k-1|k-1}^i \quad , \tag{3.19}$$

then the posterior pdf at $k-1$ is

$$p(\mathbf{z}_{k-1}|\mathbf{x}_{1:k-1}) = \sum_{i=1}^{n_z} w_{k-1|k-1}^i \delta(\mathbf{z}_{k-1} - \mathbf{z}_{k-1}^i) \quad . \tag{3.20}$$

We obtain the prediction and update equations from substitution of equation (3.20) in (3.8) and (3.9). Resulting in:

$$\begin{aligned} p(\mathbf{z}_k|\mathbf{x}_{1:k-1}) &= \sum_{i=1}^{n_z} w_{k|k-1}^i \delta(\mathbf{z}_k - \mathbf{z}_k^i) \\ w_{k|k-1}^i &\triangleq \sum_{j=1}^{n_z} w_{k-1|k-1}^j p(\mathbf{z}_k^i|\mathbf{z}_{k-1}^j) \\ p(\mathbf{z}_k|\mathbf{x}_{1:k}) &= \sum_{i=1}^{n_z} w_{k|k}^i \delta(\mathbf{z}_k - \mathbf{z}_k^i) \\ w_{k|k}^i &\triangleq \frac{w_{k|k-1}^i p(\mathbf{x}_k|\mathbf{z}_k^i)}{\sum_{j=1}^{n_z} w_{k|k-1}^j p(\mathbf{x}_k|\mathbf{z}_k^j)} \end{aligned} \tag{3.21}$$

Notice that grid-based methods consider that the distributions $p(\mathbf{z}_k|\mathbf{z}_{k-1})$ and $p(\mathbf{x}_k|\mathbf{z}_k)$ are known. However, there is not any assumption made regarding the distribution itself, i.e., the distributions can differ from the Gaussian case in contrast to the Kalman Filter.

3.1.3 Sub-optimal Algorithms

In many cases, the assumptions considered by optimal algorithms are too restrictive and cannot be held. For instance, the dependence of measurements on states might be non-linear (e.g. a time-delay that parameterizes a signal) or the noise could not be considered white and Gaussian distributed anymore. In the cases where one cannot take advantage of optimal algorithms, there exist several suboptimal algorithms that can be considered to deal with the goal of obtaining the filtering distribution of interest. In this section, we review some of the most common suboptimal algorithms found in the literature.

Extended Kalman Filter

The KF can be extended to the case of nonlinear models of the form of:

$$\begin{aligned} \mathbf{z}_k &= \mathbf{f}_{k-1}(\mathbf{z}_{k-1}) + \boldsymbol{\nu}_k \\ \mathbf{x}_k &= \mathbf{h}_k(\mathbf{z}_k) + \mathbf{n}_k \end{aligned} \tag{3.22}$$

where $\mathbf{f}_{k-1}(\cdot)$ and $\mathbf{h}_k(\cdot)$ are known nonlinear functions. $\boldsymbol{\nu}_k$ and $\mathbf{n}_k$ are mutually independent random variables drawn from a zero-mean white Gaussian probability density function with known covariance matrices $\boldsymbol{\Sigma}_{z,k}$ and $\boldsymbol{\Sigma}_{n,k}$, respectively.

The approach taken by the Extended Kalman Filter (EKF) is based on a local linearization of the model, while maintaining the Gaussian constraint on the involved density functions [Jaz70]. The EKF approximates the posterior pdf as a Gaussian in the vein of (3.15). Thus, the posterior characterization is provided by its estimated mean and covariances. Similarly as done in the KF algorithm, the mean and covariance of both predictive and updated distributions are obtained in a sequential way [And79]:

$$\begin{aligned} \hat{\mathbf{z}}_{k|k-1} &= \mathbf{f}_{k-1}(\hat{\mathbf{z}}_{k-1|k-1}) \\ \mathbf{P}_{k|k-1} &= \boldsymbol{\Sigma}_{z,k} + \hat{\mathbf{F}}_{k-1}\mathbf{P}_{k-1|k-1}\hat{\mathbf{F}}_{k-1}^T \\ \hat{\mathbf{z}}_{k|k} &= \hat{\mathbf{z}}_{k|k-1} + \mathbf{K}_k\left(\mathbf{x}_k - \mathbf{h}_k(\hat{\mathbf{z}}_{k|k-1})\right) \\ \mathbf{P}_{k|k} &= \mathbf{P}_{k|k-1} - \mathbf{K}_k\mathbf{S}_k\mathbf{K}_k^T \end{aligned} \tag{3.23}$$

where

$$\begin{aligned} \mathbf{K}_k &= \mathbf{P}_{k|k-1}\hat{\mathbf{H}}_k^T\mathbf{S}_k^{-1} \\ \mathbf{S}_k &= \mathbb{E}\left\{\left|\mathbf{x}_k - \hat{\mathbf{H}}_k\hat{\mathbf{z}}_{k|k-1}\right|^2\right\} = \hat{\mathbf{H}}_k\mathbf{P}_{k|k-1}\hat{\mathbf{H}}_k^T + \boldsymbol{\Sigma}_{n,k}\ . \end{aligned} \tag{3.24}$$

The computation of this first and second order statistics is done after linearizing measurement and/or state evolution functions in (3.22). Local linearizations of $\mathbf{f}_{k-1}(\hat{\mathbf{z}}_{k-1|k-1})$ and $\mathbf{h}_k(\hat{\mathbf{z}}_{k|k-1})$ are obtained by the Gradient evaluated at the point of interest as

$$\begin{aligned} \hat{\mathbf{F}}_{k-1} &= \left[\nabla_{\mathbf{z}_{k-1}}\mathbf{f}_{k-1}^T(\mathbf{z}_{k-1})\right]^T\Big|_{\mathbf{z}_{k-1}=\hat{\mathbf{z}}_{k-1|k-1}} \\ \hat{\mathbf{H}}_k &= \left[\nabla_{\mathbf{z}_k}\mathbf{h}_k^T(\mathbf{z}_k)\right]^T\Big|_{\mathbf{z}_k=\hat{\mathbf{z}}_{k|k-1}}, \end{aligned} \tag{3.25}$$

respectively.

As said the EKF deals with nonlinearities in the model. However, the posterior density is still modeled as being Gaussian. Thus, it might fail in applications where the Gaussian assumption is not valid or the nonlinearity is severe, which causes the true posterior to differ from Gaussianity. In addition, the EKF requires an accurate initialization of states and covariances in order to converge to the optimal solution, since the approximations in (3.25) are local.

Unscented Kalman Filter

Yet another KF-based algorithm, which aims at approximating $p(\mathbf{z}_k|\mathbf{x}_{1:k})$ under general DSS models [Jul00]. The Unscented Kalman Filter (UKF for short) is named after the Unscented Transform (UT), which is used in the process. The UKF characterizes the filtering distribution as a Gaussian pdf, thus its mean and covariance suffice to describe it (as any KF-based approach). This density parameters are obtained from a set of deterministically chosen sample points, obtained by the UT (refer to Appendix 3.B for details).

The initial assumption made by the UKF algorithm is that the filtering distribution at instant $k-1$ is Gaussian, i.e., $p(\mathbf{z}_{k-1}|\mathbf{x}_{1:k-1}) = \mathcal{N}\left(\hat{\mathbf{z}}_{k-1|k-1}, \mathbf{P}_{k-1|k-1}\right)$. Then, this distribution is represented by a set of N_{UKF} sample points and their associated weights:

$$\left\{\mathcal{Z}_{k-1}^i, \mathcal{W}_{k-1}^i\right\}_{i=1}^{N_{UKF}} , \tag{3.26}$$

obtained by the UT. These deterministically chosen points are propagated through the, possibly nonlinear, process function

$$\mathcal{Z}_{k|k-1}^i = \mathbf{f}_{k-1}\left(\mathcal{Z}_{k-1}^i\right) \tag{3.27}$$

which, along with their corresponding weights, are used to characterize the predicted filtering distribution:

$$\begin{aligned} p(\mathbf{z}_k|\mathbf{x}_{1:k-1}) &\approx \mathcal{N}\left(\hat{\mathbf{z}}_{k|k-1}, \mathbf{P}_{k|k-1}\right) \\ \hat{\mathbf{z}}_{k|k-1} &= \sum_{i=1}^{N_{UKF}} \mathcal{W}_{k-1}^i \mathcal{Z}_{k|k-1}^i \\ \mathbf{P}_{k|k-1} &= \mathbf{\Sigma}_{z,k} + \sum_{i=1}^{N_{UKF}} \mathcal{W}_{k-1}^i \left(\mathcal{Z}_{k|k-1}^i - \hat{\mathbf{z}}_{k|k-1}\right)\left(\mathcal{Z}_{k|k-1}^i - \hat{\mathbf{z}}_{k|k-1}\right)^T . \end{aligned} \tag{3.28}$$

Finally, the update step provides the desired filtering distribution at k:

$$\begin{aligned} p(\mathbf{z}_k|\mathbf{x}_{1:k}) &\approx \mathcal{N}\left(\hat{\mathbf{z}}_{k|k}, \mathbf{P}_{k|k}\right) \\ \hat{\mathbf{z}}_{k|k} &= \hat{\mathbf{z}}_{k|k-1} + \mathbf{K}_k\left(\mathbf{x}_k - \hat{\mathbf{x}}_{k|k-1}\right) \\ \mathbf{P}_{k|k} &= \mathbf{P}_{k|k-1} - \mathbf{K}_k \mathbf{S}_k \mathbf{K}_k^T , \end{aligned} \tag{3.29}$$

where

$$\begin{aligned}
\hat{\mathbf{x}}_{k|k-1} &= \sum_{i=1}^{N_{UKF}} \mathcal{W}_{k-1}^{i} \mathbf{h}_k \left(\mathcal{Z}_{k|k-1}^{i}\right) \\
\mathbf{K}_k &= \mathbf{P}_{zx}\mathbf{S}_k^{-1} \\
\mathbf{S}_k &= \mathbf{P}_{xx} + \mathbf{\Sigma}_{n,k} \\
\mathbf{P}_{zx} &= \sum_{i=1}^{N_{UKF}} \mathcal{W}_{k-1}^{i} \left(\mathcal{Z}_{k|k-1}^{i} - \hat{\mathbf{z}}_{k|k-1}\right) \left(\mathbf{h}_k \left(\mathcal{Z}_{k|k-1}^{i}\right) - \hat{\mathbf{x}}_{k|k-1}\right)^T \\
\mathbf{P}_{xx} &= \sum_{i=1}^{N_{UKF}} \mathcal{W}_{k-1}^{i} \left(\mathbf{h}_k \left(\mathcal{Z}_{k|k-1}^{i}\right) - \hat{\mathbf{x}}_{k|k-1}\right) \left(\mathbf{h}_k \left(\mathcal{Z}_{k|k-1}^{i}\right) - \hat{\mathbf{x}}_{k|k-1}\right)^T .
\end{aligned} \tag{3.30}$$

Intuitively, the sample points in (3.26) are selected by the UT to characterize the mean and covariance of $\mathcal{N}\left(\hat{\mathbf{z}}_{k-1|k-1}, \mathbf{P}_{k-1|k-1}\right)$. The goodness of the UT is that these points are *well–behaved* under nonlinear functions, meaning that the resulting sample points in (3.27) accurately characterize $\mathcal{N}\left(\hat{\mathbf{z}}_{k|k-1}, \mathbf{P}_{k|k-1}\right)$ avoiding an awkward linearization.

Two main differences exist between EKF and UKF: UKF does not linearize the functions in the DSS model, since the approximation is on the filtering distribution itself; and, as a consequence, the calculation of the Gradients is avoided in the UKF algorithm. In general, the UKF was seen to improve the results of the EKF keeping a low computational cost [Jul97, Wan00, Mer00].

Approximate Grid-based methods

Grid-based methods can also be used when the SS is whether continuous or discrete with infinite dimensionality. The idea is to *select* a finite set of discrete states and evaluate the filtering density at those points. That is to run the grid-based characterization as presented in Section 3.1.2 with the set of finite-discrete states or use these points as the basis of an interpolation of the distribution as proposed in [Buc74, Kit87].

Although simple to implement, this type of filters can be computationally consuming since the number of points required increases exponentially with the dimension of the SS, thus preventing its use in high-dimensional problems. In addition, the selection of the set of discrete states to run the algorithm is not clear, which is probably the major criticism one can argue to avoid this filters.

Sequential Monte-Carlo methods

Sequential Monte-Carlo (SMC) methods are a set of simulation-based methods which provide an appealing way to compute posterior distributions in problems that can be modeled as a dynamical SS [Dou01a, Aru02, Che03, Ris04]. These methods are applicable in very general settings (nonlinear/nonGaussian) and are computationally efficient due to its high degree of parallelization. These methods appear under several names: bootstrap filters, condensation, particle filters, Monte-Carlo filters, interacting particle approximations, survival of the fittest,... In Section 3.2 an introduction to Particle Filters (PFs) is provided in order to fix the ideas that will be used along the dissertation.

3.2 A Brief Introduction to Particle Filters

Although we can find Sequential Monte-Carlo basic ideas back in 1950s [Ham54], it will not be until the end of the 90's when they emerge as an appealing tool to deal with filtering problems. The main reason for this abandon was the low computational burden achievable at that time, so that when technology was mature enough to implement SMC based methods, the scientific community returned to investigate the topic. In the recent years SMC has played an important role in many research areas such as signal detection and demodulation, target tracking, Bayesian inference, audio processing, financial modeling, computer vision, robotics, control or biology [Spe02, Dju03, Pun03, Kar05, Hen08].

3.2.1 Monte-Carlo integration

The aim of PFs is to recursively estimate the posterior distribution $p(\mathbf{z}_{0:k}|\mathbf{x}_{1:k})$, the marginal filtering distribution $p(\mathbf{z}_k|\mathbf{x}_{1:k})$ and its associated expectations

$$I(g_k) = \mathbb{E}\left\{g_k(\mathbf{z}_{0:k})|\mathbf{x}_{1:k}\right\} = \int g_k(\mathbf{z}_{0:k})p(\mathbf{z}_{0:k}|\mathbf{x}_{1:k})d\mathbf{z}_{0:k} \ , \tag{3.31}$$

with $g_k(\cdot)$ a function of the state vector and the DSS model being as defined by equations (3.1) and (3.2) – or alternatively by (3.3) and (3.4).

PFs rely on the Monte-Carlo integration concept. Assume that we can simulate N_s independent identically distributed (*i.i.d.*) random samples from $p(\mathbf{z}_{0:k}|\mathbf{x}_{1:k})$, this set is denoted as $\{\mathbf{z}^i_{0:k}, i = 1, \ldots, N_s\}$. Then, the estimates of the distribution and its expectation

are

$$\begin{aligned} p_s(\mathbf{z}_{0:k}|\mathbf{x}_{1:k}) &= \frac{1}{N_s}\sum_{i=1}^{N_s}\delta(\mathbf{z}_{0:k}-\mathbf{z}_{0:k}^i) \\ I_s(g_k) &= \int g_k(\mathbf{z}_{0:k})p_s(\mathbf{z}_{0:k}|\mathbf{x}_{1:k})d\mathbf{z}_{0:k} = \frac{1}{N_s}\sum_{i=1}^{N_s} g_k(\mathbf{z}_{0:k}^i) \ , \end{aligned} \tag{3.32}$$

respectively. The estimate $I_s(g_k)$ is unbiased and

$$P\left\{\lim_{N_s\to\infty} I_s(g_k) = I(g_k)\right\} = 1 \ , \tag{3.33}$$

according to the law of large numbers [Cri02]. Moreover, if the variance of g_k is finite, i.e.,

$$\begin{aligned} \sigma_{g_k}^2 &= \int (g_k(\mathbf{z}_{0:k}) - I(g_k))^2 p(\mathbf{z}_{0:k}|\mathbf{x}_{1:k})d\mathbf{z}_{0:k} \\ &= \int g_k^2(\mathbf{z}_{0:k})p(\mathbf{z}_{0:k}|\mathbf{x}_{1:k})d\mathbf{z}_{0:k} - I^2(g_k) < \infty \ , \end{aligned} \tag{3.34}$$

then by the *central limit theorem* the estimation error converges in distribution, that is

$$\lim_{N_s\to\infty} \sqrt{N_s}(I_s(g_k) - I(g_k)) \sim \mathcal{N}\left(0, \sigma_{g_k}^2\right) \ . \tag{3.35}$$

Notice also that the rate of convergence is independent of the dimension of the integrant, at least in theory. However, it is well known that PFs suffer from the curse of dimensionality [Dau03]. The latter convergence results are the basis of the success of PFs, compared to other suboptimal algorithms that lack of theoretical foundations to ensure convergence to the true posterior.

At this point one can wonder why such a method is named Monte-Carlo *integration*. Actually, it is a historically nomenclature since this method was first used to numerically solve integrals [Pap01]. For example, if we want to integrate a function $f(\mathbf{z})$, we can split it into two components: one plays the role of the probability density function $\vartheta(\mathbf{z})$ while the other is the function $g(\mathbf{z})$. Thus, the integral is obtained as

$$I = \int f(\mathbf{z})d\mathbf{z} = \int g(\mathbf{z})\vartheta(\mathbf{z})d\mathbf{z} \approx \frac{1}{N_s}\sum_{i=1}^{N_s} g(\mathbf{z}^i) \ , \tag{3.36}$$

where N_s points are generated from $\vartheta(\mathbf{z})$.

3.2.2 Importance Sampling and Sequential Importance Sampling

Unfortunately, usually it is not possible to sample effectively from the posterior distribution as required in (3.32), since it can be a complicated/unknown distribution. A classical alternative is the *Importance Sampling* (IS) method [Gew89]. Imagine we can only generate samples from a density $\pi(\mathbf{z}_{0:k}|\mathbf{x}_{1:k})$ which is *similar* to $p(\mathbf{z}_{0:k}|\mathbf{x}_{1:k})$, which means that both functions have the same support (in equation (3.48) and the corresponding text, further details will be given on this issue). We refer to $\pi(\mathbf{z}_{0:k}|\mathbf{x}_{1:k})$ as the *importance* or *proposal* density function. We can write equation (3.31) as

$$\begin{aligned} I(g_k) &= \int g_k(\mathbf{z}_{0:k}) p(\mathbf{z}_{0:k}|\mathbf{x}_{1:k}) d\mathbf{z}_{0:k} \\ &= \int g_k(\mathbf{z}_{0:k}) \frac{p(\mathbf{z}_{0:k}|\mathbf{x}_{1:k})}{\pi(\mathbf{z}_{0:k}|\mathbf{x}_{1:k})} \pi(\mathbf{z}_{0:k}|\mathbf{x}_{1:k}) d\mathbf{z}_{0:k} \\ &= \int g_k(\mathbf{z}_{0:k}) \tilde{w}(\mathbf{z}_{0:k}) \pi(\mathbf{z}_{0:k}|\mathbf{x}_{1:k}) d\mathbf{z}_{0:k} \ , \end{aligned} \tag{3.37}$$

provided that $\tilde{w}(\mathbf{z}_{0:k}) = \frac{p(\mathbf{z}_{0:k}|\mathbf{x}_{1:k})}{\pi(\mathbf{z}_{0:k}|\mathbf{x}_{1:k})}$ is upper bounded. Applying the Monte-Carlo integration method, we draw N_s independent samples from the importance density function, $\{\mathbf{z}^i_{0:k}\}_{i=1}^{N_s}$, then an estimate of $I(g_k)$ is

$$I_s(g_k) = \frac{1}{N_s} \sum_{i=1}^{N_s} g_k(\mathbf{z}^i_{0:k}) w(\mathbf{z}^i_{0:k}) \ , \tag{3.38}$$

where

$$w(\mathbf{z}^i_{0:k}) = \frac{\tilde{w}(\mathbf{z}^i_{0:k})}{\sum_{j=1}^{N_s} \tilde{w}(\mathbf{z}^j_{0:k})} \tag{3.39}$$

are known as the normalized importance weights, and

$$\tilde{w}(\mathbf{z}^i_{0:k}) = \frac{p(\mathbf{z}_{0:k}|\mathbf{x}_{1:k})}{\pi(\mathbf{z}^i_{0:k}|\mathbf{x}_{1:k})} \tag{3.40}$$

are the unnormalized importance weights, which are normalized in (3.39) to obtain a proper probability density function.

The IS method has one main drawback which makes it inadequate for recursive filtering purposes: to estimate $p(\mathbf{z}_{0:k}|\mathbf{x}_{1:k})$ one needs to have all data $\mathbf{x}_{1:k}$ available. Then, when new data is available, one has to compute the importance weights over the entire state trajectory. Thus, the computational complexity increases with time. Instead, we

are interested in an algorithm that is able to include new data in the estimation process without recomputing weights from the scratch.

In an attempt to obtain a sequential algorithm relying on IS method, the *Sequential Importance Sampling* (SIS) algorithm is obtained. It is a Monte-Carlo method that forms the basis of most SMC-based filters, being the natural recursive version of IS to approach the optimal Bayesian solution. Recalling from the IS method, we have that the posterior distribution is characterized by the N_s generated points and its associated normalized weights, $\{\mathbf{z}_{0:k}^i, w_{0:k}^i\}_{i=1}^{N_s}$, as

$$\begin{aligned} p(\mathbf{z}_{0:k}|\mathbf{x}_{1:k}) &\approx \sum_{i=1}^{N_s} w_k^i \delta(\mathbf{z}_{0:k} - \mathbf{z}_{0:k}^i) \\ w_k^i &\propto \frac{p(\mathbf{z}_{0:k}^i|\mathbf{x}_{1:k})}{\pi(\mathbf{z}_{0:k}^i|\mathbf{x}_{1:k})} \ . \end{aligned} \tag{3.41}$$

Under the assumption that we have a discrete approximation of $p(\mathbf{z}_{0:k-1}|\mathbf{x}_{1:k-1})$, the aim of SIS is to obtain a set of particles that characterize the distribution at k when new measurements are received, $\mathbf{x}_k$. If we choose the importance function to factorize as

$$\begin{aligned} \pi(\mathbf{z}_{0:k}|\mathbf{x}_{1:k}) &= \pi(\mathbf{z}_k|\mathbf{z}_{0:k-1}, \mathbf{x}_{1:k})\pi(\mathbf{z}_{0:k-1}|\mathbf{x}_{1:k-1}) \\ &= \pi(\mathbf{z}_0)\prod_{t=1}^{k}\pi(\mathbf{z}_t|\mathbf{x}_{0:t-1}, \mathbf{x}_{1:t}) \ , \end{aligned} \tag{3.42}$$

then the generation of samples can be done by augmenting the existing samples

$$\left\{\mathbf{z}_{0:k-1}^i \sim \pi(\mathbf{z}_{0:k-1}|\mathbf{x}_{1:k-1})\right\}_{i=1}^{N_s} \tag{3.43}$$

with the new state

$$\left\{\mathbf{z}_k^i \sim \pi(\mathbf{z}_k|\mathbf{z}_{0:k-1}, \mathbf{x}_{1:k})\right\}_{i=1}^{N_s} \ . \tag{3.44}$$

The associated weights are computed from the following posterior recursion:

$$\begin{aligned} p(\mathbf{z}_{0:k}|\mathbf{x}_{1:k}) &= \frac{p(\mathbf{x}_k|\mathbf{z}_{0:k}, \mathbf{x}_{1:k-1})p(\mathbf{z}_{0:k}|\mathbf{x}_{1:k-1})}{p(\mathbf{x}_k|\mathbf{x}_{1:k-1})} \\ &= \frac{p(\mathbf{x}_k|\mathbf{z}_{0:k}, \mathbf{x}_{1:k-1})p(\mathbf{z}_k|\mathbf{z}_{0:k-1}, \mathbf{x}_{1:k-1})p(\mathbf{z}_{0:k-1}|\mathbf{x}_{1:k-1})}{p(\mathbf{x}_k|\mathbf{x}_{1:k-1})} \\ &= \frac{p(\mathbf{x}_k|\mathbf{z}_k)p(\mathbf{z}_k|\mathbf{z}_{k-1})}{p(\mathbf{x}_k|\mathbf{x}_{1:k-1})}p(\mathbf{z}_{0:k-1}|\mathbf{x}_{1:k-1}) \\ &\propto p(\mathbf{x}_k|\mathbf{z}_k)p(\mathbf{z}_k|\mathbf{z}_{k-1})p(\mathbf{z}_{0:k-1}|\mathbf{x}_{1:k-1}) \ , \end{aligned} \tag{3.45}$$

which only depends on the posterior at time $k-1$ and the likelihood and the prior at time k. Given that $p(\mathbf{z}_0) \triangleq p(\mathbf{z}_0|\mathbf{x}_0)$, where $\mathbf{x}_0$ is the set of no measurements, we can

assume that the required density at time $k-1$ is available in the sequential approach. Substitution of (3.42) and (3.45) in (3.41) yields to the weight update equation,

$$w_k^i \propto w_{k-1}^i \frac{p(\mathbf{x}_k|\mathbf{z}_k^i)p(\mathbf{z}_k^i|\mathbf{z}_{k-1}^i)}{\pi(\mathbf{z}_k^i|\mathbf{z}_{0:k-1}^i, \mathbf{x}_{1:k})} \ . \tag{3.46}$$

Now the recursion is closed and we are able to find an approximation of the filtering distribution given by

$$\hat{p}(\mathbf{z}_k|\mathbf{x}_{1:k}) = \sum_{i=1}^{N_s} w_k^i \delta(\mathbf{z}_k - \mathbf{z}_k^i) \ , \tag{3.47}$$

being $\delta(\cdot)$ the Kronecker's delta function. This approximation converges *a.s.* to the true posterior[6] as $N_s \to \infty$ under weak assumptions, according to the strong law of large numbers [Dou98, Cri02]. These assumptions hold if the support of the chosen importance density ($\breve{\pi}$) include the support of the filtering distribution ($\breve{p}$), i.e.,

$$\begin{aligned} \breve{\pi} &= \{\mathbf{z}_k \in \mathbb{R}^{n_z} |\ \pi(\mathbf{z}_k|\mathbf{x}_{1:k}) > 0\} \\ \breve{p} &= \{\mathbf{z}_k \in \mathbb{R}^{n_z} |\ p(\mathbf{z}_k|\mathbf{x}_{1:k}) > 0\} \\ &\quad \text{and} \qquad \breve{p} \subseteq \breve{\pi} \ . \end{aligned} \tag{3.48}$$

Thus, for the convergence results to hold we have to ensure that the importance function has the same support as the true posterior, meaning that the set closure of the set of arguments of these functions for which the value is not zero is the same.

From the new set of sample points, one can compute a number of statistics. As conceptually presented in (4.78) and (3.12), the MMSE and MAP estimators can be obtained as

$$\hat{\mathbf{z}}_k^{\text{MMSE}} = \sum_{i=1}^{N_s} w_k^i \mathbf{z}_k^i \tag{3.49}$$

$$\hat{\mathbf{z}}_k^{\text{MAP}} = \arg\max_{\mathbf{z}_k^i} \left\{ w_k^i \right\} \ , \tag{3.50}$$

respectively. The covariance (or uncertainty region) of an estimate $\hat{\mathbf{z}}_k$ can be calculated as

$$\mathbf{\Sigma}_{\hat{z}} = \sum_{i=1}^{N_s} w_k^i \left(\mathbf{z}_k^i - \hat{\mathbf{z}}_k\right) \left(\mathbf{z}_k^i - \hat{\mathbf{z}}_k\right)^T \ . \tag{3.51}$$

[6]Notice that *a.s.* convergence is equivalent to convergence *w.p.*1. Then, the convergence of the SIS estimate of the filtering distribution is expressed as

$$P\left\{\hat{p}(\mathbf{z}_k|\mathbf{x}_{1:k}) \to p(\mathbf{z}_k|\mathbf{x}_{1:k})\right\} = 1 \quad \text{as} \quad N_s \to \infty \ .$$

A pseudocode description of the SIS algorithm is shown in Algorithm 3.1. Notice that SIS is an algorithm that approximates the posterior by sequentially updating the measurement vector and propagating the importance weights. Basically, to sum up, it involves the approximation of the posterior by a set of N_s random samples taken from an *importance density function*, $\mathbf{z}_k^i \sim \pi(\mathbf{z}_k|\mathbf{z}_{0:k-1}^i, \mathbf{x}_{1:k})$, with associated importance weights w_k^i. The choice of $\pi(\cdot)$ is a critical issue in the design of any PF, which still remains as an open topic for statisticians [Dou00] and is usually an application-dependent issue. For a set of generated particles, $\{\mathbf{z}_k^i,\ w_k^i\}_{i=1}^{N_s}$, the approximation of the filtering distribution as given by PFs is obtained via equation (3.47).

Algorithm 3.1 Sequential Importance Sampling (SIS) algorithm

Require: $\{\mathbf{z}_{k-1}^i,\ w_{k-1}^i\}_{i=1}^{N_s}$ and $\mathbf{x}_k$
Ensure: $\{\mathbf{z}_k^i,\ w_k^i\}_{i=1}^{N_s}$
1: **for** $i = 1$ to N_s **do**
2: Generate $\mathbf{z}_k^i \sim \pi(\mathbf{z}_k|\mathbf{z}_{k-1}^i, \mathbf{x}_{1:k})$
3: Calculate $\tilde{w}_k^i = w_{k-1}^i \frac{p(\mathbf{x}_k|\mathbf{z}_k^i)p(\mathbf{z}_k^i|\mathbf{z}_{k-1}^i)}{\pi(\mathbf{z}_k^i|\mathbf{z}_{0:k-1}^i, \mathbf{x}_{1:k})}$
4: **end for**
5: **for** $i = 1$ to N_s **do**
6: Normalize weights: $w_k^i = \frac{\tilde{w}_k^i}{\sum_{j=1}^{N_s} \tilde{w}_k^j}$
7: **end for**

3.2.3 Resampling

Everything has its payback, and PFs are not the exception. The main drawback of the SIS algorithm is that it suffers from the so-called *degeneracy phenomenon*, which states that the variance of importance weights can only increase over time [Dou00]. In other words, after a certain number of sequential steps, one finds that the value of one of the normalized weights tends to 1 while the rest tend to 0. The problem then is to keep particle trajectories with *significant* weights and remove those which hardly contribute to the estimation of the filtering distribution. The solution was proposed in [Rub88] and is known as *resampling*: discarding samples with low importance weights and keep/multiply those with high importance weights. Resampling was proposed for SIS in a number of works [Gor93, Liu95, Ber97].

A measure of the degeneracy is the effective sample size N_{eff}, introduced in [Kon94], which is estimated as

$$\hat{N}_{eff} = \frac{1}{\sum_{i=1}^{N_s} \left(w_k^i\right)^2} \tag{3.52}$$

where $1 \leq \hat{N}_{eff} \leq N_s$ and values close to the lower bound indicate high degeneracy. The common approach is to specify a threshold such that, when the effective sample size is below, indicates the algorithm to apply resampling (see Algorithm 3.5). Although highly dependent on the chosen threshold, this approach is the most used in the literature. In [Ber99] a suggested threshold is $N_{th} = \frac{2}{3}N_s$.

Algorithm 3.2 Generic Particle Filtering with Resampling

Require: $\left\{\mathbf{z}_{k-1}^i,\ w_{k-1}^i\right\}_{i=1}^{N_s}$ and $\mathbf{x}_k$
Ensure: $\left\{\mathbf{z}_k^i,\ w_k^i\right\}_{i=1}^{N_s}$
1: $\left[\left\{\mathbf{z}_k^i,\ w_k^i\right\}_{i=1}^{N_s}\right] = \mathrm{SIS}(\left\{\mathbf{z}_{k-1}^i,\ w_{k-1}^i\right\}_{i=1}^{N_s},\ \mathbf{x}_k)$
2: Calculate $\hat{N}_{eff}$
3: **if** $\hat{N}_{eff} < N_{th}$ **then**
4: Resample Particles: $\left[\left\{\mathbf{z}_k^i,\ w_k^i\right\}_{i=1}^{N_s}\right] = \mathrm{Resample}(\left\{\mathbf{z}_k^i,\ w_k^i\right\}_{i=1}^{N_s})$
5: **end if**

The process of resampling particles can be implemented in several ways. Common schemes include multinomial resampling [Gor93], residual resampling [Liu98] and stratified/systematic resampling [Kit96, Cri01]. It is out of the scope of the dissertation the study of novel resampling strategies, in the sequel a multinomial resampling is considered which is one of the easiest to implement.

Although it solves the degeneracy phenomenon, resampling can result in a *sample impoverishment*, that is particles with high weights are selected many times. Notice that this loss of diversity is severe when process noise is small [Gor93, Hig95]. Thus, convergence results of the algorithm should be re-established [Ber97]. Another undesired aspect of resampling is that it constitutes the bottle neck in any parallel implementation of PFs [Bol05], since all particles must be combined in this process.

Nevertheless, resampling is a key step in the design of a PF since degeneracy jeopardizes posterior estimates in a way that cannot be tolerated. Many work has been directed in the design of efficient resampling strategies and architectures [MÓ7a, Bol04].

3.2.4 Selection of the importance density

One of the key points of a PF algorithm is the choice of a *good* importance density function, $\pi(\mathbf{z}_k|\mathbf{z}_{0:k-1}^i, \mathbf{x}_{1:k})$. Actually, a bad choice can lead the algorithm to a poor characterization in (3.47) and, thus, to a bad performance. Since good or bad can be rather fuzzy concepts [Nie87, First Treatise], we proceed to discuss some alternatives that one has in the design of such importance distribution.

The optimal choice

Since the aim of a PF is to characterize the filtering distribution, it is quite intuitive to say that this distribution is the *best* choice for particle generation. Indeed, the optimal distribution is the target distribution that we wish to estimate:

$$\pi(\mathbf{z}_k|\mathbf{z}^i_{0:k-1}, \mathbf{x}_{1:k}) = p(\mathbf{z}_k|\mathbf{z}^i_{0:k-1}, \mathbf{x}_{1:k}) \ , \tag{3.53}$$

which is optimal in the sense that it minimizes the variance of importance weights conditional upon the trajectory and the observations [Dou00]. The use of such an optimal importance density reduces the degeneracy effect discussed previously. In this case, the calculation of weights reduces to:

$$w^i_k \propto w^i_{k-1} p(\mathbf{x}_k|\mathbf{z}^i_{k-1}) \ , \tag{3.54}$$

which does not depend on the current particle value $\mathbf{z}^i_k$, facilitating parallelization of the PF [Bol04].

Thus, in order to use the optimal importance density, one has to (a) be able to draw samples from $p(\mathbf{z}_k|\mathbf{z}^i_{0:k-1}, \mathbf{x}_{1:k})$ and to (b) evaluate

$$p(\mathbf{x}_k|\mathbf{z}_{k-1}) = \int p(\mathbf{x}_k|\mathbf{z}_k) p(\mathbf{z}_k|\mathbf{z}_{k-1}) d\mathbf{z}_k \ . \tag{3.55}$$

Few special cases can be found that allow the generation/evaluation from these distributions. One case is when the states $\mathbf{z}_k$ are finite, as in [Dou01b]. Another case is when the DSS model is Gaussian with linear measurements [Dou00, Ris04]. Unfortunately, these two requirements may not hold in general and one has to resort to suboptimal choices.

Suboptimal choices

Since the only condition imposed on $\pi(\mathbf{z}_k|\mathbf{z}^i_{0:k-1}, \mathbf{x}_{1:k})$ is to fulfill (3.42), the amount of possible suboptimal importance densities seems huge[7]. Indeed, a general methodology for selecting an importance density is still missing, being several alternatives proposed in the literature. Actually, in most of the cases this choice highly depends on the application itself and has to be carefully designed.

The simplest approach, and the most popular, is to consider the transitional prior as the importance function. In this case, weights are proportional to the likelihood function:

$$\begin{aligned} \pi(\mathbf{z}_k|\mathbf{z}^i_{0:k-1}, \mathbf{x}_{1:k}) &= p(\mathbf{z}_k|\mathbf{z}^i_{k-1}) \\ w^i_k &\propto w^i_{k-1} p(\mathbf{x}_k|\mathbf{z}^i_k) \ . \end{aligned} \tag{3.56}$$

[7] Keeping in mind that the importance density has to share the same support as the target distribution, in order to claim convergence [Cri02].

The popularity of the transitional prior choice is due to its simple implementation and the lack of computationally intensive calculations. Note that in the Gaussian case, generation in (3.56) reduces to sample from a Gaussian distribution. Nevertheless, this choice was shown to be inefficient as it requires a large number of samples to effectively characterize the posterior distribution [Ris04]. The main reason is that, since measurements are not taken into consideration when generating particles, the algorithm is likely to exhibit a high degeneracy.

More sophisticated, though also suboptimal, alternatives aim at approximating the optimal importance density in (3.53). Although they require a higher computational burden, their performance is typically better than the one provided by the transitional prior. Some of the strategies reported in the literature include local model linearization [Dou00], Gaussian approximations [Kot03a] or the use of the unscented transform [Mer00]. In Section 3.4 of this dissertation, we consider another importance density function. The method was originally proposed in [Cev07] for an acoustic multitarget tracking problem. Basically it is based on a Gaussian approximation of the optimal distribution.

3.2.5 A plethora of possibilities

There are many PF algorithms in the literature, mostly based in the presented SIS concept. This section presents some of the most common PFs, which basically differ in the choice of the importance density and the resampling step. However, notice that many other alternatives exist and, eventually, new proposals may appear in the literature.

SIR or Bootstrap Filter

The Bootstrap Filter (BF) was proposed in [Gor93], though it can also be found in the literature under the name of *Sampling Importance Resampling* algorithm (SIR). The main characteristic of this approach is that it assumes that the importance density is the transitional prior and that resampling is performed at every recursive step. Under these assumptions, the i-th particle is generated and weighted as

$$\begin{aligned} \mathbf{z}_k^i &\sim \pi(\mathbf{z}_k|\mathbf{z}_{0:k-1}^i, \mathbf{x}_{1:k}) = p(\mathbf{z}_k|\mathbf{z}_{k-1}^i) \\ w_k^i &\propto p(\mathbf{x}_k|\mathbf{z}_k^i) \ , \end{aligned} \tag{3.57}$$

where w_k^i does not depend on the previous weight, since $\left\{w_{k-1}^i = 1/N_s\right\}_{i=1}^{N_s}$.

Similarly as argued in Section 3.2.4 when discussing the use of the transitional prior in the SIS algorithm, the BF is sensitive to outliers since the SS is explored without any knowledge of the observations by the importance density. Also, it results in a rapid

loss of diversity as resampling is performed at every instant. Nonetheless, a considerable advantage is that the importance density is easily sampled from the prior and importance weights can be computed straightforwardly from the likelihood function.

Algorithm 3.3 Sampling Importance Resampling (SIR) algorithm

Require: $\left\{\mathbf{z}_{k-1}^i\right\}_{i=1}^{N_s}$ and $\mathbf{x}_k$
Ensure: $\{\mathbf{z}_k^i\}_{i=1}^{N_s}$
1: **for** $i = 1$ to N_s **do**
2: Generate $\mathbf{z}_k^i \sim p(\mathbf{z}_k|\mathbf{z}_{k-1}^i)$
3: Calculate $\tilde{w}_k^i = p(\mathbf{x}_k|\mathbf{z}_k^i)$
4: **end for**
5: **for** $i = 1$ to N_s **do**
6: Normalize: $w_k^i = \frac{\tilde{w}_k^i}{\sum_{j=1}^{N_s} \tilde{w}_k^j}$
7: **end for**
8: Resample Particles: $\left[\{\mathbf{z}_k^i\}_{i=1}^{N_s}, -\right] = \text{Resample}(\{\mathbf{z}_k^i,\ w_k^i\}_{i=1}^{N_s})$

Auxiliary SIR Filter

The Auxiliary SIR (ASIR) filter is an alternative to the SIR filter which aims at improving its efficiency by reducing the variance of the importance weights. It was proposed in [Pit99] under the name Auxiliary Particle Filter (APF). The basic idea is to, at the $k-1$ iteration of the algorithm, use next measurements $\mathbf{x}_k$. Hence, the algorithm can increase the influence of particles with higher predictive likelihood by resampling them before propagating the particle cloud. An interested reader can refer to [Pit01, God01, Ris04].

Regularized Particle Filter

As discussed in Section 3.2.3, the resampling step reduces degeneracy but may lead to a loss of diversity among particles. This effect can cause the particles to collapse to a single point. The Regularized Particle Filter (RPF) proposed in [Mus00] is an algorithm designed to overcome this effect. The difference with the SIR algorithm is that resampling is performed by sampling from a Kernel-based continuous distribution, in contrast to SIR where the sampling is from the discrete approximation in (3.47).

Local Linearization Particle Filter

One can rely on other suboptimal algorithms to generate an importance density close to the optimal. In that vein, the work in [Dou00] proposed to implement an EKF for each particle such that the resulting Gaussian posterior characterization is used as the particle generating function. Similarly, a UKF algorithm can keep track of each importance density function as reported in [Mer00], which was seen to provide better results than the EKF solution. Not surprisingly, the performance of a Local Linearization Particle Filter (LLPF) is better than the one provided by solely using a SIR filter, since the particle generation method of the latter is very poor. In addition, the increase in the computational burden of LLPF is typically justified due to the reduction in the required number of samples.

Gaussian Particle Filter

In contrast to the SIR filter (and its modifications), the Gaussian Particle Filter (GPF) [Kot01] approximates the filtering and predictive densities as Gaussians. Hence it suffices to propagate recursively in time the mean and covariance of the densities to update the new filtering distribution estimate. GPFs are a class of Gaussian filters where Monte-Carlo methods are used to compute the mean and the covariance. The propagation of this two parameters simplify the parallelization of such methods when implemented (recall that SIR-like filters require the propagation of the N_s particles) [Kot03a, Kot03b]. Although the Gaussian assumption may seem to tight, the appealing implementation properties of GPF made this algorithm an interesting alternative.

Multiple Model Particle Filter

The use of Multiple Model Particle Filter (MMPF) [McG00, Mus00] arises in order to deal with dynamic systems having more than one mode of operation. Also, MMPFs are of interest when the DSS model consists of both continuous and discrete parts as discussed in [Ris04]. The us of this filters can be found in many applications including target tracking, multisensor data fusion [Yan04] and switching observation models [Car07].

Cost Reference Particle Filter

One of the main criticisms to PFs is the requirement of a somewhat accurate knowledge of the dynamics of the system and the underlying distributions of the DSS model. Indeed, an analytical result of the robustness [Hub81, Mar06] of such methods to model inaccuracies is still missing, though some studies were carried in [Clo09a].

To circumvent these limitations, a new class of PF was proposed in [MÓ4] which does not require the distributions of the DSS model to be a priori known. This class of PFs are referred to as Cost Reference Particle Filters (CRPFs). In contrast to standard PF approaches, the CRPF evaluates the quality of each particle trajectory using a cost function that does not necessarily use statistical information. The claim is that CRPFs are more robust and flexible than standard PFs. Actually, CRPFs were seen to be a generalization of standard PFs. Thus, providing an even more powerful approach to Bayesian filtering. The capabilities of CRPFs were tested in target tracking problems [MÓ7b, Li08] showing important improvements with respect to classical particle filtering algorithms. Marginalization of linear states was proposed in [Lu08] using a Recursive Least Squares (RLS) algorithm, in the vein of Rao-Blackwellized Particle Filters [Sch05] which are discussed in Section 3.2.6.

3.2.6 Variance Reduction by Rao-Blackwellization

The Rao-Blackwellization procedure is used in filtering as a methodology to reduce the variance of estimates. When applied to particle filtering, the resulting filter is referred to as Rao-Blackwellized Particle Filter (RBPF) [Che00, Dou01a] or Marginalized Particle Filter (MPF) [Kar05, Sch05], equivalently. In short, Rao-Blackwellization consists in taking advantage of linear/Gaussian substructures of the DSS model, which are optimally dealt by a KF. Then, a RBPF is a combination of a PF - that tackles nonlinear states, $\mathbf{z}_k^{\mathsf{nl}}$ - and a KF - to deal with the linear states, $\mathbf{z}_k^{\mathsf{l}}$. The goodness of RBPF is that it alleviates the computational demand of PFs for high dimensional state-spaces, where a large number of particles are required.

In general, the RBPF is used when the general DSS model in (3.1) and (3.2) can be reorganized as

$$\begin{aligned} \mathbf{z}_k^{\mathsf{l}} &= \mathbf{f}_{k-1}^{\mathsf{l}}(\mathbf{z}_{k-1}^{\mathsf{nl}}) + \mathbf{F}_{k-1}^{\mathsf{l}}(\mathbf{z}_{k-1}^{\mathsf{nl}})\mathbf{z}_{k-1}^{\mathsf{l}} + \mathbf{z}_{k-1}^{\mathsf{l}} + \boldsymbol{\nu}_k^{\mathsf{l}} \\ \mathbf{z}_k^{\mathsf{nl}} &= \mathbf{f}_{k-1}^{\mathsf{nl}}(\mathbf{z}_{k-1}^{\mathsf{nl}}) + \mathbf{F}_{k-1}^{\mathsf{nl}}(\mathbf{z}_{k-1}^{\mathsf{nl}})\mathbf{z}_{k-1}^{\mathsf{l}} + \boldsymbol{\nu}_k^{\mathsf{nl}} \\ \mathbf{x}_k &= \mathbf{h}_k^{\mathsf{nl}}(\mathbf{z}_k^{\mathsf{nl}}) + \mathbf{H}_k^{\mathsf{l}}(\mathbf{z}_k^{\mathsf{nl}})\mathbf{z}_k^{\mathsf{l}} + \mathbf{n}_k \end{aligned} \tag{3.58}$$

where the state-space is clearly partitioned into two sub-spaces, corresponding to its linear and non-linear parts,

$$\mathbf{z}_k = \begin{bmatrix} \mathbf{z}_k^{\mathsf{l}} \\ \mathbf{z}_k^{\mathsf{nl}} \end{bmatrix}, \tag{3.59}$$

being linear states Gaussian distributed, whereas nonlinear states can be drawn from any distribution a priori known.

The model in (3.58) assumes that state and measurement noises are white and Gaussian distributed, i.e.,

$$\boldsymbol{\nu}_k = \begin{bmatrix} \boldsymbol{\nu}_k^{\mathsf{l}} \\ \boldsymbol{\nu}_k^{\mathsf{nl}} \end{bmatrix} \sim \mathcal{N}\left(\mathbf{0}, \boldsymbol{\Sigma}_{z,k}\right) \quad , \quad \boldsymbol{\Sigma}_{z,k} = \begin{pmatrix} \boldsymbol{\Sigma}_{z^{\mathsf{l}},k} & \boldsymbol{\Sigma}_{z^{\mathsf{l,nl}},k} \\ \boldsymbol{\Sigma}_{z^{\mathsf{l,nl}},k}^T & \boldsymbol{\Sigma}_{z^{\mathsf{nl}},k} \end{pmatrix} \tag{3.60}$$

and

$$\mathbf{n}_k \sim \mathcal{N}\left(\mathbf{0}, \boldsymbol{\Sigma}_{n,k}\right) \ . \tag{3.61}$$

Under model (3.58), the recursive estimation of the filtering distribution $p(\mathbf{z}_k|\mathbf{x}_{1:k})$ can be done by a PF. Nevertheless, one can take advantage of the conditional linear substructure that is not present in general DSS models as in (3.1) and (3.2). By the chain rule of probability, linear states can be analytically marginalized out from $p(\mathbf{z}_k|\mathbf{x}_{1:k})$:

$$p(\mathbf{z}_k^{\mathsf{l}}, \mathbf{z}_{0:k}^{\mathsf{nl}}|\mathbf{x}_{1:k}) = p(\mathbf{z}_k^{\mathsf{l}}|\mathbf{z}_{0:k}^{\mathsf{nl}}, \mathbf{x}_{1:k}) p(\mathbf{z}_{0:k}^{\mathsf{nl}}|\mathbf{x}_{1:k}) \tag{3.62}$$

and, taking into consideration that $\mathbf{z}_k^{\mathsf{l}}$ generates a linear Gaussian state-space, $p(\mathbf{z}_k^{\mathsf{l}}|\mathbf{z}_k^{\mathsf{nl}}, \mathbf{x}_{1:k})$ can be updated analytically via a KF conditional on $\mathbf{z}_k^{\mathsf{nl}}$ and only the nonlinear part of $\mathbf{z}_k$ needs to be estimated via a PF. Thus, a PF is run to characterize $p(\mathbf{z}_{0:k}^{\mathsf{nl}}|\mathbf{x}_{1:k})$ and, for the i-th particle, a KF is executed to obtain $p(\mathbf{z}_k^{\mathsf{l}}|\mathbf{z}_{0:k}^{\mathsf{nl},i}, \mathbf{x}_{1:k})$. Nevertheless, as described in (3.58), both linear and nonlinear states are interdependent. The latter causes that the RBPF follows a certain sequence of operations[8], which for the i-th particle are:

KF prediction. The distribution of interest in this step is:

$$p(\mathbf{z}_k^{\mathsf{l}}|\mathbf{z}_{0:k-1}^{\mathsf{nl},i}, \mathbf{x}_{1:k-1}) = \mathcal{N}\left(\mathbf{z}_k^{\mathsf{l}};\ \hat{\mathbf{z}}_{k|k-1}^{\mathsf{l},i}, \mathbf{P}_{k|k-1}^{i}\right) \tag{3.63}$$

where the mean and covariance are obtained similarly as in (3.15).

Run PF. For the i-th particle, the PF is in charge of generating this particle

$$\mathbf{z}_k^{\mathsf{nl},i} \sim \pi(\mathbf{z}_k^{\mathsf{nl}}|\mathbf{z}_{0:k-1}^{\mathsf{nl},i}, \mathbf{x}_{1:k}) \tag{3.64}$$

and computing its importance weight:

$$w_k^i \propto w_{k-1}^i \frac{p(\mathbf{x}_k|\mathbf{z}_{0:k}^{\mathsf{nl},i}, \mathbf{x}_{1:k-1}) p(\mathbf{z}_k^{\mathsf{nl},i}|\mathbf{z}_{k-1}^{\mathsf{nl},i})}{\pi(\mathbf{z}_k^{\mathsf{nl},i}|\mathbf{z}_{0:k-1}^{\mathsf{nl},i}, \mathbf{x}_{1:k})} \ . \tag{3.65}$$

[8]The reader is referred to [Sch05] for a complete study of the possible configurations of the RBPF and the involved expressions.

Notice that, due to the dependency between linear and nonlinear states, the likelihood distribution [Che00]

$$p(\mathbf{x}_k|\mathbf{z}_{0:k}^{\mathsf{nl},i}, \mathbf{x}_{1:k-1}) = \mathcal{N}\left(\mathbf{h}_k^{\mathsf{nl}}(\mathbf{z}_k^{\mathsf{nl},i}) + \mathbf{H}_k^{\mathsf{l}}(\mathbf{z}_k^{\mathsf{nl},i})\hat{\mathbf{z}}_{k|k-1}^{\mathsf{l},i}, \right.$$
$$\left. \boldsymbol{\Sigma}_{n,k} + \mathbf{H}_k^{\mathsf{l}}(\mathbf{z}_k^{\mathsf{nl},i})\mathbf{P}_{k|k-1}^{i}\left(\mathbf{H}_k^{\mathsf{l}}(\mathbf{z}_k^{\mathsf{nl},i})\right)^T\right) \quad (3.66)$$

and the prior distribution

$$p(\mathbf{z}_k^{\mathsf{nl},i}|\mathbf{z}_{k-1}^{\mathsf{nl},i}) = \mathcal{N}\left(\mathbf{f}_{k-1}^{\mathsf{nl}}(\mathbf{z}_{k-1}^{\mathsf{nl},i}) + \mathbf{F}_{k-1}^{\mathsf{nl}}(\mathbf{z}_{k-1}^{\mathsf{nl},i})\hat{\mathbf{z}}_{k-1|k-1}^{\mathsf{l},i}, \right.$$
$$\left. \boldsymbol{\Sigma}_{z^{\mathsf{nl}},k} + \mathbf{F}_{k-1}^{\mathsf{nl}}(\mathbf{z}_{k-1}^{\mathsf{nl},i})\mathbf{P}_{k|k}^{i}\left(\mathbf{F}_{k-1}^{\mathsf{nl}}(\mathbf{z}_{k-1}^{\mathsf{nl},i})\right)^T\right) , \quad (3.67)$$

in (3.65) are analytically obtained, as derived in [Sch03]. Thus, it is remarkable to point out that the RBPF is an interleaved process in which information from linear and nonlinear states is jointly used [Ghi05].

KF update. The updated filtering distribution of linear states is

$$p(\mathbf{z}_k^{\mathsf{l}}|\mathbf{z}_{0:k}^{\mathsf{nl},i}, \mathbf{x}_{1:k}) = \mathcal{N}\left(\mathbf{z}_k^{\mathsf{l}};\ \hat{\mathbf{z}}_{k|k}^{\mathsf{l},i}, \mathbf{P}_{k|k}^{i}\right) \quad (3.68)$$

and the parameters are obtained again as in (3.15), conditioned upon nonlinear states.

After the three recursive steps of the RBPF are done for each particle, $i = \{1, \ldots, N_s\}$, a characterization of the filtering distribution is available, the MMSE estimator of $\mathbf{z}_k^{\mathsf{nl}}$ is as stated in (3.49) and the MMSE estimator of the linear states can be expressed as

$$\hat{\mathbf{z}}_k^{\mathsf{l}} = \sum_{i=1}^{N_s} w_k^i \hat{\mathbf{z}}_{k|k}^{\mathsf{l},i} \ . \quad (3.69)$$

Intuitively, there are two reason to explain the improved performance of a RBPF with respect to a standard PF for the same number of particles:

- The dimension of $p(\mathbf{z}_k^{\mathsf{nl}}|\mathbf{x}_{1:k})$ is smaller than the dimension of $p(\mathbf{z}_k|\mathbf{x}_{1:k})$, meaning that the same number of particles are swarmed in a lower dimensional state-space in the RBPF case.
- An optimal algorithm is used to deal with linear/Gaussian states, the KF. As discussed in section 3.1.2, the KF cannot be outperformed in such scenarios.

The concept used in the RBPF is a special case of a more general result. In [Rao45] and [Bla47] it was shown that the performance of an estimator can be improved by using information about conditional probabilities. The Rao-Blackwell theorem [Leh83] states the general idea,

Theorem 3.1 (Rao-Blackwell theorem)**.** *Let $\hat{\theta} = g(\mathbf{x})$ represent any unbiased estimator for θ, and $T(\mathbf{x})$ be a sufficient statistic for θ under $p(\mathbf{x}, \theta)$. Then the conditional expectation $\mathbb{E}\{g(\mathbf{x})|T(\mathbf{x})\}$ is independent of θ, and it is the uniformly minimum variance unbiased estimator.*

Proof. See [Pap01]. □

An important corollary of the Rao-Blackwell theorem is the basis for the widespread use of RBPFs:

Corollary 3.1. *Let $\hat{\theta}$ be an unbiased estimator and let $\hat{\theta}^{RB}$ be the Rao-Blackwell estimator, then*

$$\mathbb{E}\left\{\left(\theta-\hat{\theta}\right)\left(\theta-\hat{\theta}\right)^{*}\right\} \geq \mathbb{E}\left\{\left(\theta-\hat{\theta}^{RB}\right)\left(\theta-\hat{\theta}^{RB}\right)^{*}\right\} \ . \tag{3.70}$$

The result claimed in Corollary 3.1 is important since it proves that the use of a Rao-Blackwellized estimator effectively reduces the variance of the estimation error.

3.3 System Model

This section presents the DSS model considered for the multipath mitigation problem that is discussed in this chapter. First the model for the set of measurements is exposed and a SS representation is then proposed. Many alternatives can be envisaged for the latter, being an open issue. These modifications can be aimed at better describing the reality of the evolution of delays [Len08] and, thus, improving the overall performance of the algorithm. However, the scope of the dissertation is to present a multipath mitigation algorithm and the presented SS model suffices to prove the concept.

3.3.1 Measurements

Let us consider a detailed signal model that accounts for both the LOSS and the multipath signals. The received complex baseband DS–SS signal of a given satellite affected by $M-1$

multipath signals is modeled as

$$x(t) = \sum_{m=0}^{M-1} \alpha_m(t) q\left(t - \tau_m(t)\right) e^{j\phi_m(t)} + n(t) \ , \tag{3.71}$$

where $\alpha_m(t)$, $\tau_m(t)$ and $\phi_m(t)$ stand for the amplitude, delay and phase of the m–th received signal, respectively. These parameters are time–varying processes and indeed they are explicitly expressed with their time dependence. The term $n(t)$ is a zero–mean Additive Gaussian Noise (AGN) process with variance σ_n^2. Notice that the subscript $m = 0$ stands for the LOSS parameters in the model.

The DS–SS signal of the tracked satellite is denoted by $q(t) = q_I(t) + jq_Q(t)$, being composed of the sequence of data symbols and the PRN sequence (cf. Section 2.1). Since both the PRN sequence and the chip-shaping pulse are known at the receiver, it is reasonable to consider $q(t)$ known up to 180^o phase variations due to data–bit changes. However, $d(l)$ is not likely to vary within the observation time, which is typically much shorter than the bit period [FP06].

The model in (3.71) is obtained from equation (2.5), considering the contribution of only one satellite. The contribution of the rest of satellites can be neglected considering that GNSS systems use pseudorandom noise (PRN) codes with a high processing gain ($\sim$ 43 dB in case of GPS L1 C/A signal). Thus, the influence of other satellites can be considered as Gaussian noise and included in the thermal noise term since those signals are below the noise floor [Vit95]. We consider the tracking of each satellite separately by an independent channel at the receiver, in a parallel implementation approach.

Notice that Doppler-shifts are also taken into consideration in the model, being included in the phase parameter:

$$\phi_m(t) = 2\pi f_{d_m}(t)t + \phi_{m,0} \ , \tag{3.72}$$

where $f_{d_m}(t)$ and $\phi_{m,0}$ are the time–varying Doppler-shift and carrier phase of the m-th signal, respectively. Refer to Section 2.1 for further details on (3.72). The approach followed here reduces the number of unknown parameters, since phases and Doppler deviations are jointly estimated, as will be seen later this chapter.

Defining

$$\begin{aligned}
\boldsymbol{\alpha}(t) &= [\alpha_0(t), \ldots, \alpha_{M-1}(t)]^T \in \mathbb{R}^{M\times 1} \\
\boldsymbol{\phi}(t) &= [\phi_0(t), \ldots, \phi_{M-1}(t)]^T \in \mathbb{R}^{M\times 1} \\
\boldsymbol{\tau}(t) &= [\tau_0(t), \ldots, \tau_{M-1}(t)]^T \in \mathbb{R}^{M\times 1} \\
\mathbf{q}(t;\boldsymbol{\tau}(t)) &= [q(t-\tau_0(t)), \ldots, q(t-\tau_{M-1}(t))]^T \\
&= [q_0(t;\tau_0(t)), \ldots, q_{M-1}(t;\tau_{M-1}(t))]^T \in \mathbb{C}^{M\times 1} \\
\boldsymbol{\Phi}(t) &= \mathrm{diag}\{e^{j\boldsymbol{\phi}(t)}\} \in \mathbb{C}^{M\times M},
\end{aligned} \tag{3.73}$$

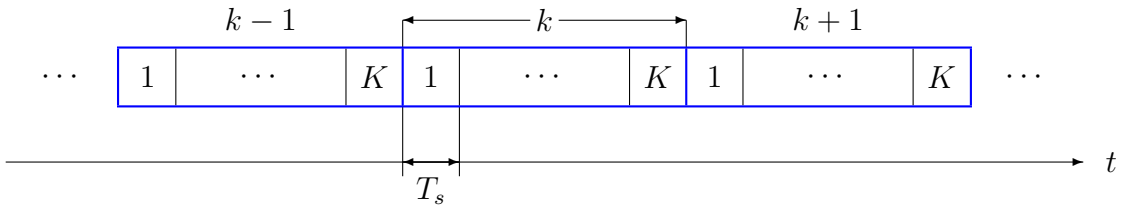

Figure 3.2: Data is processed in blocks of non-overlapped K samples, recorded at a suitable sampling rate $f_s = 1/T_s$. Index k corresponds to the processing of the corresponding set of K samples.

we can obtain the compact form of (3.71) as

$$x(t) = \mathbf{q}^T(t; \boldsymbol{\tau}(t))\boldsymbol{\Phi}(t)\boldsymbol{\alpha}(t) + n(t). \tag{3.74}$$

Considering the Software Defined Radio (SDR) philosophy [Mit00, Tsu00, Ree02, Ako03, FP06, Bor07], a GNSS receiver records K snapshots with a sampling period of T_s (see Figure 3.2). Thus, if we use $k \in \mathbb{N}$ to denote the k-th record of K samples, the model in (3.74) is extended to

$$\mathbf{x}_k = \mathbf{Q}_k^T(\boldsymbol{\tau}_k)\mathbf{a}_k + \mathbf{n}_k \tag{3.75}$$

where $\mathbf{x}_k \triangleq x(kKT_s)$, $\boldsymbol{\tau}_k \triangleq \boldsymbol{\tau}(kKT_s)$, $\boldsymbol{\Phi}_k \triangleq \boldsymbol{\Phi}(kKT_s)$, $\boldsymbol{\alpha}_k \triangleq \boldsymbol{\alpha}(kKT_s)$, $\mathbf{a}_k \triangleq \boldsymbol{\Phi}_k\boldsymbol{\alpha}_k$ and

$$\mathbf{Q}_k(\boldsymbol{\tau}_k) = [\mathbf{q}((k-1)KT_s + T_s; \boldsymbol{\tau}_k), \ldots, \mathbf{q}(kKT_s; \boldsymbol{\tau}_k)] \tag{3.76}$$

is known as the basis-function matrix and contains K samples from the delayed narrowband envelopes of each M signals, i.e., $\mathbf{Q}_k(\boldsymbol{\tau}_k) \in \mathbb{C}^{M\times K}$. The vectors containing the composite signal and the zero–mean AGN are expressed as $\mathbf{x}_k, \mathbf{n}_k \in \mathbb{C}^{K\times 1}$, respectively. The covariance matrix of the noise is left arbitrary, $\boldsymbol{\Sigma}_{n,k}$.

Notice that the unknown parameters ($\boldsymbol{\alpha}_k$, $\boldsymbol{\tau}_k$ and $\boldsymbol{\phi}_k \triangleq \boldsymbol{\phi}(kKT_s)$) are time-varying processes, as explicitly expressed by subscript k. However, we assume that they are piecewise constant during the observation interval of K samples. In addition, we take into account that amplitudes and phases can be obtained as the modulus and phase of complex amplitudes $\mathbf{a}_k$, respectively. Then, the considered real state vector is

$$\mathbf{z}_k \triangleq \begin{bmatrix} \Re\{\mathbf{a}_k\} \\ \Im\{\mathbf{a}_k\} \\ \boldsymbol{\tau}_k \end{bmatrix} \in \mathbb{R}^{3M\times 1} \ . \tag{3.77}$$

Accordingly, measurement equation in (3.75) is parameterized by the elements of $\mathbf{z}_k$

$$\mathbf{x}_k = \mathbf{Q}_k^T(\boldsymbol{\tau}_k)\mathbf{T}\ \mathbf{a}_{s,k} + \mathbf{n}_k \ , \tag{3.78}$$

where

$$\mathbf{a}_{s,k} = \begin{bmatrix} \Re\{\mathbf{a}_k\} \\ \Im\{\mathbf{a}_k\} \end{bmatrix} \in \mathbb{R}^{2M\times 1} \tag{3.79}$$

is the vector that stacks real and imaginary parts of complex amplitudes and we define

$$\mathbf{T} = \left(\mathbf{I}_M \mid j\mathbf{I}_M \right) \in \mathbb{C}^{M\times 2M}, \tag{3.80}$$

being $\mathbf{I}_M$ the M-dimensional identity matrix.

3.3.2 State-Space evolution

Following [Ilt90], states time evolution within intervals is modeled by a Markovian prior which is a first-order autoregressive model:

$$\mathbf{z}_k \sim p\left(\mathbf{z}_k|\mathbf{z}_{k-1}\right) = \mathcal{N}\left(\mathbf{F}_k\mathbf{z}_{k-1}, \mathbf{\Sigma}_{z,k}\right) \tag{3.81}$$

where we have defined

$$\begin{aligned} \mathbf{F}_k &= \text{diag}\{\mathbf{F}_{a_s,k}, \mathbf{F}_{\tau,k}\} \\ \mathbf{F}_{a_s,k} &\triangleq \text{diag}\{\mathbf{F}_{a^r,k}, \mathbf{F}_{a^i,k}\} \\ \mathbf{\Sigma}_{z,k} &= \text{diag}\{\mathbf{\Sigma}_{a_s,k}, \mathbf{\Sigma}_{\tau,k}\} \\ \mathbf{\Sigma}_{a_s,k} &\triangleq \text{diag}\{\mathbf{\Sigma}_{a^r,k}, \mathbf{\Sigma}_{a^i,k}\}\ , \end{aligned} \tag{3.82}$$

being $\mathbf{F}_{a^r,k}, \mathbf{F}_{a^i,k}$ and $\mathbf{F}_{\tau,k}$ the respective transitional matrices of each state, defined as

$$\begin{aligned} \mathbf{F}_{a^r,k} &= \begin{pmatrix} \mu_{a_0^r} & \dots & 0 \\ \vdots & \ddots & \vdots \\ 0 & \dots & \mu_{a_{M-1}^r} \end{pmatrix} \in \mathbb{R}^{M\times M} \\ \mathbf{F}_{a^i,k} &= \begin{pmatrix} \mu_{a_0^i} & \dots & 0 \\ \vdots & \ddots & \vdots \\ 0 & \dots & \mu_{a_{M-1}^i} \end{pmatrix} \in \mathbb{R}^{M\times M} \\ \mathbf{F}_{\tau,k} &= \begin{pmatrix} \mu_{\tau_0} & \dots & 0 \\ \vdots & \ddots & \vdots \\ 0 & \dots & \mu_{\tau_{M-1}} \end{pmatrix} \in \mathbb{R}^{M\times M}\ , \end{aligned} \tag{3.83}$$

where each $\mu_{(\cdot)}$ controls the dynamics of the corresponding parameter. $\mathbf{\Sigma}_{a^r,k}, \mathbf{\Sigma}_{a^i,k}$ and $\mathbf{\Sigma}_{\tau,k}$ denote the covariance matrices of the evolving states. The above state evolution model has been used in related publications due to its simplicity, see [Ilt90, Ghi05, Spa07, Kra08] for example. The values of the transitional matrices depend on the considered scenario and the dynamics of the receiver, and must be tuned accordingly.

3.4 A Particle Filtering algorithm for Multipath Mitigation

One of the core contributions of this dissertation is the proposal of a multipath mitigation tracking algorithm based on the particle filtering methodology. The algorithm tracks both LOSS and multipath time-evolving parameters, providing a Bayesian solution to the problem. Two PFs are tested: the SIR filter and the Laplace's PF. Being the latter more appealing for real-time tracking applications than the former, which actually is more likely to be thought as a recursive point-wise approximation of the ML estimator [Gil01, Cho04].

3.4.1 Rao-Blackwellization procedure

Observing the DSS model in (3.78) and (3.81), we see that the SS can be partitioned into two sub-spaces corresponding to its linear and non-linear parts. Thus, we can consider the Rao-Blackwellization procedure discussed in Section 3.2.6 to reduce the variance of importance weights. Complex amplitudes, i.e., $\mathbf{a}_{s,k}$, can be considered nuisance parameters optimally handled by a KF and time-delays are dealt by the PF. Our focus is then on the characterization of the posterior pdf of non-linear states $p(\boldsymbol{\tau}_{0:k}|\mathbf{x}_{1:k})$.

According to the SIS concept, the i-th particle in a PF is generated and weighted respectively as

$$\boldsymbol{\tau}_k^i \sim \pi(\boldsymbol{\tau}_k|\boldsymbol{\tau}_{0:k-1}^i, \mathbf{x}_{1:k}) \tag{3.84}$$

$$\tilde{w}_k^i \propto w_{k-1}^i \frac{p(\mathbf{x}_k|\boldsymbol{\tau}_{0:k}^i, \mathbf{x}_{1:k-1})p(\boldsymbol{\tau}_k^i|\boldsymbol{\tau}_{k-1}^i)}{\pi(\boldsymbol{\tau}_k^i|\boldsymbol{\tau}_{0:k-1}^i, \mathbf{x}_{1:k})}\,, \tag{3.85}$$

where $\tilde{w}_k^i$ is the i-th unnormalized importance weight. The selection of a proper importance density function is an important issue, which has to consider both particle efficiency and a feasible implementation. This is discussed in Section 3.4.2.

The algorithm requires the evaluation of the likelihood function $p(\mathbf{x}_k|\boldsymbol{\tau}_{0:k}^i, \mathbf{x}_{1:k-1})$ in order to compute the i-th weight in (3.85). That distribution can be expressed as

$$p(\mathbf{x}_k|\boldsymbol{\tau}_{0:k}^i, \mathbf{x}_{1:k-1}) = \int_{\mathbf{a}_{s,k}} p(\mathbf{x}_k|\boldsymbol{\tau}_k^i, \mathbf{a}_{s,k})p(\mathbf{a}_{s,k}|\boldsymbol{\tau}_{0:k-1}^i, \mathbf{x}_{1:k-1})d\mathbf{a}_{s,k} \tag{3.86}$$

where, from equation (3.78), we now that

$$p(\mathbf{x}_k|\boldsymbol{\tau}_k^i, \mathbf{a}_{s,k}) = \mathcal{N}\left(\mathbf{Q}_k^T(\boldsymbol{\tau}_k^i)\mathbf{T}\ \mathbf{a}_{s,k}, \boldsymbol{\Sigma}_{n,k}\right) \tag{3.87}$$

and

$$p(\mathbf{a}_{s,k}|\boldsymbol{\tau}_{0:k-1}^i, \mathbf{x}_{1:k-1}) = \mathcal{N}\left(\mathbf{a}_{s,k|k-1}^i, \mathbf{P}_{k|k-1}^i\right) \tag{3.88}$$

can be sequentially computed using a KF for each generated particle. Notice that, due to the Rao-Blackwellization procedure, the likelihood distribution is a function of the predictive posterior distribution of linear states. Therefore, the integral in (3.86) can be solved as

$$p(\mathbf{x}_k|\boldsymbol{\tau}^i_{0:k}, \mathbf{x}_{1:k-1}) = \mathcal{N}\left(\mathbf{Q}^T_k(\boldsymbol{\tau}^i_k)\mathbf{T}\ \mathbf{a}^i_{s,k|k-1}, \boldsymbol{\Sigma}_{n,k} + \mathbf{Q}^T_k(\boldsymbol{\tau}^i_k)\mathbf{P}^i_{k|k-1}\mathbf{Q}_k(\boldsymbol{\tau}^i_k)\right)\ , \tag{3.89}$$

being the equations of the prediction step of the KF:

$$\begin{aligned} \hat{\mathbf{a}}^i_{s,k|k-1} &= \mathbf{F}_{\mathbf{a}_s,k-1}\hat{\mathbf{a}}^i_{s,k-1|k-1} \\ \mathbf{P}^i_{k|k-1} &= \boldsymbol{\Sigma}_{\mathbf{a}_s,k} + \mathbf{F}_{\mathbf{a}_s,k-1}\mathbf{P}^i_{k-1|k-1}\mathbf{F}^T_{\mathbf{a}_s,k-1}. \end{aligned} \tag{3.90}$$

After generating each particle, the corresponding KF is conditionally updated following:

$$\begin{aligned} \hat{\mathbf{a}}^i_{s,k|k} &= \hat{\mathbf{a}}^i_{s,k|k-1} + \mathbf{K}^i_k\left(\mathbf{x}_k - \mathbf{G}^i_k\hat{\mathbf{a}}^i_{s,k|k-1}\right) \\ \mathbf{P}^i_{k|k} &= \mathbf{P}^i_{k|k-1} - \mathbf{K}^i_k\left(\mathbf{G}^i_k\mathbf{P}^i_{k|k-1}{\mathbf{G}^i_k}^T + \boldsymbol{\Sigma}_{n,k}\right){\mathbf{K}^i_k}^T \\ \mathbf{K}^i_k &= \mathbf{P}^i_{k|k-1}{\mathbf{G}^i_k}^T\left(\mathbf{G}^i_k\mathbf{P}^i_{k|k-1}{\mathbf{G}^i_k}^T + \boldsymbol{\Sigma}_{n,k}\right)^{-1}\ , \end{aligned} \tag{3.91}$$

where for the sake of clarity we have defined $\mathbf{G}^i_k \triangleq \mathbf{Q}^T_k(\boldsymbol{\tau}^i_k)\mathbf{T}$.

3.4.2 Selection of the importance density

One of the key points of a PF algorithm is the choice of a *good* importance density function, $\pi(\cdot)$. This is to propose an importance density function close to the optimal, which is the posterior distribution, in the sense that it minimizes the variance of importance weights. However, it is only possible to draw samples from this distribution in limited cases and other alternatives must be explored [Ris04, Dou00]. The simplest approach is to consider the transitional prior as the importance function, in which case the weights are proportional to the likelihood distribution. Nevertheless this option was shown to be inefficient as it requires a large number of samples to effectively characterize the posterior [Clo06a, Clo06e, Kra08]. Many importance function alternatives can be found in the literature, as discussed in Section 3.2.4.

In this section we consider two alternatives for the selection of the importance density, applied to the multipath mitigation problem. First, we study the use of the transitional prior, yielding to the so-called Bootstrap Filter. Secondly, an approximation of the optimal importance density is presented, which is based on a Laplacian approximation of the likelihood distribution.

Transitional prior distribution

Adopting the transitional prior as the importance density is an extensively used solution, due to its simple implementation. As pointed out in Section 3.2.4, the design of a suitable importance density is usually application dependent. In our case, the design of such distribution considers an importance function for the LOSS delay generation and another function for the parameters of multipath replicas.

On the one hand, according to the SS model in (3.81), the generation of LOSS delay particles can be expressed as

$$[\boldsymbol{\tau}_k^i]_{m=0} \sim \mathcal{N}\left(\mu_{\tau_0}[\hat{\boldsymbol{\tau}}_{k-1}]_{m=0}, \left[\hat{\boldsymbol{\Sigma}}_{\tau,k-1}\right]_{1,1}\right) \ . \tag{3.92}$$

where

$$\hat{\boldsymbol{\Sigma}}_{\tau,k} = \sum_{i=1}^{N_s} w_k^i \left(\boldsymbol{\tau}_k^i - \hat{\boldsymbol{\tau}}_k\right)\left(\boldsymbol{\tau}_k^i - \hat{\boldsymbol{\tau}}_k\right)^H \tag{3.93}$$

provides an estimation of the covariance of the estimated time–delay, $\hat{\boldsymbol{\tau}}_k$.

On the other hand, we can use side information in the generation of multipath delays. Due to physical reasons we can consider that

$$\tau_m(t) > \tau_0(t) \qquad \forall m \in \{1, \ldots, M-1\} \ , \tag{3.94}$$

in outdoor propagation channels [Jah96, Ste05, Irs05]. Taking (3.94) into account, in [Clo06e] the proposed importance density for the generation of multipath delays particles was a truncated Gaussian – which was also adopted in [Spa07]. The truncated Gaussian is a multivariate Gaussian distribution with mean the previous state estimation propagated through the state evolving equation and covariance calculated as in (3.93) at $k-1$. In addition, the i-th multipath delay particle is forced to be larger than the i-th LOSS delay particle. Hence, multipath's importance density can be expressed as

$$[\boldsymbol{\tau}_k^i]_m \sim [\boldsymbol{\tau}_k^i]_{m=0} + \left| \left(\mu_{\tau_m}[\hat{\boldsymbol{\tau}}_{k-1}]_m - [\boldsymbol{\tau}_k^i]_{m=0}\right) + \mathcal{N}\left(0, \left[\hat{\boldsymbol{\Sigma}}_{\tau,k-1}\right]_{m,m}\right) \right| \ , \tag{3.95}$$

where $m \in \{1, \ldots, M-1\}$. Figure 3.3 shows a representation of (3.95).

This choice of importance density yields to the use of the BF – a.k.a. SIR filter –, when resampling is performed each recursive step (cf. Section 3.2.5). In that case, weight update equation is given by $w_k^i \propto p(\mathbf{x}_k|\boldsymbol{\tau}_k^i)$.

The BF provides an easy implementation of a PF algorithm. However, it is not efficient in terms of particle usage, i.e., a large number of samples are required in order to obtain a certain acceptable precision in a number of applications. This was shown in [Clo06e,

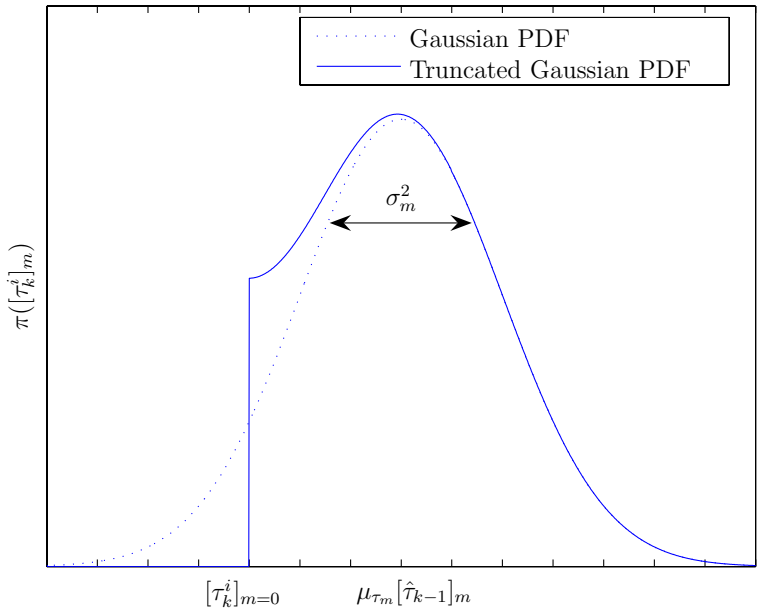

Figure 3.3: Importance density for the m-th replica. Being $\sigma_m^2 = \left[\hat{\mathbf{\Sigma}}_{\tau,k-1}\right]_{m,m}$ and $m \in \{1,\ldots,M-1\}$. This importance density ensures (3.94).

Clo06a] and the preceding work [Kra08]. The lack of efficiency is mainly caused by the fact that in the particle generation process, no use is done of the information provided by current measurements. Thus, other approaches shall be explored to make PF a more implementable tool in real-time signal processing platforms. An efficient alternative is presented hereinafter under the name of Laplace's Particle Filter.

Optimal distribution approximation by Laplace's method

In order to improve particle efficiency, we aim at using an importance density function which is close to the optimal $p(\boldsymbol{\tau}_k|\boldsymbol{\tau}_{0:k-1}, \mathbf{x}_{1:k})$, or at least closer than the transitional prior is. Since it is not possible to sample from such distribution, we consider the following approximation[9]

$$\begin{aligned} \pi(\boldsymbol{\tau}_k|\boldsymbol{\tau}_{0:k-1}, \mathbf{x}_{1:k}) &\approx p(\boldsymbol{\tau}_k|\boldsymbol{\tau}_{k-1}, \mathbf{x}_k) \\ &\propto p(\mathbf{x}_k|\boldsymbol{\tau}_k)p(\boldsymbol{\tau}_k|\boldsymbol{\tau}_{k-1}) \ , \end{aligned} \tag{3.96}$$

[9]Note that equation (3.89) provides an expression for $p(\boldsymbol{\tau}_k|\boldsymbol{\tau}_{0:k-1}, \mathbf{x}_{1:k})$ which is conditional on non-linear states that cannot be used in the generation of particles since τ_k is not already known.

which splits the posterior as being proportional to the likelihood and the prior distributions. The idea behind is that if both $p(\mathbf{x}_k|\boldsymbol{\tau}_k)$ and $p(\boldsymbol{\tau}_k|\boldsymbol{\tau}_{k-1})$ are unimodal normally distributed, then $\pi(\boldsymbol{\tau}_k|\boldsymbol{\tau}_{k-1}, \mathbf{x}_k)$ is also normal and closed form expressions for its mean and covariance matrix can be readily obtained. Whereas the prior attains these conditions, the likelihood has to be approximated. Then, a unimodal Gaussian approximation of $p(\mathbf{x}_k|\boldsymbol{\tau}_k)$ is obtained via a Laplacian approximation [Aze94] (refer to Appendix 3.C for details). Laplace's method yields analytical Gaussian approximations of densities from a Taylor series expansion at the mode of the density. In our case, the inverse Hessian of the log-likelihood is used as a covariance approximation [Gel04].

Thus, we aim at obtaining the parameters that characterize the likelihood as a Gaussian distribution: $p(\mathbf{x}_k|\boldsymbol{\tau}_k) \approx \mathcal{N}(\bar{\boldsymbol{\tau}}_k, \widehat{\boldsymbol{\Sigma}}_k)$. These two parameters are the mode $\bar{\boldsymbol{\tau}}_k$ of the likelihood and the inverse Hessian evaluated at the mode $\widehat{\boldsymbol{\Sigma}}_k$, that acts as a covariance matrix estimator. Then, the Gaussian approximation reduces to find the mode of the log-likelihood by maximizing it with respect to $\boldsymbol{\tau}_k$.

Manipulating equation (3.75), under the Gaussian assumption, it can be shown (cf. [Gol73]) that the maximization of the log-likelihood is equivalent to minimizing the following non-linear Least Squares cost function with respect to $\boldsymbol{\tau}_k$:

$$\Lambda_k\left(\boldsymbol{\tau}_k, \mathbf{a}_k\right) = \| \mathbf{x}_k - \mathbf{Q}_k^T(\boldsymbol{\tau}_k)\mathbf{a}_k \|^2 \quad . \tag{3.97}$$

Deriving (3.97) with respect to $\mathbf{a}_k$ and equating to zero, one is able to find an analytical expression for $\mathbf{a}_k$ which is a nuisance parameter in this optimization problem[10]. Then, substituting the solution for $\mathbf{a}_k$ in (3.97) and expanding the expression, the mode $\bar{\boldsymbol{\tau}}_k$ is found by minimizing

$$\begin{aligned}
\Lambda_k\left(\boldsymbol{\tau}_k\right) &= \mathbf{x}^H\mathbf{x} - \mathbf{x}^H\mathbf{H}_k\left(\mathbf{H}_k^H\mathbf{H}_k\right)^{-1}\mathbf{H}_k^H\mathbf{x} - \mathbf{x}^H\mathbf{H}_k\left(\mathbf{H}_k^H\mathbf{H}_k\right)^{-1}\mathbf{H}_k^H\mathbf{x} \\
&+ \mathbf{x}^H\mathbf{H}_k\left(\mathbf{H}_k^H\mathbf{H}_k\right)^{-1}\mathbf{H}_k^H\mathbf{H}_k\left(\mathbf{H}_k^H\mathbf{H}_k\right)^{-1}\mathbf{H}_k^H\mathbf{x} \\
&= \mathbf{x}_k^H\left(\mathbf{I} - \boldsymbol{\Pi}_k\right)\mathbf{x}_k \\
&= \| \boldsymbol{\Pi}_k^{\perp}\mathbf{x}_k \|^2 \quad ,
\end{aligned} \tag{3.98}$$

being

$$\boldsymbol{\Pi}_k\left(\boldsymbol{\tau}_k\right) \triangleq \mathbf{H}_k(\mathbf{H}_k^H\mathbf{H}_k)^{-1}\mathbf{H}_k^H \tag{3.99}$$

the projection matrix onto the subspace spanned by the columns of $\mathbf{H}_k \triangleq \mathbf{Q}_k^T(\boldsymbol{\tau}_k)$ and $\boldsymbol{\Pi}_k^{\perp}\left(\boldsymbol{\tau}_k\right)$ its orthogonal complement[11].

A regularization term is introduced in order to constrain the search space to be in the $\boldsymbol{\Sigma}_r$–neighborhood of the propagated prior estimate $\boldsymbol{\mu}_r = \mathbf{F}_{\tau,k}\hat{\boldsymbol{\tau}}_{k-1}$ to avoid divergence,

[10] Not surprisingly, the solution is given by the well-known Wiener estimator. Thus, the expression to use is $\hat{\mathbf{a}}_k = \left(\mathbf{Q}_k^*(\boldsymbol{\tau}_k)\mathbf{Q}_k^T(\boldsymbol{\tau}_k)\right)^{-1}\mathbf{Q}_k^*(\boldsymbol{\tau}_k)\mathbf{x}_k$.

[11] Recall that if $\boldsymbol{\Pi}_k$ is a projection matrix, its orthogonal complement is defined as $\boldsymbol{\Pi}_k^{\perp} \triangleq \mathbf{I} - \boldsymbol{\Pi}_k$.

mimicking [Cev07]. Thus, the optimization problem is

$$\bar{\boldsymbol{\tau}}_k = \arg\min_{\boldsymbol{\tau}_k} \left\{ \Lambda_k\left(\boldsymbol{\tau}_k\right) + r\left(\boldsymbol{\mu}_r, \boldsymbol{\Sigma}_r\right) \right\} = \arg\min_{\boldsymbol{\tau}_k} \left\{ \Lambda_k^r \right\} \ , \tag{3.100}$$

where the regularization term is constructed as:

$$r\left(\boldsymbol{\mu}_r, \boldsymbol{\Sigma}_r\right) = (\boldsymbol{\tau}_k - \boldsymbol{\mu}_r)^T \boldsymbol{\Sigma}_r^{-1} (\boldsymbol{\tau}_k - \boldsymbol{\mu}_r) \tag{3.101}$$

and

$$\Lambda_k^r = \Lambda_k\left(\boldsymbol{\tau}_k\right) + r\left(\boldsymbol{\mu}_r, \boldsymbol{\Sigma}_r\right) \ . \tag{3.102}$$

The optimization in (3.100) can be solved using the Newton-Raphson recursive algorithm. The solution is then given by the iterative expression:

$$\bar{\boldsymbol{\tau}}_k^{\ell+1} = \bar{\boldsymbol{\tau}}_k^{\ell} - \lambda^{\ell}\, \mathcal{H}_{\tau}^{-1}(\Lambda_k^r)\big|_{\bar{\boldsymbol{\tau}}_k^{\ell}}\, \nabla_{\tau}(\Lambda_k^r)|_{\bar{\boldsymbol{\tau}}_k^{\ell}} \ , \tag{3.103}$$

where index ℓ denotes iteration and λ^{ℓ} is the step-size. In particular we implement the algorithm with backtracking, meaning that after the ℓ-th solution is obtained it is compared to the previous one; if the value of the cost function is greater for the new solution, then λ^{ℓ} is reduced. See Algorithm 3.4 for a detailed pseudocode description of the algorithm. The required expressions for the Gradient and the Hessian of $\Lambda_k^r\left(\boldsymbol{\tau}_k\right)$ in (4.56) can be consulted in Appendix 3.D. The solution of the optimization problem by the Newton-Raphson algorithm provides the likelihood approximation

$$p(\mathbf{x}_k|\boldsymbol{\tau}_k) \approx \mathcal{N}\left(\bar{\boldsymbol{\tau}}_k, \widehat{\boldsymbol{\Sigma}}_k\right) \ , \tag{3.104}$$

where $\bar{\boldsymbol{\tau}}_k$ and $\widehat{\boldsymbol{\Sigma}}_k$ are the outputs of Algorithm 3.4.

Once the likelihood approximation is obtained, we now incorporate the information of each propagated particle to form the Gaussian importance density as follows:

$$\pi(\boldsymbol{\tau}_k|\boldsymbol{\tau}_{k-1}^i, \mathbf{x}_k) = \mathcal{N}\left(\boldsymbol{\mu}_{\pi}^i, \boldsymbol{\Sigma}_{\pi}\right) \tag{3.105}$$

where

$$\begin{aligned} \boldsymbol{\mu}_{\pi}^i &= \boldsymbol{\Sigma}_{\pi}\left(\widehat{\boldsymbol{\Sigma}}_k^{-1}\bar{\boldsymbol{\tau}}_k + \boldsymbol{\Sigma}_{\tau,k}^{-1}\mathbf{F}_{\tau,k}\boldsymbol{\tau}_{k-1}^i\right) \\ \boldsymbol{\Sigma}_{\pi} &= \left(\widehat{\boldsymbol{\Sigma}}_k^{-1} + \boldsymbol{\Sigma}_{\tau,k}^{-1}\right)^{-1} \ , \end{aligned} \tag{3.106}$$

as shown in Appendix 3.C.

After approximating the optimal importance function, particles can be generated and weighted according to (3.84) and (3.85), respectively. Recall that conditional linear states are taken into account when computing the likelihood in (3.89).

Algorithm 3.4 Newton-Raphson algorithm with backtracking

Require: $\hat{\boldsymbol{\tau}}_{k-1}, \lambda^0, N_\ell$
Ensure: $\bar{\boldsymbol{\tau}}_k, \widehat{\boldsymbol{\Sigma}}_k$
1: $\bar{\boldsymbol{\tau}}_k^0 = \hat{\boldsymbol{\tau}}_{k-1}$
2: **for** $\ell = 0$ to N_ℓ **do**
3: $\quad \bar{\boldsymbol{\tau}}_k^{\ell+1} = \bar{\boldsymbol{\tau}}_k^{\ell} - \lambda^\ell \, \mathcal{H}_\tau^{-1}(\Lambda_k^r)|_{\bar{\boldsymbol{\tau}}_k^\ell} \, \nabla_\tau(\Lambda_k^r)|_{\bar{\boldsymbol{\tau}}_k^\ell}$
4: $\quad$ **while** $\Lambda_k\left(\bar{\boldsymbol{\tau}}_k^{\ell+1}\right) > \Lambda_k\left(\bar{\boldsymbol{\tau}}_k^{\ell}\right)$ **do**
5: $\quad\quad \lambda^\ell = \lambda^\ell/2$
6: $\quad\quad \bar{\boldsymbol{\tau}}_k^{\ell+1} = \bar{\boldsymbol{\tau}}_k^{\ell} - \lambda^\ell \, \mathcal{H}_\tau^{-1}(\Lambda_k^r)|_{\bar{\boldsymbol{\tau}}_k^\ell} \, \nabla_\tau(\Lambda_k^r)|_{\bar{\boldsymbol{\tau}}_k^\ell}$
7: $\quad$ **end while**
8: $\quad \lambda^{\ell+1} = \lambda^0$
9: **end for**
10: $\bar{\boldsymbol{\tau}}_k = \bar{\boldsymbol{\tau}}_k^{\ell+1}$
11: $\widehat{\boldsymbol{\Sigma}}_k = \mathcal{H}_\tau^{-1}(\Lambda_k^r)|_{\bar{\boldsymbol{\tau}}_k}$

3.4.3 Estimation Objectives

The estimation objectives of the algorithm are the MMSE estimates of time-delays and complex amplitudes. From (3.49), these can be obtained as

$$\begin{aligned} \hat{\boldsymbol{\tau}}_k &= \sum_{i=1}^{N_s} w_k^i \boldsymbol{\tau}_k^i \\ \hat{\mathbf{a}}_{s,k|k} &= \sum_{i=1}^{N_s} w_k^i \hat{\mathbf{a}}_{s,k|k}^i \ , \end{aligned} \tag{3.107}$$

where $\hat{\mathbf{a}}_{s,k|k}^i$ is obtained as the output of the KF associated to the i-th particle, as given in (3.91).

3.4.4 Resampling Strategy

Many resampling strategies exist, as those presented in Section 3.2.3. In the sequel, we consider the multinomial resampling approach. In addition, for the Laplace's PF we consider that resampling is applied whenever the effective number of samples falls below threshold $N_{th} = \frac{2}{3}N_s$, as suggested in [Ber99]. In contrast for the BF, resampling is performed each time the algorithm is updated.

3.4.5 Tracking Doppler-shifts

According to equation (3.72), the linear part of the phase is due to the Doppler deviation, while the other term corresponds to the carrier phase. Hence, the Doppler–shift of the m–th signal can be tracked from the estimated complex amplitude, where $m \in \{0, \ldots, M-1\}$. Since the variation of this parameter is typically slow, compared to the sampling frequency and the estimation rate (1 estimate per K samples), a simple linear regression can be used to extract f_{d_m} from a set of phase estimates. Thus, one has to consider an observation window for $\hat{\mathbf{a}}_k$ such that the Doppler deviation has not changed significantly. We denote the length of this window by L estimates or, equivalently, LKT_s seconds. Hence, Doppler estimates at instant k are obtained as the solution to a linear Least Squares problem

$$\hat{\boldsymbol{\beta}}_k = (\boldsymbol{\Gamma}_{k-L:k}^T \boldsymbol{\Gamma}_{k-L:k})^{-1} \boldsymbol{\Gamma}_{k-L:k}^T \hat{\boldsymbol{\phi}}_{m_{k-L:k}} \ , \tag{3.108}$$

where

$$\begin{aligned} \hat{\boldsymbol{\beta}}_k &= \left[\hat{\nu}_{m_k}, \hat{\phi}_{m,0}\right]^T \\ \boldsymbol{\Gamma}_{k-LK:k}^T &= \begin{pmatrix} 2\pi(k-L)KT_s & 1 \\ \vdots & \vdots \\ 2\pi k K T_s & 1 \end{pmatrix} \\ \hat{\boldsymbol{\phi}}_{m_{k-L:k}} &= \left[\hat{\boldsymbol{\phi}}_{m_{k-L}}, \ldots, \hat{\boldsymbol{\phi}}_{m_k}\right]^T \ , \end{aligned} \tag{3.109}$$

being the latter the set of phase estimates obtained as the angle of the complex amplitude estimate given by (3.107), i.e.,

$$\hat{\boldsymbol{\phi}}_{m_k} = \angle \hat{\mathbf{a}}_{k|k} \ . \tag{3.110}$$

The tracking of the Doppler-shift for the LOSS can be done whether considering overlapped windows or not. The choice might depend on the variability of that parameter, and thus on the receiver dynamics. If tracking is performed at each k, the computational cost increases so that one has to design the algorithm depending on the scenario requirements. In that sense, the design of L depends on a number of factors and must ensure that the Doppler deviation remains piecewise constant during the window. On the one hand it depends on the variation rate of the Doppler for a given scenario. On the other hand, the designed value of L depends on parameters of the receiver such as the sampling period T_s and the number of samples used to estimate delays and complex amplitudes (K). A longer window length will provide smoother Doppler estimates, but the designed L has to ensure that the parameter remains piecewise constant in the interval, otherwise yielding to unreliable results.

Algorithm 3.5 Rao-Blackwellized Laplace's Particle Filter algorithm

Require: $\mathbf{x}_{1:k}, \mathbf{z}_0, p(\mathbf{z}_0)$
Ensure: $\hat{\boldsymbol{\alpha}}_{0:k}, \hat{\boldsymbol{\phi}}_{0:k}, \hat{\boldsymbol{\nu}}_{0:k}, \hat{\boldsymbol{\tau}}_{0:k}$

Initialization:

$\hat{\mathbf{z}}_0 \sim p(\mathbf{z}_0)$
$\sigma^2_{\tau_m} = [\boldsymbol{\Sigma}_{\tau,0}]_{m,m}$ s.t. $m \in \{0, \ldots, M-1\}$
for $i = 1$ to N_s **do**
  Generate $\tau_0^i(0) \sim \mathcal{N}\left(\hat{\tau}_0, \sigma^2_{\tau_0}\right)$
  Generate $\{\tau_m^i(0) \sim \tau_0^i(0) + \mathcal{U}\left(0, \sigma_{\tau_m}\right)\}_{m=1}^{M-1}$
  $w_0^i = 1/N_s$
  $\mathbf{P}^i_{0|0} = \text{diag}\{\boldsymbol{\Sigma}_{\alpha,0}, \boldsymbol{\Sigma}_{\phi,0}\}$
end for

Tracking:

for $k = 1$ to ∞ **do**
  Run Newton-Raphson algorithm in (4.56) $\Rightarrow \bar{\boldsymbol{\tau}}_k, \widehat{\boldsymbol{\Sigma}}_k$
  Calculate $\boldsymbol{\Sigma}_\pi$ according to (3.106).
  for $i = 1$ to N_s **do**
    i-th Kalman prediction according to (3.90).
    Calculate $\boldsymbol{\mu}_\pi^i$ according to (3.106).
    Generate $\boldsymbol{\tau}_k^i \sim \mathcal{N}\left(\boldsymbol{\mu}_\pi^i, \boldsymbol{\Sigma}_\pi\right)$
    Calculate $\tilde{w}_k^i = w_{k-1}^i \frac{p(\mathbf{x}_k|\boldsymbol{\tau}^i_{0:k}, \mathbf{x}_{1:k-1}) p(\boldsymbol{\tau}_k^i|\boldsymbol{\tau}^i_{k-1})}{\mathcal{N}\left(\boldsymbol{\tau}_k^i; \boldsymbol{\mu}_\pi^i, \boldsymbol{\Sigma}_\pi\right)}$
    i-th Kalman update according to (3.91).
  end for
  Normalize weights, w_k^i.
  Compute MMSE estimates.
  Track Doppler-shift when required, according to (3.108).
  if $\hat{N}_{eff} < \frac{2}{3} N_s$ **then**
    Resample Particles, $\{\boldsymbol{\tau}_k^i,\ w_k^i\}_{i=1}^{N_s}$.
  end if
end for

3.4.6 Estimation of the number of signals

The problem of estimating M, the number of signal replicas, is an open topic in signal processing. In order to obtain estimates of this parameter, $\hat{M}$, one can use rank tests on the data vector, such as Generalized Likelihood Ratio Tests (GLRT) [Fri02, Sto04]. Other methods exist, based on a receiver equipped with an antenna array front-end such as the Akaike's Information Criteria (AIC) [Aka73] or the Minimum Description Length (MDL) [Ris85]. However, the setup considered in this chapter considers a single antenna based receiver. An implementable solution is to assume a fixed number of replicas, maybe dependent on the environment, and perform synchronization assuming $\hat{M}$ replicas of the signal. The latter method, which has been proposed in [Nee95] and successfully implemented in NovAtel receivers, is penalized with a remaining error if $\hat{M}$ is chosen too small and may increase unnecessarily the computational burden if $\hat{M}$ is chosen too large. In the sequel, the latter approach is taken. That is, the number of signals M is assumed known or estimated by other means. However, aiming at studying how the estimation of M affects the overall performance of the proposed algorithm, simulations are provided in Section 3.5 taking this into consideration.

3.5 Simulation results

In order to assess the performance of the proposed tracking algorithm, and without loss of generality, we simulate a GPS L1 C/A signal (though the algorithm can be readily used with other GNSS signal structures) assuming an scenario composed of a LOSS and a multipath replica ($M = 2$). In GNSS, the otherwise rather simple model of one single reflection is quite representative of the multipath effect in many situations from a statistical point of view, even in the urban canyon environment (see [Ste04, Ste05] for an experimental investigation, including a high resolution measurement campaign, of the land mobile satellite navigation multipath channel).

In the following experiments, a carrier-to-noise density ratio of 45 dB-Hz for the LOSS, a signal-to-multipath ratio of 6 dB and the LOSS and multipath to be in–phase, the worst possible case [Van93], are considered. The received signal is filtered with a 2 MHz bandwidth filter, down-converted to baseband and then digitized at a sampling frequency of $f_s = 5.714$ MHz. Thus, 1 ms of recorded data corresponds to $K = 5714$ samples. The chip period is $T_c = 1/(1.023 \text{ MHz})$ in GPS C/A code. The covariance matrices involved in the simulations are $\mathbf{\Sigma}_{\tau,0}^{\frac{1}{2}} = \mathbf{\Sigma}_r^{\frac{1}{2}} = \text{diag}\{T_c, 2T_c\}$, the receiver dynamics correspond to a vehicle with a constant velocity of 22 m/s. The multipath relative delay is $\tau_1 = 0.35T_c$ with respect to the time-varying delay of the LOSS, $\tau_0(t)$. The scenario is simulated with a realistic GNSS signal generator programmed in MATLAB, thus all states evolve according

to vehicle and satellite dynamics. The evolution model considers that $\mathbf{F}_k = \mathbf{I}_{3M}$, i.e., the algorithm considers few variation between consecutive instants.

Figure 3.4 shows the RMSE performance [Kay93] (averaged over 100 Monte-Carlo simulations) of the proposed Laplace's PF algorithm when considering different numbers of particles. The results are compared to the PCRB, which is obtained using the recursion presented in Section 5.2.1. The discussion on the theoretical bounds of navigation systems is left to Chapter 5. The left-hand axis shows the RMSE of time-delay estimates normalized to T_c and the right axis corresponds to the resulting pseudorange estimation error in meters, which is propagated in the computation of user's position [Par96]. It arises from simulation results that Laplace's PF approaches the PCRB as N_s increase. In addition, Figure 3.5 presents the results obtained with the EKF and the UKF for the same scenario. It is seen from both figures that all algorithms yield similar performances for that given scenario. However, it is well known that KF-based approaches are highly dependent on a proper choice of covariance matrices, whereas particle filters are more robust to such modeling errors.

Let us assume now a different scenario in which the multipath replica is present for a given period of time, then suddenly switches off (modeling occultation) and finally it appears again. The total observation interval is 1 second and the interval in which no multipath is present in the signal is $t \in (300, 500]$ milliseconds. Figures 3.6 and 3.7 present the results obtained after 100 Monte-Carlo runs in that scenario for Laplace's PF and KF-based solutions, respectively. The most evident conclusion from these results is that Laplace's PF is by far more robust than EKF or UKF to mismodeling effects, i.e., to assume that there is a multipath replica when actually there is not. In fact, the performance of the particle filtering algorithm is hardly altered, whereas KF-based approaches suffer a severe degradation due to the bias produced by the mismodeling error, which could even cause the algorithm to diverge. This is related to the initialization of the covariance matrices in the KF: large entries in the covariance matrices aid the algorithm to converge when states evolution suffer abrupt changes, though the error due to the absence of multipath is high. On the contrary, small covariance matrices, reduce the bias effect in mismodeling situations, but the algorithm is very likely to diverge. This is shown in Figure 3.7.

In real world scenarios, multipath signals will appear/disappear arbitrarily depending on a number of phenomena such as occultation or vehicle motion and inclination. Simulations shown in 3.6 and 3.7 are meaningful since they highlight the robustness of the presented PF to this effect. Whereas EKF and UKF would require a multipath detection and/or number of replicas estimation for proper operation, the presented algorithm could use a fixed number of replicas to operate (as said $M = 2$ is quite representative in many scenarios). However, we agree in that having knowledge of the exact number of replicas would improve the efficiency of the algorithm at the expenses of increasing the computational cost. Since the model assumes that the LOSS is always present, the algorithm

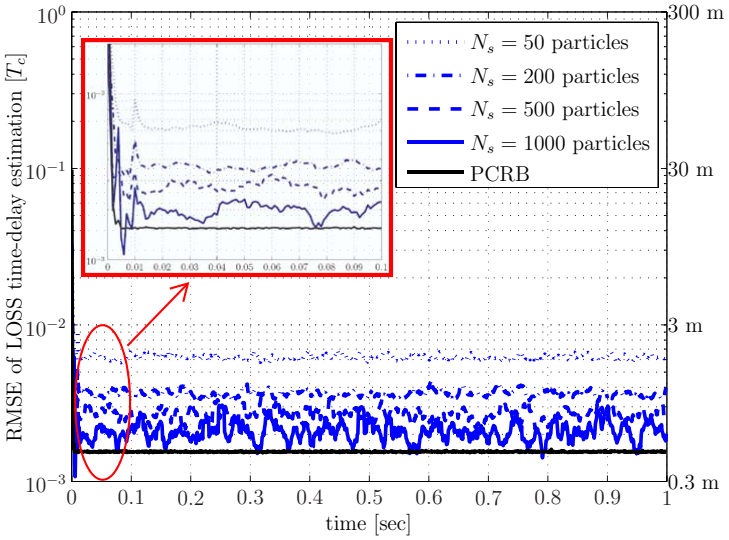

Figure 3.4: RMSE of LOSS time-delay estimation in chips and the corresponding pseudo-range estimate when Laplace's PF is considered.

fails when attempting to track it when the signal is actually blocked or not present. This drawback is shared by the other tested algorithms and could be overcome taking into account the effect in the signal model, also with a switching Markov model, and modifying the algorithm accordingly.

Figure 3.8 compares the RMSE performance of the Sampling Importance Resampling (SIR) algorithm proposed by the author in [Clo06a] and the Laplace's PF proposed in this work in terms of RMSE versus the number of particles. Actually, the former has been used as a batch processing algorithm more likely to fall in the Population Monte-Carlo (PMC) category [Cap04]. That resulted in an inefficient usage of particles, since a large number of samples are required to increase the performance significantly (which has been already confirmed in [Kra08]). Figure 3.8 highlights the efficiency of Laplace's PF in terms of N_s, when compared to SIR PF. The efficiency increase comes from the choice of an importance density function which is closer to the optimal. In contrast, using the transitional prior yields to a solution that does not take into account observations to generate particles. Thus, the posterior characterization is poorer and requires a larger number of particles for attaining similar performances as Laplaces PF does.

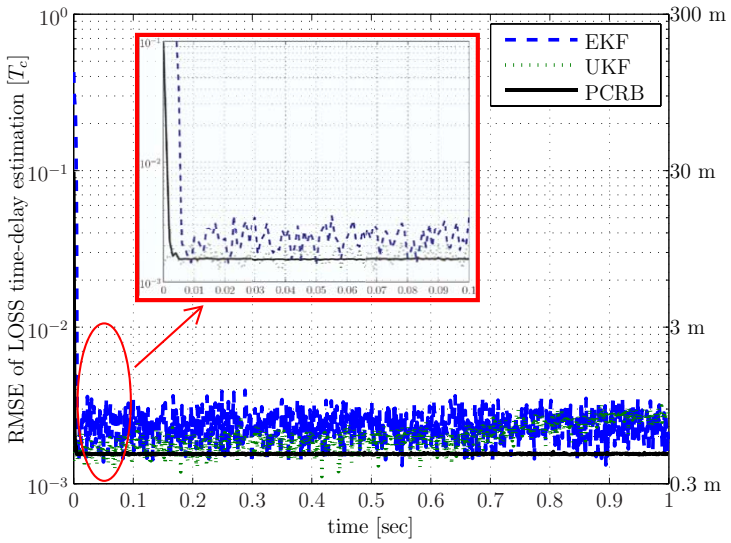

Figure 3.5: RMSE of LOSS delay estimation in chips and the corresponding pseudorange estimate when KF-based algorithms are used. RMSE averaged over 100 Monte-Carlo runs.

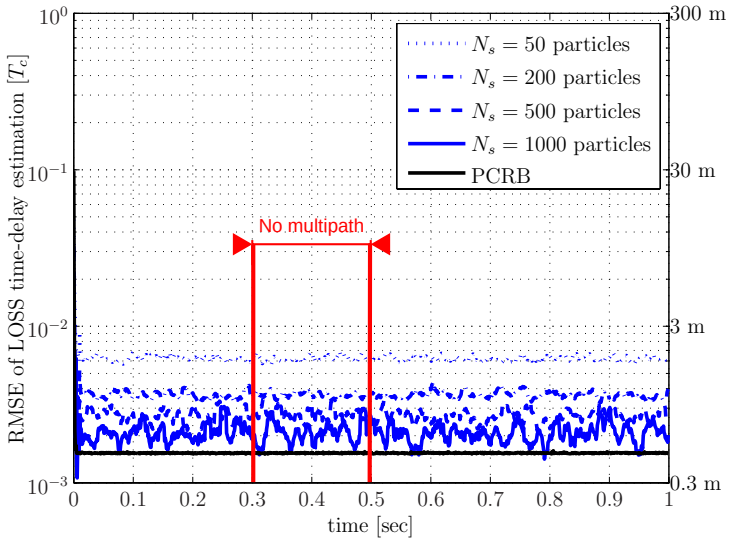

Figure 3.6: RMSE of LOSS delay estimation in chips and the corresponding pseudorange estimate for Laplace's PF. Multipath disappears/appears as shown.

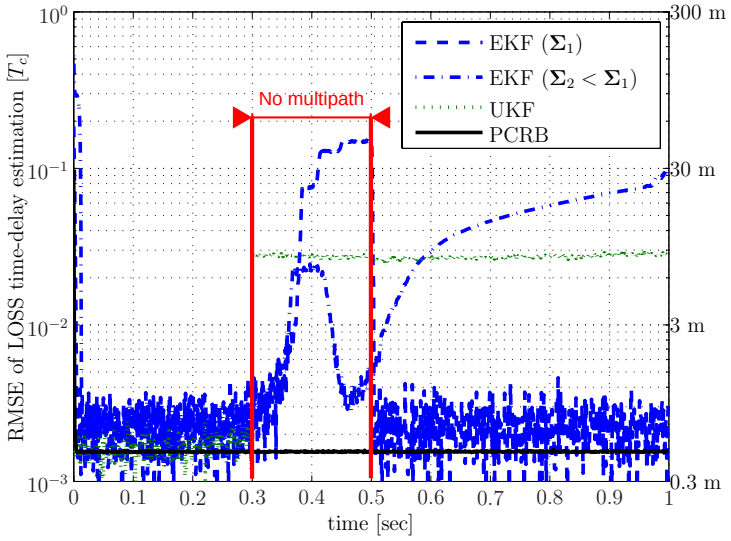

Figure 3.7: RMSE of LOSS delay estimation in chips and the corresponding pseudorange estimate using KF-based algorithms under the disappearance/appearance of a multipath replica. Here, $\mathbf{\Sigma_2} < \mathbf{\Sigma_1}$ is used to conceptually express that the diagonal entries of the covariance matrix are small in $\mathbf{\Sigma_2}$ when compared to $\mathbf{\Sigma_1}$.

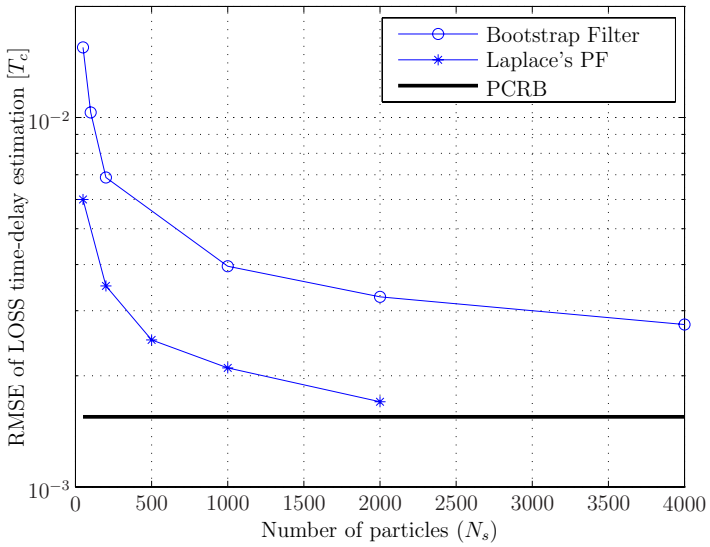

Figure 3.8: Laplace's PF is more efficient in terms of the usage of particles than SIR PF is.

3.6 Summary

This chapter dealt with the problem of multipath mitigation using a Bayesian filter. Many algorithms can be found in the literature and some of them were revisited in the first part of the chapter. Nevertheless the focus was on Sequential Monte-Carlo methods, and in particular on Particle Filters, due to its ability to deal with nonlinear/nonGaussian systems.

A simple, though useful, DSS model was proposed in Section 3.3. This system model can be further improved to accommodate more accurate prior information. However the aim of the chapter was on the algorithm rather than on the DSS model, which was used to prove the concept.

This chapter proposed a particle filtering algorithm that mitigates the multipath effect on the estimation of GNSS signal parameters, one of the dominant sources of error in high-precision applications. The SIR filter (or Bootstrap Filter) was presented, being the particle filtering architecture easiest to tune and implement. However, it was shown that it required a large number of particles in order to obtain performances close to the PCRB. The chapter presented an efficient PF which improved the performance of the SIR filter based on two features:

- The algorithm considers a variance reduction technique, referred to as Rao-Blackwellization, that estimates the linear/Gaussian part of the SS using a Kalman Filter. In our case, these states are the complex amplitudes of the received signals. The intuitive idea is clear: on the one hand, the SS dimension that the PF has to deal with is reduced and, on the other hand, linear/Gaussian setups are optimally handled by a KF.

- A method for selecting a nearly optimal importance density was presented. The main idea is to approximate both prior and likelihood distributions by Gaussian distributions. Then the posterior is also Gaussian whose parameters can be found analytically. The approximation can be accomplished by the Laplacian method. In the application under study, only the likelihood distribution had to be approximated.

The joint application of these two features provided a PF algorithm that can effectively track time–varying parameters which was not feasible at all with the SIR filter. Computer simulation results showed that, in the presence of coherent multipath, the performance of the proposed PF (referred to as Laplace's PF) improved the results of a SIR filter and that it got closer to the PCRB as the number of samples increased. A methodology for extracting Doppler-shifts from complex amplitudes was proposed in Section 3.4.5, being the slope of a linear regression constructed from the estimated phases.

Furthermore, other Bayesian filters were tested, namely the EKF and UKF algorithms. It was observed that a solution based on the KF was very sensible to abrupt changes in the scenario, i.e., appearance/disappearance of multipath replicas. In contrast, Laplace's PF was robust to this situation being its performance not altered. A further improvement of the presented algorithm can be envisaged by including a switching Markov model, as proposed in [Gir07]. Indeed, the latter could model better the appearance and disappearance of multipath signals. Improvements can be achieved at the expenses of a higher complexity.

To sum up, Laplace's PF provides an efficient algorithm to track evolving GNSS signal parameters in the presence of on/off multipath replicas that requires weaker model assumptions than KF-based solutions.

The results presented in this chapter were partially published in:

- **Journal:**

  [Clo09b] P. Closas, C. Fernández-Prades, and J. A. Fernández-Rubio, "A Bayesian Approach to Multipath Mitigation in GNSS Receivers," *IEEE J. Select. Topics in Signal Processing*, vol. 3, no. 4, August 2009.

- **Conference:**

  [Clo08b] P. Closas, C. Fernández-Prades, and J. A. Fernández-Rubio, "A Particle Filtering Tracking Algorithm for GNSS Synchronization using Laplace's method," in *Proceedings of the IEEE International Conference on Acoustics, Speech, and Signal Processing, ICASSP 2008*, Las Vegas, USA, April 2008.

  [Clo08c] P. Closas, C. Fernández-Prades, J. A. Fernández-Rubio, and D. Bernal, "Particle Filtering Strategies for Efficient Multipath Mitigation," *Proceedings of the ION GNSS 2008*, Savannah, GA, September 2008.

  [Clo06a] P. Closas, C. Fernández-Prades, and J. A. Fernández-Rubio, "Bayesian DLL for Multipath Mitigation in Navigation Systems using Particle Filters," in *Proceedings of the IEEE International Conference on Acoustics, Speech, and Signal Processing, ICASSP 2006*, Tolouse, France, May 2006.

  [Clo06d] P. Closas, C. Fernández-Prades, and J. A. Fernández-Rubio, "Sequential Monte–Carlo approximation to the ML Time–delay Estimator in a multipath channel," in *Proceedings of the* 7^{th} *IEEE International Workshop on Signal Processing Advances for Wireless Communications, SPAWC 2006*, Cannes, France, July 2006.

  [Clo06e] P. Closas, C. Fernández-Prades, J. A. Fernández-Rubio, and A. Ramírez-González, "Multipath Mitigation using Particle Filtering," in *Proceedings of the ION GNSS 2006*, Fort Worth, TX, September 2006.

Appendix 3.A Useful equalities

The Chapman-Kolmogorov equation

Conditional densities can be manipulated in order to obtain more tractable expressions by removing some variables. Denote some random variables as x_1, x_2 and x_3. If we want to remove x_2 from the joint pdf $f(x_1, x_2|x_3)$, we integrate with respect to this variable,

$$f(x_1|x_3) = \int_{-\infty}^{\infty} f(x_1|x_2, x_3)dx_2 \ . \tag{3.111}$$

On the other hand, if x_2 has to be removed from $f(x_1|x_2, x_3)$, the *Chapman-Kolmogorov* equation [Pap01] is extensively used:

$$f(x_1|x_3) = \int_{-\infty}^{\infty} f(x_1, x_2|x_3)f(x_2|x_3)dx_2 \ . \tag{3.112}$$

The Bayes' rule

Bayes' rule [Bay63] states that the probability density function of an event x conditioned to the event y can be expressed as

$$f(x|y) = \frac{p(y|x)p(x)}{p(y)} \ , \tag{3.113}$$

where the denominator can be computed using the *Total probability theorem*:

$$f(y) = \int_{-\infty}^{\infty} p(y|x)p(x)dx \ . \tag{3.114}$$

Appendix 3.B The Unscented Transform

The UT was introduced in [Jul02a, Jul02b, Jul04] and it is a key process in the UKF algorithm. The UT aims at computing the statistics of a *r.v.* at the output of a nonlinear system. At a glance, the UT deterministically selects a set of points of the *r.v.* of interest, referred to as *sigma points*, and propagates the set through the nonlinear transformation. Based on the output points, the UT proposes a mean and a covariance matrix for the resulting transformed distribution. Notice that the UT differs from a Monte-Carlo approach in the sense that the process is deterministic, whereas in the latter each realization yields to different a result.

Consider $\mathbf{a}$, a *r.v.* whose mean is denoted by $\bar{\mathbf{a}}$ and covariance $\mathbf{P}_a$. We would like to calculate the resulting mean and covariance matrix at the output of a nonlinear process $f(\cdot)$ of the transformed *r.v.* $\mathbf{b}$ using the UT. Taking into account that $f : \mathbb{R}^{n_a} \longmapsto \mathbb{R}^{n_a}$, the UT generates $2n_a + 1$ sample points selected deterministically such that the mean and covariance of $\mathbf{a}$ is completely captured. The i–th sigma point and its weight is denoted by $\mathcal{A}_i$ and $\mathcal{W}_i$, respectively. A selection scheme that achieves such mean/covariance characterization is:

$$\begin{aligned} \mathcal{A}_0 &= \bar{\mathbf{a}} \\ \mathcal{A}_i &= \bar{\mathbf{a}} + \sqrt{(n_a+\kappa)\,[\mathbf{P}_a]_{i,:}} \qquad i = 1,\ldots,n_a \\ \mathcal{A}_i &= \bar{\mathbf{a}} - \sqrt{(n_a+\kappa)\,[\mathbf{P}_a]_{i,:}} \qquad i = n_a+1,\ldots,2n_a \end{aligned} \tag{3.115}$$

where κ is a tunable scaling parameter such that $\kappa + n_a \neq 0$. A common choice is $\kappa = \kappa_1^2(n_a + \kappa_2) - n_a$, where κ_1 is a positive scaling parameter which can be made arbitrarily small to minimize higher order effects (*e.g.* 10^{-3}). κ_1 determines the spread of the sigma points around $\bar{\mathbf{a}}$. κ_2 is a secondary parameter usually set to 0. The weights associated the points in (3.115) are:

$$\begin{aligned} \mathcal{W}_0 &= \frac{\kappa}{n_a+\kappa} \\ \mathcal{W}_i &= \frac{0.5}{n_a+\kappa} \qquad i = 1,\ldots,n_a \\ \mathcal{W}_i &= \frac{0.5}{n_a+\kappa} \qquad i = n_a+1,\ldots,2n_a \end{aligned} \tag{3.116}$$

satisfying that $\sum_{i=0}^{2n_a} \mathcal{W}_i = 1$, i.e., weights are normalized.

Actually, the sigma points in (3.115) used to characterize the mean and covariance are the mean itself and a set of points located around it and controlled by the elements

in matrix $\mathbf{P}_a$. Intuitively, the objective of parameter κ is to adjust the distance among the generated sigma points and the mean. Therefore, if the dimension of the SS model increases, the distance increases also increases which forces the transform to take into account non-local effects.

In order to characterize the resulting *r.v.* after the nonlinear system, each of the generated sigma points are propagated through $f(\cdot)$,

$$\mathcal{B}_i = f\left(\mathcal{A}_i\right) \ , \tag{3.117}$$

obtaining $2n_a + 1$ sample points that are used to characterize the transformed mean and covariance of the new *r.v.* as

$$\begin{aligned} \bar{\mathbf{b}} &= \sum_{i=0}^{2n_a} \mathcal{W}_i \mathcal{B}_i \\ \mathbf{P}_b &= \sum_{i=0}^{2n_a} \mathcal{W}_i \left(\mathcal{B}_i - \bar{\mathbf{b}}\right)\left(\mathcal{B}_i - \bar{\mathbf{b}}\right)^T \ , \end{aligned} \tag{3.118}$$

respectively. The latter expressions are an accurate approximation of the first and second order statistics of the resulting stochastic process at the output of a process $f(\cdot)$ for an input $\mathbf{a}$.

To sum up, the sigma points completely capture the true mean and covariance of the Gaussian *r.v.*, and when propagated through a nonlinear system, the transformed points also capture the posterior mean and covariance accurately up to third order for any nonlinearity.

Appendix 3.C Selection of Importance Density using Laplace's approximation

The idea behind the choice of $\pi(\boldsymbol{\tau}_k|\boldsymbol{\tau}_{k-1}, \mathbf{x}_k) \propto p(\mathbf{x}_k|\boldsymbol{\tau}_k)p(\boldsymbol{\tau}_k|\boldsymbol{\tau}_{k-1})$ in equation (3.96) is that if both likelihood and prior distributions are unimodal and Gaussian, the resulting importance density is also unimodal and Gaussian. Furthermore, analytical expressions for its mean and covariance can be derived from those of $p(\mathbf{x}_k|\boldsymbol{\tau}_k)$ and $p(\boldsymbol{\tau}_k|\boldsymbol{\tau}_{k-1})$. In our application the prior pdf is already Gaussian and unimodal, but the likelihood has to be approximated. The latter is done using Laplace's method, which yields analytical Gaussian approximations of densities from a Taylor series expansion at the mode of the density ($\bar{\boldsymbol{\tau}}_k$). Considering second order terms, the log-likelihood can be approximated as

$$\begin{aligned} \mathcal{L}(\boldsymbol{\tau}_k) &\triangleq \ln p(\mathbf{x}_k|\boldsymbol{\tau}_k) \\ &\approx \mathcal{L}|_{\bar{\boldsymbol{\tau}}_k} + \frac{1}{2}(\boldsymbol{\tau}_k - \bar{\boldsymbol{\tau}}_k)^T \mathcal{H}_\tau(\mathcal{L})|_{\bar{\boldsymbol{\tau}}_k} (\boldsymbol{\tau}_k - \bar{\boldsymbol{\tau}}_k) \ , \end{aligned} \tag{3.119}$$

where we have recognized that $\nabla_\tau(\mathcal{L})|_{\bar{\boldsymbol{\tau}}_k} = \mathbf{0}$, since it is being evaluated at the mode. Identifying terms in (3.119), the following Gaussian approximation of the likelihood function arises

$$p(\mathbf{x}_k|\boldsymbol{\tau}_k) \approx \mathcal{N}\left(\bar{\boldsymbol{\tau}}_k, \widehat{\boldsymbol{\Sigma}}_k\right) \ , \tag{3.120}$$

where the mode, $\bar{\boldsymbol{\tau}}_k$, and the inverse Hessian evaluated at the mode, i.e., $\widehat{\boldsymbol{\Sigma}}_k = \mathcal{H}_\tau^{-1}(\mathcal{L})|_{\bar{\boldsymbol{\tau}}_k}$, are its mean and covariance respectively.

Hence, the importance density is Gaussian and can be obtained as the result of a product of Gaussians:

$$\begin{aligned} \pi(\boldsymbol{\tau}_k|\boldsymbol{\tau}_{k-1}, \mathbf{x}_k) &\propto p(\mathbf{x}_k|\boldsymbol{\tau}_k)p(\boldsymbol{\tau}_k|\boldsymbol{\tau}_{k-1}) \\ &= \mathcal{N}\left(\bar{\boldsymbol{\tau}}_k, \widehat{\boldsymbol{\Sigma}}_k\right) \mathcal{N}\left(\mathbf{F}_{\tau,k}\boldsymbol{\tau}_{k-1}, \boldsymbol{\Sigma}_{\tau,k}\right) \end{aligned} \tag{3.121}$$

and $\pi(\boldsymbol{\tau}_k|\boldsymbol{\tau}_{k-1}, \mathbf{x}_k)$ can also be expressed as $\mathcal{N}\left(\boldsymbol{\mu}_\pi, \boldsymbol{\Sigma}_\pi\right)$, being the problem to analytically obtain $\boldsymbol{\mu}_\pi$ and $\boldsymbol{\Sigma}_\pi$.

Taking logarithms and neglecting additive constants, we can express (3.121) as

$$\begin{aligned} \ln\left(\mathcal{N}\left(\boldsymbol{\mu}_\pi, \boldsymbol{\Sigma}_\pi\right)\right) &\propto \frac{1}{2}(\boldsymbol{\tau}_k - \bar{\boldsymbol{\tau}}_k)^T \widehat{\boldsymbol{\Sigma}}_k^{-1}(\boldsymbol{\tau}_k - \bar{\boldsymbol{\tau}}_k) \\ &+ \frac{1}{2}(\boldsymbol{\tau}_k - \mathbf{F}_{\tau,k}\boldsymbol{\tau}_{k-1})^T \boldsymbol{\Sigma}_{\tau,k}^{-1}(\boldsymbol{\tau}_k - \mathbf{F}_{\tau,k}\boldsymbol{\tau}_{k-1}) \ , \end{aligned} \tag{3.122}$$

which can be reorganized, neglecting the multiplicative constant, as

$$\begin{aligned}\ln\left(\mathcal{N}\left(\boldsymbol{\mu}_\pi, \boldsymbol{\Sigma}_\pi\right)\right) \propto\ & \boldsymbol{\tau}_k^T \left(\widehat{\boldsymbol{\Sigma}}_k^{-1} + \boldsymbol{\Sigma}_{\tau,k}^{-1}\right) \boldsymbol{\tau}_k \\ -\ & \boldsymbol{\tau}_k^T \left(\widehat{\boldsymbol{\Sigma}}_k^{-1} \bar{\boldsymbol{\tau}}_k + \boldsymbol{\Sigma}_{\tau,k}^{-1} \mathbf{F}_{\tau,k} \boldsymbol{\tau}_{k-1}\right) \\ -\ & \left(\widehat{\boldsymbol{\Sigma}}_k^{-1} \bar{\boldsymbol{\tau}}_k + \boldsymbol{\Sigma}_{\tau,k}^{-1} \mathbf{F}_{\tau,k} \boldsymbol{\tau}_{k-1}\right)^T \boldsymbol{\tau}_k \\ +\ & \left(\bar{\boldsymbol{\tau}}_k^T \widehat{\boldsymbol{\Sigma}}_k^{-1} \bar{\boldsymbol{\tau}}_k + \boldsymbol{\tau}_{k-1}^T \mathbf{F}_{\tau,k}^T \boldsymbol{\Sigma}_{\tau,k}^{-1} \mathbf{F}_{\tau,k} \boldsymbol{\tau}_{k-1}\right) , \end{aligned} \tag{3.123}$$

yielding to

$$\begin{aligned}\boldsymbol{\tau}_k^T \boldsymbol{\Sigma}_\pi^{-1} \boldsymbol{\tau}_k &= \boldsymbol{\tau}_k^T \left(\widehat{\boldsymbol{\Sigma}}_k^{-1} + \boldsymbol{\Sigma}_{\tau,k}^{-1}\right) \boldsymbol{\tau}_k \\ \boldsymbol{\tau}_k^T \boldsymbol{\Sigma}_\pi^{-1} \boldsymbol{\mu}_\pi &= \boldsymbol{\tau}_k^T \left(\widehat{\boldsymbol{\Sigma}}_k^{-1} \bar{\boldsymbol{\tau}}_k + \boldsymbol{\Sigma}_{\tau,k}^{-1} \mathbf{F}_{\tau,k} \boldsymbol{\tau}_{k-1}\right) \\ \boldsymbol{\mu}_\pi^T \boldsymbol{\Sigma}_\pi^{-1} \boldsymbol{\tau}_k &= \left(\widehat{\boldsymbol{\Sigma}}_k^{-1} \bar{\boldsymbol{\tau}}_k + \boldsymbol{\Sigma}_{\tau,k}^{-1} \mathbf{F}_{\tau,k} \boldsymbol{\tau}_{k-1}\right)^T \boldsymbol{\tau}_k \\ \boldsymbol{\mu}_\pi^T \boldsymbol{\Sigma}_\pi^{-1} \boldsymbol{\mu}_\pi &= \left(\bar{\boldsymbol{\tau}}_k^T \widehat{\boldsymbol{\Sigma}}_k^{-1} \bar{\boldsymbol{\tau}}_k + \boldsymbol{\tau}_{k-1}^T \mathbf{F}_{\tau,k}^T \boldsymbol{\Sigma}_{\tau,k}^{-1} \mathbf{F}_{\tau,k} \boldsymbol{\tau}_{k-1}\right) . \end{aligned} \tag{3.124}$$

From the latter, it is lengthy (but straightforward) to obtain the mean and covariance of the Gaussian importance density in (3.121):

$$\begin{aligned}\boldsymbol{\mu}_\pi &= \boldsymbol{\Sigma}_\pi \left(\widehat{\boldsymbol{\Sigma}}_k^{-1} \bar{\boldsymbol{\tau}}_k + \boldsymbol{\Sigma}_{\tau,k}^{-1} \mathbf{F}_{\tau,k} \boldsymbol{\tau}_{k-1}\right) \\ \boldsymbol{\Sigma}_\pi &= \left(\widehat{\boldsymbol{\Sigma}}_k^{-1} + \boldsymbol{\Sigma}_{\tau,k}^{-1}\right)^{-1} , \end{aligned} \tag{3.125}$$

respectively.

This result is obtained under the assumption that $\bar{\boldsymbol{\tau}}_k \approx \mathbf{F}_{\tau,k} \boldsymbol{\tau}_{k-1}$, such that the equality for $\boldsymbol{\mu}_\pi^T \boldsymbol{\Sigma}_\pi^{-1} \boldsymbol{\mu}_\pi$ in (3.124) holds. The latter is reasonable since the evolution of the parameter is supposed to be small compared to the observation interval of K samples.

Appendix 3.D Gradient and Hessian of $\Lambda_k^r(\boldsymbol{\tau}_k)$

This Appendix is devoted to the derivation of the Gradient and the Hessian of the cost function:

$$\Lambda_k^r(\boldsymbol{\tau}_k) = \| \boldsymbol{\Pi}_k^{\perp}\mathbf{x}_k \|^2 + (\boldsymbol{\tau}_k - \boldsymbol{\mu}_r)^T \boldsymbol{\Sigma}_r^{-1}(\boldsymbol{\tau}_k - \boldsymbol{\mu}_r) \ , \tag{3.126}$$

as defined in (3.102). These operators are required in the Newton-Raphson algorithm run to obtain the importance density in Laplace's PF.

The expressions for the Gradient and the Hessian of $\Lambda_k^r(\boldsymbol{\tau}_k)$ can be obtained as

$$\begin{aligned} \nabla_\tau(\Lambda_k^r) &= -\mathbf{x}_k^H \nabla_\tau(\boldsymbol{\Pi}_k(\boldsymbol{\tau}_k))\mathbf{x}_k + \boldsymbol{\Sigma}_r^{-1}(\boldsymbol{\tau}_k - \boldsymbol{\mu}_r) \\ \mathcal{H}_\tau(\Lambda_k^r) &= -\mathbf{x}_k^H \mathcal{H}_\tau(\boldsymbol{\Pi}_k(\boldsymbol{\tau}_k))\mathbf{x}_k + \boldsymbol{\Sigma}_r^{-1} \ , \end{aligned} \tag{3.127}$$

respectively. The first terms in the expressions in (3.127) are obtained taking into account the definition of the orthogonal complement of a projection matrix. Then, the problem of computing $\nabla_\tau(\Lambda_k^r)$ and $\mathcal{H}_\tau(\Lambda_k^r)$ is solved after obtaining $\nabla_\tau(\boldsymbol{\Pi}_k)$ and $\mathcal{H}_\tau(\boldsymbol{\Pi}_k)$. In the sequel, we provide some guides to analytically obtain these expressions.

From the definition of the Projection matrix $\boldsymbol{\Pi}_k \triangleq \mathbf{H}_k(\mathbf{H}_k^H\mathbf{H}_k)^{-1}\mathbf{H}_k^H$ it arises, after lengthy but straightforward mathematical manipulation, that its Gradient and Hessian respectively are

$$\begin{aligned} \nabla_\tau(\boldsymbol{\Pi}_k) &= \boldsymbol{\Pi}_k^{\perp}\nabla_\tau(\mathbf{H}_k)\mathbf{H}_k^{\dagger} + \left(\boldsymbol{\Pi}_k^{\perp}\nabla_\tau(\mathbf{H}_k)\mathbf{H}_k^{\dagger}\right)^H \\ \mathcal{H}_\tau(\boldsymbol{\Pi}_k) &= \nabla_\tau(\boldsymbol{\Pi}_k^{\perp})\nabla_\tau(\mathbf{H}_k)\mathbf{H}_k^{\dagger} + \boldsymbol{\Pi}_k^{\perp}\mathcal{H}_\tau(\mathbf{H}_k)\mathbf{H}_k^{\dagger} \\ &+ \boldsymbol{\Pi}_k^{\perp}\nabla_\tau(\mathbf{H}_k)\nabla_\tau(\mathbf{H}_k^{\dagger}) + \Big(\nabla_\tau(\boldsymbol{\Pi}_k^{\perp})\nabla_\tau(\mathbf{H}_k)\mathbf{H}_k^{\dagger} \\ &+ \boldsymbol{\Pi}_k^{\perp}\mathcal{H}_\tau(\mathbf{H}_k)\mathbf{H}_k^{\dagger} + \boldsymbol{\Pi}_k^{\perp}\nabla_\tau(\mathbf{H}_k)\nabla_\tau(\mathbf{H}_k^{\dagger})\Big)^H \ , \end{aligned} \tag{3.128}$$

where $\boldsymbol{\Pi}_k^{\perp} \triangleq \mathbf{I} - \boldsymbol{\Pi}_k$ and thus $\nabla_\tau(\boldsymbol{\Pi}_k^{\perp}) = -\nabla_\tau(\boldsymbol{\Pi}_k)$. A detailed derivation of the expressions in (3.128) can be found in [FP06, p. 96-98] and [Ott93], where a similar problem was addressed. An interested reader is referred to this reference for further details.

For the sake of clarity, we introduced the Moore-Penrose pseudoinverse in the notation

$$\mathbf{H}_k^{\dagger} \triangleq (\mathbf{H}_k^H\mathbf{H}_k)^{-1}\mathbf{H}_k^H, \tag{3.129}$$

whose Gradient can be obtained as

$$\nabla_\tau(\mathbf{H}_k^{\dagger}) = (\mathbf{H}_k^H\mathbf{H}_k)^{-1}\nabla_\tau(\mathbf{H}_k)^H\boldsymbol{\Pi}_k^{\perp} - \mathbf{H}_k^{\dagger}\nabla_\tau(\mathbf{H}_k)\mathbf{H}_k^{\dagger} \ . \tag{3.130}$$

Thus, after obtaining $\nabla_\tau(\mathbf{H}_k)$ and $\mathcal{H}_\tau(\mathbf{H}_k)$, the expressions in equation (3.128) can be evaluated from which one is able to compute $\nabla_\tau(\Lambda_k^r)$ and $\mathcal{H}_\tau(\Lambda_k^r)$ in (3.127). The derivation of the required expressions is provided in Appendix 3.E.

Appendix 3.E Gradient and Hessian of matrix $\mathbf{H}_k$

As showed in Appendix 3.D, the computation of $\nabla_\tau(\Lambda_k^r)$ and $\mathcal{H}_\tau(\Lambda_k^r)$ requires obtaining $\nabla_\tau(\mathbf{H}_k)$ and $\mathcal{H}_\tau(\mathbf{H}_k)$. This is the aim of this appendix.

First, we note that $\nabla_\tau(\mathbf{H}_k)$ can be decomposed as the derivative with respect to each element of $\boldsymbol{\tau}$

$$\nabla_\tau(\mathbf{H}_k) = \begin{bmatrix} \nabla_{\tau_0}(\mathbf{H}_k) \\ \vdots \\ \nabla_{\tau_{M-1}}(\mathbf{H}_k) \end{bmatrix} \tag{3.131}$$

and recalling that $\mathbf{H}_k \triangleq \mathbf{Q}_k^T(\boldsymbol{\tau}_k)$, where $\mathbf{Q}_k$ is defined as the basis function matrix in equation (3.76).

Then, the Gradient of $\mathbf{H}_k$ with respect to the i-th element of $\boldsymbol{\tau}$ is

$$\nabla_{\tau_i}(\mathbf{H}_k) = \begin{pmatrix} \mathbf{0} & \nabla_{\tau_i}(q_i((k-1)K+1;\tau_{i,k})) & \mathbf{0} \\ \vdots & \vdots & \vdots \\ \mathbf{0} & \nabla_{\tau_i}(q_i(kK;\tau_{i,k})) & \mathbf{0} \end{pmatrix} , \tag{3.132}$$

whose dimensions are $K \times M$ and

$$\nabla_{\tau_i}(q_i(k';\tau_{i,k})) = -\dot{q}_i(k';\tau_{i,k}) , \tag{3.133}$$

where $\dot{q}_i(k';\tau_{i,k})$ stands for the *d*erivative *o*f *t*ime of waveform $q_i(t;\tau_{i,k})$ evaluated at instant k'.

Similarly, the Hessian of $\mathbf{H}_k$ is defined as

$$\mathcal{H}_\tau(\mathbf{H}_k) = \begin{pmatrix} \triangle_{\tau_0}^{\tau_0}(\mathbf{H}_k) & \dots & \triangle_{\tau_{M-1}}^{\tau_0}(\mathbf{H}_k) \\ \vdots & \ddots & \vdots \\ \triangle_{\tau_{M-1}}^{\tau_0}(\mathbf{H}_k) & \dots & \triangle_{\tau_{M-1}}^{\tau_{M-1}}(\mathbf{H}_k) \end{pmatrix} , \tag{3.134}$$

where

$$\begin{aligned} \triangle_{\tau_i}^{\tau_j}(\mathbf{H}_k) &= \mathbf{0} \quad , \forall i \neq j \\ \triangle_{\tau_i}^{\tau_i}(\mathbf{H}_k) &= \begin{pmatrix} \mathbf{0} & \triangle_{\tau_i}^{\tau_i}(q_i((k-1)K+1;\tau_{i,k})) & \mathbf{0} \\ \vdots & \vdots & \vdots \\ \mathbf{0} & \triangle_{\tau_i}^{\tau_i}(q_i(kK;\tau_{i,k})) & \mathbf{0} \end{pmatrix} \end{aligned} \tag{3.135}$$

and

$$\triangle_{\tau_i}^{\tau_i}(q_i(k';\tau_{i,k})) = \ddot{q}_i(k';\tau_{i,k}) , \tag{3.136}$$

$\ddot{q}_i(k';\tau_{i,k})$ standing for the second *d*erivative *o*f *t*ime of waveform $q_i(t;\tau_{i,k})$ evaluated at instant k'.

4

Direct Position Estimation

DIVIDE and Conquer. This is the approach taken in many signal processing applications due to its ability to split complex mathematical problems in several problems of reduced complexity. In addition, this methodology allows the exploitation of parallel structures in hardware architectures; or make use of concurrency and multithreading scheduling when designing under the Software-Defined Radio (SDR) paradigm. The design of GNSS receivers provides one of the clearest examples of this approach. Ultimately, the aim of a GNSS receiver is to estimate its position, based on the signals emitted by a constellation of satellites. As discussed in Chapter 2, the estimation is composed of two steps: synchronization and trilateration. At a glance, the receiver computes its relative distance to each visible satellite from the estimated synchronization parameters (time-delays and Doppler-shifts, gathered in vectors $\boldsymbol{\tau}$ and $\mathbf{f}_d$ respectively) and uses these distances to calculate its position $\mathbf{p}$ through solving a geometrical problem. This methodology (depicted in the upper diagram of Figure 4.1) has been widespread used in the design of GNSS receivers and, thus, we refer to it as the *conventional approach* to GNSS positioning.

The conventional approach is computationally affordable and a number of algorithms can be found in the literature to estimate synchronization parameters, refer to Chapter 2. However, [Par96] pointed out some of its drawbacks:

- The estimation errors committed in $\hat{\boldsymbol{\tau}}$ are propagated to the next step, the position calculation. These estimates can be severely distorted by a number of effects, as

seen in Chapter 2. One of these sources of error is the multipath propagation, which introduces a bias relatively large under coherent multipath. Chapter 3 proposed an algorithm to mitigate this effect, however, we saw that there is still a remaining error which is indeed propagated to the positioning algorithm. It is not evident how these errors are propagated when transformed by the nonlinear system of equations that yield to the position calculation, but it seems clear that little can be done at that point when observables are corrupted. Chapter 5 will treat the transformation of synchronization errors into positioning errors.

- The conventional approach requires independent and uncoupled estimators for each channel (satellite). The implications are twofold. On the one hand, the implementation of such approach requires replicate hardware or software structures. On the other hand, the approach does not take into consideration possible dependencies among channels, which could improve the estimation performance.

- Related to the previous point, a GNSS receiver can have a minimum of 8–12 parallel channels. Since the ultimate parameter of interest is the PVT solution (i.e., position, velocity and time defined in a three dimensional space), it seems that there exists a possible redundancy because the receiver estimates in a higher dimensional parameter space (code and carrier phase for each channel). Thus, the conventional approach increases the dimensionality of the problem with respect to the one strictly (and theoretically) required.

- The use of prior information is not straightforward when dealing with synchronization parameters. From Chapter 3, one can conclude that a number of Bayesian filters can be used to track and estimate synchronization parameters, but the state-space evolution of these time-varying parameters is not evident and many alternatives exist. The model proposed in Section 3.3.2 is a useful simplification of reality, but more realistic SS models would require expensive test-field campaigns [Ste04] and the ability of the algorithm to discern among a number of synchronization evolution models depending on the dynamics of the receiver. This is by far more difficult than considering prior information when the parameter of interest is user's position itself, where the physical meaning of the parameter helps the inclusion of side information as will be seen in Section 4.8.

- Although the cross-correlation properties of spreading sequences used in GNSS signals provide a rather high processing gain, there is indeed a remaining Multiple Access Interference (MAI) that is not combated in conventional receivers (cf. Chapter 2). To overcome such limitation, one could incorporate multiple access techniques [Vit95] to GNSS receivers, jointly processing signals from different satellites [Ilt94].

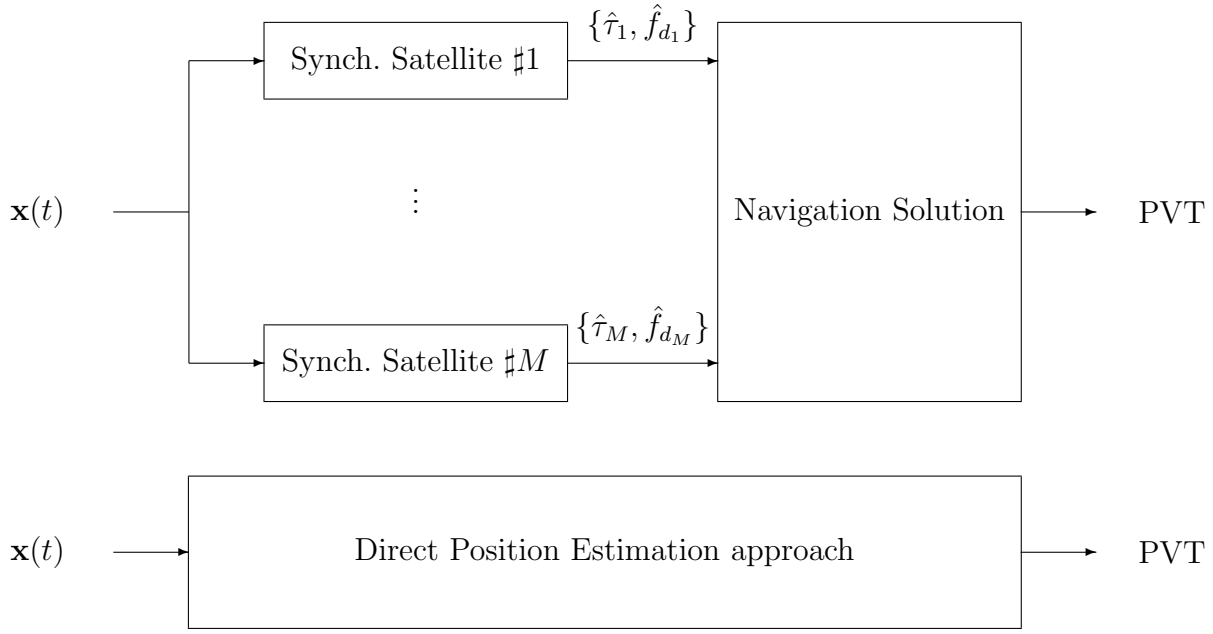

Figure 4.1: Block diagram comparing the operation of a conventional GNSS receiver and the proposed Direct Position Estimation approach.

This dissertation proposes to avoid the two-steps position calculation in order to overcome the above drawbacks. The chapter presents what is referred to as the Direct Position Estimation (DPE) approach. DPE takes a different approach to the positioning problem. DPE focuses on the estimation (directly from the received and sampled IF signal, $\mathbf{x}(t)$) of position coordinates, which are indeed the parameters of interest to the end-user. The avoidance of intermediate estimation steps will be seen to help to partially overcome some limitations of the conventional approach, such as the degradation in position accuracy due to multipath and severe channel fading conditions. The lower diagram in Figure 4.1 shows the conceptual operation, as compared to the conventional receiver in the upper side.

The chapter is organized as follows. Section 4.1 presents the DPE concept and a motivation for its use consisting in proving that the two-steps approach cannot overcome the performance of a direct estimation. The latter is a general result, which applied to the GNSS case justifies the design of receivers under the DPE framework. Section 4.2 describes the signal model considered along the discussion. Two main differences exist between this model and the one considered in Chapter 3. On the one hand, the model in Chapter 3 accounted for the LOSS of a given satellite and $M-1$ multipath replicas. In contrast, the signal model in Section 4.2 explicitly describes the LOSSs of all visible satellites and does not consider multipath replicas, implicitly included in the noise term. In this case, we use M to denote the number of visible satellites. Notice that we are not using the notation M_s, as introduced in Chapter 2, for the sake of clarity. On the other

hand, this chapter assumes the more general receiver composed of an antenna array front-end. The optimal position estimation under the ML criterion is discussed in Section 4.3, whose asymptotical efficiency is proved. In Section 4.4 a comparison between DPE and conventional approaches is provided. Section 4.5 presents the concept of *position-based synchronization*, which considers the extraction of synchronization parameters from the estimated position under the DPE framework. Position-based synchronization proposes a synchronization methodology which is the other way around of the conventional approach. A number of algorithms to implement the ML estimator of position in a SDR receiver are discussed in Section 4.6. Recalling that the final objective for proposing a DPE framework to design GNSS receivers is the inclusion of prior information in a natural way, Section 4.8 presents the Bayesian counterpart of DPE. This is referred to as the Bayesian Direct Position Estimation (BDPE) in the sequel. Finally, at the light of the DPE framework, previous related work is exposed and discussed. Thus, Section 4.10 provides some insight to other work that share the idea of a direct position estimation.

4.1 Direct Position Estimation approach: background and motivation

Although the conventional two-steps position determination is the approach taken traditionally, it is seen to have a number of drawbacks. In contrast, DPE proposes an alternative where the estimation of user's position is performed directly from the received and sampled signal. Thus, avoiding intermediate steps and jointly considering signals from all satellites when estimating $\mathbf{p}$.

Both approaches are illustrated in Figure 4.1. The conventional approach (upper diagram) was discussed in Chapter 2, consisting in a two-steps procedure:

1. **Estimation of synchronization parameters.** The receiver is equipped with a number of tracking channels, in charge of estimating both time-delays and Doppler-shifts of the acquired satellites. In general, this estimation is performed independently among channels by a bank of Delay/Phase Lock Loops or more sophisticated signal processing techniques.. We denote as τ_i and f_{d_i} the delay and Doppler deviation of the i-th satellite, being the i-th entries in vectors $\boldsymbol{\tau}$ and $\mathbf{f}_d$ respectively.

2. **Position calculation.** As discussed in Chapter 2, these estimates provide a measure of the relative distance between the receiver an each satellite. Then, an estimate of the receiver's position is obtained by solving a geometrical problem, referred to as trilateration. This is typically done relying on LS or WLS algorithms.

The lower diagram in Figure 4.1 shows the conceptual idea of DPE approach: merging the two-steps approach into a single estimation problem. DPE addresses some of the inherent drawbacks of the conventional two-steps approach. The dependencies between channels are efficiently exploited, in the sense that signals from visible satellites are jointly processed to obtain user's position (which is the common driving parameter of these signals). Due to the joint processing of satellite signals, MAI is also optimally mitigated.

A recent result in [Ama08b] provides the means to show that the conventional two-steps approach cannot overcome the performance of DPE. This interesting result is the core of Proposition 4.1.

Proposition 4.1. *Let* $\boldsymbol{\upsilon} \in \Upsilon \subset \mathbb{R}^{n_\upsilon}$ *and* $\boldsymbol{\gamma} \in \Gamma \subset \mathbb{R}^{n_\gamma}$ *be two unknown parameters s.t. there exist an injective function* $g(\cdot) : \Gamma \longmapsto \Upsilon$,

$$\boldsymbol{\upsilon} = g(\boldsymbol{\gamma}) \ , \forall \boldsymbol{\gamma} \in \Gamma \tag{4.1}$$

that relates both. Function $g(\cdot)$ *has a unique inverse mapping*

$$\boldsymbol{\gamma} = g^{-1}(\boldsymbol{\upsilon}) \ , \forall \boldsymbol{\upsilon} \in \bar{\Upsilon} \tag{4.2}$$

under the subset $\bar{\Upsilon} = \{\boldsymbol{\upsilon} \mid \boldsymbol{\upsilon} = g(\boldsymbol{\gamma}), \forall \boldsymbol{\gamma} \in \Gamma\} \subset \Upsilon$.

Denote by $\hat{\boldsymbol{\gamma}}_1$ *and* $\hat{\boldsymbol{\gamma}}_2$ *the* K*-samples estimators of* $\boldsymbol{\gamma}$ *based on single–step and two–steps approaches, respectively. Similarly,* $\boldsymbol{\Sigma}(\hat{\boldsymbol{\gamma}}_1)$ *and* $\boldsymbol{\Sigma}(\hat{\boldsymbol{\gamma}}_2)$ *represent the covariance matrix of each estimator.*

Then,

$$\mathbf{C} \triangleq \lim_{K \to \infty} \left(\boldsymbol{\Sigma}(\hat{\boldsymbol{\gamma}}_2) - \boldsymbol{\Sigma}(\hat{\boldsymbol{\gamma}}_1) \right) \tag{4.3}$$

is a positive semidefinite matrix.

Proof. See Appendix 4.A. □

Proposition 4.1 provides the mathematical justification to the DPE approach. Roughly speaking, the result means that the covariance of the two-steps approach cannot be smaller than the covariance of the one-step estimator [Clo09e]. Thus, the estimation performance of the conventional approach can only be, at most, equal than the one provided by the DPE approach, in the MSE sense. The latter claim is stated in Corollary 4.1, for the sake of clarity. This is a strong result that is the basis of DPE framework, as it opens the door to the design of future GNSS receivers with enhanced performance.

Corollary 4.1. *Direct Position Estimation approach outperforms conventional two-steps positioning, in the MSE sense.*

This chapter is devoted to the study and evaluation of DPE approach for GNSS receivers. Signal model, optimal estimator (in the ML sense), algorithms, architectures and inclusion of prior data is discussed, emphasizing the similarities and differences of the approach with respect to the conventional approach taken by GNSS receivers.

4.2 Signal Model

A GNSS antenna receives measurements which are considered to be a superposition of plane waves corrupted by noise and, possibly, interferences and multipath. An antenna receives M scaled, time–delayed and Doppler–shifted signals with known signal structure. Each signal correspond to the line-of-sight signal (LOSS) of one of the M visible satellites. The receiving complex baseband [Pro94] signal can be modeled as

$$x(t) = \sum_{i=1}^{M} a_i q_i(t - \tau_i) \exp\{j2\pi f_{d_i} t\} + n(t) \ , \tag{4.4}$$

where $q_i(t)$ is the transmitted complex baseband low–rate navigation signal spread by the pseudorandom code of the i–th satellite, considered known. a_i is its complex amplitude, τ_i is the time-delay, f_{d_i} the Doppler deviation and $n(t)$ represents zero-mean additive noise and other unmodeled terms. The model in (4.4) is obtained from (2.1)–(2.5) and (2.12) with $a_i = \alpha_i \exp\{j\phi_{i,0}\}$, $q_i(t) = q_{I,i}(t) + jq_{Q,i}(t)$ and only considering LOSS propagation.

In the multiple antenna receiver, an N element antenna array receives M scaled, time–delayed and Doppler–shifted signals with known structure. Each antenna element receives a replica of the complex baseband signal modeled by equation (4.4), with a different phase depending on the array geometry and the Directions Of Arrival (DOA) [Mon80, Joh93, Tre02]. Then, the single-snapshot model can be expressed in compact form as

$$\mathbf{x}(t) = \mathbf{G}(\boldsymbol{\theta}, \boldsymbol{\phi})\mathbf{A}\mathbf{d}(t, \boldsymbol{\tau}, \mathbf{f}_d) + \mathbf{n}(t) \tag{4.5}$$

where each row corresponds to one antenna and

- $\mathbf{x}(t) \in \mathbb{C}^{N\times 1}$ is the observed signal vector,
- $\mathbf{G}(\boldsymbol{\theta}, \boldsymbol{\phi}) \in \mathbb{C}^{N\times M}$ is the spatial signature matrix (see Appendix 4.B), related to the array geometry and the DOA of the impinging signals. $\boldsymbol{\theta}, \boldsymbol{\phi} \in \mathbb{R}^{M\times 1}$ stand for the azimuth and elevation vectors of the M sources, respectively,
- $\mathbf{A} \in \mathbb{C}^{M\times M}$ is a diagonal matrix with the elements of complex amplitude vector $\mathbf{a} = [a_1, \ldots, a_M]^T \in \mathbb{C}^{M\times 1}$ along its diagonal,

- $\boldsymbol{\tau}, \mathbf{f}_d \in \mathbb{R}^{M\times 1}$ are column vectors which contain time-delays and Doppler–shifts of each satellite,
- $\mathbf{d}(t, \boldsymbol{\tau}, \mathbf{f}_d) = [d_1(t), \ldots, d_M(t)]^T \in \mathbb{C}^{M\times 1}$, where each component is defined by

$$d_i(t) = q_i(t - \tau_i) \exp\{j2\pi f_{d_i} t\} \ ,$$

  the delayed Doppler–shifted narrowband signals envelopes, and
- $\mathbf{n}(t) \in \mathbb{C}^{N\times 1}$ represents additive noise and all other disturbing terms, like multipath of each signal or interferences. Statistically, this term is considered a zero-mean, complex, temporally white, circularly symmetric Gaussian vector process with an unknown arbitrary covariance matrix, $\boldsymbol{\Sigma}_n$. Thus, given two instants t_i and t_j, it holds that:

$$\begin{aligned} \mathbb{E}\{\mathbf{n}(t)\} &= \mathbf{0} \\ \mathbb{E}\{\mathbf{n}(t_i)\mathbf{n}^T(t_j)\} &= \mathbf{0} \\ \mathbb{E}\{\mathbf{n}(t_i)\mathbf{n}^H(t_j)\} &= \boldsymbol{\Sigma}_n \delta(t_i - t_j) \ . \end{aligned}$$

This model is built upon the *narrowband array assumption*, in which the time required for the signal to propagate along the array aperture is much smaller than the inverse of the signal bandwidth. Thus, a phase–shift can be used to describe the propagation from one antenna to another. For instance, current GPS L1 C/A navigation signals are reported to be emitted with a 20 MHz bandwidth [Ser06a], whose inverse is 50 nanoseconds or 15 meters in spatial terms. Therefore the array is expected to be much smaller, since the carrier wavelength is on the order of 20 centimeters, for the assumption to be reasonable. In the same way, we have assumed that the Doppler effect can be modeled by a frequency shift, which is commonly referred to as the *narrowband signal assumption* [Sto96]. This assumption is also reasonable provided that navigation systems are placed in the L band, with a carrier frequency on the order of 1 GHz, being much more larger than the signal bandwidth.

Consider that K snapshots of the impinging signal are taken at a suitable sampling rate f_s. Then, the sampled data can be expressed as[1]

$$\mathbf{X} = \mathbf{G}(\boldsymbol{\theta}, \boldsymbol{\phi})\mathbf{A}\mathbf{D}(\boldsymbol{\tau}, \mathbf{f}_d) + \mathbf{N} \tag{4.6}$$

[1]Rigorously, the model in (4.6) should be expressed as

$$\mathbf{X}_k = \mathbf{G}(\boldsymbol{\theta}_k, \boldsymbol{\phi}_k)\mathbf{A}_k\mathbf{D}(\boldsymbol{\tau}_k, \mathbf{f}_{d_k}) + \mathbf{N}_k \ ,$$

where the time dependence of the parameters is made explicit. However, for the sake of clarity, we have omitted the discrete time instant subscript k, since the parameters of interest are assumed piecewise constant during the observation interval. Thus, if not otherwise stated, the main problem is to estimated the deterministic and unknown parameters of the model.

using the following definitions:

- $\mathbf{X} = [\mathbf{x}(t_0), \ldots, \mathbf{x}(t_{K-1})] \in \mathbb{C}^{N \times K}$, referred to as the spatiotemporal data matrix.
- $\mathbf{D}(\boldsymbol{\tau}, \mathbf{f}_d) = [\mathbf{d}(t_0, \boldsymbol{\tau}, \mathbf{f}_d), \ldots, \mathbf{d}(t_{K-1}, \boldsymbol{\tau}, \mathbf{f}_d)] \in \mathbb{C}^{M \times K}$, known as the basis–function matrix.
- $\mathbf{N} = [\mathbf{n}(t_0), \ldots, \mathbf{n}(t_{K-1})] \in \mathbb{C}^{N \times K}$, a matrix containing all undesired contributions to $\mathbf{X}$. This matrix will be assumed having a Gaussian distribution, with zero mean, and with an arbitrary and unknown covariance matrix $\boldsymbol{\Sigma}_n$.
- $f_s = 1/T_s$, being $T_s = t_k - t_{k-1}$.

Notice that we assume that the parameters of interest of the model and the covariance matrix of the error are piecewise constant during the observation interval, i.e., they do not change in K/f_s seconds. However, small variations are allowed in the long term, i.e., among different observation windows. This assumption is reasonable in GNSS since this interval is on the order of tens of milliseconds and the variation of such parameters is typically much slower [Par96].

We can rearrange spatial signatures and complex amplitudes in an equivalent channel matrix $\mathbf{H} = \mathbf{G}(\boldsymbol{\theta}, \boldsymbol{\phi})\mathbf{A} + \mathbf{E}$, which is assumed arbitrary and unknown. The resulting unstructured spatial response model is given by

$$\mathbf{X} = \mathbf{H}\mathbf{D}(\boldsymbol{\tau}, \mathbf{f}_d) + \mathbf{N} \ , \tag{4.7}$$

where $\mathbf{H}$ takes into account possible mismodeling errors, gathered in matrix $\mathbf{E}$. Notice that the structure of matrix $\mathbf{H}$ is arbitrary, in contrast to $\mathbf{GA}$. The contribution of $\mathbf{E}$ is typically bounded, meaning that these errors are considered small. This is expressed as

$$\| \mathbf{E} \|_F \ \leq \epsilon \quad , \quad \epsilon > 0 \ . \tag{4.8}$$

The model in equation (4.7) is the approach taken hereinafter, which provides desirable advantages with respect to the structured model in (4.6):

- In many GNSS applications, it seems reasonable to consider that DOAs of impinging signals are a priori known. However, this knowledge implies that somewhat complex DOA estimation algorithms must be used and that a nearly perfect calibration is required. The latter presents a technological challenge and many possible sources of errors might jeopardize the operation of the algorithm [Swi98]. To name a few: errors in the antenna elements gain/phase measurements, unmodeled mutual coupling, quantization error (if a beamforming algorithm is used), environmental changes, mechanical modifications of the antenna hardware, etc.

- The above calibration errors are gathered in $\mathbf{H}$, which is treated as a channel matrix and estimated. This is possible because DOAs and amplitudes do not force $\mathbf{H}$ to have a certain structure, indeed its structure is arbitrary. The payback is its inability to estimate carrier phases, since the spatial reference is lost in the unstructured model case.

- It was seen in [FP06] that the asymptotical performance of an estimator based on the unstructured array model is the same as a solution based on (4.6). This is because synchronization and DOA parameters are uncoupled [Dog01, FP09a], meaning that theoretically an estimator of $\boldsymbol{\tau}$ and/or $\mathbf{f}_d$ does not require the knowledge of the angles $\boldsymbol{\theta}$ and $\boldsymbol{\phi}$. As a consequence, it is not only easier to implement the unstructured approach than the structured one, but asymptotically equivalent.

The signal model presented so far is valid for the conventional approach, where the incoming signal is parameterized by synchronization parameters. These parameters include time–delay and Doppler–shifts, which we gather in an unknown vector:

$$\boldsymbol{\upsilon} = \begin{bmatrix} \boldsymbol{\tau} \\ \mathbf{f}_d \end{bmatrix} , \tag{4.9}$$

for the sake of clarity.

DPE approach is based on a simple fact: synchronization parameters of each satellite can be expressed as functions of the same common parameters (including user position). After inspecting GNSS observables in (2.21) and (2.22), one can easily identify that

$$\begin{aligned} \boldsymbol{\tau} &\triangleq \boldsymbol{\tau}(\boldsymbol{\gamma}) \\ \mathbf{f}_d &\triangleq \mathbf{f}_d(\boldsymbol{\gamma}) \end{aligned} , \tag{4.10}$$

being $\boldsymbol{\gamma} \in \mathbb{R}^{n_\gamma}$ a vector gathering all considered motion parameters, whose simplest configuration is $\boldsymbol{\gamma} = \left[\mathbf{p}^T, \mathbf{v}^T, \delta t\right]^T$, i.e., receiver's position, velocity and clock bias respectively. However, DPE is a quite general approach and $\boldsymbol{\gamma}$ can include a plethora of parameters [BS01, Gus02]. Specifically, the i-th satellite's synchronization parameters can be written in terms of the elements of $\boldsymbol{\gamma}$ as:

$$\begin{aligned} c\tau_i &= \| \mathbf{p}_i - \mathbf{p} \| + c(\delta t - \delta t_i) \\ f_{d_i} &= -(\mathbf{v}_i - \mathbf{v})^T \frac{\mathbf{p}_i - \mathbf{p}}{\| \mathbf{p}_i - \mathbf{p} \|} \frac{f_c}{c} \end{aligned} , \tag{4.11}$$

with the definitions done in (2.21) and (2.22): $\mathbf{p}_i$ and $\mathbf{v}_i$ are the position and velocity of the i-th satellite; f_c is the carrier frequency; and c represents the speed of light.

Then, whereas equation (4.4) is a time-frequency parameterization of the incoming signals, the signal model considered in the DPE approach is parameterized by $\boldsymbol{\gamma}$. Considering (4.10), the received complex baseband is modeled as

$$x(t) = \sum_{i=1}^{M} a_i q_i(t - \tau_i(\boldsymbol{\gamma})) \exp\{j2\pi f_{d_i}(\boldsymbol{\gamma})\, t\} + n(t) \ , \tag{4.12}$$

being the DPE counterpart of the array model in (4.7)

$$\mathbf{X} = \mathbf{H}\mathbf{D}(\boldsymbol{\gamma}) + \mathbf{N}. \tag{4.13}$$

where the same definitions hold as in the conventional signal model. $\boldsymbol{\gamma}$ stands for the vector containing all considered position and motion parameters to be estimated in the Direct Position Estimation approach, as well as the receiver clock bias[2].

4.3 Maximum Likelihood Estimation of Position in GNSS receivers

Parameter estimation methods have been thoroughly covered in the literature [Leh83, Kay93]. The Maximum Likelihood (ML) principle presents an optimal paradigm to obtain a parameter estimator that asymptotically attain its lower variance bound, i.e., the Cramér-Rao Bound (CRB), as the number of samples goes to infinity. ML is based on the maximization of the distribution of measurements conditional on the value of the parameter. Thus, for a set of K recorded samples gathered in $\mathbf{x}$, the Maximum Likelihood Estimator (MLE) of a parameter $\boldsymbol{\xi}$ is the solution to

$$\hat{\boldsymbol{\xi}}_{\mathrm{ML}} = \arg\max_{\boldsymbol{\xi}} \{p(\mathbf{x}|\boldsymbol{\xi})\} \ . \tag{4.14}$$

Under mild regularity conditions, the asymptotical distribution (for large data sets) of the estimator satisfies that

$$\hat{\boldsymbol{\xi}}_{\mathrm{ML}} \sim \mathcal{N}\left(\boldsymbol{\xi}, \mathbf{J}_F^{-1}(\boldsymbol{\xi})\right) \ , \tag{4.15}$$

where $\mathbf{J}_F(\boldsymbol{\xi})$ is the Fisher Information Matrix (FIM) evaluated at the true value of parameter $\boldsymbol{\xi}$ – concepts developed in Section 5.1 –. Thus, the claim is that the MLE is

[2]It is important to keep in mind that, in the sequel, $\boldsymbol{\upsilon}$ is the vector containing time-delay and Doppler-shift of each visible satellite. Notice that $\boldsymbol{\upsilon}$ is the target parameter in the conventional positioning approach. In contrast, $\boldsymbol{\gamma}$ gathers all unknown parameters of the DPE approach, such as position, velocity or clock bias.

asymptotically efficient, i.e., it attains the lowest variance predicted by the CRB as K increases. The regularity conditions include the existence of the derivatives of the log-likelihood function and the FIM being non-zero. For further details and a rigorous proof, refer to [Kay93, Appendix 7.B].

This section provides the derivation of the MLE of position for the general case of an antenna array based receiver. For the particularization to the single antenna case, refer to Appendix 4.D. The asymptotical consistency of the MLE of position is proved in Appendix 4.E, considering both front-end architectures.

The derivation of the MLE of position is performed taking advantage of the invariance principle of ML estimates [Kay93]. Hence, first $\hat{\boldsymbol{\upsilon}}_{\mathrm{ML}}$ is computed [FP06] and then, using equations (2.21) and (2.22), $\hat{\boldsymbol{\gamma}}_{\mathrm{ML}}$ is obtained. This strategy is adopted in order to highlight the differences among both frameworks, being equivalent to a direct derivation of the MLE of $\boldsymbol{\gamma}$.

Applying the logarithm to the likelihood function of measurements in equation (4.7), and neglecting irrelevant additive and multiplicative constants, we obtain the negative log-likelihood function which depends on the unknown parameters of the model[3] $\boldsymbol{\Sigma}_n$, $\mathbf{H}$ and $\boldsymbol{\upsilon}$

$$\Lambda_1\left(\boldsymbol{\Sigma}_n, \mathbf{H}, \boldsymbol{\upsilon}\right) = \ln\left(\det\left(\boldsymbol{\Sigma}_n\right)\right) + \mathrm{Tr}\left(\boldsymbol{\Sigma}_n^{-1}\mathbf{C}\left(\mathbf{H}, \boldsymbol{\upsilon}\right)\right) \ , \tag{4.16}$$

being $\mathbf{C}\left(\mathbf{H}, \boldsymbol{\upsilon}\right)$ defined as

$$\mathbf{C}\left(\mathbf{H}, \boldsymbol{\upsilon}\right) = \frac{1}{K}\left(\mathbf{X} - \mathbf{H}\mathbf{D}(\boldsymbol{\upsilon})\right)\left(\mathbf{X} - \mathbf{H}\mathbf{D}(\boldsymbol{\upsilon})\right)^H . \tag{4.17}$$

With the following cross-correlation definitions

$$\begin{aligned} \hat{\mathbf{R}}_{xx} &= \frac{1}{K}\mathbf{X}\mathbf{X}^H & \hat{\mathbf{R}}_{xd}(\boldsymbol{\upsilon}) &= \frac{1}{K}\mathbf{X}\mathbf{D}^H(\boldsymbol{\upsilon}) \\ \hat{\mathbf{R}}_{dx}(\boldsymbol{\upsilon}) &= \hat{\mathbf{R}}_{xd}^H(\boldsymbol{\upsilon}) & \hat{\mathbf{R}}_{dd}(\boldsymbol{\upsilon}) &= \frac{1}{K}\mathbf{D}(\boldsymbol{\upsilon})\mathbf{D}^H(\boldsymbol{\upsilon}) \end{aligned} \tag{4.18}$$

equation (4.17) can be expressed as

$$\mathbf{C}\left(\mathbf{H}, \boldsymbol{\upsilon}\right) = \hat{\mathbf{R}}_{xx} - \hat{\mathbf{R}}_{xd}\mathbf{H}^H - \mathbf{H}\hat{\mathbf{R}}_{xd}^H + \mathbf{H}\hat{\mathbf{R}}_{dd}\mathbf{H}^H \ , \tag{4.19}$$

where we have omitted the dependence on $\boldsymbol{\upsilon}$ for the sake of clarity.

Thus, the joint ML estimate of $\boldsymbol{\Sigma}_n$, $\mathbf{H}$, and $\boldsymbol{\upsilon}$ is given by the minimization of the resulting cost function

$$\hat{\boldsymbol{\Sigma}}_{n,\mathrm{ML}}, \hat{\mathbf{H}}_{\mathrm{ML}}, \hat{\boldsymbol{\upsilon}}_{\mathrm{ML}} = \arg\min_{\boldsymbol{\Sigma}_n, \mathbf{H}, \boldsymbol{\upsilon}} \left\{\Lambda_1\left(\boldsymbol{\Sigma}_n, \mathbf{H}, \boldsymbol{\upsilon}\right)\right\} . \tag{4.20}$$

[3] where the trace property $\mathbf{z}^H\mathbf{B}\mathbf{z} = \mathrm{Tr}\left(\mathbf{B}\mathbf{z}\mathbf{z}^H\right)$ is used.

Using the following standard matrix calculus results

$$\begin{aligned} \frac{\delta \ln\left(\det\left(\mathbf{Z}\right)\right)}{\delta \mathbf{Z}} &= (\mathbf{Z}^{-1})^T = (\mathbf{Z}^T)^{-1} \\ \frac{\delta \operatorname{Tr}(\mathbf{Z}^{-1}\mathbf{B})}{\delta \mathbf{Z}} &= -\mathbf{Z}^{-1}\mathbf{B}\mathbf{Z}^{-1} \end{aligned} \tag{4.21}$$

we obtain the gradient of (4.16) with respect to the covariance matrix,

$$\frac{\delta \Lambda_1}{\delta \boldsymbol{\Sigma}_n} = \boldsymbol{\Sigma}_n^{-1} - \boldsymbol{\Sigma}_n^{-1}\mathbf{C}\left(\mathbf{H}, \boldsymbol{\upsilon}\right)\boldsymbol{\Sigma}_n^{-1} \ . \tag{4.22}$$

Assuming that $K \geq N + M$, so that matrix $\mathbf{C}\left(\mathbf{H}, \boldsymbol{\upsilon}\right)$ is invertible *w.p.*1., the MLE of the covariance matrix is given by

$$\hat{\boldsymbol{\Sigma}}_{n,\mathrm{ML}} = \mathbf{C}\left(\mathbf{H}, \boldsymbol{\upsilon}\right)\Big|_{\mathbf{H}=\hat{\mathbf{H}}_{\mathrm{ML}}, \boldsymbol{\upsilon}=\hat{\boldsymbol{\upsilon}}_{\mathrm{ML}}} \ . \tag{4.23}$$

A cost function dependent on $\mathbf{H}$ and $\boldsymbol{\upsilon}$ is obtained by substituting (4.23) in (4.16),

$$\Lambda_2\left(\mathbf{H}, \boldsymbol{\upsilon}\right) = \ln\left(\det\left(\hat{\mathbf{R}}_{xx} - \hat{\mathbf{R}}_{xd}\mathbf{H}^H - \mathbf{H}\hat{\mathbf{R}}_{xd}^H + \mathbf{H}\hat{\mathbf{R}}_{dd}\mathbf{H}^H\right)\right) \ . \tag{4.24}$$

Adding and subtracting $\hat{\mathbf{R}}_{xd}\hat{\mathbf{R}}_{dd}^{-1}\hat{\mathbf{R}}_{xd}^H$ to the argument of the determinant in (4.24) and using the hermitian property of the autocorrelation matrix, the cost function can be expressed as

$$\begin{aligned} \Lambda_2\left(\mathbf{H}, \boldsymbol{\upsilon}\right) &= \ln\Big(\det\Big(\hat{\mathbf{R}}_{xx} - \hat{\mathbf{R}}_{xd}\hat{\mathbf{R}}_{dd}^{-1}\hat{\mathbf{R}}_{xd}^H + \\ &+ \left(\mathbf{H} - \hat{\mathbf{R}}_{xd}\hat{\mathbf{R}}_{dd}^{-1}\right)\hat{\mathbf{R}}_{dd}\left(\mathbf{H} - \hat{\mathbf{R}}_{xd}\hat{\mathbf{R}}_{dd}^{-1}\right)^H\Big)\Big) \\ &\geq \ln\left(\det\left(\hat{\mathbf{R}}_{xx} - \hat{\mathbf{R}}_{xd}\hat{\mathbf{R}}_{dd}^{-1}\hat{\mathbf{R}}_{xd}^H\right)\right) \ , \end{aligned} \tag{4.25}$$

where we use the fact that the determinant is a nondecreasing function, which means that for any positive definite matrix $\hat{\mathbf{W}}$ and any non-negative definite matrix $\hat{\mathbf{V}}$, it satisfies

$$\det\left(\hat{\mathbf{W}} + \hat{\mathbf{V}}\right) \geq \det\left(\hat{\mathbf{W}}\right) \ , \tag{4.26}$$

where the equality only holds for $\hat{\mathbf{V}} = \mathbf{0}$. Inspecting (4.25), we can identify the terms:

$$\hat{\mathbf{V}} = \left(\mathbf{H} - \hat{\mathbf{R}}_{xd}\hat{\mathbf{R}}_{dd}^{-1}\right)\hat{\mathbf{R}}_{dd}\left(\mathbf{H} - \hat{\mathbf{R}}_{xd}\hat{\mathbf{R}}_{dd}^{-1}\right)^H \tag{4.27}$$

$$\hat{\mathbf{W}} = \hat{\mathbf{R}}_{xx} - \hat{\mathbf{R}}_{xd}\hat{\mathbf{R}}_{dd}^{-1}\hat{\mathbf{R}}_{xd}^H \tag{4.28}$$

where it is straightforward that see that (4.27) is a non-negative definite matrix due to its quadratic form. We used Proposition 4.2 to verify the positive definiteness of (4.28).

Proposition 4.2. *Considering the correlation definitions in (4.18),*

$$\hat{\mathbf{W}} = \hat{\mathbf{R}}_{xx} - \hat{\mathbf{R}}_{xd}\hat{\mathbf{R}}_{dd}^{-1}\hat{\mathbf{R}}_{xd}^{H} \tag{4.29}$$

is a positive definite matrix. Meaning that, for any real vector $\mathbf{u} \neq \mathbf{0}$*, we have that*

$$\mathbf{u}^T\hat{\mathbf{W}}\mathbf{u} > 0 \ . \tag{4.30}$$

Proof. See Appendix 4.C. □

The value of the channel matrix that nulls $\hat{\mathbf{V}}$ and therefore minimizes Λ_2 is the ML estimator

$$\hat{\mathbf{H}}_{\mathrm{ML}} = \hat{\mathbf{R}}_{xd}\hat{\mathbf{R}}_{dd}^{-1}\Big|_{\boldsymbol{\upsilon}=\hat{\boldsymbol{\upsilon}}_{\mathrm{ML}}} \tag{4.31}$$

also known as the Wiener estimator. Substitution of the latter in equation (4.23) shows that $\hat{\mathbf{W}}$ is the ML estimate of $\boldsymbol{\Sigma}_n$, i.e.,

$$\hat{\boldsymbol{\Sigma}}_{n,\mathrm{ML}} = \hat{\mathbf{W}} \tag{4.32}$$

The ML estimation of time-delays and Doppler-shifts is then obtained by minimizing the nonlinear cost function resulting from the substitution of (4.31) in (4.24),

$$\hat{\boldsymbol{\upsilon}}_{\mathrm{ML}} = \arg\min_{\boldsymbol{\upsilon}} \left\{ \ln\left(\det\left(\hat{\mathbf{R}}_{xx} - \hat{\mathbf{R}}_{xd}\hat{\mathbf{R}}_{dd}^{-1}\hat{\mathbf{R}}_{xd}^{H} \right) \right) \right\} \ , \tag{4.33}$$

i.e., the minimization of the logarithm of the determinant of the covariance estimate:

$$\boxed{\begin{array}{c} \text{Maximum Likelihood synchronization:} \\ \\ \hat{\boldsymbol{\upsilon}}_{\mathrm{ML}} = \arg\min_{\boldsymbol{\upsilon}} \left\{ \ln\left(\det\left(\hat{\mathbf{W}}\left(\boldsymbol{\upsilon}\right) \right) \right) \right\} \\ \hat{\mathbf{W}}\left(\boldsymbol{\upsilon}\right) = \hat{\mathbf{R}}_{xx} - \hat{\mathbf{R}}_{xd}\left(\boldsymbol{\upsilon}\right)\hat{\mathbf{R}}_{dd}^{-1}\left(\boldsymbol{\upsilon}\right)\hat{\mathbf{R}}_{xd}^{H}\left(\boldsymbol{\upsilon}\right) \end{array}} \ . \tag{4.34}$$

Our aim is to obtain an expression of the likelihood function dependent on the target motion vector $\boldsymbol{\gamma}$, i.e., as a function of user position instead of the synchronization parameters. Recall that $\boldsymbol{\gamma} \triangleq \boldsymbol{\upsilon}(\boldsymbol{\gamma})$, or equivalently $\boldsymbol{\tau} \triangleq \boldsymbol{\tau}(\boldsymbol{\gamma})$ and $\mathbf{f}_d \triangleq \mathbf{f}_d(\boldsymbol{\gamma})$, as evidenced in equations (4.10) and (4.11). Thus, the ML estimation of position is given by the vector $\boldsymbol{\gamma}$ that optimizes the likelihood cost function

$$\boxed{\begin{array}{c} \text{Maximum Likelihood positioning:} \\ \\ \hat{\boldsymbol{\gamma}}_{\mathrm{ML}} = \arg\min_{\boldsymbol{\gamma}} \left\{ \ln\left(\det\left(\hat{\mathbf{W}}\left(\boldsymbol{\gamma}\right) \right) \right) \right\} \\ \hat{\mathbf{W}}\left(\boldsymbol{\gamma}\right) = \hat{\mathbf{R}}_{xx} - \hat{\mathbf{R}}_{xd}\left(\boldsymbol{\gamma}\right)\hat{\mathbf{R}}_{dd}^{-1}\left(\boldsymbol{\gamma}\right)\hat{\mathbf{R}}_{xd}^{H}\left(\boldsymbol{\gamma}\right) \end{array}} \ , \tag{4.35}$$

due to the invariance principle of the ML estimates under injective functions [Pap01]. In the sequel, we use the definitions

$$\Lambda\left(\boldsymbol{\upsilon}\right) \triangleq \ln\left(\det\left(\hat{\mathbf{W}}\left(\boldsymbol{\upsilon}\right)\right)\right) \tag{4.36}$$

$$\Lambda\left(\boldsymbol{\gamma}\right) \triangleq \ln\left(\det\left(\hat{\mathbf{W}}\left(\boldsymbol{\gamma}\right)\right)\right) \ , \tag{4.37}$$

that represent the cost functions in (4.34) and (4.35), respectively. Notice from (4.32) that the matrix in the optimization problem is the MLE of the unknown covariance matrix. The determinant of the covariance matrix is commonly known as the generalized variance [Wil32]. Intuitive interpretations of the MLE can be found in [FP09b].

4.4 Comparison of Conventional and Direct Position Estimation frameworks

The two frameworks have core differences in several aspects. This section is devoted to the *qualitative* comparison of conventional and DPE approaches. The aim of this section is to highlight the pros and cons of both alternatives and to discuss their characteristics.

4.4.1 Optimization problem

Important differences appear when considering the optimization problems in equations (4.34) and (4.35), i.e., finding the ML estimate of synchronization parameters $\boldsymbol{\upsilon}$ or the ML estimate of vector $\boldsymbol{\gamma}$.

The most apparent difference is that whereas in the synchronization–parameter based positioning a two-dimensional optimization has to be performed per tracked satellite, the position-dependent cost function takes into account signals coming from all satellites to obtain a position estimate, dealing with a single multivariate optimization problem. Thus, in the conventional approach M two-dimensional optimization problems must be solved to estimate each pair $\{\tau_i, f_{d_i}\}_{i=1}^{M} \triangleq \{\boldsymbol{\upsilon}_i\}_{i=1}^{M}$. Hence, particularizing (4.34) to solve the parameters of the i-th satellite we have that

$$\hat{\boldsymbol{\upsilon}}_i = \arg\min_{\boldsymbol{\upsilon}_i}\left\{\ln\left(\det\left(\hat{\mathbf{W}}\left(\boldsymbol{\upsilon}_i\right)\right)\right)\right\} \qquad i = \{1, \ldots, M\}$$

$$\hat{\mathbf{W}}\left(\boldsymbol{\upsilon}_i\right) = \hat{\mathbf{R}}_{xx} - \frac{1}{K}\mathbf{X}\mathbf{d}_i^H(\boldsymbol{\upsilon}_i)\left(\mathbf{d}_i(\boldsymbol{\upsilon}_i)\mathbf{d}_i^H(\boldsymbol{\upsilon}_i)\right)^{-1}\mathbf{d}_i(\boldsymbol{\upsilon}_i)\mathbf{X}^H \ , \tag{4.38}$$

where we use the definition $\mathbf{d}_i(\boldsymbol{\upsilon}_i) \triangleq [d_i(t_0), \ldots, d_i(t_{K-1})]$. Notice that M optimizations according to (4.38) are performed independently and in parallel. In contrast, a $\dim\{\boldsymbol{\gamma}\}$-dimensional problem has to be faced in the DPE's framework, as provided by (4.35).

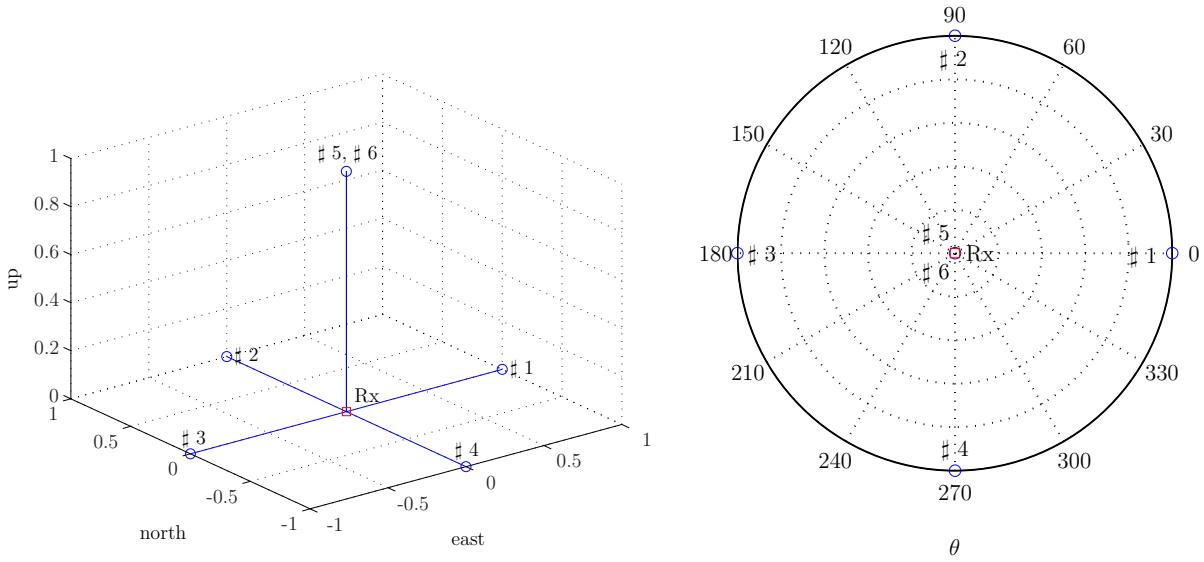

(a) (b)

Figure 4.2: Optimum constellation to minimize GDOP with $M = 6$ satellites. Three-dimensional illustration in (a) and a zenithal perspective in (b).

In order to gain some insight into the optimization problems at hand, the resulting ML cost functions for two distinct scenarios are plotted and discussed. For the conventional two-steps approach the plotted function is that of a particular satellite, as expressed by (4.38). The latter results in a two-dimensional function, which can be plotted as a function of time-delay and Doppler deviation. However, notice that in general the problem dealt by a DPE approach is n_γ-dimensional, with $n_\gamma = \dim\{\boldsymbol{\gamma}\}$. The minimum dimension of the Γ space is 4, i.e., when $\boldsymbol{\gamma}$ is composed of the three-dimensional receiver position and its clock bias (if there is not any side–information regarding any of the parameters in $\boldsymbol{\gamma}$ that allows marginalization). This fact makes impossible to plot the ML cost function $\Lambda(\boldsymbol{\gamma})$. For the sake of clarity, we now consider that one of the coordinates (say z) and the receiver clock bias are known (or vary slowly with time and can be tracked by other methods) so that we can plot the three-dimensional cost function for the problem consisting in estimating $\boldsymbol{\gamma} = [x, y]^T$. Nevertheless, we remark that this setting is only for qualitative analysis purposes performed within this section and that $\boldsymbol{\gamma}$ has to be composed of all unknown motion parameters for a given scenario (as done in Section 4.7 to provide realistic simulation results).

With this setup, a number of simulations are performed, evaluating the cost function for different coordinate errors. Normalized ML cost functions are shown considering two

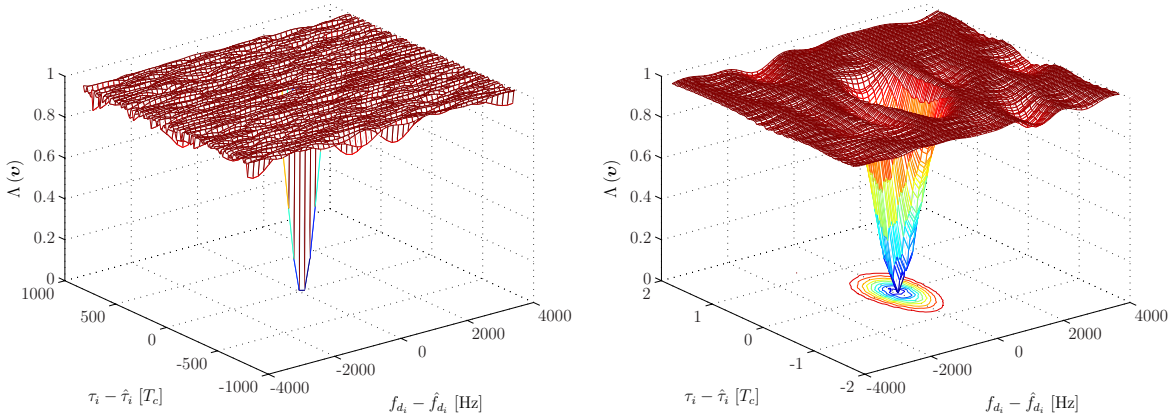

(a) Coarse Acquisition (b) Fine Synchronization

Figure 4.3: The ML cost function in equation (4.38) as a function of synchronization parameters of the locally generated code of the i-th satellite. Whereas in (a) there is a wide ambiguity region, fine synchronism focuses on a reduced search-space as in (b). The latter is the case of tracking loops.

types of front-end architectures for the GNSS receiver: a single antenna and a circular antenna array composed of 8 antenna elements. A benchmark scenario is simulated composed of 6 satellites in a constellation that minimizes the Geometric Dilution Of Precision (GDOP), according to [Par96]. The GDOP provides a measure of the *quality* of a satellite constellation. Roughly speaking, small GDOP values correspond to better geometries. The constellation is shown in Figure 4.2 in east-north-up (ENU) coordinates [Gre01], the satellites form a four-sided pyramid in a hemisphere with two satellites at zenith, being all satellites equally spaced. In particular, the considered constellation simulates C/A code on the L1 carrier of the GPS signal with a chip rate of 1.023 MHz. Carrier-to-noise density ratios are set for all satellites to 45 dB-Hz. Signals are bandpass filtered at the receiver with a bandwidth of 2 MHz, downconverted to an Intermediate Frequency of 4.309 MHz and digitized at a sampling frequency of 5.714 MHz. The observation period is 1 ms or, equivalently, $K = 5714$ recorded samples.

Figure 4.3 shows the ML cost function obtained as a function of $\boldsymbol{v}_i$. Without loss of generality, these figures consider $N = 1$ antenna. Initially, the search space has to be expanded to account for all possible delay and Doppler values [Par96] in what is referred to as *signal acquisition*. Afterwards, the search space is reduced for fine synchronization. The latter is carried typically by tracking loops (DLL and PLL) running for each satellite. After optimizing the cost function for each visible satellite, synchronization estimates are used to obtain an estimation of user's position, as discussed in Chapter 2.

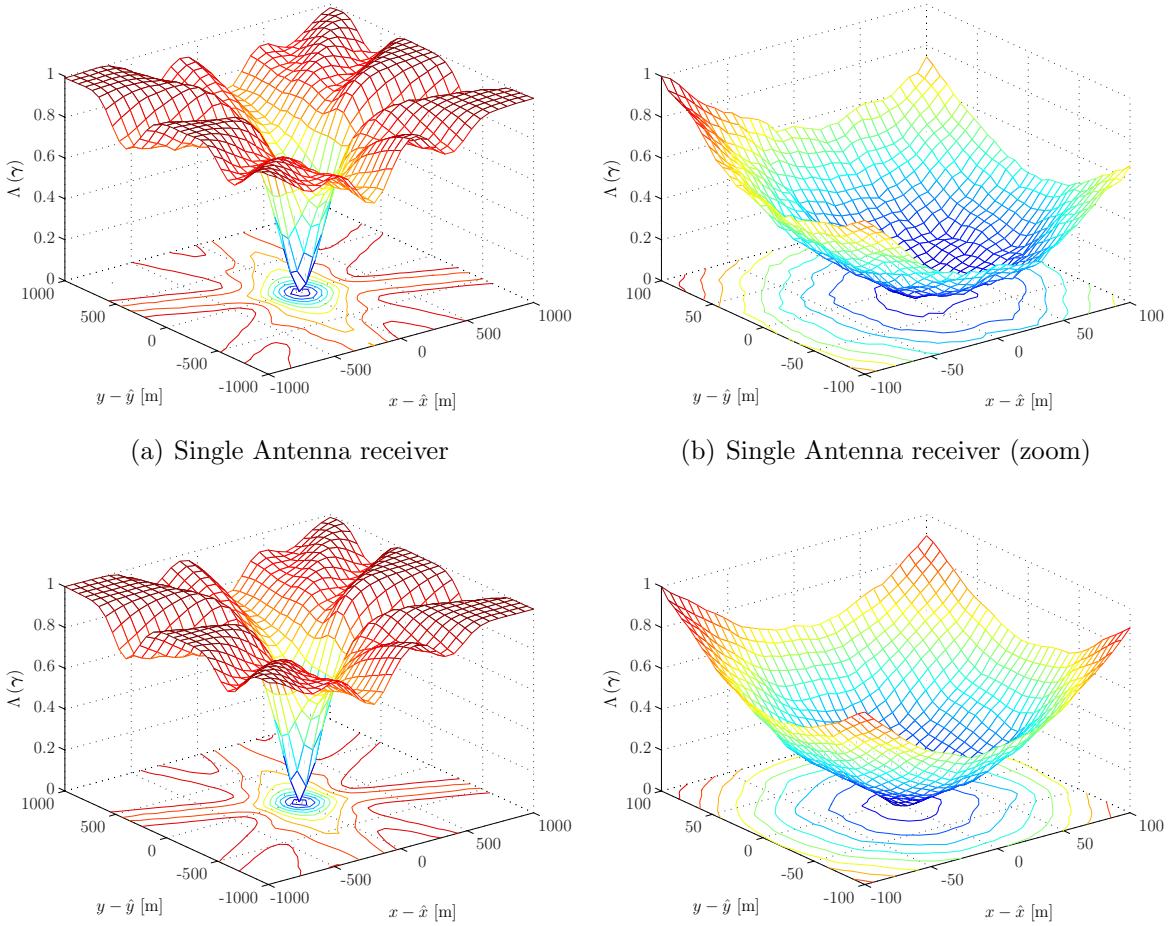

(a) Single Antenna receiver

(b) Single Antenna receiver (zoom)

(c) Antenna Array receiver

(d) Antenna Array receiver (zoom)

Figure 4.4: The ML cost function in equation (4.37) as a function of the unknown motion parameters of the receiver, $\boldsymbol{\gamma} \triangleq [x, y]^T$.

Analogously, Figure 4.4 shows the ML cost function for the considered reference scenario when the optimization problem consists in finding the value of γ that minimizes $\Lambda(\boldsymbol{\gamma})$, i.e., the DPE problem. Although from these Figures we can guess that the function is minimized when the true values of γ are evaluated, a prove on the consistency of the MLE of position can be found in Appendix 4.E, which states that for $K \to \infty$ the cost function attains its global optimum when evaluated at the true value of γ, i.e., when no error is committed. Figure 4.4 presents the results for the two architectures under study (single antenna and antenna array receivers). As done in Figure 4.3, the cost function is plotted twice: first with a wide search space and then with a reduced interval. The latter

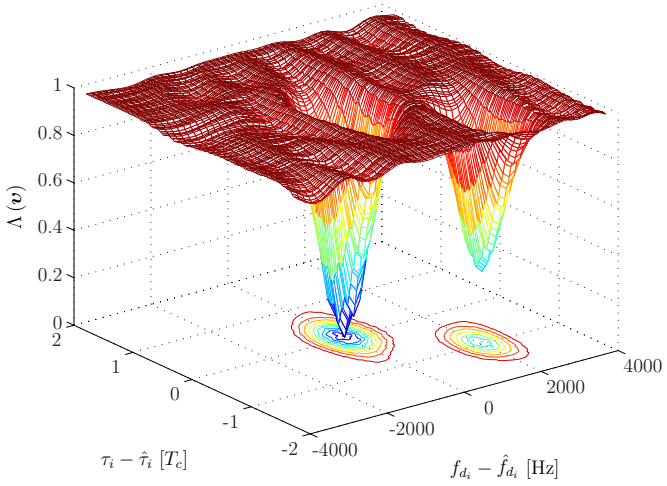

Figure 4.5: ML cost function for the conventional two-steps approach in the presence of a multipath replica: multiple optima can degrade synchronization's performance.

points out that the optimization problem is not convex [Boy03], as the surface of the cost function appears to be rough, i.e., not smooth. This is an important result since, from the latter figures, one could wrongly state that the optimization problem can be considered convex in the neighborhood of the true value of $\boldsymbol{\gamma}$. Thus, when designing optimization algorithms in Section 4.6, one must be aware of that characteristic of $\Lambda(\boldsymbol{\gamma})$.

In addition to the benchmark scenario, a multipath replica for satellite ♯1 is introduced. Its signal-to-multipath ratio (SMR) is 3 dB, impinging the receiver with same elevation as the LOSS and an azimuth of $\theta_1 + 180^o$, where θ_i represents the azimuth of the LOSS of the i-th satellite as defined in Appendix 4.B. The relative delay is 1 chip with respect to the LOSS and the Doppler-shift is 2000 Hz. For the conventional approach, it can be seen in Figure 4.5 the effect of the multipath replica in the cost function: an additional local minimum appears for each multipath replica in the scenario. This is caused due to the high correlation between the LOSS and this kind of interference. Indeed, this can complicate the operation of an optimization algorithm in order to avoid local optima. Multipath with relative delays lower than the chip period are referred to as coherent multipath, representing the dominant source of error in high precision applications as it may cause a bias in delay and carrier–phase estimations [Van93]. The simplest implementation of the ML cost function in the conventional approach is the DLL (Delay Lock Loop). The problem which arises is that the order of this estimator (the DLL) is chosen according to the assumption that only the LOSS is present. This means that this estimator tries to estimate the relative propagation delay of only the LOSS. As said, in case the LOSS is corrupted by several (or a single) superimposed delayed replicas, i.e., multipath, this estimator becomes biased. Aiming at reducing multipath's effect, many alternatives have

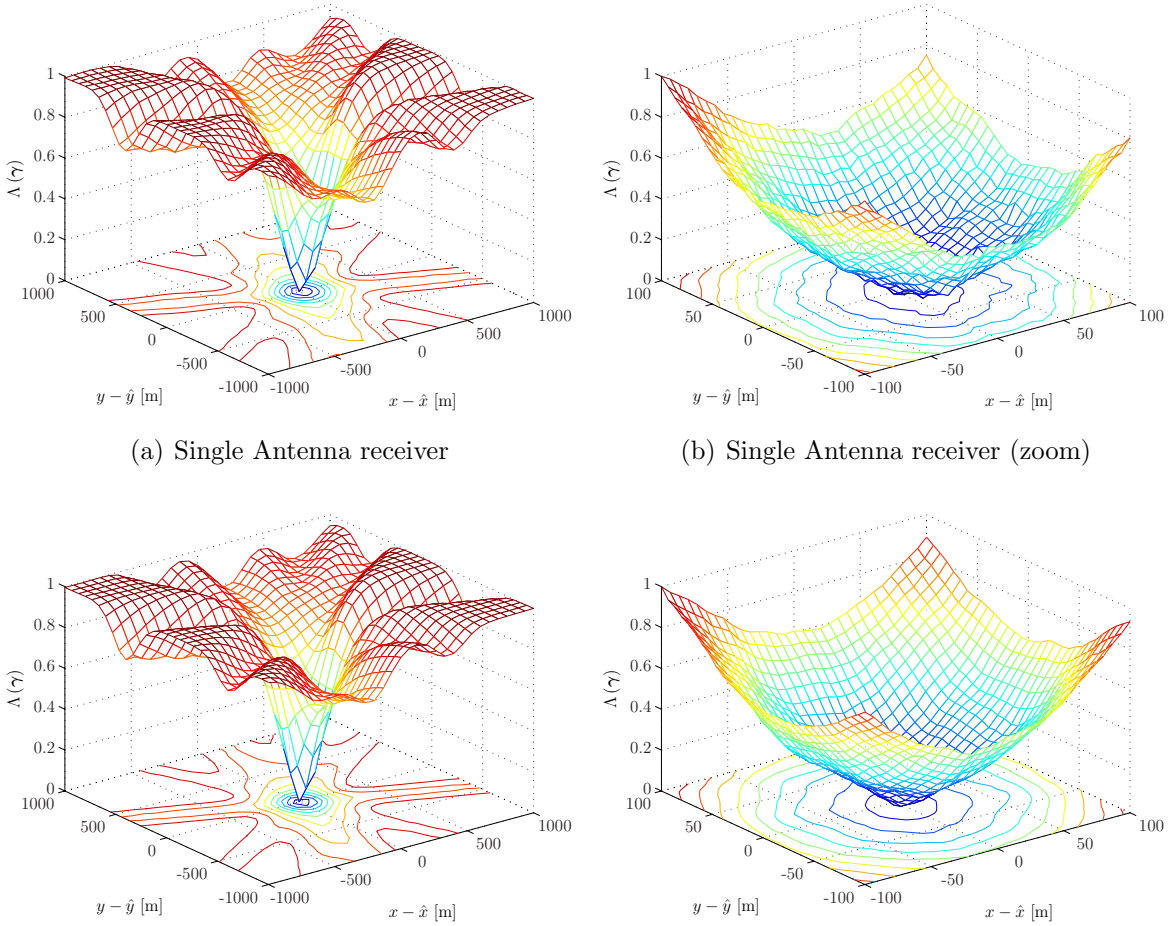

(a) Single Antenna receiver

(b) Single Antenna receiver (zoom)

(c) Antenna Array receiver

(d) Antenna Array receiver (zoom)

Figure 4.6: The ML cost function in equation (4.37) as a function of the unknown position of the user receiver, $\boldsymbol{\gamma}$, for a single antenna based receiver and an antenna array architecture. A multipath replica is present in the scenario with SMR = 3 dB and a relative delay of 1 chip with respect to the LOSS.

been proposed in the literature (including those proposed in Chapter 3) and the reader is referred to Chapter 2 for an overview.

In contrast, the effect of multipath seems to be diametrically opposed when adopting DPE. Figure 4.6 depicts DPE's cost function under that setup. It is remarkable that no secondary optimum appears due to multipath replica. Considering that position is jointly estimated with the information (measurements) of all in–view satellites, a diversity is introduced in this estimation as the propagation path for each satellite link is independent.

The approach presented takes advantage of this diversity, being robust against fading multipath channels [Clo06c]. Thus, we can claim that DPE provides an appealing framework for multipath mitigation purposes – claim which has to be yet validated in Section 4.7 with computer simulation results and in Chapter 5 by evaluating the theoretical variance bound of the estimator. Similarly, the adoption of DPE helps when the LOSS is blocked, which might occur when a severe fading affects a given satellite link due to obstacles in the LOSS direction. In that situation, the rest of in–view satellites provide information regarding user position and the estimation of $\boldsymbol{\gamma}$ can be performed. Figures for the signal blockage scenario are omitted, as they would be similar to those in Figure 4.4.

4.4.2 Receiver's architecture and requirements

In Chapter 2, the two possible architectures for an antenna array based receiver were discussed. Namely, DBF and statistical array processing. Either alternatives were depicted in Figures 2.6 and 2.7, respectively. Figures 4.7 and 4.8 provide the DPE's counterpart to those architectures, correspondingly. In the former, a DBF technique is selected to compute array weights and, then, DPE's solution corresponds to the case of a single antenna receiver ($N = 1$ antenna element). The MLE of position under this setup can be consulted in Appendix 4.D. Along this dissertation, we are interested in the statistical array processing approach, i.e., finding the MLE of position as the solution to the optimization problem given by (4.35). Henceforth, we do not have to worry about designing DBF algorithms since we are taking a statistical array processing approach (see Appendix 2.A). Nevertheless, DBF could be considered as in Figure 4.7, relying on a single antenna DPE's approach.

The proposed DPE paradigm claims to provide a framework to overcome inherent limitations of conventional GNSS receivers. Nevertheless, the potential benefits of DPE do not come at no cost. On the one hand, the computational complexity of DPE is higher to that of the 2-steps approach. Whereas in the former a single multivariate non-convex optimization problem has to be faced, the latter splits the solution in several lower dimensional problems (which in addition can be lightly handled by efficient correlation structures, refer to Chapter 2). Therefore, an effort should be done in order to find efficient algorithms to implement DPE in real-time GNSS receivers, topic discussed in Section 4.6. On the other hand, the transmitters have to be highly accurate in transmitting the signals synchronously. This assumption is reasonable in the GNSS application since satellites are continuously monitored for that purpose. In addition, an accurate estimation of the i-th satellite clock bias – performed by the control segment – is broadcasted in the navigation message in order to correct this possible source of error.

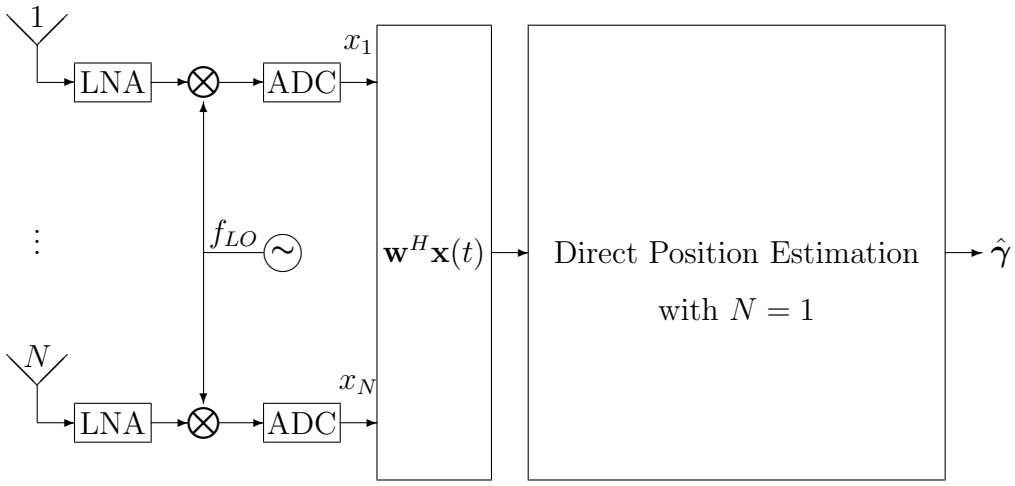

Figure 4.7: DPE approach in a SDR GNSS receiver with DBF. The optimization is particularized for $N = 1$, with the array being equivalent to a single steerable antenna.

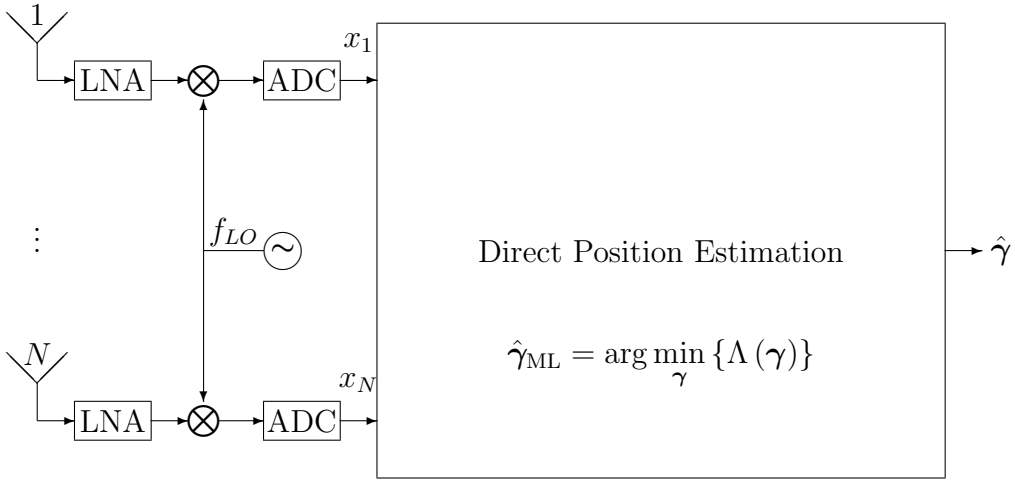

Figure 4.8: DPE approach in a SDR antenna array GNSS receiver. A multivariate optimization problem provides user's position.

Some analogies hold between conventional and DPE positioning. The optimization in (4.35), the core operation in DPE's approach, can be regarded as the analogous operation to signal tracking (plus navigation solution) in conventional GNSS receivers. In the sense that this optimization is performed periodically, tracing the values of the elements in $\boldsymbol{\gamma}$. Similarly, tracking modules usually require a prior estimation of the parameter of interest, vector $\boldsymbol{\gamma}$ in this case. Indeed, this prior estimate reminds of the signal acquisition carried out in conventional GNSS receivers, where a coarse estimation of synchronization parameters is performed. Figure 4.9 illustrates the blocks composing either acquisition and tracking modules of both positioning approaches. The corresponding operations are as follows:

Conventional approach. First, digitized signal is processed in order to obtain a coarse value of synchronization parameters (estimates of time-delays and Doppler-shifts, gathered in $\hat{\boldsymbol{\upsilon}}_c$). This is referred to as signal *acquisition*, probably constituting one of the most computationally demanding operations of a GNSS receiver. Afterwards, the receiver starts a *tracking* mode where, on the one hand, synchronization parameters are continuously traced to obtain finer estimates, denoted by $\hat{\boldsymbol{\upsilon}}_f$. On the other hand, a navigation solution is computed, which involves the demodulation of the low-rate navigation message, construction of observables using $\hat{\boldsymbol{\upsilon}}_f$ and position calculation as discussed in Section 2.2.3. The process undertaken in Figure 4.9(a) was already discussed in Chapter 2, where further comments can be found.

DPE approach. In this case, the receiver also follows the two modes of operation: *acquisition* and *tracking*, as depicted in Figure 4.9(b). Acquisition involves a coarse estimation of synchronization parameters as in the conventional approach. These estimates are obtained after correlation of the received signal with locally generated satellite codes, $\hat{\boldsymbol{\upsilon}}_c$. These estimates are used to demodulate the navigation message and compute a coarse positioning solution, $\hat{\boldsymbol{\gamma}}_c$, which serves as an initialization point for the optimization algorithm in charge of (4.35). The error values of these synchronization coarse estimates is typically on the order of $\pm\frac{T_c}{2}$ for GPS C/A receivers. Roughly, this is equivalent to an error of ± 150 meters. We saw in Section 4.4.1 that an initialization point with these requirements will be located in the neighborhood of the global optimum, being a good candidate for algorithm warm up. Notice that other GNSS signals produce even lower acquisition errors.

The two-steps approach of conventional receivers can be clearly identified in Figure 4.9(a) within receiver's tracking mode (consisting in fine synchronization and position computation). In contrast, DPE's tracking mode consists of the optimization problem that implements the MLE of position, i.e., a single-step approach. Do not confuse the two-steps with acquisition and tracking, which are the modes of operation of either receivers.

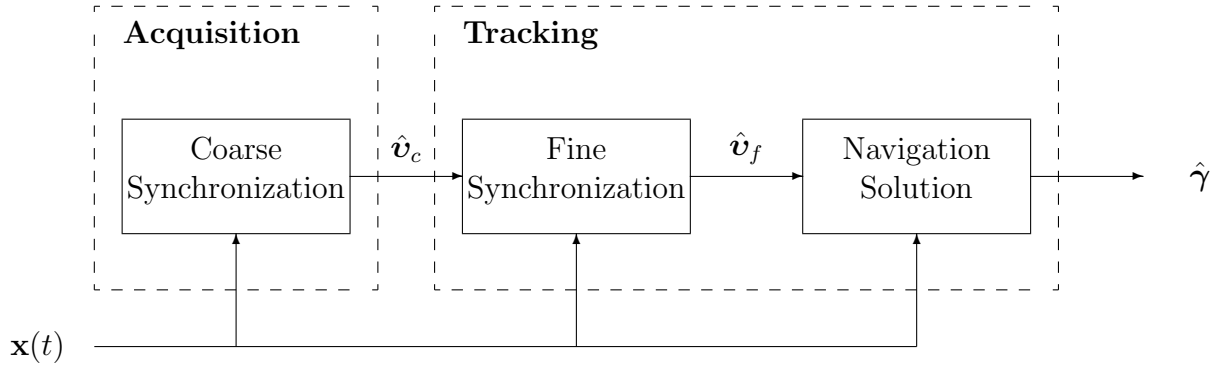

(a) Conventional approach

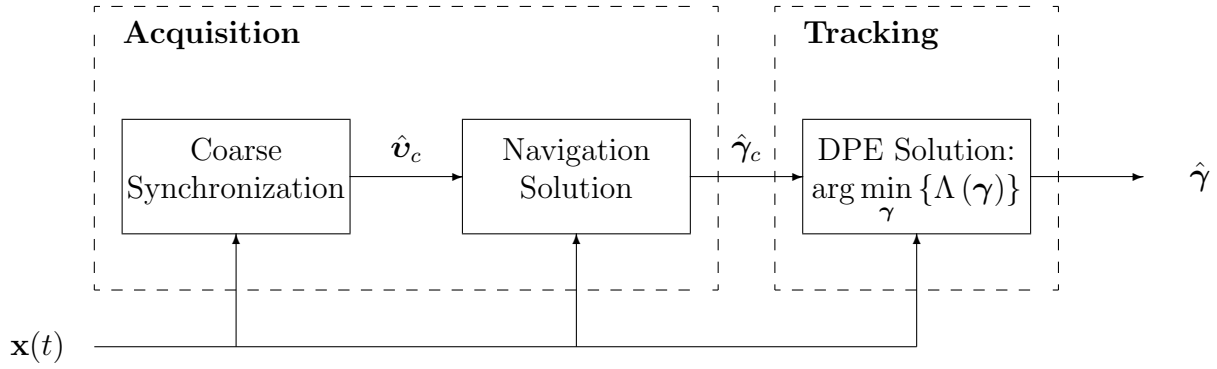

(b) DPE approach

Figure 4.9: Acquisition and Tracking schemes for (a) conventional and (b) DPE positioning approaches.

4.4.3 Asymptotical accuracy

The theoretical lower bound of accuracy of any unbiased estimator is given by the Cramér-Rao Bound (CRB). Thus, it seems suitable that one needs to derive the bound to answer the question: "how better can DPE perform compared to the conventional approach?". Due to its importance, Chapter 5 is devoted to the study and comparison of conventional and DPE bounds. Nevertheless these bounds are used in Section 4.7 this Chapter as a benchmark for the proposed implementation of the MLE of position.

4.5 The concept of Position-based Synchronization

Although estimates obtained with the proposed approach are the user coordinates themselves, it might be desirable to obtain synchronization parameters. This can be accomplished by undoing the transformations in (2.21) and (2.24) as these transformations are expressed by injective functions. The estimation of synchronization parameters relying on position estimates is referred to as *Position-based Synchronization* [Clo06c], which can be used as a figure of merit when comparing DPE performance to algorithms that estimate synchronization parameters. Let the contribution of M visible satellites be gathered in the measured vector $\mathbf{x}(t)$. Then, DPE is in charge of estimating $\boldsymbol{\gamma}$ as discussed hereinbefore. Time-delays and Doppler-shifts of each satellite (included in vector $\boldsymbol{\upsilon}$) can be expressed in terms of observables, which are related to user's motion parameters. Recalling from (2.21) and (2.24), this relation reads as

$$\begin{aligned} \rho_i(\boldsymbol{\gamma}) &= \| \mathbf{p}_i - \mathbf{p} \| + c\,(\delta t - \delta t_i) + \epsilon_i \\ \dot{\rho}_i(\boldsymbol{\gamma}) &= (\mathbf{v}_i - \mathbf{v})^T \frac{\mathbf{p}_i - \mathbf{p}}{\| \mathbf{p}_i - \mathbf{p} \|} + c\left(\dot{\delta t} - \dot{\delta t}_i\right) + \epsilon_{f_i} \,, \end{aligned} \tag{4.39}$$

where $i \in \{1, \ldots, M\}$. Therefore, τ_i and f_{d_i} can be univocally obtained from $\hat{\boldsymbol{\gamma}}$ using (4.39) and (2.22) as

$$\begin{aligned} \tau_i &= \frac{1}{c}\rho_i(\boldsymbol{\gamma}) \\ f_{d_i} &= \left(\left(\dot{\delta t} - \dot{\delta t}_i\right) - \frac{1}{c}\dot{\rho}_i(\boldsymbol{\gamma})\right) f_c \,, \end{aligned} \tag{4.40}$$

where f_c is the carrier frequency of the signal. Figure 4.10 shows the conceptual idea, where we use the definitions

$$\boldsymbol{\rho}(\hat{\boldsymbol{\gamma}}) \triangleq \begin{pmatrix} \rho_1(\boldsymbol{\gamma}) \\ \vdots \\ \rho_M(\boldsymbol{\gamma}) \end{pmatrix} \quad \text{and} \quad \dot{\boldsymbol{\rho}}(\hat{\boldsymbol{\gamma}}) \triangleq \begin{pmatrix} \dot{\rho}_1(\boldsymbol{\gamma}) \\ \vdots \\ \dot{\rho}_M(\boldsymbol{\gamma}) \end{pmatrix} . \tag{4.41}$$

Position-based Synchronization can aid when tracking satellites with low carrier-to-noise density ratios since position is jointly estimated considering information of all in–view satellites. Thus, taking advantage of this diversity, for instance in indoor navigation or in environments where the loss of tracking with certain satellites might occur due to severe fading conditions and signal blockages, among other scenario-dependant nuisance effects.

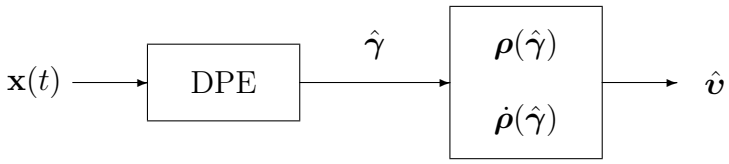

Figure 4.10: Position-based Synchronization. Time-delays and Doppler-shifts can be obtained from DPE solution.

4.6 Optimization algorithms

As discussed thus far, DPE involves the optimization of (4.35), i.e., a multivariate/nonlinear cost function which is not convex at all. Thus, obtaining the MLE of position requires the design of algorithms to perform the aforementioned optimization problem in finite time. A number of alternatives can be explored [Ant07, Mic96]. This section discusses some of the possible choices and presents the algorithm used hereinafter when presenting DPE results in Section 4.7.

A first approach could be to use a brute force method, evaluating the function on a coarse grid to roughly locate the global minimum, and then resorting to other methods to iteratively attain the optimum. As proposed in [FP06], one can combine a grid-based methodology with a spline interpolation of the cost function in the vicinity of the optimum [Bar98]. This algorithm has the advantage of being simple to implement, whose only tunable parameters are the number of points in the grid and the distance among them. However, it is not suitable for high-dimensional problems since the grid of points where the cost function has to be evaluated increases exponentially with the dimensionality of $\boldsymbol{\gamma}$. Hence, although this approach is optimal in the sense that it attains the instantaneous optimum of the cost function for an appropriate grid setup, its implementation can be computationally prohibitive.

Gradient-like methods provide an iterative solution for functional optimization [Arf01], e.g., Steepest Descent [Cau47] and Newton-Raphson algorithms. These algorithms are based on the computation of the functional gradient, which carries information about the slope of the function and, thus, the location of the optimum. Notice that this approach is valid for the optimization of convex functions, which is not the case in the DPE problem. A variation suited for the problem at hand can consist in performing a smoothing of the cost function or a quadratic approximation.

A general method for finding ML estimates that are too complex for direct solution is given by the Space-Alternating Generalized Expectation-Maximization (SAGE) algorithm [Fes94]. SAGE is a generalization of the Expectation-Maximization algorithm presented in [Dem77]. SAGE allows a complex multivariate optimization problem to be simplified into a number of decoupled optimization problems and solved in two steps: E-step and

M-step. First, the state-space is divided in subsets. Then, the expectation of the likelihood is evaluated for some subset of parameters while the others are assumed known. In the M-step, the maximization of the expectation found in the E-step provides the ML estimates of the parameters in the subset. The algorithm iterates E and M steps with the unknown subset of parameters being replaced.

Another alternative is to consider Monte-Carlo methods to design a well-suited optimization algorithm, e.g. the Metropolis-Hastings algorithm [Dou05]. To this aim, Sequential Monte-Carlo (SMC) methods were investigated and adapted to the multivariate optimization problem at hand in [Clo06b]. Basically, the algorithm generates a set of support points in which the ML cost function is evaluated, the trial point associated to the lowest weight is then propagated to the next iteration until convergence. The proposed algorithm resembles Population Monte–Carlo (PMC) optimization algorithms [Cap04]. Although its performance was seen to overcome other tested methods [Clo06c], it involves intensive computational operations which prevents its use when implementing DPE.

Therefore, the need for an efficient, simple and computationally affordable algorithm is still an issue. Hereinafter we suggest an optimization algorithm that accomplishes the three requirements: the Accelerated Random Search (ARS) algorithm [App04]. ARS is a modification of the Pure Random Search (PRS) algorithm. Thus, we first sketch the operation of the latter to provide the foundations of the former.

Let $\Lambda(\boldsymbol{\gamma})$ be a real-valued, bounded function with compact support $\Gamma \subset \mathbb{R}^{n_\gamma}$. PRS attempts to solve the generic problem

$$\min_{\boldsymbol{\gamma}\in\Gamma} \{\Lambda(\boldsymbol{\gamma})\} \ , \tag{4.42}$$

by generating a stream of N_s *i.i.d.* realizations of $\boldsymbol{\gamma}$, denoted as $\{\boldsymbol{\gamma}\}_{i=1}^{N_s}$. These samples are generated uniformly on Γ. Then, (4.42) is found after computing $M_i = \min\{\Lambda(\boldsymbol{\gamma}) : \ i = 1, \ldots, N_s\}$. The analogous problem of finding the maximum of the function can be dealt similarly. The goodness of PRS is that the sequence M_i converges *a.s.* to the minimum under a mild requirement: the function must be measurable. Unfortunately, the convergence of the PRS is extremely slow in many cases (e.g. when n_γ is large) and one might require a large number of trial points to converge.

ARS is an iterative algorithm to solve (4.42). It presents some modifications, which are basically focused to alleviate the convergence issues of PRS. Hereinafter we index the iterations of the algorithm by $i = \{0, \ldots, N_{\text{iter}} - 1\}$. Basically, at the i-th iteration, the algorithm proposes to draw sample points ($\tilde{\boldsymbol{\gamma}}$) from a uniform distribution on a closed ball centered at the current minimizer ($\boldsymbol{\gamma}^i$). Let the closed ball of radius $\mathbf{d}^i$ centered at $\boldsymbol{\gamma}^i$ be defined as

$$\mathcal{B}\left(\boldsymbol{\gamma}^i, \mathbf{d}^i\right) = \left\{\tilde{\boldsymbol{\gamma}} \in \Gamma \ : \ |\tilde{\boldsymbol{\gamma}} - \boldsymbol{\gamma}^i| < \mathbf{d}^i\right\} \ , \tag{4.43}$$

then a sample point is generated as

$$\tilde{\boldsymbol{\gamma}} \sim \mathcal{U}\left(\mathcal{B}\left(\boldsymbol{\gamma}^i, \mathbf{d}^i\right)\right) \ , \tag{4.44}$$

at the i-th iteration. Thus, $\mathcal{B}\left(\boldsymbol{\gamma}^i, \mathbf{d}^i\right) \subset \Gamma$ for any $\boldsymbol{\gamma}^i \in \Gamma$. The radius of the ball in (4.43) is regulated as follows:

- if the value of the function evaluated at the new sample point is smaller than the previous one (i.e., $\Lambda\left(\tilde{\boldsymbol{\gamma}}\right) < \Lambda\left(\boldsymbol{\gamma}^i\right)$), the former is set as the minimizer and the radius of the ball is set to its maximum value $\mathbf{d}_{\max}$. This is done in order to avoid being trapped in local minima.
- when the value of the function evaluated at the generated sample is larger than the previous trial, the new sample is discarded and the radius of the ball is reduced by a contraction factor c_f. As a rule of thumb, the contraction factor is set to $c_f = 2$ if not otherwise stated. This strategy improves the accuracy of the optimization, as the search space is reduced by reducing the ball's hypervolume.
- whenever the radius falls below a minimum threshold, $\mathbf{d}_{\min}$, it is restarted to its initial value. In general, it is convenient to fix the initial value of the radius to its maximum.
- In general, the radius of the ball can be different for each component in $\boldsymbol{\gamma}^i$. Meaning that it can be designed according to the particularities of each element in the unknown parameter vector.

The application of the ARS algorithm to the DPE problem is detailed in Algorithm 4.1. The simplicity of the algorithm presents it as an appealing alternative to compute the ML estimates under the DPE framework. The claim for its simple implementation and reduced computational cost is twofold. First, it only requires the evaluation of the cost function in (4.35), as opposite to other more complex approaches where the computation of the gradient and hessian are required. Secondly, ARS is an algorithm that requires few parameters to be tuned. This contrast with the majority of Monte-Carlo based methods, which typically involve the adjustment of a large number of parameters for proper operation, e.g. the Simulated Annealing algorithm [Laa88, Ott89].

4.7 Simulation results

This section studies the performance of the MLE of position under the DPE framework, as compared to the conventional two-steps approach. We considered the civilian GPS

Algorithm 4.1 Direct Position Estimation by the Accelerated Random Search (ARS) algorithm

Require: $\mathbf{d}_{\min}, \mathbf{d}_{\max}, c_f, N_{\text{iter}}$
Ensure: $\hat{\boldsymbol{\gamma}}_{\text{ML}} = \arg\min_{\boldsymbol{\gamma}\in\Gamma} \{\Lambda(\boldsymbol{\gamma})\}$

Initialization:

$\mathbf{d}^0 = \mathbf{d}_{\max}$
$\boldsymbol{\gamma}^0$ from acquisition or previous estimate.

Algorithm iterations:

for $i = 0$ to $N_{\text{iter}} - 1$ **do**
  Generate $\tilde{\boldsymbol{\gamma}} \sim \mathcal{U}(\mathcal{B}(\boldsymbol{\gamma}^i, \mathbf{d}^i))$
  if $\Lambda(\tilde{\boldsymbol{\gamma}}) < \Lambda(\boldsymbol{\gamma}^i)$ **then**
    $\boldsymbol{\gamma}^{i+1} = \tilde{\boldsymbol{\gamma}}$
    $\mathbf{d}^{i+1} = \mathbf{d}_{\max}$
  else
    $\boldsymbol{\gamma}^{i+1} = \boldsymbol{\gamma}^i$
    $\mathbf{d}^{i+1} = \frac{\mathbf{d}^i}{c_f}$
  end if
  if $\mathbf{d}^{i+1} < \mathbf{d}_{\min}$ **then**
    $\mathbf{d}^{i+1} = \mathbf{d}_{\max}$
  end if
end for
$\hat{\boldsymbol{\gamma}}_{\text{ML}} = \boldsymbol{\gamma}^{N_{\text{iter}}-1}$

navigation signal, as described in Section 2.1.1. The simulated receiver filtered the signal with a pre-correlation filter with a 1.1 MHz cutoff frequency and digitized it at a sampling rate of $f_s = 5.714$ MHz. The observation time was 1 ms, which corresponds to $K = 5714$ samples. Two receiver architectures were considered: one considering a single antenna receiver ($N = 1$) and another with an 8-element circular antenna array ($N = 8$). The receiver was considered static in either cases. The recreated scenario corresponded to a realistic constellation geometry, with an elevation mask of 5^o and with $M = 7$ visible satellites. Table 4.1 shows PRN code numbers [Par96], azimuth and elevations of the generated satellites.

PRN ♯	9	12	17	18	26	28	29
Azimuth, $\boldsymbol{\theta}$	288.9	215.2	87.9	295.4	123.5	46.1	130.6
Elevation, $\boldsymbol{\phi}$	46.9	24.5	29.1	32.1	71.5	24.4	60.7

Table 4.1: Azimuth and elevation values (in degrees) of the visible satellites.

The optimality criterion considered is the Mean Squared Error (MSE). Let $\hat{\boldsymbol{\xi}}$ be an estimator of an unknown vector parameter $\boldsymbol{\xi}$, then the MSE matrix is defined as

$$\mathbf{S}(\hat{\boldsymbol{\xi}}) = \mathbb{E}_{\mathbf{x}|\boldsymbol{\xi}} \left\{ \left(\hat{\boldsymbol{\xi}} - \boldsymbol{\xi} \right) \left(\hat{\boldsymbol{\xi}} - \boldsymbol{\xi} \right)^T \right\} , \tag{4.45}$$

which measures the averaged mean squared deviation of the estimator from the true value of the parameter. The MSE matrix can be decomposed in two terms:

$$\mathbf{S}(\hat{\boldsymbol{\xi}}) = \mathbf{C}(\hat{\boldsymbol{\xi}}) + \mathbf{b}(\hat{\boldsymbol{\xi}})\mathbf{b}^T(\hat{\boldsymbol{\xi}}) , \tag{4.46}$$

where

$$\begin{aligned} \mathbf{C}(\hat{\boldsymbol{\xi}}) &\triangleq \mathbb{E}_{\mathbf{x}|\boldsymbol{\xi}} \left\{ \left(\hat{\boldsymbol{\xi}} - \mathbb{E}_{\mathbf{x}|\boldsymbol{\xi}} \left\{ \hat{\boldsymbol{\xi}} \right\} \right) \left(\hat{\boldsymbol{\xi}} - \mathbb{E}_{\mathbf{x}|\boldsymbol{\xi}} \left\{ \hat{\boldsymbol{\xi}} \right\} \right)^T \right\} \\ b(\hat{\boldsymbol{\xi}}) &\triangleq \mathbb{E}_{\mathbf{x}|\boldsymbol{\xi}} \left\{ \hat{\boldsymbol{\xi}} \right\} - \boldsymbol{\xi} \end{aligned} \tag{4.47}$$

represent the covariance matrix and bias of the estimator, respectively. Thus, when assessing the performance of an estimator, we have to keep in mind that the MSE value has the contribution of both statistical measures. An estimator is said to be unbiased when $\mathbb{E}_{\mathbf{x}|\boldsymbol{\xi}} \left\{ \hat{\boldsymbol{\xi}} \right\} = \boldsymbol{\xi}$ and in that case we have that $\mathbf{S}(\hat{\boldsymbol{\xi}}) = \mathbf{C}(\hat{\boldsymbol{\xi}})$. The unbiased assumption is considered in the derivation of the CRB in Section 5.1, which provides a bound on $\mathbf{C}(\hat{\boldsymbol{\xi}})$. For the sake of clarity, we consider the Root MSE (RMSE) of position as the standard metric hereinafter. This metric is defined from the MSE of the coordinates of $\mathbf{p}$ as

$$\begin{aligned} \mathrm{RMSE}\{\hat{\mathbf{p}}\} &\triangleq \sqrt{\mathrm{MSE}\{\hat{\mathbf{p}}\}} \\ \mathrm{MSE}\{\hat{\mathbf{p}}\} &\triangleq \mathbb{E}\left\{ (\mathbf{p} - \hat{\mathbf{p}})^T (\mathbf{p} - \hat{\mathbf{p}}) \right\} \\ &= \mathbb{E}\left\{ (x - \hat{x})^2 \right\} + \mathbb{E}\left\{ (y - \hat{y})^2 \right\} + \mathbb{E}\left\{ (z - \hat{z})^2 \right\} \\ &= \mathrm{MSE}\{\hat{x}\} + \mathrm{MSE}\{\hat{y}\} + \mathrm{MSE}\{\hat{z}\} \end{aligned} \tag{4.48}$$

and the CRB of position is plotted similarly, following (5.77).

As discussed in Section 4.6, DPE was implemented using the ARS algorithm (see Algorithm 4.1). In order to provide a fair comparison between DPE and the two-steps approach, the parallel optimization of synchronization parameters in (4.38) was implemented also with the ARS algorithm. The designed values for either cases are shown in Table 4.2. Notice that

$$\mathbf{d}_{\min} = [d_{\min,x}, d_{\min,y}, d_{\min,z}]^T \quad \text{and} \quad \mathbf{d}_{\max} = [d_{\max,x}, d_{\max,y}, d_{\max,z}]^T \tag{4.49}$$

are specified in units of meters in the DPE case and that we have different values in

$$\mathbf{d}_{\min} = [d_{\min,\tau}, d_{\min,f_d}]^T \quad \text{and} \quad \mathbf{d}_{\max} = [d_{\max,\tau}, d_{\max,f_d}]^T \tag{4.50}$$

Parameter	Value	Units
$d_{\min,x}$, $d_{\min,y}$, $d_{\min,z}$	1	[m]
$d_{\max,x}$, $d_{\max,y}$, $d_{\max,z}$	50	[m]
c_f	2	-
N_{iter}	200	-

$\Uparrow$
ML positioning

Parameter	Value	Units
$d_{\min,\tau}$	$10\ T_c$	[s]
$d_{\max,\tau}$	$10^{-3}\ T_c$	[s]
$d_{\min,f_d}$	10^{-3}	[Hz]
$d_{\max,f_d}$	1000	[Hz]
c_f	2	-
N_{iter}	200	-

$\Uparrow$
ML synchronization

Table 4.2: ARS algorithm parameters used to compute the MLE of position and the MLE of synchronization parameters.

for the estimation of time-delays and Doppler-shifts. Therefore, the pairs $\{d_{\min,\tau}, d_{\max,\tau}\}$ and $\{d_{\min,f_d}, d_{\max,f_d}\}$ are expressed in units of time and frequency, respectively.

After obtaining synchronization estimates by the ARS algorithm, in the two-steps positioning approach, these estimates were used to compute user's position. This calculus was done with the LS and WLS solutions, as provided in equations (2.29) and (2.31), respectively. Thus, the figures depict the actual positioning error of both approaches. As commented in Chapter 2, the construction of weighting matrix $\mathbf{\Omega}_w$ is not unique. In the sequel, we consider that the diagonal entries in $\mathbf{\Omega}_w$ are the carrier-to-noise density ratios (C/N_0) of the corresponding satellites, normalized to the highest C/N_0 value. Thus, if $(C/N_0)_i$ denotes the C/N_0 of the i-th satellite, the weighting matrix of the WLS problem in (2.31) is constructed as

$$\mathbf{\Omega}_w = \frac{1}{\eta}\ \text{diag}\left\{(C/N_0)_1, \cdots, (C/N_0)_M\right\}\ , \tag{4.51}$$

with

$$\eta = \max\left\{(C/N_0)_1, \cdots, (C/N_0)_M\right\} \tag{4.52}$$

being a normalizing factor.

With this setup, a number of scenarios were tested, averaging the results over 200 independent Monte Carlo runs. These scenarios were used also in Section 5.3, computing the CRBs used in this chapter. Namely, these scenarios are:

Scenario 1: All satellites are assumed with equal C/N_0, with this value being swept from 20 to 50 dB-Hz.

Scenario 2: All satellites in the constellation are received with $C/N_0 = 45$ dB-Hz but satellite ♯9, whose C/N_0 is swept from 10 to 55 dB-Hz. This configuration models,

for instance, the blockage of that satellite which is seen as a reduction of its received strength.

Scenario 3: A multipath replica for satellite ♯9 is present, whose SMR is 3 dB. The relative azimuth of the replica with respect to the LOSS is 180^o, with the same elevation angle. All satellites are received with a $C/N_0 = 45$ dB-Hz. The swept parameter in this case is the relative delay between the LOSS of ♯9 and its replica, which is varied from 0 to $2T_c$.

Scenario 4: Similar as *Scenario 3*, but in addition to multipath propagation for satellite ♯9, we have that $(C/N_0)_{\sharp 9} = 25$ dB-Hz and SMR $= -20$ dB.

Recreating *Scenario 1*, the results of each position estimator are shown in Figure 4.11(a). It arises that the RMSE performances attain their corresponding CRBs and that both estimators have similar asymptotical bounds. However, we can see that the variance of DPE's estimator is smaller than the one achieved by a LS processing of ML estimates of time-delays and Doppler-shifts. Notice that, for this scenario, LS and WLS solutions are equivalent. In addition, a close look will reveal that the CRB derived under DPE's framework is lower than the bound of a conventional 2-steps approach. This was already predicted by Corollary 4.1. However, simulation results point out that the bound provided by the CRB might not be valid for low C/N_0. The reason is that the CRB falls in the category of *small-error bounds*, meaning that its validity is conditional on having *small* estimation errors. Thus, other bounds could be explored to have more accurate benchmarks under that regime as discussed in Chapter 5 (cf. [Tre07]).

Figure 4.11(b) plots the results for *Scenario 2*. As expected, the two-steps WLS solution outperforms the performance of the LS approach. An interesting effect is seen after satellite ♯9 reaches $C/N_0 = 45$ dB-Hz, i.e., the power level of the rest of satellites. At that point, the overall position RMSE degrades due to an increase of the Multiple Access Interference (MAI) that satellite ♯9 induces to the rest. Since the estimation of synchronization parameters is performed independently, a conventional receiver is not immune to MAI. In contrast, DPE provides an optimal ML approach to jointly process all signals, analogously as done in multiuser communication systems [Vit95]. Again, the CRB is not tight enough for low C/N_0 values.

Figure 4.12 presents the results for the multipath environments recreated by *Scenarios 3* and *4*. As pointed out many times in the literature (cf. [Sou02], for instance), time-delay ML estimates are biased for close multipath. That bias is propagated through the LS-based (or WLS-based) positioning solution. Similarly, we can detect the same effect in the DPE solution. However, the degradation is less severe in the latter, as can be seen from the bias curves depicted in Figure 4.13 for the case of *Scenario 3*. Notice that we plotted the bias for each coordinate in $\hat{\mathbf{p}}$. From the figures we cannot conclude that the y coordinate

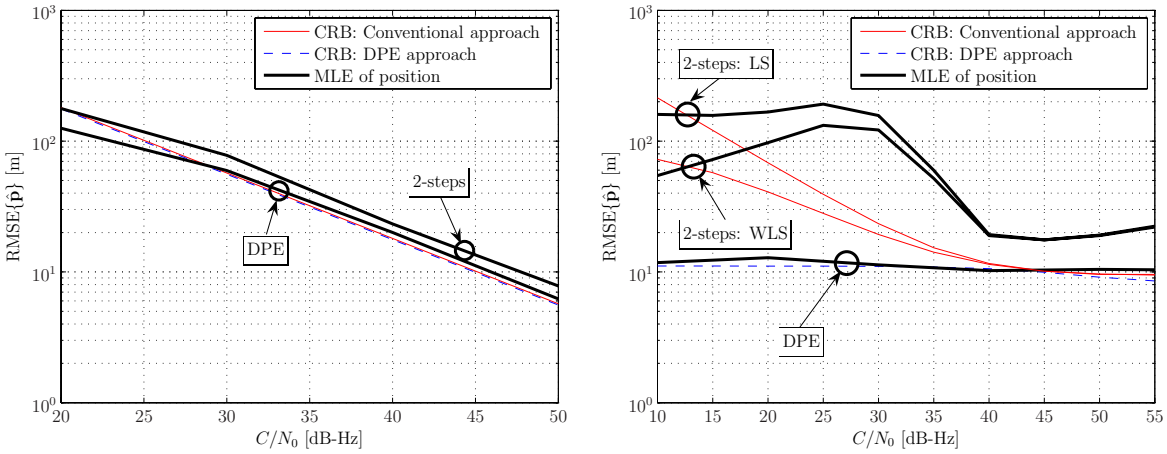

(a) (b)

Figure 4.11: RMSE$\{\hat{\mathbf{p}}\}$ of MLE of position against the corresponding CRB. *Scenario 1* in (a) and *Scenario 2* in (b), with $N = 1$ antenna.

has a smaller bias in general, and we can only claim that for the specific setup simulated it does. However, it gives the idea that the geometry of the problem will indeed affect the actual bias of each coordinate.

4.8 Bayesian Direct Position Estimation approach

The proposed DPE framework parameterizes signal model with motion parameters ($\boldsymbol{\gamma}$) instead of being synchronization dependent ($\boldsymbol{\upsilon}$). This fact is not only seen to provide performance improvements when implementing the corresponding MLEs, but it also allows the use of prior information in a more natural way. The latter claim comes after observing the parameters of interest under each positioning approach. Under the conventional approach it is difficult to propose an evolution model or a prior distribution for $\boldsymbol{\upsilon}$, i.e., time-delays and Doppler-shifts. We experienced this challenge in Chapter 3, where a rather simplistic DSS model was considered (cf. Section 3.3.2). Although the assumed prior distribution in (3.81) was useful and exhibited relatively good performance results, it is evident that it is not capturing the true evolution of synchronization parameters. Establishing such a model represents a tough problem to deal with. In contrast, DPE arises as an appealing framework for the inclusion of prior information since the modeling of motion parameters gathered in $\boldsymbol{\gamma}$ has been vastly addressed in the literature, for instance [Gus02] and the references therein. The aprioristic information regarding user's coordi-

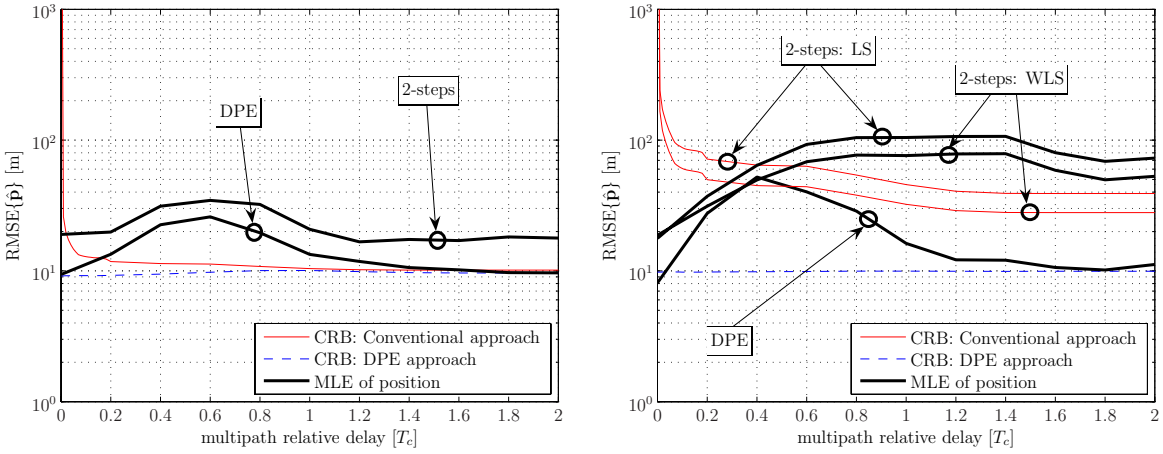

(a) SMR = 3 dB (b) SMR = −20 dB

Figure 4.12: RMSE{$\hat{\mathbf{p}}$} of MLE of position against CRBs as a function of the relative multipath delay. *Scenario 3* in (a) and *Scenario 4* in (b), with $N = 1$ antenna.

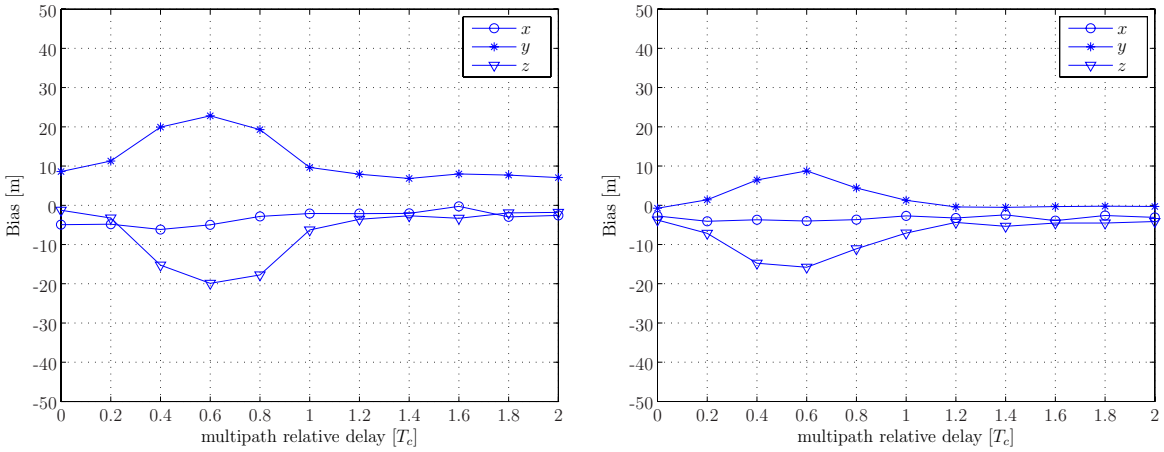

(a) two-steps and LS position estimation (b) DPE approach

Figure 4.13: Bias committed in each position coordinate using both MLEs of position as a function of the relative multipath delay. *Scenario 3* and $N = 1$ antenna.

nates can either be obtained from existing motion models [BS01], delivered by an Inertial Measurement Unit (IMU) in an ultra-tight integration configuration [Gre01, Far99] or by any other available source of information concerning user's motion like altimeters or dead reckoning methods. Therefore, we can claim that the use of prior information when the target parameter is $\boldsymbol{\gamma}$ is conceptually easier than in the conventional $\boldsymbol{\upsilon}$-based positioning approach, where the use of prior information is somehow less apparent since the evolution of these parameters cannot be modeled easily[4].

The aim of this section is to present, formulate and propose a Bayesian framework following DPE's philosophy. We refer to the use of prior information under DPE's approach as the Bayesian Direct Position Estimation (BDPE) approach to GNSS positioning. Section 4.8.1 presents the considered system model, which is expressed as a discrete state-space (DSS) model. A DSS model is composed of a measurement equation and a state evolution equation. The former admits few modifications and is obtained straightforwardly from the DPE signal model already discussed hereinbefore. In contrast, the latter accepts a number of alternatives which might be only limited by the specific application and the available side information. Some of the possible state equations are discussed, but it is important to keep in mind that many other alternatives can be considered, being the list not limited to those examples. Finally, Section 4.8.2 discusses the algorithms that can be contemplated in order to implement the BDPE paradigm in a GNSS receiver. In particular, simulation results are provided using a Particle Filtering algorithm to verify the feasibility of BDPE's approach.

4.8.1 System model

The Bayesian approach is the natural way to account for prior information. It relies on the marginal posterior distribution $p(\boldsymbol{\gamma}_k|\mathbf{x}_{1:k})$ to estimate $\boldsymbol{\gamma}_k$, given all available measurements $\mathbf{x}_{1:k}$ up to time k. Therefore, we deal with the filtering problem, in contrast to the static parameter estimation problem adopted so far under DPE's framework. An overview of Bayesian theoretical foundations and algorithms can be consulted in Section 3.1, the reader is referred to this part of the dissertation for further information. Hereinafter we consider the tracking of $\boldsymbol{\gamma}_k \in \mathbb{R}^{n_\gamma}$ given measurements $\mathbf{x}_k \in \mathbb{C}^{n_x}$ at time index k, where n_γ and n_x are the dimensions of the state and measurement vectors, respectively. The problem is generically represented by a DSS model. State equation models the evolution

[4]Actually, the inclusion of prior information in the conventional approach is generally done when computing the navigation solution. Notice that there is a subtle difference in using prior information in the DPE framework and its conventional counterpart. Whereas the latter operates at the observable level, DPE manipulates the received sampled signal. This has important repercussions from a signal processing point of view since, in the conventional approach, prior information is introduced after $\boldsymbol{\upsilon}$ is estimated, possibly affected by its inherent errors, e.g. multipath biases.

of target states (on which measurements depend on) as a discrete–time stochastic model, in general

$$\boldsymbol{\gamma}_k = \mathbf{f}_{k-1}(\boldsymbol{\gamma}_{k-1}, \boldsymbol{\nu}_k) \ , \tag{4.53}$$

where $\mathbf{f}_{k-1}(\cdot)$ is a known, possibly non-linear, function of the state $\boldsymbol{\gamma}_k$ and $\boldsymbol{\nu}_k$ is referred to as process noise. $\boldsymbol{\nu}_k$ gathers any mismodeling effect or disturbances in the state characterization. The relation between measurements and states is generically expressed as

$$\mathbf{x}_k = \mathbf{h}_k(\boldsymbol{\gamma}_k, \mathbf{n}_k) \ , \tag{4.54}$$

where $\mathbf{h}_k(\cdot)$ is a known possibly non-linear function and $\mathbf{n}_k$ is referred to as measurement noise. Both process and measurement noise are assumed white, with known statistics and mutually independent. The initial *a priori* distribution of the state vector is assumed to be known, $p(\boldsymbol{\gamma}_0)$.

Hereinbelow, we proceed to identify the possible configurations of the general DSS model described by (4.53) and (4.54). First, the measurement model is described. As said, the considered measurement model is inspired in DPE's signal model, but including the time dependency of parameters (or states). Afterwards, examples of state equations are proposed, bearing in mind that the list is not limited to those. Namely, we discuss motion models, Inertial Measurement Unit's data, atmospheric models and map matching alternatives.

Measurement equation

For the sake of simplicity, we consider the single antenna based receiver hereinafter. Similarly as done in Appendix 4.D, the K-snapshots signal model reads as:

$$\mathbf{x}_k = \mathbf{c}_k \mathbf{D}(\boldsymbol{\gamma}_k) + \mathbf{n}_k \ , \tag{4.55}$$

where

- $\mathbf{x}_k \in \mathbb{C}^{1\times K}$ is the observed signal vector, digitized at a suitable sampling rate of $f_s = 1/T_s$,
- $\mathbf{c}_k \triangleq \operatorname{diag}\{\mathbf{A}_k\}$ and $\mathbf{A}_k \in \mathbb{C}^{M\times M}$ is the diagonal matrix whose elements are the complex amplitudes of the M received signals[5],
- $\mathbf{D}(\boldsymbol{\gamma}_k) = [\mathbf{d}(kKT_s, \boldsymbol{\gamma}_k), \ldots, \mathbf{d}((k+1)KT_s - T_s, \boldsymbol{\gamma}_k)] \in \mathbb{C}^{M\times K}$, known as the basis–function matrix and

[5]We are not taking the risk of confusing the reader with the same notation for complex amplitudes and acceleration vector. For this reason complex amplitudes are denoted by $\mathbf{c}_k$ hereinafter this section.

- $\mathbf{n}_k \in \mathbb{C}^{1\times K}$ represents K snapshots of zero-mean AWGN with piecewise constant variance σ_n^2 during the observation interval.

Refer to Section 4.2 for further explanations and definitions of the elements in equation (4.55), where the static parameter problem was treated. As a difference, the model in (4.55) assumes that K samples are recorded each time-instant k, thus, it accounts for evolving states.

State equation: a bunch of alternatives

We present a number of examples from the myriad of alternatives that can be considered for the choice of a state equation in (4.53). Namely: motion models, Inertial Measurement Unit's data, atmospheric models and map matching techniques.

1. **Motion models.** If one is merely interested in the modeling of position ($\mathbf{p}_k$), velocity ($\mathbf{v}_k$) and/or acceleration ($\mathbf{a}_k$), then the following motion models provide an appealing and simple approach to it [Gus02]. From the differential equations $\dot{\mathbf{p}}_t = \mathbf{v}_t$, $\dot{\mathbf{v}}_t = \mathbf{a}_t$ and Newton's law (relating forces to acceleration), we obtain:

$$\begin{aligned} \text{Constant velocity:} \quad & \mathbf{p}_t = \mathbf{p}_0 + \mathbf{v}_0 t \\ \text{Constant acceleration:} \quad & \mathbf{p}_t = \mathbf{p}_0 + \mathbf{v}_0 t + \mathbf{a}_0 \tfrac{t^2}{2} \ , \end{aligned} \tag{4.56}$$

   which are continuous-time models for motion [Tip78]. In the sequel we consider the discrete-time model by introducing the states update period $\mathcal{T}_s$. The value of $\mathcal{T}_s$ has to be chosen according to the time elapsed between two consecutive time instants k and $k+1$. Agreeing with the definitions in (4.55), we can identify that $\mathcal{T}_s = KT_s$ in our case.

   The general state equation can be rearranged to take into account that some states are inputs of the system (measurable somehow), defined as $\mathbf{u}_k$. Thus, state evolution can be split in the contribution of two terms: previous state vector and measured inputs. We can broadly express the linear discrete-time state model as

$$\boldsymbol{\gamma}_k = \mathbf{F}_\gamma \boldsymbol{\gamma}_{k-1} + \mathbf{F}_u \mathbf{u}_{k-1} + \boldsymbol{\nu}_k \ , \tag{4.57}$$

   where $\mathbf{F}_\gamma$ is the transitional matrix and $\mathbf{F}_u$ is the matrix that relates inputs with states. The noise term $\boldsymbol{\nu}_k$ is regarded as zero-mean and Gaussian distributed with covariance matrix $\boldsymbol{\Sigma}_{\gamma,k}$. In the sequel, a number of motion models are considered. However, it is worth saying that there exist a plethora of possibilities depending on the application itself and that combinations of the following models are possible.

- *Velocity measurable:* If the velocity is assumed to be measurable, for instance by a speedometer, equation (4.57) reduces to,

$$\underbrace{\mathbf{p}_k}_{\boldsymbol{\gamma}_k} = \underbrace{\mathbf{p}_{k-1}}_{\mathbf{F}_\gamma \boldsymbol{\gamma}_{k-1}} + \underbrace{\mathcal{T}_s \mathbf{v}_{k-1}}_{\mathbf{F}_u \mathbf{u}_{k-1}} + \boldsymbol{\nu}_k \ . \tag{4.58}$$

  Under this motion model, only position is considered in the state vector and acceleration is not taken into consideration. Indeed, this is the simplest model that can be considered in a positioning application.

- *Velocity and Acceleration measurable:* If measurements of acceleration are also available, this information can be introduced in the state equation by increasing the input vector, resulting in

$$\underbrace{\mathbf{p}_k}_{\boldsymbol{\gamma}_k} = \underbrace{\mathbf{p}_{k-1}}_{\mathbf{F}_\gamma \boldsymbol{\gamma}_{k-1}} + \underbrace{\begin{pmatrix} \mathcal{T}_s \cdot \mathbf{I}_3 & \frac{\mathcal{T}_s^2}{2} \cdot \mathbf{I}_3 \end{pmatrix} \begin{pmatrix} \mathbf{v}_{k-1} \\ \mathbf{a}_{k-1} \end{pmatrix}}_{\mathbf{F}_u \mathbf{u}_{k-1}} + \boldsymbol{\nu}_k \ , \tag{4.59}$$

  where $\mathbf{I}_3$ is the 3×3 identity matrix. This might be the case of car and plane applications, where other devices (apart from the GNSS receiver itself) can feed such side information to the state equation.

- *Acceleration measurable:* Notice that for the models in (4.58) and (4.59) we assume a perfect knowledge of velocity and acceleration values. If only acceleration can be measurable, as is the case of many navigation applications, we can model the true acceleration $\breve{\mathbf{a}}_k$ as being the sum of the observed acceleration and a bias term:

$$\breve{\mathbf{a}}_k = \mathbf{a}_k + \delta \mathbf{a}_k \ . \tag{4.60}$$

  With this setup, acceleration is the measured input signal and both velocity vector and acceleration bias are part of the state vector. Thus, our state equation is now of the form:

$$\begin{aligned} \underbrace{\begin{pmatrix} \mathbf{p}_k \\ \mathbf{v}_k \\ \delta \mathbf{a}_k \end{pmatrix}}_{\boldsymbol{\gamma}_k} &= \underbrace{\begin{pmatrix} \mathbf{I}_3 & \mathcal{T}_s \cdot \mathbf{I}_3 & \frac{\mathcal{T}_s^2}{2} \cdot \mathbf{I}_3 \\ \mathbf{0} & \mathbf{I}_3 & \mathcal{T}_s \cdot \mathbf{I}_3 \\ \mathbf{0} & \mathbf{0} & \mathbf{I}_3 \end{pmatrix} \begin{pmatrix} \mathbf{p}_{k-1} \\ \mathbf{v}_{k-1} \\ \delta \mathbf{a}_{k-1} \end{pmatrix}}_{\mathbf{F}_\gamma \boldsymbol{\gamma}_{k-1}} \\ &+ \underbrace{\begin{pmatrix} \frac{\mathcal{T}_s^2}{2} \cdot \mathbf{I}_3 \\ \mathcal{T}_s \cdot \mathbf{I}_3 \\ \mathbf{0} \end{pmatrix} \mathbf{a}_{k-1}}_{\mathbf{F}_u \mathbf{u}_{k-1}} + \boldsymbol{\nu}_k \ . \end{aligned} \tag{4.61}$$

2. **Inertial Measurement Unit data.** The use of IMUs to improve the position solution provided by conventional GNSS receivers has been widely studied in the literature. The sensors used in an IMU could be a triad of gyros for measuring angular-rate and accelerometers for measuring acceleration or specific forces, $\widetilde{\boldsymbol{\omega}}_{ib}^{b}$ and $\widetilde{\mathbf{f}}_{ib}^{b}$ respectively. Other configurations include an additional axis for calibration purposes.

   An Inertial Navigation System (INS) is a self-contained navigator that generates an attitude (a.k.a. orientation), velocity and position solution at rates higher than those achievable by a GNSS receiver. An INS is the device that combines these IMU sensors and navigation algorithms. The INS algorithms for generating attitude, velocity and position involve, in part, performing the mathematical operation of integration at the output of these sensors. Thus, any error at the output of the sensors leads to correlated attitude, position, and velocity errors that are potentially unbounded. A GNSS receiver, on the other hand, generates position and velocity estimates with bounded errors. Their error characteristics are complementary, being this the main reason to integrate GNSS/INS systems in many applications. GNSS/INS integration architectures can be classified into loose, tight and ultra-tight coupling, depending on the degree of integration between both systems [Gre01, Lac07]. Loose GNSS/INS integration makes the GNSS receiver and the INS operate as independent navigation systems whose positions estimates are blended to form an integrated third position solution. Tight GNSS/INS integration, in contrast, reduces GNSS and INS to their basic sensor functions, that is, pseudorange, accelerations, and gyro measurements are used to generate a single blended navigation solution. In general, classical tight architectures provide more accurate solutions than loose approaches [Gro08]. Furthermore, tight integration is able to keep extracting useful information from a GNSS receiver in situations where fewer than four satellites are visible. Ultra-tight constitutes the most complex GNSS/INS integration architecture [Bab04, Ber08b]. In this case, the outputs of the IMU are used to dynamically tune the parameters that govern the inner tracking loops of the GNSS receiver, e.g. DLL bandwidth.

   Herein we consider an integration of INS data with GNSS measurements under the BDPE framework. This integration scheme might resemble the ultra-tight architecture, in the sense that INS data is used to rule the estimation of position directly from the received signal stream.

   The general state propagation model considers attitude, velocity and position - referenced to, and resolved in, the ECEF frame [Gre01]-, together with the accelerometer ($\mathbf{b}_a$) and gyro biases ($\mathbf{b}_g$) referenced in the body frame. The INS partition of the

state vector comprises the following 15 states:

$$\boldsymbol{\gamma}_k = \begin{pmatrix} \mathbf{C}^e_{b_k} \\ \mathbf{v}^e_{ib_k} \\ \mathbf{p}^e_{ib_k} \\ \mathbf{b}^b_{a_k} \\ \mathbf{b}^b_{g_k} \end{pmatrix} , \tag{4.62}$$

where the superscript e is used to denote the ECEF frame and the superscript b is used to denote the body frame, that read as e-frame and b-frame respectively. Subscript k denotes the discrete time index. To obtain the INS system model, the time derivative of each state must be calculated. The attitude propagation is derived first, followed by velocity, position, accelerometer and gyro biases propagation.

The attitude evolution uses the angular-rate measurement $\widetilde{\boldsymbol{\omega}}^b_{ib}$ provided by the INS. This attitude is expressed as the body-to-Earth-frame coordinate transformation matrix:

$$\mathbf{C}^e_{b_k} = \mathbf{C}^e_{b_{k-1}} \left(\mathbf{I}_3 + \boldsymbol{\Omega}^b_{ib_{k-1}} T \right) - \boldsymbol{\Omega}^e_{ie} \mathbf{C}^e_{b_{k-1}} \mathcal{T}_s \ , \tag{4.63}$$

where $\boldsymbol{\Omega}^b_{ib}$ is a skew-symmetric matrix[6] with the contributions of the gyro angular rate measurements and the gyro bias. At the k-th time instant, it is constructed as,

$$\begin{aligned} \boldsymbol{\Omega}^b_{ib_k} &= \left[\boldsymbol{\omega}^b_{ib_k} \times \right] \\ \boldsymbol{\omega}^b_{ib_k} &= \left[\omega^b_{ib,x}, \omega^b_{ib,y}, \omega^b_{ib,z} \right]^T \Big|_k \\ &= \widetilde{\boldsymbol{\omega}}^b_{ib_k} - \mathbf{b}^b_{g_k} \ , \end{aligned} \tag{4.64}$$

where $\left[\boldsymbol{\omega}^b_{ib_k} \times \right]$ denotes the skew-symmetric matrix defined as

$$\left[\boldsymbol{\omega}^b_{ib_k} \times \right] \triangleq \begin{pmatrix} 0 & -\omega^b_{ib,z} & \omega^b_{ib,y} \\ \omega^b_{ib,z} & 0 & -\omega^b_{ib,x} \\ -\omega^b_{ib,y} & \omega^b_{ib,x} & 0 \end{pmatrix} \Bigg|_k . \tag{4.65}$$

In equation (4.63), $\mathcal{T}_s$ is the interval between the input of successive accelerometer and gyro outputs to the inertial navigation equations and matrix $\boldsymbol{\Omega}^e_{ie}$ is the angular rate matrix for Earth rotation in the e-frame:

$$\boldsymbol{\Omega}^e_{ie} = \begin{pmatrix} 0 & -\omega_{ie} & 0 \\ \omega_{ie} & 0 & 0 \\ 0 & 0 & 0 \end{pmatrix} , \tag{4.66}$$

[6] $\mathbf{A}$ is a skew-symmetric matrix if it satisfies that $\mathbf{A}^T = -\mathbf{A}$.

in the WGS84[7] [EUR98] value for the Earth's angular rate is $\omega_{ie} = 7.292115 \times 10^{-5}$ rad/s.

The velocity and position update equations use the specific forces measured along the b-frame coordinate system, $\widetilde{\mathbf{f}}^b_{ib}$. Hence, we have to change the coordinate system to the e-frame. The velocity update equation reads as

$$\mathbf{v}^e_{ib_k} = \mathbf{v}^e_{ib_{k-1}} + \left(\mathbf{C}^e_{b_{k-1}}\mathbf{f}^b_{ib_{k-1}} + \mathbf{g}^e_b - 2\boldsymbol{\Omega}^e_{ie}\mathbf{v}^e_{ib_{k-1}}\right)\mathcal{T}_s \ , \tag{4.67}$$

where vector $\mathbf{g}^e_b$ represents the gravity vector calculated in the e-frame and $\mathbf{f}^b_{ib}$ is computed with the specific force measurements and the accelerometer bias:

$$\mathbf{f}^b_{ib_{k-1}} = \widetilde{\mathbf{f}}^b_{ib_{k-1}} - \mathbf{b}^b_{a_{k-1}} \ . \tag{4.68}$$

Similarly, the position update equation is computed as

$$\begin{aligned} \mathbf{p}^e_{ib_k} &= \mathbf{p}^e_{ib_{k-1}} + \mathbf{v}^e_{ib_{k-1}}\mathcal{T}_s \\ &+ \left(\mathbf{C}^e_{b_{k-1}}\mathbf{f}^b_{ib_{k-1}} + \mathbf{g}^e_b - 2\boldsymbol{\Omega}^e_{ie}\mathbf{v}^e_{ib_{k-1}}\right)\frac{\mathcal{T}_s^2}{2} \ . \end{aligned} \tag{4.69}$$

We can assume that accelerometer and gyro biases are constant except for a random component that we can represent as random processes:

$$\begin{aligned} \mathbf{b}^b_{a_k} &= \mathbf{b}^b_a + \boldsymbol{\upsilon}_{a_{k-1}} \\ \mathbf{b}^b_{g_k} &= \mathbf{b}^b_g + \boldsymbol{\upsilon}_{g_{k-1}} \ , \end{aligned} \tag{4.70}$$

whereas $\mathbf{b}^b_a$ and $\mathbf{b}^b_g$ are constant and depend on the manufacturer, $\boldsymbol{\upsilon}_a$ and $\boldsymbol{\upsilon}_g$ are $r.v.$ which represent the accelerometers and gyros noises, respectively.

As one can see, the main sources of system noise on the inertial navigation solution are random walk on the velocity due to noise on the accelerometer specific-force measurements and random walk of the attitude due to the noise on the gyro angular-rate measurements. In addition, where separate accelerometer and gyro dynamic bias states are not estimated, the in-run time variation of the accelerometer and gyro biases can be approximated as white noise.

3. **Atmospheric models.** The propagation of GNSS signals through the atmosphere affects its reception. In particular, the uppermost and the lower parts of the

[7]The World Geodetic System (WGS) is an international standard for navigation coordinates. The standard comprises a coordinate frame for the Earth, a reference ellipsoid and a gravitational equipotential surface (a.k.a. the geoid) that defines the *nominal sea level*. There have been a number of versions, being the latest released in 1984 and denoted by WGS84.

atmosphere cause non-negligible effects, ionosphere and troposphere respectively [Par96, Gre01].

The free electrons in the ionosphere (due to gases ionized by solar radiation) causes GNSS signal to propagate through a dispersive medium. In that case, the propagation velocity is no longer the vacuum speed of light, but a function of the carrier frequency ($\propto 1/f_c^2$). This is seen as a delay in the signal modulation (i.e., pseudorange is delayed) and as an advancement of the phase of the signal in an identical amount. There are 3 alternatives to combat the effect of ionosphere in observable measurements:

(a) A parametric model of such delays is available due to Klobuchar [Klo76], with its parameters being broadcasted in the navigation message by the satellites. For instance, conventional single-frequency GPS receivers make use of the eight coefficients of the Ionospheric Correction Algorithm (ICA) model [Klo87], which are transmitted in the GPS navigation message. Other ionospheric models can be found in the literature such as DGR [Gio90] and NeQuick [IR97].

(b) More sophisticated dual-frequency GNSS receivers can directly solve for the delay, taking advantage of its dependency with the carrier frequency. We are not taking this approach in the dissertation, as we consider single-frequency receivers.

(c) Another solution is to rely on a real-time correction network, which broadcasts ionospheric corrections for a number of reference stations. This is referred to as differential operation. In Satellite-Based Augmentation systems (SBAS) like WAAS or EGNOS, the correction for the ionospheric delay is achieved by transmitting a grid of vertical ionospheric delay values and performing some kind of interpolation [Rho05].

Regarding the tropospheric delay, it is a function of elevation and altitude of the receiver, and is dependent on many factors such as atmospheric pressure, temperature and relative humidity. Unlike the ionospheric delay, the tropospheric delay is not frequency-dependent (because it is not a dispersive medium at GNSS frequencies) and it cannot therefore be eliminated through linear combinations of observations on different frequency bands. Thus, it becomes the dominant source of atmospheric error in multiple-frequency receivers. In contrast to ionosphere-induced delays, the tropospheric path delay lengthens the propagation time equally for code and carrier signal components. The mitigation of such effect is typically achieve by differential techniques and interpolation, due to its high spatial correlation. Refer to [Hop69, Saa73, Jan91, HW97] for an overview of tropospheric models, which remains as an open topic due to the difficulty in modeling the water vapor (the basic component of troposphere).

Taking these atmospheric effects into consideration, the pseudorange observable of the i-th satellite presented in (2.21) can be better described as

$$\rho_i = \| \mathbf{p}_i - \mathbf{p} \| + c\left(\delta t - \delta t_i\right) + c\Delta_I + c\Delta_T + \epsilon_i \ , \tag{4.71}$$

where c is the speed of light and the same definitions assumed in (2.21) hold. The ionospheric and tropospheric caused delays are denoted by Δ_I and Δ_T, respectively. These delays are obtained either using atmospheric models or by differential techniques. Thus, Δ_I and Δ_T can be regarded as inputs of the DSS model. Considering a generic unknown state vector $\boldsymbol{\gamma}_k$, the general filtering problem can be augmented to account for such side-information

$$\begin{aligned} \boldsymbol{\gamma}_k &= \mathbf{f}_{k-1}\left(\boldsymbol{\gamma}_{k-1}, \Delta_{I_k}, \Delta_{T_k}, \boldsymbol{\nu}_k\right) \\ \Delta_{I_k}, \Delta_{T_k} &\Longleftarrow \text{Atmospheric models or differential techniques .} \end{aligned} \tag{4.72}$$

The inclusion of atmospheric information is thus independent of the state evolution and can run independently. All state equation alternatives allow the use of such data, which will improve its results since, at the end, they all rely on the observable equation (4.71). It is out of the scope of this dissertation the study of atmospheric models and an interested reader is referred to the provided references. At this point, it suffices to say that these values can be straightforwardly computed from the navigation message and/or by differential approaches.

4. **Map matching.** Finally, in order to show the versatility of the approach, a way of integrating information from maps is sketched. At a glance, car navigation by map matching consists in matching trajectories to a possible path in the road network. Map matching can be easily incorporated in the state-evolution function within the BDPE framework. The process of map matching is represented by the functional

$$\mathcal{M}(\cdot) : \Gamma \longmapsto \Gamma \ , \tag{4.73}$$

where Γ is the subset in $\mathbb{R}^{n_\gamma}$ that contains γ. Then, $\mathcal{M}(\cdot)$ is a function that maps state evolution into the space of possible states (e.g., force the trajectory of a car to be inside highway lanes). Including the time instant subindex k, the state equation turns to:

$$\boldsymbol{\gamma}_k = \mathcal{M}_k\left(\mathbf{f}_{k-1}\left(\boldsymbol{\gamma}_{k-1}, \boldsymbol{\nu}_k\right)\right) \ , \tag{4.74}$$

where $\boldsymbol{\gamma}_k$ can be composed of any motion parameter, as explained before. Actually this model is complementary with the ones discussed previously since $\mathbf{f}_{k-1}(\cdot)$ is left arbitrary (as in the atmospheric data case). However it is presented here to reinforce the framework nature of BDPE, which can be considered as a way to gather any sort of prior information in the position computation.

4.8.2 Algorithms and simulation results

Section 4.8.1 presents some of the alternatives for the design of the DSS model in the BDPE approach. As a conclusion, we can say that the model is composed of a nonlinear measurement equation and that a large number of state configurations can be envisaged, depending on the particular application. Some of them being linear and others nonlinear.

The algorithms that can be used to deal with such DSS models were extensively described in the first part of Chapter 3, where Bayesian filtering was discussed. Due to the nonlinearity of the measurement equation (and possible nonlinearities in the state evolution), we have to deal with suboptimal algorithms as those presented in Section 3.1.3. For example, Extended Kalman Filter, Gaussian Filters (e.g. the Unscented Kalman Filter) [Ito00] or Particle Filters are possible candidates. However, the list is not limited to these algorithms, and the selection of a given filtering algorithm is closely related to the application and, consequently, to the DSS model. Thus, the design of a BDPE algorithm should be determined on a case-by-case basis. It is not the aim of this dissertation to present rather complex BDPE algorithms, but to prove the feasibility of such approach. Therefore, without loss of generality, the Bootstrap Filter (BF for short) is used in the simulation results herein due to its simple implementation (see Section 3.2.5 for details). Recall that the BF is a particular implementation of a PF. At a glance, PFs sequentially characterize the posterior distribution of a filtering problem based on Monte-Carlo integration convergence results and the Sequential Importance Sampling (SIS) concept [Dju03, Dou01a, Ris04]. Basically, this characterization involves the approximation of the filtering distribution by a set of N_s random samples taken from an *importance density function*, $\pi(\cdot)$, with associated importance weights w_k^i. In general,

$$\begin{aligned} \boldsymbol{\gamma}_k^i &\sim \pi(\boldsymbol{\gamma}_k|\boldsymbol{\gamma}_{k-1}^i, \mathbf{x}_{1:k}) \\ \tilde{w}_k^i &\propto w_{k-1}^i \frac{p(\mathbf{x}_k|\boldsymbol{\gamma}_k^i)p(\boldsymbol{\gamma}_k^i|\boldsymbol{\gamma}_{k-1}^i)}{\pi(\boldsymbol{\gamma}_k^i|\boldsymbol{\gamma}_{k-1}^i, \mathbf{x}_k)} \end{aligned} \tag{4.75}$$

and

$$w_k^i = \frac{\tilde{w}_k^i}{\sum_{j=1}^{N_s} \tilde{w}_k^j} \tag{4.76}$$

are the normalized weights. For a set of generated particles, $\{\boldsymbol{\gamma}_k^i,\ w_k^i\}_{i=1}^{N_s}$, the characterization of the marginal posterior distribution is given by

$$\hat{p}(\boldsymbol{\gamma}_k|\mathbf{x}_{1:k}) = \sum_{i=1}^{N_s} w_k^i \delta(\boldsymbol{\gamma}_k - \boldsymbol{\gamma}_k^i)\ , \tag{4.77}$$

Parameter	Value	Units
f_s	5.714	[MHz]
f_c	1.023	[MHz]
B	1.1	[MHz]
K	10^{-3}	[s]
M	7	-
PRN♯	9 - 12 - 17 - 18 - 26 - 28 - 29	-
elev. cutoff	5^o	[degrees]

Table 4.3: Parameters of the generated signal.

being $\delta(\cdot)$ the Kronecker's delta function. Then, the MMSE estimate of $\boldsymbol{\gamma}_k$ can be computed as

$$\hat{\boldsymbol{\gamma}}_k = \sum_{i=1}^{N_s} w_k^i \boldsymbol{\gamma}_k^i \ . \tag{4.78}$$

The BF considers a particular setup for the equations in (4.75), where the transitional prior is used as the importance density function, i.e.,

$$\begin{aligned} \boldsymbol{\gamma}_k^i &\sim p(\boldsymbol{\gamma}_k^i | \boldsymbol{\gamma}_{k-1}^i) \\ \tilde{w}_k^i &\propto w_{k-1}^i p(\mathbf{x}_k | \boldsymbol{\gamma}_k^i) \ , \end{aligned} \tag{4.79}$$

and, in the following simulations, we have considered that resampling is systematically performed whenever the condition $\hat{N}_{eff} < \frac{2}{3} N_s$ holds. $\hat{N}_{eff}$ is the effective sample size, as defined in (3.52).

The trajectory of a mobile receiver is simulated using SatNav Toolbox of GPSoft, see left-hand side in Figure 4.14. The resulting trajectory is then used to feed a signal generation tool, aiming at testing BDPE under realistic conditions. The simulated signal follows the standard for GPS C/A code signal. The main characteristics of the recreated environment are summarized in Table 4.3. Right-hand side of Figure 4.14 plots the evolving Signal-to-Noise ratios (SNR) of each visible satellite, for the whole considered interval of 60 seconds.

The Bootstrap Filter (BF) algorithm designed for the following simulations considers that $\boldsymbol{\gamma}_k$ contains the 3-D position coordinates of the mobile receiver and that the model in equation (4.58) is used to model the transition between states, that is the algorithm has knowledge of the 3-D velocity of the receiver. Figure 4.15 shows the RMSE of each position coordinate as obtained by the BF implementing the Bayesian DPE concept when considering $N_s = \{50, 200\}$ particles. The algorithm processes K samples at each instant k and outputs a filtered state $\boldsymbol{\gamma}_k$. With the simulated setup, it is equivalent to say that each millisecond the filter processes 5714 samples. From simulation results, BDPE stands as a

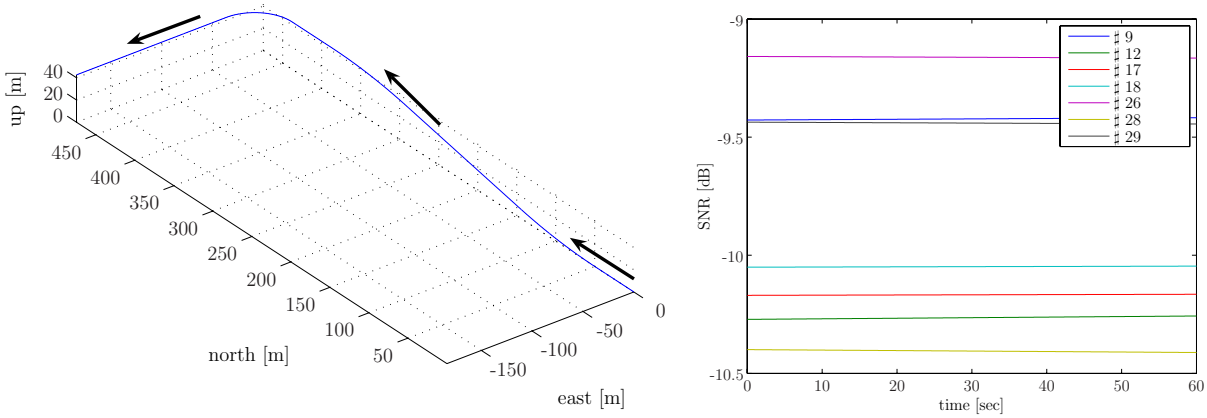

(a) (b)

Figure 4.14: Recreated scenario. Simulated trajectory using SatNav Toolbox for Matlab by GPSoft in (a) and SNRs of the visible satellites in (b).

reliable approach to positioning while considering side information. As discussed earlier, other state evolutions can be used which could eventually improve the results presented of this simple example. Nevertheless, the aim of the section is to point out the applicability of BDPE. A further improvement of the results, in terms of variance reduction, is to average over a few of milliseconds (as it is usually done in conventional receivers).

4.9 DPE vs BDPE: open and closed loop interpretations

We can say that DPE and BDPE are the obverse and reverse of the same coin: although they share many important features, important differences exist between them. So far we distinguished DPE and BDPE as being the ML and Bayesian counterparts of the same concept, respectively. We stressed that their main difference is whether the parameter of interest is static or dynamic, respectively. However, this is not strictly true since DPE – following the ML paradigm – can be considered for time-varying parameters by assuming it piecewise constant during the observation interval and applying the estimator each time a new set of samples become available. The optimum static parameter estimator, under the ML criterion, was derived in Section 4.3 and the Bayesian approach was discussed in Section 4.8. Furthermore, we claimed that the use of a priori data constitutes an inherent difference between both alternatives. When considered, the dynamical model

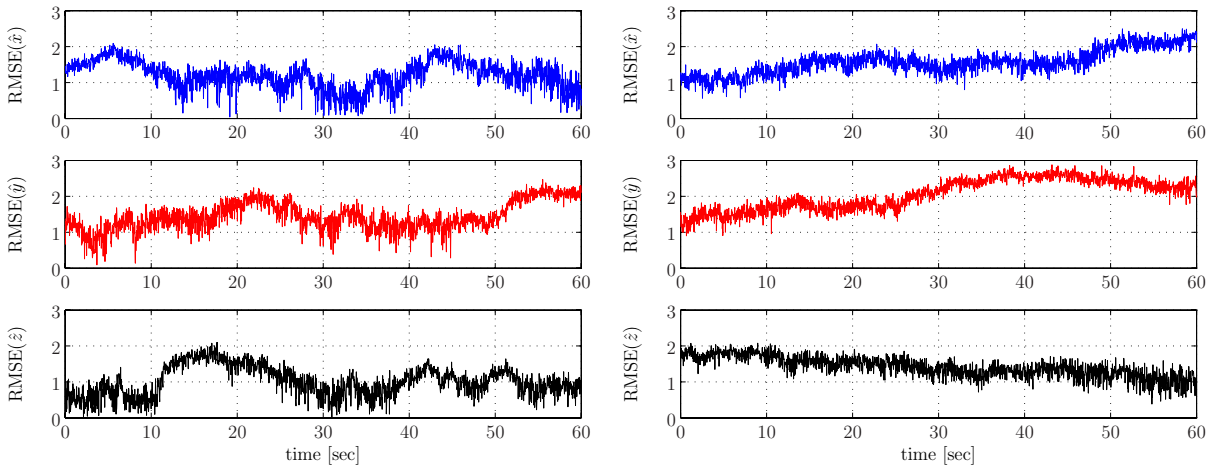

(a) $N_s = 50$ particles (b) $N_s = 200$ particles

Figure 4.15: RMSE of the BDPE position coordinates solution, implemented by a BF

plays an important role as discussed earlier. Yet another interpretation can be given to these approaches. From an implementation point of view, whereas DPE describes an open loop architecture, BDPE is a closed loop implementation of the direct positioning approach proposed in the dissertation.

As exposed in Section 4.3, the solution of DPE's approach requires the optimization of a cost function, denoted by $\Lambda(\tilde{\boldsymbol{\gamma}}; \mathbf{x}_k)$ and defined in (4.35). Notice that here we make explicit its dependence with measurements, $\mathbf{x}_k$. In Section 4.6 a number of optimization methods were analyzed, with the ARS algorithm being selected. In Figure 4.16 the operation of such algorithm is sketched. Observe that the bulk of optimization algorithms are in accordance to that diagram, substituting the dashed boxed with its corresponding operations. Therefore, it arises that one deals with an open loop scheme when implementing DPE in a GNSS receiver. Although the algorithm operates in an iterative way, it is not using feedback from the output to control its operation. The ARS algorithm in particular provides an estimate of $\boldsymbol{\gamma}$ given the measurements in k after N_{iter} iterations. Thus, if T_s denotes the sampling period and $\mathbf{x}_k$ is composed of K samples, the algorithm has to ensure that its execution is performed before the next set of sample data is available, i.e., $t_{\text{e}} N_{\text{iter}} \leq K T_s$ with t_{e} being the execution time of one iteration of the algorithm.

Conversely, BDPE is implemented under the Bayesian filtering paradigm. A number of algorithms can be considered to that aim, the larger part of them sharing the same closed loop architecture. For example, if one implements BDPE by means of a KF-like algorithm, the resulting scheme is shown in Figure 4.17(a). Similarly, a generic PF implementation

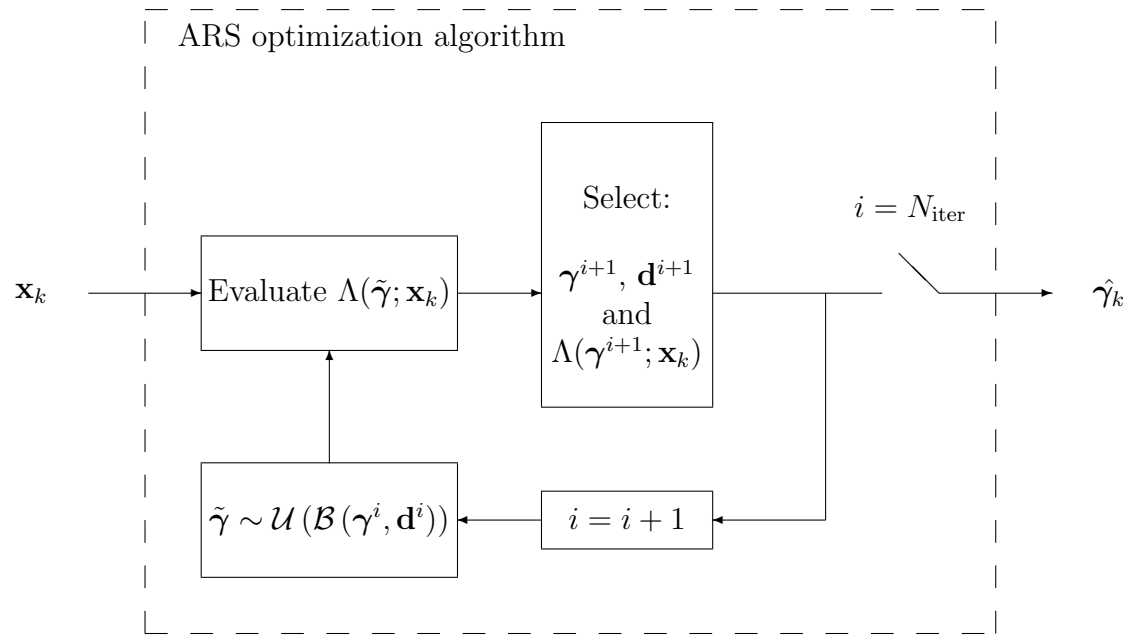

Figure 4.16: Open loop architecture of DPE approach, as implemented by the ARS algorithm.

would provide the closed loop algorithm depicted in Figure 4.17(b). Although both algorithms are conceptually different, their architectures are alike. Either algorithms take into consideration measurements and previous estimates to perform the classical prediction-update steps, discussed in Section 3.1. Generally, closed loop systems are used to obtain more accurate results or improve adaptive control. In this case, it is necessary provide feedback of the output of the system to the filtering algorithm. A particular advantage of using this scheme is that measurements can be handled sequentially as they are received, avoiding large memory sizes for further calculations (as is the case of DPE and its cost function optimization).

4.10 Related work

As far as the author knows, Direct Position Estimation is a novel topic in the GNSS positioning application. Nevertheless, there is some related work in the literature which is worth mentioning. In particular, two interesting ideas share some of the concepts of DPE. Namely, a GNSS receiver architecture that breaks the independency among tracking loops

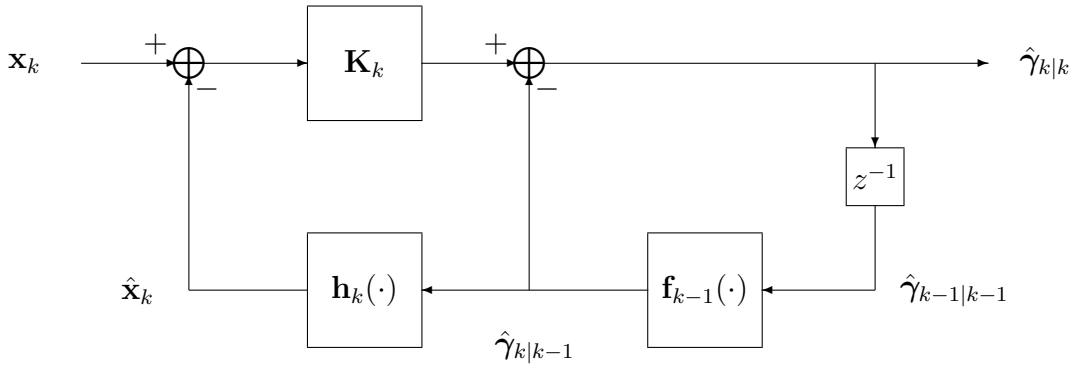

(a) KF-based implementation

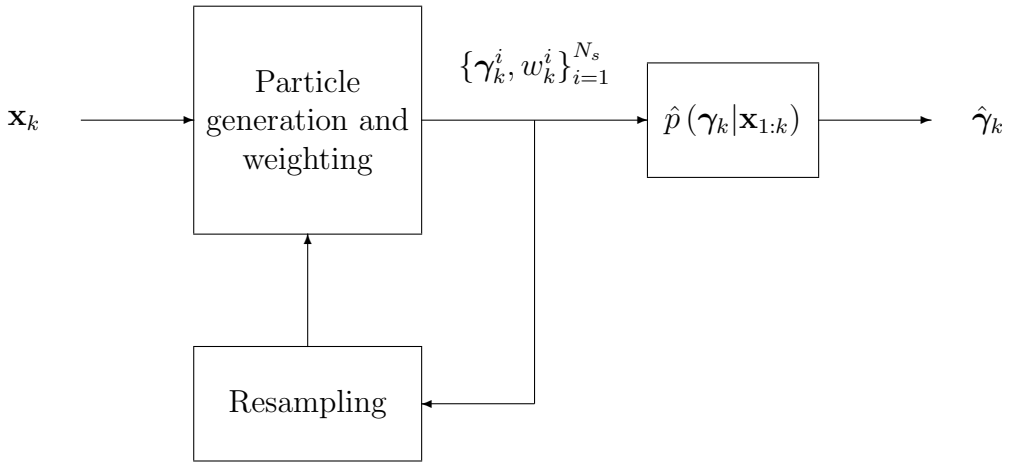

(b) PF-based implementation

Figure 4.17: KF like (a) and PF (b) implementations of BDPE, either describe a closed loop architecture.

and a single-step radiolocation procedure. These contributions are discussed in Sections 4.10.1 and 4.10.2 respectively.

4.10.1 Vector Delay Locked Loop

In [Par96], the idea of jointly processing all visible satellites was initially proposed. The so-called Vector Delay Locked Loop (VDLL) merges the two possible loops in a GNSS receiver: delay lock loops and position loops. The former are the bank of DLLs and FLLs; the latter loop comes after making the LS positioning problem recursive, then one deals with an EKF loop where the states are the position coordinates and the measurement consists of the set of outputs of the PRN code correlators. Thus, a VDLL replaces tracking loops by the navigation processor, since it indeed controls the code and carrier NCO. Actually, the VDLL algorithm can be seen as a particularization of the BDPE approach when using the EKF algorithm with a specific DSS model configuration. The VDLL has the feature of not requiring additional hardware equipment, thus its implementation does not involve any increase in power, weight or size. It was seen that the VDLL provides good performances in weak signal conditions and in the presence of interferences [Pan06, Las07].

4.10.2 Radiolocation by Direct Position Determination

The two-steps approach is also the basis of radiolocation and geolocation applications, refer to [Foy76] and the references therein. The problem in this case is to locate a radiating emitter using a set of receivers[8]. The mobile terminal radiolocation problem is depicted in Figure 4.18. With this setup, the i-th Base Station (BS) estimates one or more location dependent signal parameters from its measurements, denoted by $\mathbf{x}_i(t)$. For instance, these parameters can be the Time Of Arrival (TOA), Angle Of Arrival (AOA), Doppler-shift or signal strength [Tor84]. Notice that these parameters are used to infer a relative distance between the emitter and the i-th BS. Afterwards, the estimated distances to each receiver are jointly processed to compute the mobile's position in a Fusion Center (FC).

Recently, [Wei04] proposed to merge the two-steps in a single estimation process. This approach was termed as Direct Position Determination (DPD) in [Ama05], where the localization of multiple emitters was faced. In [Ama08a] this principle was applied to the

[8]Unfortunately, it is not difficult to imagine a number of military applications of radiolocation. Actually, the research interest in that field increased during World War II due to its evident usage. Nevertheless, nowadays one can find civilian geolocation applications such as the international cooperation programme Cospas/Sarsat [Sca84], which aims at supporting Search and Rescue teams in catastrophes and accidents by locating the emitter of a distress beacon. Cospas/Sarsat has received some attention in the literature, due to its inclusion as a payload of Galileo satellites [FP05a, FP06].

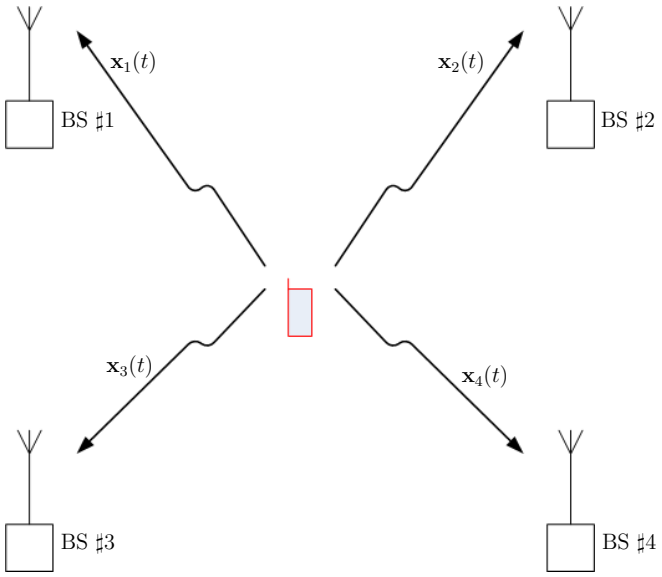

Figure 4.18: Radiolocation problem: location of an emitter by a set of receivers.

radiolocation of emitters using Doppler measurements. In a DPD approach, the FC gathers all measurements acquired by the BSs, which are jointly processed to compute emitter's position without intermediate steps. This implies an increased network complexity since the amount of data to be transmitted to the FC is larger than the conventional approach, where only the estimated relative distances are transmitted from each BS to the FC.

Although conceptually opposed to the GNSS problem, which is the positioning of a receiver instead of an emitter, the signal processing methodology of both applications is similar. DPD shares the basic idea of the DPE approach proposed in this dissertation: reducing the conventional two-steps position solution to a direct estimation of position coordinates. The main difference between both is conceptual. DPD was envisaged for the radiolocation problem, i.e., computing the position of a transmitter by measuring its relative distance to a number of BSs. Thus, a Fusion Center is in charge of determining the position of the transmitter based on the measurements of the BSs. Conversely, a GNSS receiver aims at locating itself by measuring its relative distance to a number of transmitters (satellites). Hence, the fundamental problem is different in the GNSS application. DPD and DPE can provide parallel and overlapped work notwithstanding, which is worth to take into consideration.

4.11 Summary

Conventional GNSS receivers are based on a two-steps procedure to compute user's position: estimation of synchronization parameters and position calculation by trilateration. With this idea being already reviewed in Chapter 2, the present chapter emphasized the drawbacks of this approach. Basically, the main problems associated to this positioning procedure are due to independent estimation of synchronization parameters, neglecting the existing constraints among them. Namely, the fact that time-delays and Doppler-shifts can be parameterized by common parameters, i.e., position, velocity and clock bias.

The core contribution of this chapter is the study of a Direct Position Estimation (DPE) approach, as an alternative to conventional two-steps positioning approach. By proving Proposition 4.1, we were able to claim that DPE outperforms a two-steps procedure in the MSE sense. Bearing this in mind, we developed a framework where GNSS receivers with improved capabilities can be conceived. DPE was studied from many points of view:

- The MLE of position was derived in Section 4.3, consisting in a nonlinear multivariate optimization problem. Notice that, in general, this estimator is different from that obtained after solving the MLE of synchronization parameters and plugging in the WLS trilateration problem. This difference became evident in computer simulation results discussed in Section 4.7, where both positioning alternatives were compared. A number of significative scenarios were tested, validating Proposition 4.1 and its Corollary. Also, DPE was seen to be a twofold promising alternative. On the one hand, improving the performance in scenarios where independent sources of errors among satellite links were affecting the receiver (e.g. multipath propagation). On the other hand, providing an optimal way to deal with MAI, in the ML sense.

- In simulations, the optimization was performed by the Accelerated Random Search (ARS) algorithm, which was deemed a suitable algorithm after inspecting the nature of the optimization problem (cf. Section 4.6). ARS is an iterative optimization algorithm with the particularity of having few tunable parameters and providing *a.s.* convergence to the optimum. With such algorithm, the MLE of position was seen to be asymptotically efficient in the sense that it attains the CRB.

- A qualitative comparison of DPE and two-steps approaches was given in Section 4.4, in contrast to the quantitative analysis in Section 4.7. Section 4.4.1 involved a comparison of the optimization problem arose by MLE of position and synchronization parameters, DPE and conventional approaches respectively. Following the SDR paradigm, in Section 4.4.2 the basic block diagram of a GNSS receiver implementing DPE was outlined. In addition, its possible operation was discussed and

compared to the conventional *acquisition* and *tracking* modes. The comparison of both alternatives in terms of positioning accuracy was left to the simulation results (MSE performance) and Chapter 5 (theoretical variance bounds).

- Position-based synchronization proposes the other way around to the conventional approach, that is to say, obtaining synchronization parameters from user's position computed under DPE's approach. This concept was introduced in Section 4.5.

- Apart from its improved performance in the static parameter case, DPE has another important feature: it allows the use of prior information naturally when estimating user's position. Since the parameter of interest includes (being not limited to) motion parameters, elicitation of prior distributions or evolution models for such parameters is easer when compared to the case of synchronization parameters. Thus, DPE was seen to provide a general foundation for the inclusion of prior information in GNSS receivers, as discussed in Section 4.8. The Bayesian counterpart of DPE's approach was termed as Bayesian Direct Position Estimation (BDPE). The general framework to study such approach is Bayesian filtering, including DSS modeling of the system. Whereas measurement equation admits few alternatives, selection of the state equation is not restricted to a specific configuration. Therefore, a number of state configurations were proposed considering prior data of different nature (from INS data to atmospheric information, including motion models). Simulation results showed the feasibility of BDPE.

- Section 4.9 compared the possible implementations of DPE and BDPE concepts. An interpretation in terms of open and closed loop architectures was given for DPE and its Bayesian version, respectively.

Summarizing, this chapter proposed a novel alternative for GNSS positioning where the conventional two-steps approach is combined into a single optimization problem. DPE was seen to provide, at least, the same performance than the conventional approach and improved capabilities in hazardous scenario conditions. Due to its novelty, a number of open issues are yet to be investigated as will be commented in Chapter 6.

Contributions on Direct Position Estimation were published in:

- **Journal:**

  [Clo07b] P. Closas, C. Fernández-Prades, and J. A. Fernández-Rubio, "Maximum Likelihood Estimation of Position in GNSS," *IEEE Signal Processing Lett.*, vol. 14, no. 5, pp. 359–362, May 2007.

- **Conference:**

[Clo09e] P. Closas, C. Fernández-Prades, and J. A. Fernández-Rubio, "Direct Position Estimation approach outperforms conventional two-steps positioning", *Proc. XVII European Signal Processing Conference, EUSIPCO*, Glasgow,Scotland, August 2009, in Special Session.

[FP09b] C. Fernández-Prades, and P. Closas, "Synchronization of GNSS Signals with Unstructured Antenna Arrays by a Multivariate Minimization of the Generalized Variance", *16th International Conference on Digital Signal Processing (DSP 2009)*, Santorini, Greece, July 2009.

[Clo08a] P. Closas, C. Fernández-Prades, D. Bernal, and J. A. Fernández-Rubio, "Bayesian Direct Position Estimation," *Proceedings of the ION GNSS 2008*, Savannah, GA, September 2008.

[Clo07c] P. Closas, C. Fernández-Prades, and J. A. Fernández-Rubio, "ML Estimation of Position in a GNSS Receiver using the SAGE Algorithm," in *Proceedings of the IEEE International Conference on Acoustics, Speech, and Signal Processing, ICASSP 2007*, Hawaii, USA, April 2007

[Clo06f] P. Closas, C. Fernández-Prades, J. A. Fernández-Rubio, and A. Ramírez-González, "On the Maximum Likelihood Estimation of Position," in *Proceedings of the ION GNSS 2006*, Fort Worth, TX, September 2006.

[Clo06b] P. Closas, C. Fernández-Prades, and J. A. Fernández-Rubio, "Optimizing the Likelihood with Sequential Monte–Carlo methods," in *XXI Simposium Nacional de la Unión Científica Internacional de Radio (URSI)*, Oviedo, Spain, September 2006.

[Clo06c] P. Closas, C. Fernández-Prades, and J. A. Fernández-Rubio, "Particle Filtering applied to Robust Multivariate Likelihood Optimization in the absence of a closed-form solution," in *IEEE Nonlinear Statistical Signal Processing Workshop, NSSPW'06*, Cambridge, UK, September 2006.

Appendix 4.A Proof of Proposition 4.1

Denote the log-likelihood function of measurements $\mathbf{x}$ given $\boldsymbol{\gamma}$ by $\mathcal{L}\left(\mathbf{x}|g(\boldsymbol{\gamma})\right) \triangleq \ln p\left(\mathbf{x}|g(\boldsymbol{\gamma})\right)$. Then, the MLE of $\boldsymbol{\gamma}$ is

$$\hat{\boldsymbol{\gamma}}_{\mathrm{ML}} = \arg\max_{\boldsymbol{\gamma}\in\boldsymbol{\Gamma}} \left\{\mathcal{L}\left(\mathbf{x}|g(\boldsymbol{\gamma})\right)\right\} \ , \tag{4.80}$$

which equals $\boldsymbol{\gamma}_1$ by definition. Notice that the optimization search in (4.80) shall be performed only over the space $\boldsymbol{\Gamma}$.

The two-steps approach consists in first estimating the MLE of $\boldsymbol{\upsilon}$ as the solution to

$$\hat{\boldsymbol{\upsilon}}_{\mathrm{ML}} = \arg\max_{\boldsymbol{\upsilon}\in\boldsymbol{\Upsilon}} \left\{\mathcal{L}(\mathbf{x}|\boldsymbol{\upsilon})\right\} \ , \tag{4.81}$$

and, then, use this estimate to obtain $\boldsymbol{\gamma}_2$ using its relation with $\boldsymbol{\upsilon}$. For instance, the second estimation step can be done by a WLS, which is the common choice in conventional GNSS receivers:

$$\begin{aligned} \hat{\boldsymbol{\gamma}}_2 &= \arg\min_{\boldsymbol{\gamma}\in\boldsymbol{\Gamma}} \left\{\Lambda(\boldsymbol{\gamma})\right\} \\ &= \arg\min_{\boldsymbol{\gamma}\in\boldsymbol{\Gamma}} \left\{\left(\hat{\boldsymbol{\upsilon}}_{\mathrm{ML}} - g(\boldsymbol{\gamma})\right)^T \boldsymbol{\Omega}_w \left(\hat{\boldsymbol{\upsilon}}_{\mathrm{ML}} - g(\boldsymbol{\gamma})\right)\right\} \ , \end{aligned} \tag{4.82}$$

where $\boldsymbol{\Omega}_w$ is a real, positive definite and symmetric weighting matrix.

To prove (4.3), we first obtain the asymptotical expressions of the covariance matrices of the estimators, $\boldsymbol{\Sigma}(\hat{\boldsymbol{\gamma}}_1)$ and $\boldsymbol{\Sigma}(\hat{\boldsymbol{\gamma}}_2)$ respectively.

Since the one-step estimator is the MLE, it is well-known that it is asymptotically efficient under regularity conditions [Sch91]. This means that its asymptotical covariance equals the inverse of the Fisher Information Matrix (FIM), defined as $\mathbf{J}_F(\boldsymbol{\gamma}) \in \mathbb{R}^{n_\gamma \times n_\gamma}$. Thus,

$$\begin{aligned} \lim_{K\to\infty} \boldsymbol{\Sigma}(\hat{\boldsymbol{\gamma}}_1) &= \left(\mathbb{E}\left\{\frac{\partial\mathcal{L}\left(\mathbf{x}|g(\boldsymbol{\gamma})\right)}{\partial\boldsymbol{\gamma}}\left(\frac{\partial\mathcal{L}\left(\mathbf{x}|g(\boldsymbol{\gamma})\right)}{\partial\boldsymbol{\gamma}}\right)^T\right\}\right)^{-1} \\ &\triangleq \mathbf{J}_F^{-1}(\boldsymbol{\gamma}) \ . \end{aligned} \tag{4.83}$$

Using the chain rule we can extend the derivative as

$$\frac{\partial\mathcal{L}\left(\mathbf{x}|g(\boldsymbol{\gamma})\right)}{\partial\boldsymbol{\gamma}} = \frac{\partial\mathcal{L}\left(\mathbf{x}|\boldsymbol{\upsilon}\right)}{\partial\boldsymbol{\gamma}} = \frac{\partial\boldsymbol{\upsilon}^T}{\partial\boldsymbol{\gamma}}\frac{\partial\mathcal{L}\left(\mathbf{x}|\boldsymbol{\upsilon}\right)}{\partial\boldsymbol{\upsilon}} \ , \tag{4.84}$$

which substituted in (4.83) results in

$$\begin{aligned}\lim_{K\to\infty}\boldsymbol{\Sigma}(\hat{\boldsymbol{\gamma}}_1) &= \left(\mathbb{E}\left\{\left(\frac{\partial\boldsymbol{\upsilon}^T}{\partial\boldsymbol{\gamma}}\frac{\partial\mathcal{L}\left(\mathbf{x}|\boldsymbol{\upsilon}\right)}{\partial\boldsymbol{\upsilon}}\right)\left(\frac{\partial\boldsymbol{\upsilon}^T}{\partial\boldsymbol{\gamma}}\frac{\partial\mathcal{L}\left(\mathbf{x}|\boldsymbol{\upsilon}\right)}{\partial\boldsymbol{\upsilon}}\right)^T\right\}\right)^{-1}\\ &= \left(\mathbb{E}\left\{\frac{\partial\boldsymbol{\upsilon}^T}{\partial\boldsymbol{\gamma}}\frac{\partial\mathcal{L}\left(\mathbf{x}|\boldsymbol{\upsilon}\right)}{\partial\boldsymbol{\upsilon}}\frac{\partial\mathcal{L}^T\left(\mathbf{x}|\boldsymbol{\upsilon}\right)}{\partial\boldsymbol{\upsilon}}\frac{\partial\boldsymbol{\upsilon}}{\partial\boldsymbol{\gamma}}\right\}\right)^{-1}\\ &= \left(\frac{\partial\boldsymbol{\upsilon}^T}{\partial\boldsymbol{\gamma}}\mathbb{E}\left\{\frac{\partial\mathcal{L}\left(\mathbf{x}|\boldsymbol{\upsilon}\right)}{\partial\boldsymbol{\upsilon}}\frac{\partial\mathcal{L}^T\left(\mathbf{x}|\boldsymbol{\upsilon}\right)}{\partial\boldsymbol{\upsilon}}\right\}\frac{\partial\boldsymbol{\upsilon}}{\partial\boldsymbol{\gamma}}\right)^{-1}\\ &= \left(\frac{\partial\boldsymbol{\upsilon}^T}{\partial\boldsymbol{\gamma}}\,\mathbf{J}_F(\boldsymbol{\upsilon})\,\frac{\partial\boldsymbol{\upsilon}}{\partial\boldsymbol{\gamma}}\right)^{-1}, \end{aligned} \tag{4.85}$$

where $\mathbf{J}_F(\boldsymbol{\upsilon})\in\mathbb{R}^{n_\upsilon\times n_\upsilon}$ is the FIM of $\boldsymbol{\upsilon}$.

Now we focus on the covariance matrix of $\boldsymbol{\gamma}_2$. According to [Che05], for large data sets,

$$\boldsymbol{\Sigma}(\hat{\boldsymbol{\gamma}}_2)\simeq\left(\mathbb{E}_{\hat{\boldsymbol{\upsilon}}}\left\{\frac{\partial^2\Lambda(\boldsymbol{\gamma})}{\partial\boldsymbol{\gamma}^2}\right\}\right)^{-1}\mathbb{E}_{\hat{\boldsymbol{\upsilon}}}\left\{\frac{\partial\Lambda(\boldsymbol{\gamma})}{\partial\boldsymbol{\gamma}}\frac{\partial\Lambda^T(\boldsymbol{\gamma})}{\partial\boldsymbol{\gamma}}\right\}\left(\mathbb{E}_{\hat{\boldsymbol{\upsilon}}}\left\{\frac{\partial^2\Lambda(\boldsymbol{\gamma})}{\partial\boldsymbol{\gamma}^2}\right\}\right)^{-1} \tag{4.86}$$

can be used as an approximation. We know that:

$$\begin{aligned}\Lambda(\boldsymbol{\gamma}) &\triangleq \left(\hat{\boldsymbol{\upsilon}}_{\mathrm{ML}}-g(\boldsymbol{\gamma})\right)^T\boldsymbol{\Omega}_w\left(\hat{\boldsymbol{\upsilon}}_{\mathrm{ML}}-g(\boldsymbol{\gamma})\right)\\ \frac{\partial\Lambda(\boldsymbol{\gamma})}{\partial\boldsymbol{\gamma}} &= -2\frac{\partial\boldsymbol{\upsilon}^T}{\partial\boldsymbol{\gamma}}\boldsymbol{\Omega}_w\left(\hat{\boldsymbol{\upsilon}}_{\mathrm{ML}}-g(\boldsymbol{\gamma})\right)\\ \frac{\partial^2\Lambda(\boldsymbol{\gamma})}{\partial\boldsymbol{\gamma}^2} &= 2\frac{\partial\boldsymbol{\upsilon}^T}{\partial\boldsymbol{\gamma}}\boldsymbol{\Omega}_w\frac{\partial\boldsymbol{\upsilon}}{\partial\boldsymbol{\gamma}}, \end{aligned} \tag{4.87}$$

which, substituted in (4.86), yields to

$$\begin{aligned}\boldsymbol{\Sigma}(\hat{\boldsymbol{\gamma}}_2)\simeq&\left(\mathbb{E}_{\hat{\boldsymbol{\upsilon}}}\left\{2\frac{\partial\boldsymbol{\upsilon}^T}{\partial\boldsymbol{\gamma}}\boldsymbol{\Omega}_w\frac{\partial\boldsymbol{\upsilon}}{\partial\boldsymbol{\gamma}}\right\}\right)^{-1}\\ &\mathbb{E}_{\hat{\boldsymbol{\upsilon}}}\left\{2\frac{\partial\boldsymbol{\upsilon}^T}{\partial\boldsymbol{\gamma}}\boldsymbol{\Omega}_w\left(\hat{\boldsymbol{\upsilon}}_{\mathrm{ML}}-g(\boldsymbol{\gamma})\right)\left(2\frac{\partial\boldsymbol{\upsilon}^T}{\partial\boldsymbol{\gamma}}\boldsymbol{\Omega}_w\left(\hat{\boldsymbol{\upsilon}}_{\mathrm{ML}}-g(\boldsymbol{\gamma})\right)\right)^T\right\}\\ &\left(\mathbb{E}_{\hat{\boldsymbol{\upsilon}}}\left\{2\frac{\partial\boldsymbol{\upsilon}^T}{\partial\boldsymbol{\gamma}}\boldsymbol{\Omega}_w\frac{\partial\boldsymbol{\upsilon}}{\partial\boldsymbol{\gamma}}\right\}\right)^{-1}. \end{aligned} \tag{4.88}$$

The first and last expectations in (4.88) do not contain terms with $\hat{\boldsymbol{\upsilon}}$, thus we can neglect the expectation there

$$\boldsymbol{\Sigma}(\hat{\boldsymbol{\gamma}}_2) \simeq \left(\frac{\partial \boldsymbol{\upsilon}^T}{\partial \boldsymbol{\gamma}} \boldsymbol{\Omega}_w \frac{\partial \boldsymbol{\upsilon}}{\partial \boldsymbol{\gamma}}\right)^{-1} \frac{\partial \boldsymbol{\upsilon}^T}{\partial \boldsymbol{\gamma}} \boldsymbol{\Omega}_w \mathbb{E}_{\hat{\boldsymbol{\upsilon}}} \left\{ \left(\hat{\boldsymbol{\upsilon}}_{\mathrm{ML}} - g(\boldsymbol{\gamma})\right) \left(\hat{\boldsymbol{\upsilon}}_{\mathrm{ML}} - g(\boldsymbol{\gamma})\right)^T \right\} \boldsymbol{\Omega}_w \frac{\partial \boldsymbol{\upsilon}}{\partial \boldsymbol{\gamma}} \left(\frac{\partial \boldsymbol{\upsilon}^T}{\partial \boldsymbol{\gamma}} \boldsymbol{\Omega}_w \frac{\partial \boldsymbol{\upsilon}}{\partial \boldsymbol{\gamma}}\right)^{-1} . \quad (4.89)$$

We now recall that the covariance matrix of $\hat{\boldsymbol{\upsilon}}_{\mathrm{ML}}$ tends to the inverse FIM under regularity conditions, then

$$\lim_{K\to\infty} \boldsymbol{\Sigma}(\hat{\boldsymbol{\gamma}}_2) = \left(\frac{\partial \boldsymbol{\upsilon}^T}{\partial \boldsymbol{\gamma}} \boldsymbol{\Omega}_w \frac{\partial \boldsymbol{\upsilon}}{\partial \boldsymbol{\gamma}}\right)^{-1} \frac{\partial \boldsymbol{\upsilon}^T}{\partial \boldsymbol{\gamma}} \boldsymbol{\Omega}_w \mathbf{J}_F(\boldsymbol{\upsilon}) \boldsymbol{\Omega}_w \frac{\partial \boldsymbol{\upsilon}}{\partial \boldsymbol{\gamma}} \left(\frac{\partial \boldsymbol{\upsilon}^T}{\partial \boldsymbol{\gamma}} \boldsymbol{\Omega}_w \frac{\partial \boldsymbol{\upsilon}}{\partial \boldsymbol{\gamma}}\right)^{-1} . \quad (4.90)$$

Defining

$$\begin{aligned} \mathbf{V}_1 &= \frac{\partial \boldsymbol{\upsilon}^T}{\partial \boldsymbol{\gamma}} \\ \mathbf{V}_2 &= \left(\mathbf{V}_1 \boldsymbol{\Omega}_w \mathbf{V}_1^T\right)^{-1} \mathbf{V}_1 \boldsymbol{\Omega}_w , \end{aligned} \quad (4.91)$$

for the sake of clarity, we have that the asymptotical variances can be expressed as

$$\lim_{K\to\infty} \boldsymbol{\Sigma}(\hat{\boldsymbol{\gamma}}_1) = \left(\mathbf{V}_1 \mathbf{J}_F(\boldsymbol{\upsilon}) \mathbf{V}_1^T\right)^{-1} \quad (4.92)$$

$$\lim_{K\to\infty} \boldsymbol{\Sigma}(\hat{\boldsymbol{\gamma}}_2) = \mathbf{V}_2 \mathbf{J}_F(\boldsymbol{\upsilon}) \mathbf{V}_2^T . \quad (4.93)$$

Substituting (4.92) and (4.93) into (4.3),

$$\mathbf{C} \triangleq \mathbf{V}_2 \mathbf{J}_F(\boldsymbol{\upsilon}) \mathbf{V}_2^T - \left(\mathbf{V}_1 \mathbf{J}_F(\boldsymbol{\upsilon}) \mathbf{V}_1^T\right)^{-1} , \quad (4.94)$$

we are ready to verify its positive semidefiniteness, i.e., for any real vector $\mathbf{u} \neq \mathbf{0}$, we have that

$$\mathbf{u}^T \mathbf{C} \mathbf{u} \geq 0 . \quad (4.95)$$

Define the vectors

$$\begin{aligned} \mathbf{a} &= \mathbf{J}_F^{-1/2}(\boldsymbol{\upsilon}) \mathbf{V}_2^T \mathbf{u} \\ \mathbf{b} &= \mathbf{J}_F^{1/2}(\boldsymbol{\upsilon}) \mathbf{V}_1^T \left(\mathbf{V}_1 \mathbf{J}_F(\boldsymbol{\upsilon}) \mathbf{V}_1^T\right)^{-1} \mathbf{u} \end{aligned} \quad (4.96)$$

and, by the Cauchy-Schwartz inequality[9], we have

$$\left(\mathbf{u}^T\mathbf{V}_2\mathbf{J}_F(\boldsymbol{\upsilon})\mathbf{V}_2^T\mathbf{u}\right)\left(\mathbf{u}^T\left(\mathbf{V}_1\mathbf{J}_F(\boldsymbol{\upsilon})\mathbf{V}_1^T\right)^{-1}\mathbf{u}\right)-\left(\mathbf{u}^T\left(\mathbf{V}_1\mathbf{J}_F(\boldsymbol{\upsilon})\mathbf{V}_1^T\right)^{-1}\mathbf{u}\right)^2\geq 0\ . \quad (4.97)$$

Recalling that $\left(\mathbf{V}_1\mathbf{J}_F(\boldsymbol{\upsilon})\mathbf{V}_1^T\right)^{-1}$ is a non-negative definite matrix, since it represents a covariance matrix, we can write (4.97) as

$$\mathbf{u}^T\left(\mathbf{V}_2\mathbf{J}_F(\boldsymbol{\upsilon})\mathbf{V}_2^T-\left(\mathbf{V}_1\mathbf{J}_F(\boldsymbol{\upsilon})\mathbf{V}_1^T\right)^{-1}\right)\mathbf{u}\geq 0\ , \quad (4.98)$$

proving (4.95), *q.e.d.* □

Notice that the inequality in (4.98) becomes equality when we choose the weighting matrix such that $\boldsymbol{\Omega}_w = \mathbf{J}_F(\boldsymbol{\upsilon})$. However, the true value of $\boldsymbol{\upsilon}$ is not available, which reinforces the idea that the one-step estimation cannot be outperformed by the two-steps approach.

[9]Cauchy-Schwartz inequality: $\| \mathbf{a} \|^2 \| \mathbf{b} \|^2 - (\mathbf{a}^T\mathbf{b})^2 \geq 0$

Appendix 4.B Derivation of the Spatial Signature Matrix

An *East-North-Up* (ENU) local plane coordinate system is used in the receiver calculations, with the phase center of the array being typically considered as the origin (see Figure 4.19).

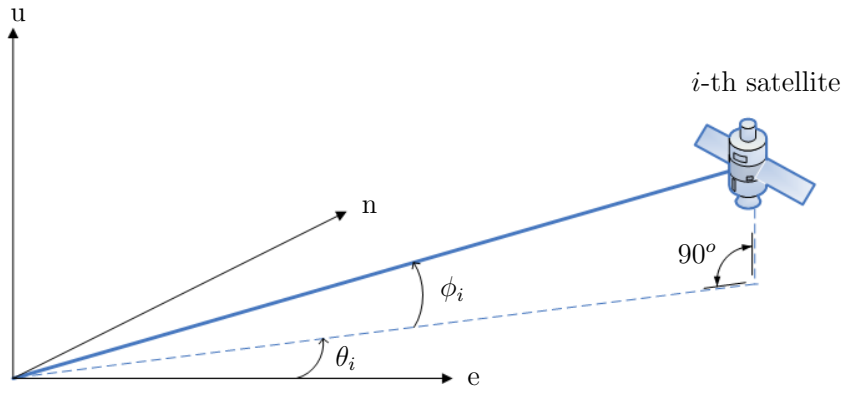

Figure 4.19: Definition of the azimuth and elevation angles for the i-th satellite, θ_i and ϕ_i respectively. The origin of the ENU coordinate system is the phase center of the array.

Considering M sources and N antennas with arbitrary geometry, we are interested in the time delay of each source observed in each antenna. This can be expressed in a matrix form as

$$\mathbf{G}^T = \exp\{j\pi\mathbf{K}\mathbf{R}\} \ , \tag{4.99}$$

where $\mathbf{K} \in \mathbb{R}^{M\times 3}$ is referred to as the wavenumber matrix, defined as

$$\mathbf{K} = \begin{pmatrix} \cos(\theta_1)\cos(\phi_1) & \sin(\theta_1)\cos(\theta_1) & \sin(\phi_1) \\ \vdots & \vdots & \vdots \\ \cos(\theta_M)\cos(\phi_M) & \sin(\theta_M)\cos(\theta_M) & \sin(\phi_M) \end{pmatrix} \tag{4.100}$$

and having its rows pointing toward the corresponding emitter, being θ_i the angle of the i-th source defined anticlockwise from the e axis on the en plane and ϕ_i the angle respect the en plane. The other term in (4.99),

$$\mathbf{R} = \begin{pmatrix} r_{e_1} & \dots & r_{e_N} \\ r_{n_1} & \dots & r_{n_N} \\ r_{u_1} & \dots & r_{u_N} \end{pmatrix} \ , \tag{4.101}$$

is the matrix of sensor element position, normalized to units of half wavelengths with respect the e, n and u axes.

Appendix 4.C Proof of Proposition 4.2

To prove that $\hat{\mathbf{W}} = \hat{\mathbf{R}}_{xx} - \hat{\mathbf{R}}_{xd}\hat{\mathbf{R}}_{dd}^{-1}\hat{\mathbf{R}}_{xd}^{H}$ is a positive definite matrix, we use the cross–correlation definitions in equation (4.18) in $\hat{\mathbf{W}}$ to obtain

$$\begin{aligned}\hat{\mathbf{W}} &= \frac{1}{K}\left(\mathbf{HD}+\mathbf{N}\right)\left(\mathbf{HD}+\mathbf{N}\right)^{H} \\ &- \frac{1}{K}\left(\mathbf{HD}+\mathbf{N}\right)\mathbf{D}^{H}\left(\mathbf{DD}^{H}\right)^{-1}\mathbf{D}\left(\mathbf{HD}+\mathbf{N}\right)^{H} \ . \end{aligned} \tag{4.102}$$

Neglecting irrelevant constants, we can further manipulating equation (4.102):

$$\begin{aligned}\hat{\mathbf{W}} \ \propto \ & \mathbf{HDD}^{H}\mathbf{H}^{H} + \mathbf{HDN}^{H} + \mathbf{ND}^{H}\mathbf{H}^{H} + \mathbf{NN}^{H} \\ - \ & \mathbf{HDD}^{H}\left(\mathbf{DD}^{H}\right)^{-1}\mathbf{DD}^{H}\mathbf{H}^{H} - \mathbf{HDD}^{H}\left(\mathbf{DD}^{H}\right)^{-1}\mathbf{DN}^{H} \\ - \ & \mathbf{ND}^{H}\left(\mathbf{DD}^{H}\right)^{-1}\mathbf{DD}^{H}\mathbf{H}^{H} - \mathbf{ND}^{H}\left(\mathbf{DD}^{H}\right)^{-1}\mathbf{DN}^{H} \ , \end{aligned}$$

which yields to:

$$\begin{aligned}\hat{\mathbf{W}} \ \propto \ & \mathbf{HDD}^{H}\mathbf{H}^{H} + \mathbf{HDN}^{H} + \mathbf{ND}^{H}\mathbf{H}^{H} + \mathbf{NN}^{H} \\ - \ & \mathbf{HDD}^{H}\mathbf{H}^{H} - \mathbf{HDN}^{H} \\ - \ & \mathbf{ND}^{H}\mathbf{H}^{H} - \mathbf{ND}^{H}\left(\mathbf{DD}^{H}\right)^{-1}\mathbf{DN}^{H} \ . \end{aligned} \tag{4.103}$$

The expression in (4.103) is clearly equivalent to:

$$\begin{aligned}\hat{\mathbf{W}} &\propto \mathbf{NN}^{H} - \mathbf{ND}^{H}\left(\mathbf{DD}^{H}\right)^{-1}\mathbf{DN}^{H} \\ &= \mathbf{N}\left(\mathbf{I} - \mathbf{D}^{H}\left(\mathbf{DD}^{H}\right)^{-1}\mathbf{D}\right)\mathbf{N}^{H} \\ &= \mathbf{N}\left(\mathbf{I} - \mathbf{D}^{H}\left(\mathbf{D}^{H}\right)^{\dagger}\right)\mathbf{N}^{H} \\ &= \mathbf{N}\left(\mathbf{I} - \mathbf{P}_{\mathbf{D}^{H}}\right)\mathbf{N}^{H} \ , \end{aligned} \tag{4.104}$$

where $\mathbf{I}$ is the identity matrix and $\mathbf{P}_{\mathbf{D}^{H}} = \mathbf{D}^{H}\left(\mathbf{D}^{H}\right)^{\dagger}$ is the projection matrix over the subspace spanned by the columns of $\mathbf{D}^{H}$. Notice that $\mathbf{I} - \mathbf{P}_{\mathbf{D}^{H}}$ is also a projection matrix, which projects over the subspace orthogonal to the latter. As projection matrices are non–negative definite and the expression obtained in (4.104) has a quadratic form, the proof on the positive definiteness of matrix $\hat{\mathbf{W}}$ is concluded. □

Appendix 4.D MLE of position in single–antenna based receivers

The K-snapshots array signal model in (4.13) has its single antenna counterpart in:

$$\mathbf{x} = \mathbf{a}\mathbf{D}(\boldsymbol{\upsilon}) + \mathbf{n} \ , \tag{4.105}$$

where

- $\mathbf{x} \in \mathbb{C}^{1\times K}$ is the observed signal vector,
- $\mathbf{a} \in \mathbb{C}^{1\times M}$ is a vector whose elements are the complex amplitudes of the M received signals $\mathbf{a} = [a_1, \ldots, a_M]$,
- $\boldsymbol{\upsilon} \in \mathbb{R}^{2M\times 1}$ gathers $\boldsymbol{\tau}$ and $\mathbf{f}_d$, i.e., time-delays and Doppler-shifts of each visible satellite,
- $\mathbf{D}(\boldsymbol{\upsilon}) = [\mathbf{d}(t_0, \boldsymbol{\upsilon}), \ldots, \mathbf{d}(t_{K-1}, \boldsymbol{\upsilon})] \in \mathbb{C}^{M\times K}$, known as the basis–function matrix and
- $\mathbf{n} \in \mathbb{C}^{1\times K}$ represents K snapshots of zero-mean AWGN with piecewise constant variance σ_n^2 during the observation interval.

We first take into account that the MLE is equivalent to the solution obtained by a Least Squares (LS) criterion under the assumption of zero-mean AWGN. Neglecting additive and multiplicative constants, maximizing the likelihood function of measurement equation (4.13) is equivalent to minimizing

$$\Lambda\left(\mathbf{a}, \boldsymbol{\tau}, \mathbf{f}_d\right) \triangleq \Lambda\left(\mathbf{a}, \boldsymbol{\upsilon}\right) = \frac{1}{K}\left|\left|\mathbf{x} - \mathbf{a}\mathbf{D}(\boldsymbol{\upsilon})\right|\right|^2 \tag{4.106}$$

with respect to $\mathbf{a}, \boldsymbol{\upsilon}$. With the following cross-correlations estimation definitions:

$$\begin{aligned} \hat{r}_{xx} &= \frac{1}{K}\mathbf{x}\mathbf{x}^H & \hat{\mathbf{R}}_{xd}(\boldsymbol{\upsilon}) &= \frac{1}{K}\mathbf{x}\mathbf{D}^H(\boldsymbol{\upsilon}) \\ \hat{\mathbf{R}}_{dx}(\boldsymbol{\upsilon}) &= \hat{\mathbf{R}}_{xd}^H(\boldsymbol{\upsilon}) & \hat{\mathbf{R}}_{dd}(\boldsymbol{\upsilon}) &= \frac{1}{K}\mathbf{D}(\boldsymbol{\upsilon})\mathbf{D}^H(\boldsymbol{\upsilon}) \ , \end{aligned} \tag{4.107}$$

it is straightforward to obtain the MLE of amplitudes as

$$\hat{\mathbf{a}}_{\mathrm{ML}} = \hat{\mathbf{R}}_{xd}(\boldsymbol{\upsilon})\hat{\mathbf{R}}_{dd}^{-1}(\boldsymbol{\upsilon})\Big|_{\boldsymbol{\tau}=\hat{\boldsymbol{\tau}}_{\mathrm{ML}}, \mathbf{f}_d=\hat{\mathbf{f}}_{d_{\mathrm{ML}}}} \ , \tag{4.108}$$

which is the Wiener solution.

The ML estimation of synchronization parameters is then obtained by minimizing the nonlinear cost function resulting from the substitution of (4.108) in (4.106),

$$\begin{aligned}\hat{\boldsymbol{\tau}}_{\mathrm{ML}}, \hat{\mathbf{f}}_{d_{\mathrm{ML}}} &= \arg\min_{\boldsymbol{\tau},\mathbf{f}_d}\left\{\Lambda\left(\boldsymbol{\tau},\mathbf{f}_d\right)\right\} = \arg\min_{\boldsymbol{\upsilon}}\left\{\Lambda\left(\boldsymbol{\upsilon}\right)\right\} \\ &= \arg\min_{\boldsymbol{\tau},\mathbf{f}_d}\left\{\hat{r}_{xx} - \hat{\mathbf{R}}_{xd}(\boldsymbol{\upsilon})\hat{\mathbf{R}}_{dd}^{-1}(\boldsymbol{\upsilon})\hat{\mathbf{R}}_{xd}^{H}(\boldsymbol{\upsilon})\right\} . \end{aligned} \tag{4.109}$$

Our aim is to obtain an expression of the likelihood function dependent on $\boldsymbol{\gamma}$, i.e., as a function of user position instead of the synchronization parameters. Notice that $\tau \triangleq \tau(\boldsymbol{\gamma})$ and $f_d \triangleq f_d(\boldsymbol{\gamma})$, as described by equations (2.21) and (2.22). Thus the MLE of user position is given by the vector $\boldsymbol{\gamma}$ that maximizes the likelihood function or, equivalently, the vector $\boldsymbol{\gamma}$ that minimizes $\Lambda\left(\boldsymbol{\gamma}\right)$. As thanks to the invariance principle of the ML estimates under injective functions [Pap01]. Hence,

$$\begin{aligned}\hat{\boldsymbol{\gamma}}_{\mathrm{ML}} &= \arg\min_{\boldsymbol{\gamma}}\left\{\Lambda\left(\boldsymbol{\gamma}\right)\right\} \\ &= \arg\min_{\boldsymbol{\gamma}}\left\{\hat{r}_{xx} - \hat{\mathbf{R}}_{xd}\left(\boldsymbol{\gamma}\right)\hat{\mathbf{R}}_{dd}^{-1}\left(\boldsymbol{\gamma}\right)\hat{\mathbf{R}}_{xd}^{H}\left(\boldsymbol{\gamma}\right)\right\} . \end{aligned} \tag{4.110}$$

Appendix 4.E Consistency of the MLE of position

An estimator of a parameter $\boldsymbol{\gamma}$ is said to be consistent if its estimates converge in probability to the true value (hereinafter denoted by $\breve{\boldsymbol{\gamma}}$) of the parameter as $K \to \infty$, being K the number of samples used. We first deal with the single antenna based receiver and then, treat the more general antenna array case.

• Single–antenna case:

The asymptotic values of the correlation terms in (4.107) are

$$\lim_{K\to\infty} \hat{\mathbf{R}}_{xd} = \lim_{K\to\infty} \frac{1}{K} \left(\mathbf{a}\mathbf{D}(\breve{\boldsymbol{\gamma}}) + \mathbf{n}\right) \mathbf{D}^H(\boldsymbol{\gamma}) = \mathbf{a}\mathbf{C}_{dd}(\breve{\boldsymbol{\gamma}}, \boldsymbol{\gamma}) \tag{4.111}$$

$$\lim_{K\to\infty} \hat{r}_{xx} = r_{xx} \quad , \quad \lim_{K\to\infty} \hat{\mathbf{R}}_{dd} = \mathbf{C}_{dd}(\boldsymbol{\gamma}, \boldsymbol{\gamma}) \tag{4.112}$$

$$\text{where} \qquad \mathbf{C}_{dd}(n, m) = \lim_{K\to\infty} \frac{1}{K} \mathbf{D}(n)\mathbf{D}^H(m) \ . \tag{4.113}$$

The limit of the ML cost function in (4.110) is constructed from substitution of the latter expressions in $\Lambda(\boldsymbol{\gamma})$. Then, adding and subtracting $\mathbf{a}\mathbf{C}_{dd}(\breve{\boldsymbol{\gamma}}, \breve{\boldsymbol{\gamma}})\mathbf{a}^H$, we have:

$$\begin{aligned} \lim_{K\to\infty} \Lambda(\boldsymbol{\gamma}) &= r_{xx} - \mathbf{a}\mathbf{C}_{dd}(\breve{\boldsymbol{\gamma}}, \boldsymbol{\gamma})\mathbf{C}_{dd}^{-1}(\boldsymbol{\gamma}, \boldsymbol{\gamma})\mathbf{C}_{dd}^{H}(\breve{\boldsymbol{\gamma}}, \boldsymbol{\gamma})\mathbf{a}^H \\ &= \mathbf{a}\boldsymbol{\Omega}\mathbf{a}^H + \lim_{K\to\infty} \Lambda(\breve{\boldsymbol{\gamma}}) \qquad (4.114) \\ \boldsymbol{\Omega} &= \mathbf{C}_{dd}(\breve{\boldsymbol{\gamma}}, \breve{\boldsymbol{\gamma}}) - \mathbf{C}_{dd}(\breve{\boldsymbol{\gamma}}, \boldsymbol{\gamma})\mathbf{C}_{dd}^{-1}(\boldsymbol{\gamma}, \boldsymbol{\gamma})\mathbf{C}_{dd}^{H}(\breve{\boldsymbol{\gamma}}, \boldsymbol{\gamma}) \ . \qquad (4.115) \end{aligned}$$

The problem is prove that $\breve{\boldsymbol{\gamma}}$ minimizes the ML cost function

$$\lim_{K\to\infty} \Lambda(\boldsymbol{\gamma}) \geq \lim_{K\to\infty} \Lambda(\breve{\boldsymbol{\gamma}}) \quad , \forall \boldsymbol{\gamma} \tag{4.116}$$

which occurs if $\boldsymbol{\Omega}$ is a non–negative definite matrix, since is straightforward to prove that $\Lambda(\boldsymbol{\gamma})$ is a positive definite matrix. Notice that $\boldsymbol{\Omega}$ is the Schur complement of $\mathbf{C}_{dd}(\boldsymbol{\gamma}, \boldsymbol{\gamma})$ in the matrix formed as

$$\begin{pmatrix} \mathbf{C}_{dd}(\breve{\boldsymbol{\gamma}}, \breve{\boldsymbol{\gamma}}) & \mathbf{C}_{dd}(\breve{\boldsymbol{\gamma}}, \boldsymbol{\gamma}) \\ \mathbf{C}_{dd}^{H}(\breve{\boldsymbol{\gamma}}, \boldsymbol{\gamma}) & \mathbf{C}_{dd}(\boldsymbol{\gamma}, \boldsymbol{\gamma}) \end{pmatrix} = \lim_{K\to\infty} \frac{1}{K} \begin{pmatrix} \mathbf{D}(\breve{\boldsymbol{\gamma}}) \\ \mathbf{D}(\boldsymbol{\gamma}) \end{pmatrix} \begin{pmatrix} \mathbf{D}^H(\breve{\boldsymbol{\gamma}}) & \mathbf{D}^H(\boldsymbol{\gamma}) \end{pmatrix} , \tag{4.117}$$

being the matrix non-negative, due to its quadratic form, any Schur complement of it is also non-negative, *q.e.d.*

• Antenna array case:

The asymptotic values of the correlation terms in equation (4.18) are:

$$\begin{aligned}
\lim_{K\to\infty} \hat{\mathbf{R}}_{xx} &= \mathbf{R}_{xx} \\
\lim_{K\to\infty} \hat{\mathbf{R}}_{xd} &= \lim_{K\to\infty} \frac{1}{K} \left(\mathbf{H}\mathbf{D}(\breve{\boldsymbol{\gamma}}) + \mathbf{N}\right) \mathbf{D}^H(\boldsymbol{\gamma}) \\
&= \mathbf{H}\mathbf{C}_{dd}(\breve{\boldsymbol{\gamma}}, \boldsymbol{\gamma}) \\
\lim_{K\to\infty} \hat{\mathbf{R}}_{dd} &= \mathbf{C}_{dd}(\boldsymbol{\gamma}, \boldsymbol{\gamma}) \ ,
\end{aligned} \tag{4.118}$$

where we define

$$\mathbf{C}_{dd}(n, m) = \lim_{K\to\infty} \frac{1}{K} \mathbf{D}(n)\mathbf{D}^H(m) \tag{4.119}$$

and take into account that noise is uncorrelated with the signal space.

For the sake of clarity, $\Lambda(\boldsymbol{\gamma})$ stands for the ML cost function in equation (4.35):

$$\begin{aligned}
\Lambda(\boldsymbol{\gamma}) &= \ln \left| \hat{\mathbf{W}}(\boldsymbol{\gamma}) \right| \\
&= \ln \left| \hat{\mathbf{R}}_{xx} - \hat{\mathbf{R}}_{xd}(\boldsymbol{\gamma}) \hat{\mathbf{R}}_{dd}^{-1}(\boldsymbol{\gamma}) \hat{\mathbf{R}}_{xd}^H(\boldsymbol{\gamma}) \right|
\end{aligned} \tag{4.120}$$

and the limit of $\Lambda(\boldsymbol{\gamma})$ is constructed from substitution of the asymptotic correlation expressions and the addition and subtraction of $\mathbf{H}\mathbf{C}_{dd}(\breve{\boldsymbol{\gamma}}, \breve{\boldsymbol{\gamma}})\mathbf{H}^H$, resulting in:

$$\begin{aligned}
\lim_{K\to\infty} \Lambda(\boldsymbol{\gamma}) &= \ln \left| \mathbf{R}_{xx} - \mathbf{H}\mathbf{C}_{dd}(\breve{\boldsymbol{\gamma}}, \boldsymbol{\gamma}) \mathbf{C}_{dd}^{-1}(\boldsymbol{\gamma}, \boldsymbol{\gamma}) \mathbf{C}_{dd}^H(\breve{\boldsymbol{\gamma}}, \boldsymbol{\gamma}) \mathbf{H}^H \right| \\
&= \ln \left| \mathbf{R}_{xx} - \mathbf{H}\mathbf{C}_{dd}(\breve{\boldsymbol{\gamma}}, \breve{\boldsymbol{\gamma}}) \mathbf{H}^H \right. \\
&+ \left. \mathbf{H} \left(\mathbf{C}_{dd}(\breve{\boldsymbol{\gamma}}, \breve{\boldsymbol{\gamma}}) - \mathbf{C}_{dd}(\breve{\boldsymbol{\gamma}}, \boldsymbol{\gamma}) \mathbf{C}_{dd}^{-1}(\boldsymbol{\gamma}, \boldsymbol{\gamma}) \mathbf{C}_{dd}^H(\breve{\boldsymbol{\gamma}}, \boldsymbol{\gamma}) \right) \mathbf{H}^H \right| \ .
\end{aligned} \tag{4.121}$$

We make use of a linear algebra result: the determinant is a nondecreasing function. Therefore, for any possible matrix $\mathbf{B}_1$ and any possible non-negative definite matrix $\mathbf{B}_2$, the determinant satisfies that

$$\begin{aligned}
|\mathbf{B}_1 + \mathbf{B}_2| &= \left| \mathbf{B}_1 \left(\mathbf{I} + \mathbf{B}_1^{-1} \mathbf{B}_2 \right) \right| \\
&= |\mathbf{B}_1| \cdot \left| \mathbf{I} + \mathbf{B}_1^{-1} \mathbf{B}_2 \right| \\
&\geq |\mathbf{B}_1| \ ,
\end{aligned} \tag{4.122}$$

since the eigenvalues of $\mathbf{I} + \mathbf{B}_1^{-1}\mathbf{B}_2$ are greater or equal than 1, and the equality only holds when $\mathbf{B}_2 = \mathbf{0}$. Applying this result to equation (4.121), we can identify the term

$$\begin{aligned}
\mathbf{B}_2 &= \mathbf{H}\boldsymbol{\Omega}(\breve{\boldsymbol{\gamma}}, \boldsymbol{\gamma})\mathbf{H}^H \\
\boldsymbol{\Omega}(\breve{\boldsymbol{\gamma}}, \boldsymbol{\gamma}) &= \mathbf{C}_{dd}(\breve{\boldsymbol{\gamma}}, \breve{\boldsymbol{\gamma}}) - \mathbf{C}_{dd}(\breve{\boldsymbol{\gamma}}, \boldsymbol{\gamma}) \mathbf{C}_{dd}^{-1}(\boldsymbol{\gamma}, \boldsymbol{\gamma}) \mathbf{C}_{dd}^H(\breve{\boldsymbol{\gamma}}, \boldsymbol{\gamma}) \ .
\end{aligned} \tag{4.123}$$

Notice that $\mathbf{B}_2$ is non-negative definite since $\mathbf{\Omega}$ is the Schur complement of $\mathbf{C}_{dd}(\boldsymbol{\gamma},\boldsymbol{\gamma})$ in the matrix formed as

$$\begin{pmatrix} \mathbf{C}_{dd}(\breve{\boldsymbol{\gamma}},\breve{\boldsymbol{\gamma}}) & \mathbf{C}_{dd}(\breve{\boldsymbol{\gamma}},\boldsymbol{\gamma}) \\ \mathbf{C}_{dd}^{H}(\breve{\boldsymbol{\gamma}},\boldsymbol{\gamma}) & \mathbf{C}_{dd}(\boldsymbol{\gamma},\boldsymbol{\gamma}) \end{pmatrix} = \lim_{K\to\infty} \frac{1}{K} \begin{pmatrix} \mathbf{D}(\breve{\boldsymbol{\gamma}}) \\ \mathbf{D}(\boldsymbol{\gamma}) \end{pmatrix} \begin{pmatrix} \mathbf{D}^{H}(\breve{\boldsymbol{\gamma}}) & \mathbf{D}^{H}(\boldsymbol{\gamma}) \end{pmatrix} , \tag{4.124}$$

being the matrix non-negative, due to its quadratic form, any Schur complement of it is also non-negative. This proves that

$$\lim_{K\to\infty} \Lambda(\boldsymbol{\gamma}) \geq \ln \left| \mathbf{R}_{xx} - \mathbf{H}\mathbf{C}_{dd}(\breve{\boldsymbol{\gamma}},\breve{\boldsymbol{\gamma}})\mathbf{H}^{H} \right| = \lim_{K\to\infty} \Lambda(\breve{\boldsymbol{\gamma}}) \quad , \forall \boldsymbol{\gamma} \tag{4.125}$$

and the equality holds if and only $\mathbf{\Omega}(\breve{\boldsymbol{\gamma}},\boldsymbol{\gamma}) = \mathbf{0}$, which is only possible when $\boldsymbol{\gamma} = \breve{\boldsymbol{\gamma}}$, *q.e.d.*

5

Fundamental Bounds in GNSS Positioning

THE variance of any unbiased estimator is lower bounded. This can be somewhat frustrating, since it states that, no matter how hard we try, the *best* estimator we can envisage cannot outperform the theoretical performance bound for a given scenario. However, being honest, one cannot expect that a given estimator performs identically (and ideally) under different scenarios. For example, if we aim at estimating the value of a DC level corrupted by thermal noise, it is intuitive that the higher the noise power, the worse our estimates will be (as proved in [Kay93], for instance). Thus, after the initial deception, the knowledge of such a bound turns to provide benefits from a statistical signal processing perspective. First, the bound can be used as a benchmark to compare the performance of any unbiased estimator. Secondly, if an estimator is seen to attain the theoretical bound, one can claim that it is the Minimum Variance Unbiased (MVU) estimator. Last, but not least, the variance bound can be used to have a quantitative result on the accuracy of the MVU estimator. The latter provides the feasible performance values that one can expect when implementing an unbiased estimator, thus, providing a reference for performance benchmarking.

Many variance bounds can be found in the literature. A comprehensive overview and a collection of the most relevant papers on the topic can be found in [Tre07]. These bounds

can be divided into two main categories: classical and Bayesian bounds. Whereas the former considers a nonrandom parameter of interest, the latter assumes that the parameter is drawn from a given distribution [Tre07]. Based on the *covariance inequality* [Leh83, p. 123], we can consider a number of bounds under the aforementioned classification. Classical variance bounds are – in increasing hierarchy, i.e., tighter bounds – the Cramér-Rao Bound (or CRB for short) [Fis22, Rao45, Cra46]; the Bhattacharyya Bound [Bha46]; and the Barankin Bound [Bar49]. The Bayesian counterparts of these variance bounds are the Posterior or Bayesian CRB (PCRB) [Shu57, Tre68]; the Weighted PCRB [Bob87]; the Bayesian Bhattacharyya Bound [Tre68]; the Bobrovsky-Zakai Bound [Bob75, Bob87, Reu97]; and the Weiss-Weinstein Bound] [Wei85]. Also listed in an increasing hierarchy.

The above are bounds on the variance of an unbiased estimator[1], or equivalently on its covariance matrix. However, there are other types of bounds such as the Ziv-Zakai family [Ziv69]. Ziv-Zakai bounds relate the MSE in the estimation problem to the probability of error in a binary hypothesis testing problem.

The CRB falls in the category of *small-error bounds*, meaning that its validity is conditional on having *small* estimation errors. Thus, for instance, the value of the CRB for low SNR or finite samples size conditions might not be accurate, even providing a meaningless bound in these cases. The Bhattacharyya inequality provides also a small error-bound. On the contrary, Barankin bound is of the class of *large-error bounds*, which gives tighter results for a wider range of cases. Although the CRB is the less tighter, it is one of the most used bounds in statistical signal processing when assessing the performance of parameter estimation algorithms [Kay93]. This is because, in general, the CRB is by far the easiest to evaluate compared to the rest of existing bounds. Hereinafter, we will focus on the CRB, letting as future work the derivation of other bounds.

Although we focus on the deterministic (or conditional) CRB, a number of alternatives were proposed in the literature which are listed here for the sake of completeness. The *modified* CRB proposed in [D'A94] provides a bound more relaxed than the CRB which is usually not possible to attain, whose goodness is that it can deal with nuisance parameters in the model. The modified CRB is used in a communications framework, with data symbols being treated as nuisance parameters in synchronization algorithms. The *stochastic* CRB [Ott93, Ger01, Sto01] deals with the case of unknown noise distributions. Thus, the target parameter is extended to include the parameters that describe the noise term of the model. In [Sto98] a *constrained* CRB was proposed, useful when the parameter estimation process considers differentiable and deterministic constraints. Recently, the *intrinsic* CRB [Smi05] extended the CRB to the case in which the parameter space is a connected Riemannian manifold. In contrast, the CRB considers that the parameter

[1]They can be adapted for the biased estimator case, see [Abe93] for instance.

space represents an open subset of some Euclidean space. The latter is not always true [Xav05].

Our aim is to study the theoretical variance bounds of the unbiased estimators treated along the dissertation for the different GNSS positioning problems. In that vein, we can distinguish three problems:

1. What is the lowest attainable positioning accuracy of the conventional two-steps approach?
2. We know from Proposition 4.1 that a Direct Position Estimation (DPE) approach cannot be outperformed by the conventional approach, but, what is the quantitative improvement of using DPE? and, under which conditions we obtain such a significant improvement in the MSE sense?
3. Dealing with the nonlinear filtering problem presented in Chapter 3, we might be interested in evaluating how far the tested Bayesian algorithms are from the theoretical bound.

The first two points refer to the study of the theoretical lower bound of the two existing GNSS positioning approaches. Namely, the conventional two-steps approach and the DPE approach proposed in Chapter 4. Whereas the CRB of synchronization parameters has been addressed in the literature, its relation to the final positioning error has not been revealed yet. For example, [SG00] and [FP06] developed the CRB expressions for the synchronization, DOA and amplitude parameters considering an antenna array receiver. Previously, [Wei94] derived an easy-to-compute formula for the single antenna receiver, stating that the lowest standard deviation of any unbiased time–delay estimator $\hat{\tau}_i$ is

$$\sigma_{\tau_i} = \frac{3.444 \cdot 10^{-4}}{\sqrt{(C/N_0)_i B T_{\text{obs}}}} \leq \sqrt{\mathbb{E}\left\{(\hat{\tau}_i - \tau_i)^2\right\}}\ , \tag{5.1}$$

where index i refers to the i-th satellite, $(C/N_0)_i$ is the corresponding carrier-to-noise density ratio, B is the bandwidth of the low-pass filter at the receiver and T_{obs} the observation time. This bound has the advantage of having a simple formula, which can be implemented without tedious signal simulations. However, it has potential pitfalls such as the inability to take into account complex scenarios, for instance considering interference or multipath propagation. In that sense, the bounds reported in [SG00, FP06] are more versatile and tighter, at the expenses of an increased computational complexity when evaluated. Surprisingly, obtaining an accurate positioning error bound has not been addressed in the literature. The approach taken so far has been to compute the CRB of synchronization parameters – for example as in (5.1) – and obtain the order of magnitude of the positioning error as the error committed in the pseudorange estimate,

i.e., $\sigma_{\rho_i} = c\ \sigma_{\tau_i}$ where c stands for the speed of light constant [Gre01]. This computation provides a coarse order of magnitude of the positioning error committed, but it is rather clumsy when one aims at computing the real CRB of position, where the contribution of all visible satellites is taken into consideration. In Section 5.1.1 we will obtain the CRB of position for the conventional approach, based on the results by [FP06] on the CRB of synchronization parameters. Thus, establishing a rigorous link between the well-known problem of GNSS synchronization and the final estimated position. Section 5.1.2 presents the CRB analysis of the DPE approach, that is to say the lower bound of a direct estimation of position. The latter is also a novel result which constitutes a valuable tool to compare both positioning approaches. Notice that the results in Section 5.1 refer to the classical parameter estimation case, where no prior data is used.

Section 5.2 discusses the third point in the above list. In that case, the aim is to provide a benchmark bound for the Bayesian tracking algorithms considered in Chapter 3. Thus, the PCRB is studied for general DSS models and particularized for the model dealt in Chapter 3 to track synchronization and amplitude parameters of both the LOSS and its multipath replicas.

5.1 Cramér-Rao Bound

The multiple-parameter CRB states that, for any unbiased estimate of a generic, real-valued parameter vector $\boldsymbol{\xi}$, the covariance matrix of the estimates

$$\mathbf{C}(\hat{\boldsymbol{\xi}}) \triangleq \mathbb{E}_{\mathbf{x}|\boldsymbol{\xi}} \left\{ \left(\hat{\boldsymbol{\xi}} - \boldsymbol{\xi} \right) \left(\hat{\boldsymbol{\xi}} - \boldsymbol{\xi} \right)^T \right\} \tag{5.2}$$

is bounded as

$$\mathbf{C}(\hat{\boldsymbol{\xi}}) \geq \mathbf{J}_F^{-1}(\boldsymbol{\xi}) \ , \tag{5.3}$$

where $\mathbf{J}_F(\boldsymbol{\xi})$ is commonly referred to as the Fisher Information Matrix or FIM, whose inverse is the CRB matrix [Sch91]. The matrix inequality in (5.3) means that $\mathbf{C}(\hat{\boldsymbol{\xi}}) - \mathbf{J}_F^{-1}(\boldsymbol{\xi})$ is a non-negative definite matrix. With $\ln p(\mathbf{x}|\boldsymbol{\xi})$ being the log-likelihood function, the FIM elements are defined by

$$\begin{aligned} \left[\mathbf{J}_F(\boldsymbol{\xi})\right]_{u,v} &\triangleq \mathbb{E}_{\mathbf{x}|\boldsymbol{\xi}} \left\{ \frac{\partial \ln p(\mathbf{x}|\boldsymbol{\xi})}{\partial \xi_u} \frac{\partial \ln p(\mathbf{x}|\boldsymbol{\xi})}{\partial \xi_v} \right\} \\ &= -\mathbb{E}_{\mathbf{x}|\boldsymbol{\xi}} \left\{ \frac{\partial^2 \ln p(\mathbf{x}|\boldsymbol{\xi})}{\partial \xi_u \partial \xi_v} \right\} \ , \end{aligned} \tag{5.4}$$

with the expectations being over the distribution of data $\mathbf{x}$ conditioned upon parameter $\boldsymbol{\xi}$, i.e., $p(\mathbf{x}|\boldsymbol{\xi})$.

Therefore, this result provides a lower bound on the variance of any unbiased estimator of the parameter ξ_u:

$$\mathbb{E}_{\mathbf{x}|\boldsymbol{\xi}}\left\{\left(\hat{\xi}_u - \xi_u\right)^2\right\} \geq \left[\mathbf{J}_F^{-1}(\boldsymbol{\xi})\right]_{u,u} \ , \tag{5.5}$$

if the equality holds, the estimator $\hat{\xi}_u$ is said to be *efficient*, meaning that its variance attains the CRB by efficiently using data. An interesting result states that for $\hat{\boldsymbol{\xi}}_{ML}$ being the MLE of $\boldsymbol{\xi}$, it is asymptotically distributed (for large data sets) according to

$$\hat{\boldsymbol{\xi}}_{ML} \sim \mathcal{N}\left(\boldsymbol{\xi}, \mathbf{J}_F^{-1}(\boldsymbol{\xi})\right) \ , \tag{5.6}$$

meaning that ML estimators are asymptotically unbiased and asymptotically efficient, as they attain the CRB.

Let us consider the generic single snapshot signal model expressed as

$$\mathbf{x}(t_k) = \boldsymbol{\mu}_x(t_k, \boldsymbol{\xi}) + \mathbf{n}(t_k) \in \mathbb{C}^N \tag{5.7}$$

for convenience, with $\mathbf{n}(t_k)$ being additive complex Gaussian noise with an arbitrary covariance matrix $\boldsymbol{\Sigma}_n$ [Woo56]. For this model the likelihood function is

$$p(\mathbf{x}|\boldsymbol{\xi}) = \frac{1}{\det\left(\pi^N \boldsymbol{\Sigma}_n\right)} \exp\left(-\left(\mathbf{x}(t_k) - \boldsymbol{\mu}_x(t_k, \boldsymbol{\xi})\right)^H \boldsymbol{\Sigma}_n^{-1} \left(\mathbf{x}(t_k) - \boldsymbol{\mu}_x(t_k, \boldsymbol{\xi})\right)\right) \ . \tag{5.8}$$

Under these assumptions, using the Slepian-Bang's formula [Kay93, Sto97], we know that the u, v-th element of the FIM for the generic K snapshots case is

$$\begin{aligned}\left[\mathbf{J}_F(\boldsymbol{\xi})\right]_{u,v} &= K \operatorname{Tr}\left\{\boldsymbol{\Sigma}_n^{-1} \frac{\partial \boldsymbol{\Sigma}_n}{\partial \xi_v} \boldsymbol{\Sigma}_n^{-1} \frac{\partial \boldsymbol{\Sigma}_n}{\partial \xi_u}\right\} \\ &+ 2\Re\left\{\sum_{k=0}^{K-1} \frac{\partial(\boldsymbol{\mu}_{\mathbf{x}}(t_k, \boldsymbol{\xi}))^H}{\partial \xi_u} \boldsymbol{\Sigma}_n^{-1} \frac{\partial \boldsymbol{\mu}_{\mathbf{x}}(t_k, \boldsymbol{\xi})}{\partial \xi_v}\right\} \ .\end{aligned} \tag{5.9}$$

The rest of the section particularizes (5.9) to obtain the CRB of position of conventional and DPE approaches, Sections 5.1.1 and 5.1.2 respectively. The former is based on the transformation of the CRB of synchronization parameters using the WLS equation in (2.31). This equation relates synchronization parameters to the position of the receiver in the conventional approach. For the sake of clarity, each section reproduces the corresponding signal model which was already presented in Section 4.2, *repetita juvant*.

5.1.1 Conventional positioning approach

In the multiple antenna receiver, an N element antenna array receives M scaled, time–delayed and Doppler–shifted signals with known structure. M corresponds to the number

of visible satellites. Each antenna element receives a replica of the complex baseband signal modeled by equation (4.4), with a different phase depending on the array geometry and the Directions Of Arrival (DOA) [Mon80, Joh93, Tre02]. Then, the single-snapshot model for the conventional approach can be expressed in compact form as

$$\mathbf{x}(t) = \mathbf{G}(\boldsymbol{\theta}, \boldsymbol{\phi})\mathbf{A}\mathbf{d}(t, \boldsymbol{\tau}, \mathbf{f}_d) + \mathbf{n}(t) \tag{5.10}$$

where each row corresponds to one antenna and

- $\mathbf{x}(t) \in \mathbb{C}^{N\times 1}$ is the observed signal vector,
- $\mathbf{G}(\boldsymbol{\theta}, \boldsymbol{\phi}) \in \mathbb{C}^{N\times M}$ is the spatial signature matrix, related to the array geometry and the DOA of the impinging signals. $\boldsymbol{\theta}, \boldsymbol{\phi} \in \mathbb{R}^{M\times 1}$ stand for the azimuth and elevation vectors of the M sources, respectively,
- $\mathbf{A} \in \mathbb{C}^{M\times M}$ is a diagonal matrix with the elements of complex amplitude vector $\mathbf{a} = [a_1, \ldots, a_M]^T \in \mathbb{C}^{M\times 1}$ along its diagonal,
- $\boldsymbol{\tau}, \mathbf{f}_d \in \mathbb{R}^{M\times 1}$ are column vectors which contain time-delays and Doppler–shifts of each satellite,
- $\mathbf{d}(t, \boldsymbol{\tau}, \mathbf{f}_d) = [d_1, \ldots, d_M]^T \in \mathbb{C}^{M\times 1}$, where each component is defined by

  $$d_i = q_i(t - \tau_i)\exp\{j2\pi f_{d_i} t\} \ ,$$

  the delayed Doppler–shifted narrowband signals envelopes, and
- $\mathbf{n}(t) \in \mathbb{C}^{N\times 1}$ represents additive noise and all other disturbing terms, like multipath of each signal or interferences. Statistically, this term is considered Gaussian with an arbitrary covariance matrix, $\boldsymbol{\Sigma}_n$.

In this case, from equation (5.10) we have that

$$\boldsymbol{\mu}_x(t_k, \boldsymbol{\xi}_A) = \mathbf{G}(\boldsymbol{\theta}, \boldsymbol{\phi})\mathbf{A}\mathbf{d}(t_k, \boldsymbol{\tau}, \mathbf{f}_d) \tag{5.11}$$

and the vector of unknown parameters is

$$\boldsymbol{\xi}_A = \begin{pmatrix} \boldsymbol{\alpha} \\ \boldsymbol{\psi} \\ \boldsymbol{\upsilon} \end{pmatrix} \ , \tag{5.12}$$

which can be split into amplitudes $\boldsymbol{\alpha}$, Directions of Arrival $\boldsymbol{\psi}$ and synchronization parameters $\boldsymbol{\upsilon}$:

$$\begin{aligned} \boldsymbol{\alpha} &= \left[\Re\{\mathbf{a}\}^T, \Im\{\mathbf{a}\}^T\right]^T \in \mathbb{R}^{2M\times 1} \\ \boldsymbol{\psi} &= \left[\boldsymbol{\theta}^T, \boldsymbol{\phi}^T\right]^T \in \mathbb{R}^{2M\times 1} \\ \boldsymbol{\upsilon} &= \left[\boldsymbol{\tau}^T, \mathbf{f}_d^T\right]^T \in \mathbb{R}^{2M\times 1} \ . \end{aligned} \tag{5.13}$$

Therefore, the FIM can be expressed with submatrices, $2M \times 2M$ sized:

$$\mathbf{J}_F(\boldsymbol{\xi}_A) = \begin{pmatrix} \mathbf{J}_{\boldsymbol{\alpha\alpha}} & \mathbf{J}_{\boldsymbol{\psi\alpha}}^T & \mathbf{J}_{\boldsymbol{\upsilon\alpha}}^T \\ \mathbf{J}_{\boldsymbol{\psi\alpha}} & \mathbf{J}_{\boldsymbol{\psi\psi}} & \mathbf{J}_{\boldsymbol{\upsilon\psi}}^T \\ \mathbf{J}_{\boldsymbol{\upsilon\alpha}} & \mathbf{J}_{\boldsymbol{\upsilon\psi}} & \mathbf{J}_{\boldsymbol{\upsilon\upsilon}} \end{pmatrix} . \tag{5.14}$$

The elements of such submatrices can be computed using the definition obtained in equation (5.9), accounting that $\boldsymbol{\Sigma}_n$ is independent of $\boldsymbol{\xi}_A$. For $u, v \in \{1, ..., 2M\}$:

$$\mathbf{J}_{\alpha_u\alpha_v} = 2\Re\left\{\sum_{k=0}^{K-1} \mathbf{d}(t_k)^H \frac{\partial \mathbf{A}^H}{\partial \alpha_u} \mathbf{G}^H \boldsymbol{\Sigma}_n^{-1} \mathbf{G} \frac{\partial \mathbf{A}}{\partial \alpha_v} \mathbf{d}(t_k)\right\} \tag{5.15}$$

$$\mathbf{J}_{\psi_u\alpha_v} = 2\Re\left\{\sum_{k=0}^{K-1} \mathbf{d}(t_k)^H \mathbf{A}^H \frac{\partial \mathbf{G}^H}{\partial \psi_u} \boldsymbol{\Sigma}_n^{-1} \mathbf{G} \frac{\partial \mathbf{A}}{\partial \alpha_v} \mathbf{d}(t_k)\right\} \tag{5.16}$$

$$\mathbf{J}_{\upsilon_u\alpha_v} = 2\Re\left\{\sum_{k=0}^{K-1} \frac{\partial \mathbf{d}(t_k)^H}{\partial \upsilon_u} \mathbf{A}^H \mathbf{G}^H \boldsymbol{\Sigma}_n^{-1} \mathbf{G} \frac{\partial \mathbf{A}}{\partial \alpha_v} \mathbf{d}(t_k)\right\} \tag{5.17}$$

$$\mathbf{J}_{\psi_u\psi_v} = 2\Re\left\{\sum_{k=0}^{K-1} \mathbf{d}(t_k)^H \mathbf{A}^H \frac{\partial \mathbf{G}^H}{\partial \psi_u} \boldsymbol{\Sigma}_n^{-1} \frac{\partial \mathbf{G}}{\partial \psi_v} \mathbf{A}\mathbf{d}(t_k)\right\} \tag{5.18}$$

$$\mathbf{J}_{\upsilon_u\psi_v} = 2\Re\left\{\sum_{k=0}^{K-1} \frac{\partial \mathbf{d}(t_k)^H}{\partial \upsilon_u} \mathbf{A}^H \mathbf{G}^H \boldsymbol{\Sigma}_n^{-1} \frac{\partial \mathbf{G}}{\partial \psi_v} \mathbf{A}\mathbf{d}(t_k)\right\} \tag{5.19}$$

$$\mathbf{J}_{\upsilon_u\upsilon_v} = 2\Re\left\{\sum_{k=0}^{K-1} \frac{\partial \mathbf{d}(t_k)^H}{\partial \upsilon_u} \mathbf{A}^H \mathbf{G}^H \boldsymbol{\Sigma}_n^{-1} \mathbf{G}\mathbf{A} \frac{\partial \mathbf{d}(t_k)}{\partial \upsilon_v}\right\} , \tag{5.20}$$

where $\frac{\partial \mathbf{A}}{\partial \alpha_i}$ is an all-zero $2M \times 2M$ matrix except for a 1 in the u, u position in case of $1 \leq u \leq M$, and an all-zero $2M \times 2M$ matrix except for a $j = \sqrt{-1}$ in the u, u position in case of $M < u \leq 2M$. Here, the case $1 \leq u \leq M$ stands for the derivative with respect to the elements of $\Re\{\mathbf{a}\}$ and the case $M < u \leq 2M$ stands for the derivative with respect to the elements of $\Im\{\mathbf{a}\}$.

Let define $\mathbf{G}^T = \exp\{j\pi\mathbf{K}\mathbf{R}\}$, where $\mathbf{K} \in \mathbb{R}^{M\times 3}$ is the wavenumber matrix, defined as

$$\mathbf{K} = \begin{pmatrix} \cos(\theta_1)\cos(\phi_1) & \sin(\theta_1)\cos(\theta_1) & \sin(\phi_1) \\ \vdots & \vdots & \vdots \\ \cos(\theta_M)\cos(\phi_M) & \sin(\theta_M)\cos(\theta_M) & \sin(\phi_M) \end{pmatrix} \tag{5.21}$$

and having its rows pointing toward the corresponding emitter, with θ_i being the angle of the source i defined anticlockwise from the x axis on the xy plane and ϕ_i the angle respect the xy plane. Refer to Appendix 4.B for details on the spatial signature matrix.

On the other hand,

$$\mathbf{R} = \begin{pmatrix} r_{x_1} & \dots & r_{x_N} \\ r_{y_1} & \dots & r_{y_N} \\ r_{z_1} & \dots & r_{z_N} \end{pmatrix} \tag{5.22}$$

is the matrix of sensor element position normalized to units of half wavelengths with respect the x, y and z axes. Then, the derivative of $\mathbf{G}$ is

$$\frac{\partial \mathbf{G}}{\partial \psi_u} = j\pi \mathbf{R}^T \frac{\partial \mathbf{K}^T}{\partial \psi_u} \odot \exp\left\{ j\pi \mathbf{R}^T \mathbf{K}^T \right\} \ , \tag{5.23}$$

where the derivatives of $\mathbf{K}$, are:

$$\frac{\partial \mathbf{K}}{\partial \psi_u} = \left[-\sin(\theta_u)\cos(\phi_u), \cos^2(\theta_u) - \sin^2(\theta_u), 0 \right] \qquad \text{for } 1 \leq u \leq M \tag{5.24}$$

for the u–th row and zeros otherwise; and

$$\frac{\partial \mathbf{K}}{\partial \psi_u} = \left[-\cos(\theta_{(u-M)})\sin(\phi_{(u-M)}), 0, \cos(\phi_{(u-M)}) \right] \qquad \text{for } M < u \leq 2M \tag{5.25}$$

for the $(u-M)$–th row and zeros otherwise. Hence, in (5.24) the derivative is with respect to the elements of $\boldsymbol{\theta}$ and in (5.25) with respect to the elements of $\boldsymbol{\phi}$. Finally,

$$\frac{\partial \mathbf{d}(t_k)}{\partial \upsilon_u} = \begin{pmatrix} 0 \\ \vdots \\ -\dot{q}_u(t_k - \tau_u) e^{j2\pi f_{d_u} t_k} \\ \vdots \\ 0 \end{pmatrix} \qquad \text{for } 1 \leq u \leq M \tag{5.26}$$

and

$$\frac{\partial \mathbf{d}(t_k)}{\partial \upsilon_u} = \begin{pmatrix} 0 \\ \vdots \\ j2\pi t_k q_{(u-M)}(t_k - \tau_{(u-M)}) e^{j2\pi f_{d_{(u-M)}} t_k} \\ \vdots \\ 0 \end{pmatrix} \qquad \text{for } M < u \leq 2M \tag{5.27}$$

stand for the derivatives with respect to the elements of $\boldsymbol{\tau}$ and $\mathbf{f}_d$, respectively. In the first case, $\dot{q}_i(t)$ is the *d*erivative *o*f *t*ime of the waveform $q_i(t)$.

Using equations (5.23-5.27) into (5.15-5.20), the FIM is completely defined and therefore the CRB for all the parameters can be directly computed by inverting (5.14).

The conventional approach provides a deterministic mapping between time-delay estimates and the positioning solution, as provided by equation (2.31). Thus, it suffices to transform the CRB obtained for the former to evaluate the CRB of the latter. According to [Kay93], if the desired estimate can be expressed as $[\hat{\mathbf{p}}^T, \hat{\delta t}]^T = g(\hat{\boldsymbol{\tau}})$, then its covariance matrix is bounded by

$$\mathbf{C}(\hat{\mathbf{p}}, \hat{\delta t}) \geq \frac{\partial g(\boldsymbol{\tau})}{\partial \boldsymbol{\tau}} \, \mathbf{J}_{\tau\tau}^{-1} \, \frac{\partial g(\boldsymbol{\tau})^T}{\partial \boldsymbol{\tau}} \ , \tag{5.28}$$

where $\mathbf{J}_{\tau\tau}$ is the FIM of the time-delay parameter, obtained from (5.20) with $1 \leq \{u, v\} \leq M$. In this case we know from (2.28) and (2.31) that

$$g(\boldsymbol{\tau}) = \begin{pmatrix} \mathbf{p}^o \\ 0 \end{pmatrix} + \left(\mathbf{T}^H \boldsymbol{\Omega}_w \mathbf{T}\right)^{-1} \mathbf{T}^H \boldsymbol{\Omega}_w \mathbf{y} \ , \tag{5.29}$$

where its Jacobian matrix is

$$\frac{\partial g(\boldsymbol{\tau})}{\partial \boldsymbol{\tau}} = c \left(\mathbf{T}^H \boldsymbol{\Omega}_w \mathbf{T}\right)^{-1} \mathbf{T}^H \boldsymbol{\Omega}_w \ , \tag{5.30}$$

considering that the linearization point is the true position, i.e., $\mathbf{p}^o = \mathbf{p}$, and c is the speed of light. Notice that we consider the conventional positioning approach with pseudorange measurements, therefore it is not justified to observe that Doppler deviations are not explicitly used in (5.28). Indeed, as justified in Chapter 2, Doppler shifts are implicitly used in order to stabilize the tracking loops in charge of estimating $\boldsymbol{\tau}$.

From the above it follows that the covariance matrix of position and clock offset estimates in the conventional approach is lower bounded by the CRB matrix as

$$\mathbf{C}(\hat{\mathbf{p}}, \hat{\delta t}) \geq c^2 \left(\left(\mathbf{T}^H \boldsymbol{\Omega}_w \mathbf{T}\right)^{-1} \mathbf{T}^H \boldsymbol{\Omega}_w\right) \mathbf{J}_{\tau\tau}^{-1} \left(\left(\mathbf{T}^H \boldsymbol{\Omega}_w \mathbf{T}\right)^{-1} \mathbf{T}^H \boldsymbol{\Omega}_w\right)^T \ , \tag{5.31}$$

where $\mathbf{J}_{\tau\tau}^{-1}$ is expressed in units of time.

5.1.2 Direct Position Estimation approach

In the multiple antenna receiver, an N element antenna array receives M scaled, time–delayed and Doppler–shifted signals with known structure. M corresponds to the number of visible satellites. Each antenna element receives a replica of the complex baseband signal modeled by equation (4.12), with a different phase depending on the array geometry and the Directions Of Arrival (DOA) [Mon80, Joh93, Tre02]. Then, the single-snapshot model for the DPE approach can be expressed in compact form as

$$\mathbf{x}(t) = \mathbf{G}(\boldsymbol{\theta}, \boldsymbol{\phi}) \mathbf{A} \mathbf{d}(t, \boldsymbol{\gamma}) + \mathbf{n}(t) \tag{5.32}$$

where each row corresponds to one antenna and

- $\mathbf{x}(t) \in \mathbb{C}^{N\times 1}$ is the observed signal vector,
- $\mathbf{G}(\boldsymbol{\theta}, \boldsymbol{\phi}) \in \mathbb{C}^{N\times M}$ is the spatial signature matrix, related to the array geometry and the DOA of the impinging signals. $\boldsymbol{\theta}, \boldsymbol{\phi} \in \mathbb{R}^{M\times 1}$ stand for the azimuth and elevation vectors of the M sources, respectively,
- $\mathbf{A} \in \mathbb{C}^{M\times M}$ is a diagonal matrix with the elements of complex amplitude vector $\mathbf{a} = [a_1, \ldots, a_M]^T \in \mathbb{C}^{M\times 1}$ along its diagonal,
- $\boldsymbol{\gamma} \in \mathbb{R}^{n_\gamma \times 1}$ is the column vector gathering all considered motion parameters, whose simplest configuration is $\boldsymbol{\gamma} = \left[\mathbf{p}^T, \mathbf{v}^T, \delta t\right]^T$,
- $\mathbf{d}(t, \boldsymbol{\gamma}) = [d_1, \ldots, d_M]^T \in \mathbb{C}^{M\times 1}$, where each component is defined by

$$d_i = q_i(t - \tau_i(\boldsymbol{\gamma})) \exp\{j2\pi f_{d_i}(\boldsymbol{\gamma})t\} \ ,$$

  the delayed Doppler–shifted narrowband signals envelopes as functions of $\boldsymbol{\gamma}$, and
- $\mathbf{n}(t) \in \mathbb{C}^{N\times 1}$ represents additive noise and all other disturbing terms, like multipath of each signal or interferences. Statistically, this term is considered Gaussian with an arbitrary covariance matrix, $\boldsymbol{\Sigma}_n$.

In this case,

$$\boldsymbol{\mu}_x(t_k, \boldsymbol{\xi}_B) = \mathbf{G}(\boldsymbol{\theta}, \boldsymbol{\phi})\mathbf{A}\mathbf{d}(t_k, \boldsymbol{\gamma}) \tag{5.33}$$

and the vector of unknown parameters is

$$\boldsymbol{\xi}_B = \begin{pmatrix} \boldsymbol{\alpha} \\ \boldsymbol{\psi} \\ \boldsymbol{\gamma} \end{pmatrix} \ , \tag{5.34}$$

where $\boldsymbol{\gamma}$ can include any parameter related to the position and motion of the receiver, and the receiver clock drift.

Therefore, the FIM can be expressed with submatrices:

$$\mathbf{J}_F(\boldsymbol{\xi}_B) = \begin{pmatrix} \mathbf{J}_{\boldsymbol{\alpha}\boldsymbol{\alpha}} & \mathbf{J}_{\boldsymbol{\psi}\boldsymbol{\alpha}}^T & \mathbf{J}_{\boldsymbol{\gamma}\boldsymbol{\alpha}}^T \\ \mathbf{J}_{\boldsymbol{\psi}\boldsymbol{\alpha}} & \mathbf{J}_{\boldsymbol{\psi}\boldsymbol{\psi}} & \mathbf{J}_{\boldsymbol{\gamma}\boldsymbol{\psi}}^T \\ \mathbf{J}_{\boldsymbol{\gamma}\boldsymbol{\alpha}} & \mathbf{J}_{\boldsymbol{\gamma}\boldsymbol{\psi}} & \mathbf{J}_{\boldsymbol{\gamma}\boldsymbol{\gamma}} \end{pmatrix} \ , \tag{5.35}$$

where $\mathbf{J}_{\boldsymbol{\alpha}\boldsymbol{\alpha}}$, $\mathbf{J}_{\boldsymbol{\psi}\boldsymbol{\alpha}}$ and $\mathbf{J}_{\boldsymbol{\psi}\boldsymbol{\psi}}$ are $2M \times 2M$ sized, previously defined in (5.15), (5.16) and (5.18) respectively. Then, we have to determine the values of $\mathbf{J}_{\boldsymbol{\gamma}\boldsymbol{\alpha}}, \mathbf{J}_{\boldsymbol{\gamma}\boldsymbol{\psi}} \in \mathbb{R}^{\dim\{\boldsymbol{\gamma}\}\times 2M}$ and $\mathbf{J}_{\boldsymbol{\gamma}\boldsymbol{\gamma}} \in \mathbb{R}^{\dim\{\boldsymbol{\gamma}\}\times\dim\{\boldsymbol{\gamma}\}}$:

$$\mathbf{J}_{\gamma_u\alpha_v} = 2\Re\left\{\sum_{k=0}^{K-1}\frac{\partial\mathbf{d}(t_k)^H}{\partial\gamma_u}\mathbf{A}^H\mathbf{G}^H\mathbf{Q}^{-1}\mathbf{G}\frac{\partial\mathbf{A}}{\partial\alpha_v}\mathbf{d}(t_k)\right\} \tag{5.36}$$

$$\mathbf{J}_{\gamma_u\psi_v} = 2\Re\left\{\sum_{k=0}^{K-1}\frac{\partial\mathbf{d}(t_k)^H}{\partial\gamma_u}\mathbf{A}^H\mathbf{G}^H\mathbf{Q}^{-1}\frac{\partial\mathbf{G}}{\partial\psi_v}\mathbf{A}\mathbf{d}(t_k)\right\} \tag{5.37}$$

$$\mathbf{J}_{\gamma_u\gamma_v} = 2\Re\left\{\sum_{k=0}^{K-1}\frac{\partial\mathbf{d}(t_k)^H}{\partial\gamma_u}\mathbf{A}^H\mathbf{G}^H\mathbf{Q}^{-1}\mathbf{G}\mathbf{A}\frac{\partial\mathbf{d}(t_k)}{\partial\gamma_v}\right\}\ , \tag{5.38}$$

where the expression for $\frac{\partial\mathbf{d}(t_k)}{\partial\gamma_u}$ is the one lacking in these expressions.

Recalling the model in (5.32), we can express the basis-function vector as

$$\mathbf{d}(t_k,\boldsymbol{\gamma}) = \mathbf{q}(t_k-\boldsymbol{\tau}(\boldsymbol{\gamma}))\odot\exp\{j2\pi\mathbf{f}_d(\boldsymbol{\gamma})t_k\}\ , \tag{5.39}$$

with $\mathbf{q}(t_k-\boldsymbol{\tau}(\boldsymbol{\gamma}))\in\mathbb{C}^{M\times 1}$ being the vector containing $q_i(t_k-\tau_i(\boldsymbol{\gamma}))$ in its i–th row, i.e.,

$$\mathbf{q}(t_k-\boldsymbol{\tau}(\boldsymbol{\gamma})) = \begin{pmatrix} q_1(t_k-\tau_1(\boldsymbol{\gamma})) \\ \vdots \\ q_M(t_k-\tau_M(\boldsymbol{\gamma})) \end{pmatrix}\ . \tag{5.40}$$

Then, derivating (5.39) with respect to γ_u – the u-th element in $\boldsymbol{\gamma}$ – we have

$$\begin{aligned}\frac{\partial\mathbf{d}(t_k)}{\partial\gamma_u} &= \frac{\partial\mathbf{q}(t_k-\boldsymbol{\tau}(\boldsymbol{\gamma}))}{\partial\gamma_u}\odot\exp\{j2\pi\mathbf{f}_d(\boldsymbol{\gamma})t_k\} \\ &+ \mathbf{q}(t_k-\boldsymbol{\tau}(\boldsymbol{\gamma}))\odot\frac{\partial\exp\{j2\pi\mathbf{f}_d(\boldsymbol{\gamma})t_k\}}{\partial\gamma_u}\ ,\end{aligned} \tag{5.41}$$

where

$$\begin{aligned}\frac{\partial\mathbf{q}(t_k-\boldsymbol{\tau}(\boldsymbol{\gamma}))}{\partial\gamma_u} &= \begin{pmatrix} \frac{\partial q_1(t_k-\tau_1(\boldsymbol{\gamma}))}{\partial\gamma_u} \\ \vdots \\ \frac{\partial q_M(t_k-\tau_M(\boldsymbol{\gamma}))}{\partial\gamma_u} \end{pmatrix} \\ &= \begin{pmatrix} -\frac{\partial\tau_1(\boldsymbol{\gamma})}{\partial\gamma_u}\dot{q}_1(t_k-\tau_1(\boldsymbol{\gamma})) \\ \vdots \\ -\frac{\partial\tau_M(\boldsymbol{\gamma})}{\partial\gamma_u}\dot{q}_M(t_k-\tau_M(\boldsymbol{\gamma})) \end{pmatrix} \overset{(a)}{=} \sum_{i=1}^{M}\frac{\partial\mathbf{d}(t_k)}{\partial\tau_i}\end{aligned} \tag{5.42}$$

and

$$\frac{\partial \exp\{j2\pi \mathbf{f}_d(\boldsymbol{\gamma})t_k\}}{\partial \gamma_u} = \begin{pmatrix} \frac{\partial \exp\{j2\pi f_{d_1}(\boldsymbol{\gamma})t_k\}}{\partial \gamma_u} \\ \vdots \\ \frac{\partial \exp\{j2\pi f_{d_M}(\boldsymbol{\gamma})t_k\}}{\partial \gamma_u} \end{pmatrix} = \begin{pmatrix} j2\pi t_k \exp\{j2\pi f_{d_1}(\boldsymbol{\gamma})t_k\} \frac{\partial f_{d_1}(\boldsymbol{\gamma})\}}{\partial \gamma_u} \\ \vdots \\ j2\pi t_k \exp\{j2\pi f_{d_M}(\boldsymbol{\gamma})t_k\} \frac{\partial f_{d_M}(\boldsymbol{\gamma})\}}{\partial \gamma_u} \end{pmatrix}, \tag{5.43}$$

in (a) we used the result in equation (5.26).

Substituting (5.42) and (5.42) in (5.41), and rearranging terms, it results that

$$\frac{\partial \mathbf{d}(t_k)}{\partial \gamma_u} = \left(\sum_{i=1}^{M} \frac{\partial \mathbf{d}(t_k)}{\partial \tau_i} \right) \odot \frac{\partial \boldsymbol{\tau}(\boldsymbol{\gamma})}{\partial \gamma_u} + \left(\sum_{i=1}^{M} \frac{\partial \mathbf{d}(t_k)}{\partial f_{d_i}} \right) \odot \frac{\partial \mathbf{f}_d(\boldsymbol{\gamma})}{\partial \gamma_u}, \tag{5.44}$$

where $\frac{\partial \mathbf{d}(t_k)}{\partial \tau_i}$ and $\frac{\partial \mathbf{d}(t_k)}{\partial f_{d_i}}$ are calculated using equations (5.26) and (5.27), respectively.

In the sequel we consider that

$$\boldsymbol{\gamma} \triangleq \begin{pmatrix} \mathbf{p} \\ \mathbf{v} \\ \delta t \end{pmatrix}, \tag{5.45}$$

i.e., the parameter of interest gathers position coordinates $\mathbf{p} = [x, y, z]^T$, velocity coordinates $\mathbf{v} = [v_x, v_y, v_z]^T$ and the bias of the receiver clock δt. Thus, we have that $\dim\{\boldsymbol{\gamma}\} = 7$. In that case, the i–th row of matrices $\frac{\partial \boldsymbol{\tau}(\boldsymbol{\gamma})}{\partial \boldsymbol{\gamma}}$ and $\frac{\partial \mathbf{f}_d(\boldsymbol{\gamma})}{\partial \boldsymbol{\gamma}}$ are

$$\frac{\partial \tau_i(\boldsymbol{\gamma})}{\partial \boldsymbol{\gamma}} = \begin{pmatrix} \frac{\partial \tau_i(\boldsymbol{\gamma})}{\partial \mathbf{p}} \\ \frac{\partial \tau_i(\boldsymbol{\gamma})}{\partial \mathbf{v}} \\ \frac{\partial \tau_i(\boldsymbol{\gamma})}{\partial \delta t} \end{pmatrix}^T \quad \text{and} \quad \frac{\partial f_{d_i}(\boldsymbol{\gamma})}{\partial \boldsymbol{\gamma}} = \begin{pmatrix} \frac{\partial f_{d_i}(\boldsymbol{\gamma})}{\partial \mathbf{p}} \\ \frac{\partial f_{d_i}(\boldsymbol{\gamma})}{\partial \mathbf{v}} \\ \frac{\partial f_{d_i}(\boldsymbol{\gamma})}{\partial \delta t} \end{pmatrix}^T, \tag{5.46}$$

respectively. The derivatives in (5.46) can be found in Appendices 5.A and 5.B. The derivatives with respect to γ_u of the synchronization parameters $\boldsymbol{\tau}(\boldsymbol{\gamma})$ and $\mathbf{f}_d(\boldsymbol{\gamma})$ follow from their definitions in equations (2.21) and (2.22), respectively.

At this point, all the elements in equation (5.35) can be computed. Therefore, the inversion of the FIM matrix in (5.35) yields to the computation of the CRB of position under the DPE framework.

5.2 Posterior Cramér-Rao Bound

The Posterior Cramér-Rao Bound (PCRB) provides a lower bound on the MSE matrix for random parameters[2]. The Bayesian paradigm considers that the parameter of interest $\boldsymbol{\xi}$ is random with a given a priori distribution, denoted by $p(\boldsymbol{\xi})$. Then, the estimation error

$$\mathbf{C}(\hat{\boldsymbol{\xi}}) \triangleq \mathbb{E}_{\mathbf{x},\boldsymbol{\xi}} \left\{ \left(\hat{\boldsymbol{\xi}} - \boldsymbol{\xi} \right) \left(\hat{\boldsymbol{\xi}} - \boldsymbol{\xi} \right)^T \right\} \tag{5.47}$$

is bounded as

$$\mathbf{C}(\hat{\boldsymbol{\xi}}) \geq \mathbf{J}_B^{-1}(\boldsymbol{\xi}) \ , \tag{5.48}$$

where $\mathbf{J}_B^{-1}(\boldsymbol{\xi})$ is referred to as the Bayesian Information Matrix (BIM), its inverse provides the PCRB matrix [Tre07]. The matrix inequality in (5.48) means that $\mathbf{C}(\hat{\boldsymbol{\xi}}) - \mathbf{J}_B^{-1}(\boldsymbol{\xi})$ is a non-negative definite matrix. The BIM elements are computed as

$$\begin{aligned} [\mathbf{J}_B(\boldsymbol{\xi})]_{u,v} &\triangleq \mathbb{E}_{\mathbf{x},\boldsymbol{\xi}} \left\{ \frac{\partial \ln p(\mathbf{x},\boldsymbol{\xi})}{\partial \xi_u} \frac{\partial \ln p(\mathbf{x},\boldsymbol{\xi})}{\partial \xi_v} \right\} \\ &= -\mathbb{E}_{\mathbf{x},\boldsymbol{\xi}} \left\{ \frac{\partial^2 \ln p(\mathbf{x},\boldsymbol{\xi})}{\partial \xi_u \partial \xi_v} \right\} \ , \end{aligned} \tag{5.49}$$

with the expectations being over the joint distribution of data $\mathbf{x}$ and the parameter $\boldsymbol{\xi}$, i.e., $p(\mathbf{x},\boldsymbol{\xi})$. Similarly as in the CRB, an Bayesian estimator of a random parameter is said to be Bayesian efficient when its variance attains the PCRB.

The BIM can be expressed as the summation of two terms: $\mathbf{J}_D(\boldsymbol{\xi})$ and $\mathbf{J}_P(\boldsymbol{\xi})$ [Tre68]. The former corresponds to the contribution of data measurements and the latter represents the information provided by prior, i.e.,

$$\mathbf{J}_B(\boldsymbol{\xi}) = \mathbf{J}_D(\boldsymbol{\xi}) + \mathbf{J}_P(\boldsymbol{\xi}) \ , \tag{5.50}$$

where the u,v-th element of each term is obtained as

$$\begin{aligned} [\mathbf{J}_D(\boldsymbol{\xi})]_{u,v} &\triangleq \mathbb{E}_{\mathbf{x},\boldsymbol{\xi}} \left\{ \frac{\partial \ln p(\mathbf{x}|\boldsymbol{\xi})}{\partial \xi_u} \frac{\partial \ln p(\mathbf{x}|\boldsymbol{\xi})}{\partial \xi_v} \right\} \\ &= -\mathbb{E}_{\mathbf{x},\boldsymbol{\xi}} \left\{ \frac{\partial^2 \ln p(\mathbf{x}|\boldsymbol{\xi})}{\partial \xi_u \partial \xi_v} \right\} \\ &= \mathbb{E}_{\boldsymbol{\xi}} \left\{ -\mathbb{E}_{\mathbf{x}|\boldsymbol{\xi}} \left\{ \frac{\partial^2 \ln p(\mathbf{x}|\boldsymbol{\xi})}{\partial \xi_u \partial \xi_v} \right\} \right\} \\ &= \mathbb{E}_{\boldsymbol{\xi}} \left\{ [\mathbf{J}_F(\boldsymbol{\xi})]_{u,v} \right\} \end{aligned} \tag{5.51}$$

[2]We can also find the Posterior Cramér-Rao Bound in the literature under the name of Bayesian Cramér-Rao Bound. Along the dissertation we used the former, as it is widespread used in nonlinear filtering literature.

and

$$\begin{aligned}\left[\mathbf{J}_P(\boldsymbol{\xi})\right]_{u,v} &\triangleq \mathbb{E}_{\boldsymbol{\xi}}\left\{\frac{\partial \ln p(\boldsymbol{\xi})}{\partial \xi_u}\frac{\partial \ln p(\boldsymbol{\xi})}{\partial \xi_v}\right\} \\ &= -\mathbb{E}_{\boldsymbol{\xi}}\left\{\frac{\partial^2 \ln p(\boldsymbol{\xi})}{\partial \xi_u \partial \xi_v}\right\} . \end{aligned} \tag{5.52}$$

From (5.51) we observe that the contribution of data to the Bayesian bound is equivalent to the expected value of $\mathbf{J}_F(\boldsymbol{\xi})$ over the distribution $p(\boldsymbol{\xi})$. Thus, the data contribution to the Bayesian estimation process corresponds to the averaged information matrix of the deterministic case, i.e., the FIM. Moreover, when no prior data is considered, $\mathbf{J}_D(\boldsymbol{\xi})$ equals $\mathbf{J}_F(\boldsymbol{\xi})$ and the term $\mathbf{J}_P(\boldsymbol{\xi})$ disappears. Which reduces to the deterministic case discussed in Section 5.1.

So far, the PCRB was discussed from a static parameter estimation point of view. In other words, parameter $\boldsymbol{\xi}$ was the realization of a *r.v.* which we wanted to estimate. Another setup is possible. Dealing with the nonlinear filtering problem, tracking the time evolution of the parameter of interest (a.k.a. state vector) is the objective. As extensively discussed in Chapter 3 a state-space model can be used to characterize the evolution of the system and, particularly, we considered the discrete state-space model. We will see in Section 5.2.1 that, in that case, the evaluation of the PCRB can be demanding due to a dimensionality growth with time. Fortunately, a result due to [Tic98] allows one to compute the bound recursively. The result was extended in [Sim01] to the prediction and smoothing problems discussed in Section 3.1.

5.2.1 Recursive computation of the PCRB for Nonlinear Filtering

Let $\mathbf{x}_k \in \mathbb{C}^{n_x}$ be a vector of measured data, $\mathbf{z}_k \in \mathbb{R}^{n_z}$ an unknown random parameter and $\hat{\mathbf{z}}_k(\mathbf{x}_{1:k})$ an estimator of $\mathbf{z}_k$ considering available data at time instant k, $\mathbf{x}_{1:k} = \{\mathbf{x}_1, \ldots, \mathbf{x}_k\}$. The discrete state-space model provides a twofold characterization of the system under study, i.e., evolution of states and measurement dependence with states:

$$\mathbf{z}_k = \mathbf{f}_{k-1}(\mathbf{z}_{k-1}, \boldsymbol{\nu}_k) \tag{5.53}$$

$$\mathbf{x}_k = \mathbf{h}_k(\mathbf{z}_k, \mathbf{n}_k) , \tag{5.54}$$

respectively. $\mathbf{f}_{k-1}(\cdot)$ and $\mathbf{h}_k(\cdot)$ are known, possibly nonlinear, functions of the state $\mathbf{z}_k$. $\boldsymbol{\nu}_k$ and $\mathbf{n}_k$ are referred to as process and measurement noises, respectively. Both noises are assumed with known statistics and mutually independent. The initial *a priori* distribution of the state vector is assumed known, $p(\mathbf{z}_0)$.

For the filtering problem, the minimum theoretical achievable error variance is given by the PCRB [Ris04, Tre07, Ber01]. The PCRB states that the covariance matrix of the estimation error is bounded by the inverse of the Bayesian Information Matrix[3], $\mathbf{J}_k \in \mathbb{R}^{n_z \times n_z}$, i.e.,

$$\mathbf{C}_k(\mathbf{z}_k) \triangleq \mathbb{E}_{\mathbf{x}_k,\mathbf{z}_k}\left\{(\hat{\mathbf{z}}_k(\mathbf{x}_{1:k}) - \mathbf{z}_k)(\hat{\mathbf{z}}_k(\mathbf{x}_{1:k}) - \mathbf{z}_k)^T\right\} \geq \mathbf{J}_k^{-1} \ , \tag{5.55}$$

where the expectation is with respect to both measurements and states. The inequality in (5.55) means that the difference $\mathbf{C}_k(\mathbf{z}_k) - \mathbf{J}_k^{-1}$ is a positive semidefinite matrix and, if the equality holds, the estimator is said to be statistically efficient. Let the Trajectory Information Matrix, $\mathbf{J}(\mathbf{z}_{0:k}) \in \mathbb{R}^{(k+1)n_z \times (k+1)n_z}$, be the information matrix derived from the joint distribution for estimating $\mathbf{z}_{0:k}$ and defined as

$$\mathbf{J}(\mathbf{z}_{0:k}) = \mathbb{E}_{\mathbf{x}_k,\mathbf{z}_k}\left\{-\triangle_{\mathbf{z}_{0:k}}^{\mathbf{z}_{0:k}} \ln p(\mathbf{x}_{1:k}, \mathbf{z}_{0:k})\right\} \ , \tag{5.56}$$

where we define $\mathbf{z}_{0:k} = \{\mathbf{z}_0, \ldots, \mathbf{z}_k\}$ as the entire trajectory of state-vectors. We are interested in the problem of computing the BIM for estimating $\mathbf{x}_k$, to compute the bound in (5.55). Decomposing $\mathbf{z}_{0:k}$ and $\mathbf{J}(\mathbf{z}_{0:k})$ as

$$\mathbf{z}_{0:k} = \begin{pmatrix} \mathbf{z}_{0:k-1} \\ \mathbf{z}_k \end{pmatrix} \tag{5.57}$$

and

$$\begin{aligned} \mathbf{J}(\mathbf{z}_{0:k}) &= \begin{pmatrix} \mathbf{A}_k & \mathbf{B}_k \\ \mathbf{B}_k^T & \mathbf{C}_k \end{pmatrix} \qquad (5.58) \\ &\triangleq \begin{pmatrix} \mathbb{E}_{\mathbf{x}_k,\mathbf{z}_k}\left\{-\triangle_{\mathbf{z}_{0:k-1}}^{\mathbf{z}_{0:k-1}} \ln p(\mathbf{x}_{1:k}, \mathbf{z}_{0:k})\right\} & \mathbb{E}_{\mathbf{x}_k,\mathbf{z}_k}\left\{-\triangle_{\mathbf{z}_{0:k-1}}^{\mathbf{z}_k} \ln p(\mathbf{x}_{1:k}, \mathbf{z}_{0:k})\right\} \\ \mathbb{E}_{\mathbf{x}_k,\mathbf{z}_k}\left\{-\triangle_{\mathbf{z}_k}^{\mathbf{z}_{0:k-1}} \ln p(\mathbf{x}_{1:k}, \mathbf{z}_{0:k})\right\} & \mathbb{E}_{\mathbf{x}_k,\mathbf{z}_k}\left\{-\triangle_{\mathbf{z}_k}^{\mathbf{z}_k} \ln p(\mathbf{x}_{1:k}, \mathbf{z}_{0:k})\right\} \end{pmatrix} \ , \end{aligned}$$

respectively, we can compute the PCRB, $\mathbf{J}_k^{-1} \in \mathbb{R}^{n_z \times n_z}$, as the lower-right corner of $\mathbf{J}^{-1}(\mathbf{z}_{0:k})$, i.e.,

$$\mathbf{J}_k = \mathbf{C}_k - \mathbf{B}_k^T \mathbf{A}_k^{-1} \mathbf{B}_k \ . \tag{5.59}$$

Notice that the computation of the $n_z \times n_z$ BIM involves either the inversion of $\mathbf{A}_k \in \mathbb{R}^{kn_z \times kn_z}$ or the inversion of $\mathbf{J}^{-1}(\mathbf{z}_{0:k})$. Clearly, this can imply a high computational cost.

[3] where we dropped the subindex B for the sake of clarity, while keeping in mind that

$$\begin{aligned} \mathbf{J}_k &\triangleq \mathbf{J}_B(\mathbf{z}_k) \\ &= \mathbf{J}_D(\mathbf{z}_k) + \mathbf{J}_P(\mathbf{z}_k) \\ &= \mathbb{E}_{\mathbf{x}_k,\mathbf{z}_k}\left\{\frac{\partial \ln p(\mathbf{x}_k|\mathbf{z}_k)}{\partial \mathbf{z}_k} \frac{\partial \ln p(\mathbf{x}_k|\mathbf{z}_k)}{\partial \mathbf{z}_k}\right\} + \mathbb{E}_{\mathbf{z}_k}\left\{\frac{\partial \ln p(\mathbf{z}_k|\mathbf{z}_{k-1})}{\partial \mathbf{z}_k} \frac{\partial \ln p(\mathbf{z}_k|\mathbf{z}_{k-1})}{\partial \mathbf{z}_k}\right\} \ . \end{aligned}$$

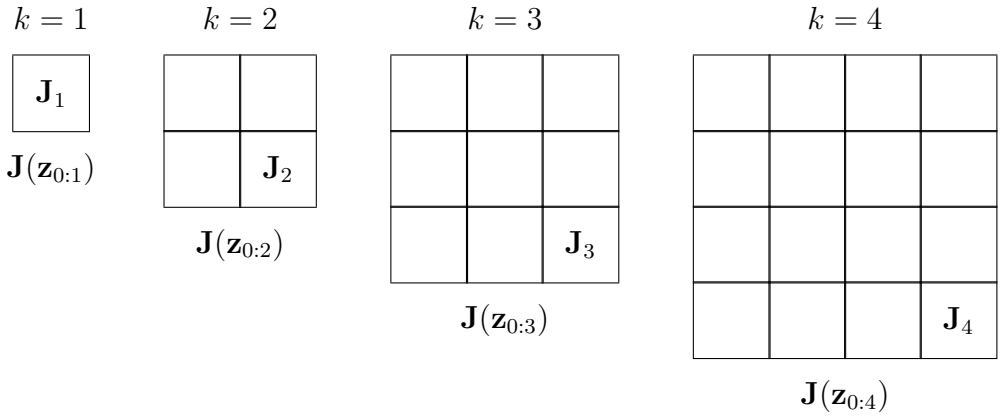

Figure 5.1: Dimensionality growth of the Trajectory Information Matrix with k.

As depicted in Figure 5.1, the dimensionality of $\mathbf{J}(\mathbf{z}_{0:k})$ grows with k. This poses a computational problem to the computation of the PCRB, which conveys the idea of deriving a recursive computation of the bound. Some papers proposed to relate the nonlinear filtering problem to an *equivalent* linear system, e.g., [Bob75]. However, the problem is partially solved in these approaches and still the recursion was to be found by [Tic98]. The latter provides a recipe for computing $\mathbf{J}_k$ without manipulating large matrices, such as $\mathbf{J}(\mathbf{z}_{0:k})$. Proposition 5.1 states the main result of that work.

Proposition 5.1. *The sequence* $\{\mathbf{J}_k\}$ *of posterior information submatrices for estimating state vectors* $\{\mathbf{z}_k\}$ *can be obtained using the following recursion:*

$$\mathbf{J}_{k+1} = \mathbf{D}_k^{22} - \mathbf{D}_k^{21} \left(\mathbf{J}_k + \mathbf{D}_k^{11}\right)^{-1} \mathbf{D}_k^{12} \ , \tag{5.60}$$

where

$$\begin{aligned}
\mathbf{D}_k^{11} &= \mathbb{E}_{\mathbf{z}_k,\mathbf{z}_{k+1}} \left\{ -\triangle_{\mathbf{z}_k}^{\mathbf{z}_k} \ln p(\mathbf{z}_{k+1}|\mathbf{z}_k) \right\} \\
\mathbf{D}_k^{12} &= \mathbb{E}_{\mathbf{z}_k,\mathbf{z}_{k+1}} \left\{ -\triangle_{\mathbf{z}_k}^{\mathbf{z}_{k+1}} \ln p(\mathbf{z}_{k+1}|\mathbf{z}_k) \right\} \\
\mathbf{D}_k^{21} &= \mathbb{E}_{\mathbf{z}_k,\mathbf{z}_{k+1}} \left\{ -\triangle_{\mathbf{z}_{k+1}}^{\mathbf{z}_k} \ln p(\mathbf{z}_{k+1}|\mathbf{z}_k) \right\} = \left[\mathbf{D}_k^{12}\right]^T \\
\mathbf{D}_k^{22} &= \mathbb{E}_{\mathbf{z}_k,\mathbf{z}_{k+1}} \left\{ -\triangle_{\mathbf{z}_{k+1}}^{\mathbf{z}_{k+1}} \ln p(\mathbf{z}_{k+1}|\mathbf{z}_k) \right\} \\
&+ \mathbb{E}_{\mathbf{z}_{k+1},\mathbf{x}_{k+1}} \left\{ -\triangle_{\mathbf{z}_{k+1}}^{\mathbf{z}_{k+1}} \ln p(\mathbf{x}_{k+1}|\mathbf{z}_{k+1}) \right\}
\end{aligned} \tag{5.61}$$

and the initialization is done considering the prior density of the states:

$$\mathbf{J}_0 = \mathbb{E}_{\mathbf{z}_0} \left\{ -\triangle_{\mathbf{z}_0}^{\mathbf{z}_0} \ln p(\mathbf{z}_0) \right\} \ . \tag{5.62}$$

Proof. See Appendix 5.C. □

The recursion in (5.60) is extremely useful in many cases where the computation of the PCRB is mathematically untractable. In addition, matrices involved in the recursive formula are $n_z \times n_z$, in contrast to the problem in equation (5.56) which has a dimension that increases with k (see Figure 5.1).

When the general DSS model described by (5.53) and (5.54) is particularized, some simplifications apply to the recursive computation of the PCRB in (5.60) and (5.61). The rest of the section is devoted to present three of those particularizations, with the latter being the model considered in Chapter 3.

Additive Gaussian Noise

In this case, the general DSS model is expressed as:

$$\begin{aligned} \mathbf{z}_k &= \mathbf{f}_{k-1}(\mathbf{z}_{k-1}) + \boldsymbol{\nu}_k \\ \mathbf{x}_k &= \mathbf{h}_k(\mathbf{z}_k) + \mathbf{n}_k \ , \end{aligned} \tag{5.63}$$

where both process and measurement noise are zero-mean and Gaussian distributed, with covariance matrices being $\boldsymbol{\Sigma}_{z,k}$ and $\boldsymbol{\Sigma}_{n,k}$ respectively. Then, we have that

$$\begin{aligned} -\ln p(\mathbf{z}_{k+1}|\mathbf{z}_k) &= c_1 + \frac{1}{2}\left(\mathbf{z}_{k+1} - \mathbf{f}_k(\mathbf{z}_k)\right)^T \boldsymbol{\Sigma}_{z,k}^{-1}\left(\mathbf{z}_{k+1} - \mathbf{f}_k(\mathbf{z}_k)\right) \\ -\ln p(\mathbf{x}_{k+1}|\mathbf{z}_{k+1}) &= c_2 + \frac{1}{2}\left(\mathbf{x}_{k+1} - \mathbf{h}_{k+1}(\mathbf{z}_{k+1})\right)^T \boldsymbol{\Sigma}_{n,k+1}^{-1}\left(\mathbf{x}_{k+1} - \mathbf{h}_{k+1}(\mathbf{z}_{k+1})\right) \ , \end{aligned} \tag{5.64}$$

where c_1 and c_2 are constants, and

$$\begin{aligned} \mathbf{D}_k^{11} &= \mathbb{E}_{\mathbf{z}_k}\left\{\tilde{\mathbf{F}}_k^T \boldsymbol{\Sigma}_{z,k}^{-1} \tilde{\mathbf{F}}_k\right\} \\ \mathbf{D}_k^{12} &= -\mathbb{E}_{\mathbf{z}_k}\left\{\tilde{\mathbf{F}}_k^T\right\} \boldsymbol{\Sigma}_{z,k}^{-1} \\ \mathbf{D}_k^{22} &= \boldsymbol{\Sigma}_{z,k}^{-1} + \mathbb{E}_{\mathbf{z}_{k+1}}\left\{\tilde{\mathbf{H}}_{k+1}^T \boldsymbol{\Sigma}_{k+1,n}^{-1} \tilde{\mathbf{H}}_{k+1}\right\} \ . \end{aligned} \tag{5.65}$$

In (5.65) we use the definitions of Jacobian of $\mathbf{h}_k(\mathbf{z}_k)$ and $\mathbf{h}_k(\mathbf{z}_k)$ evaluated at the true value of $\mathbf{z}_k$:

$$\begin{aligned} \tilde{\mathbf{H}}_k &= \left[\nabla_{\mathbf{z}_k} \mathbf{h}_k^T(\mathbf{z}_k)\right]^T \\ \tilde{\mathbf{F}}_k &= \left[\nabla_{\mathbf{z}_k} \mathbf{f}_k^T(\mathbf{z}_k)\right]^T \ , \end{aligned} \tag{5.66}$$

respectively.

The difficulty in evaluating (5.65) comes due to the need of performing the expectation over $\mathbf{z}_k$ and $\mathbf{z}_{k+1}$. The common approach is to approximate such expectations using Monte-Carlo simulation, i.e., create a significative number of state-vector trajectories, calculate the corresponding PCRB and average them to obtain the theoretical PCRB of the system under study. In certain cases, where the process noise is small, the expectation can be dropped out as a good approximation.

Linear systems under Additive Gaussian Noise

The linear DSS model corrupted by AGN reduces to :

$$\begin{aligned} \mathbf{z}_k &= \mathbf{F}_{k-1}\mathbf{z}_{k-1} + \boldsymbol{\nu}_k \\ \mathbf{x}_k &= \mathbf{H}_k\mathbf{z}_k + \mathbf{n}_k \ , \end{aligned} \tag{5.67}$$

where $\mathbf{F}_{k-1}$ and $\mathbf{H}_k$ are known matrices that represent linear functions, referred to as *transitional* and *measurement* matrices respectively. $\boldsymbol{\nu}_k$ and $\mathbf{n}_k$ are mutually independent random variables drawn from a zero-mean white Gaussian probability density function with known covariance matrices, $\boldsymbol{\Sigma}_{z,k}$ and $\boldsymbol{\Sigma}_{n,k}$ respectively.

In this case, it is straightforward to show that the recursion can be expressed as:

$$\mathbf{J}_{k+1} = \boldsymbol{\Sigma}_{z,k}^{-1} - \boldsymbol{\Sigma}_{z,k}^{-1}\mathbf{F}_k \left(\mathbf{J}_k + \mathbf{F}_k^T\boldsymbol{\Sigma}_{z,k}^{-1}\mathbf{F}_k\right)^{-1} \mathbf{F}_k^T\boldsymbol{\Sigma}_{z,k}^{-1} + \mathbf{H}_{k+1}^T\boldsymbol{\Sigma}_{k+1,n}^{-1}\mathbf{H}_{k+1} \ , \tag{5.68}$$

and using the matrix inversion lemma

$$\mathbf{J}_{k+1} = \left(\boldsymbol{\Sigma}_{z,k} + \mathbf{F}_k^T\mathbf{J}_k^{-1}\mathbf{F}_k\right)^{-1} + \mathbf{H}_{k+1}^T\boldsymbol{\Sigma}_{k+1,n}^{-1}\mathbf{H}_{k+1} \tag{5.69}$$

we obtain an expression with two terms: one corresponds to the process prediction and the other to the measurement update.

Linear states and nonlinear measurements under Additive Gaussian Noise

Consider a DSS model as:

$$\begin{aligned} \mathbf{z}_k &= \mathbf{F}_{k-1}\mathbf{z}_{k-1} + \boldsymbol{\nu}_k \\ \mathbf{x}_k &= \mathbf{h}_k(\mathbf{z}_k) + \mathbf{n}_k \ , \end{aligned} \tag{5.70}$$

where the previous definitions hold. Some simplifications apply to (5.65 under that DSS model. Considering that states are drawn from a Gaussian pdf and $p(\mathbf{z}_0) = \mathcal{N}\left(\bar{\mathbf{z}}_0, \boldsymbol{\Sigma}_{0,z}\right)$, after mathematical manipulation of equation (5.62) we obtain that $\mathbf{J}_0 = \boldsymbol{\Sigma}_{0,z}^{-1}$. In addition,

$$\begin{aligned} \mathbf{D}_k^{11} &= \mathbf{F}_k^T\boldsymbol{\Sigma}_{z,k}^{-1}\mathbf{F}_k \\ \mathbf{D}_k^{12} &= -\mathbf{F}_k^T\boldsymbol{\Sigma}_{z,k}^{-1} \\ \mathbf{D}_k^{22} &= \boldsymbol{\Sigma}_{z,k}^{-1} + \mathbb{E}_{\mathbf{z}_{k+1}}\left\{\tilde{\mathbf{H}}_{k+1}^T\boldsymbol{\Sigma}_{k+1,n}^{-1}\tilde{\mathbf{H}}_{k+1}\right\} \ , \end{aligned} \tag{5.71}$$

where we use the definitions in (5.66). Notice that, after simplifications due to the model at hand, matrices $\mathbf{D}_k^{11}$, $\mathbf{D}_k^{12}$ and $\mathbf{D}_k^{21}$ are deterministic and can be easily obtained. However, due to the non-linearity in the measurement model, the expectation operator in the computation of $\mathbf{D}_k^{22}$ cannot be dropped out. In order to compute this expectation, a Monte-Carlo approximation can be performed as previously commented.

The particularization in (5.70) is the case of the model considered in Chapter 3. Recalling from Section 3.3, maintaining the definitions therein, we can express the studied DSS model as

$$\begin{aligned} \mathbf{z}_k &= \mathbf{F}_{k-1}\mathbf{z}_{k-1} + \boldsymbol{\nu}_k \\ \mathbf{x}_k &= \underbrace{\mathbf{Q}_k^T(\boldsymbol{\tau}_k)\mathbf{T}\begin{bmatrix} \Re\{\mathbf{a}_k\} \\ \Im\{\mathbf{a}_k\} \end{bmatrix}}_{\mathbf{h}_k(\mathbf{z}_k)} + \mathbf{n}_k \ , \end{aligned} \tag{5.72}$$

where $\mathbf{T} = \begin{pmatrix} \mathbf{I}_M \mid j\mathbf{I}_M \end{pmatrix}$ and with

$$\mathbf{z}_k \triangleq \begin{bmatrix} \Re\{\mathbf{a}_k\} \\ \Im\{\mathbf{a}_k\} \\ \boldsymbol{\tau}_k \end{bmatrix} \in \mathbb{R}^{3M\times 1} \ . \tag{5.73}$$

being the state vector (complex amplitudes and time-delays). Notice that M stands for the number of received signals from a given satellite (LOSS plus multipath replicas). With this setup

$$\begin{aligned} \tilde{\mathbf{H}}_k &= \left[\nabla_{\mathbf{z}_k}\mathbf{h}_k^T(\mathbf{z}_k)\right]^T \\ &= \left[\left[\nabla_{a_k^r}\mathbf{h}_k^T(\mathbf{z}_k)\right]^T, \left[\nabla_{a_k^i}\mathbf{h}_k^T(\mathbf{z}_k)\right]^T, \left[\nabla_{\tau_k}\mathbf{h}_k^T(\mathbf{z}_k)\right]^T\right] \end{aligned} \tag{5.74}$$

with

$$\begin{aligned} \left[\nabla_{a_k^r}\mathbf{h}_k^T(\mathbf{z}_k)\right]^T &= \left[\mathbf{Q}_k^T(\boldsymbol{\tau}_k)\mathbf{T}\ \mathbf{1}_1, \ldots, \mathbf{Q}_k^T(\boldsymbol{\tau}_k)\mathbf{T}\ \mathbf{1}_M\right] \\ \left[\nabla_{a_k^i}\mathbf{h}_k^T(\mathbf{z}_k)\right]^T &= \left[\mathbf{Q}_k^T(\boldsymbol{\tau}_k)\mathbf{T}\ \mathbf{1}_{M+1}, \ldots, \mathbf{Q}_k^T(\boldsymbol{\tau}_k)\mathbf{T}\ \mathbf{1}_{2M}\right] \end{aligned} \tag{5.75}$$

where $\mathbf{1}_i$ represents the all-zeros vector except for a 1 in the i-th position. The gradient $\left[\nabla_{\tau_k}\mathbf{h}_k^T(\mathbf{z}_k)\right]^T$ following Appendix 3.E.

5.3 Computer Simulations

The expressions for the CRB of both approaches can be applied to any of the existing GNSS signal structures. In particular, we considered hereinafter the well-known Global

Positioning System, GPS for short. The civilian GPS signal is referred to as the Coarse Acquisition (C/A) code and it is a spread–spectrum signal transmitted at a carrier frequency of $f_c = 1575.42$ MHz with a chip rate of 1.023 MHz, see Chapter 2. For the considered GPS receiver architecture, the received signal was filtered with a 1.1 MHz bandwidth filter, down-converted to baseband and then digitized at a sampling frequency of $f_s = 5.714$ MHz. The observation time was 1 ms, which corresponds to $K = 5714$ samples. Two receiver architectures were considered: one considering a single antenna receiver ($N = 1$) and another with an 8-element circular antenna array ($N = 8$). The receiver was considered static in both cases, i.e., $\mathbf{v} = \mathbf{0}^T$, without loss of generality.

The recreated scenario corresponds to a realistic constellation geometry, with an elevation mask of 5^o. In particular, two versions were simulated. The first one consisted of $M = 7$ satellites, whose azimuth and elevation angles were (in degrees)

$$\begin{aligned} \boldsymbol{\theta} &= [288.9, 215.2, 87.9, 295.4, 123.5, 46.1, 130.6]^T \\ \boldsymbol{\phi} &= [46.9, 24.5, 29.1, 32.1, 71.5, 24.4, 60.7]^T \ , \end{aligned} \tag{5.76}$$

respectively. The corresponding PRN code numbers [Par96] of each satellite in (5.76) were $\{9, 12, 17, 18, 26, 28, 29\}$. The second considered scenario was one with $M = 4$ satellites, those with PRN numbers $\{9, 12, 17, 18\}$, with the same geometry described by (5.76). Basically, the latter emulates the occultation of three satellites (i.e., $\{26, 28, 29\}$) in the first considered scenario. Both geometries are illustrated in Figure 5.2.

In order to avoid plotting the bounds for the three position coordinates, the following figures depict the CRB of the three-dimensional position vector, defined as

$$\sigma_p^2 \triangleq \mathbb{E}\left\{(\mathbf{p} - \hat{\mathbf{p}})^T(\mathbf{p} - \hat{\mathbf{p}})\right\} = \sigma_x^2 + \sigma_y^2 + \sigma_z^2 \ , \tag{5.77}$$

where σ_x^2, σ_y^2 and σ_z^2 are the CRBs of each coordinate, as computed by the corresponding CRB. Recall that what is referred to as the conventional approach is the positioning solution given by first estimating synchronization parameters independently and using those estimates to compute user's location.

With this setup, Figure 5.3 shows a comparison of both derived CRBs of position as a function of the C/N_0 of the visible satellites. For the sake of simplicity, we considered that all satellites had the same C/N_0. Under that scenario, both conventional and DPE approaches appear to have similar bounds in terms of position accuracy. Hence, potentially both positioning alternatives are able to obtain same performances in such *ideal* scenario.

DPE performance improvement was seen to came from the fact that each satellite has its independent propagation channel. This introduces a kind of diversity which we can refer to as *satellital diversity* [Clo06f]. The diversity feature of a direct positioning approach was pointed out also in [Ama05, Ama08a], for the radiolocation problem. Aiming at proving this concept, an scenario where all but one satellites had the same $C/N_0 = 45$

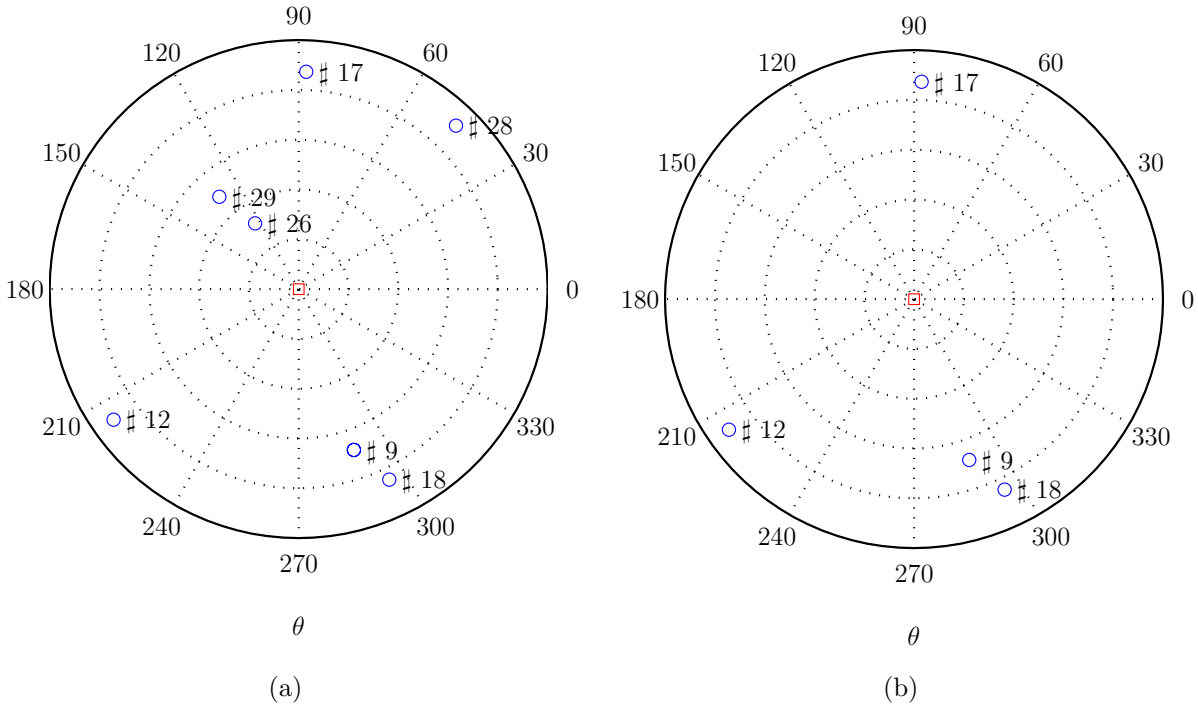

Figure 5.2: Constellation geometries considered in the simulations, the red box represents the receiver location with respect to satellites. (a) corresponds to $M = 4$ satellites and (b) to $M = 7$ visible satellites.

dB-Hz whereas one varied its C/N_0 in a range was tested. The results are plotted in Figure 5.4. It can be seen that DPE exhibits some robustness against sudden shadowing of one of the satellites in the constellation. This is because the rest of visible satellites are used to estimate user's position, overcoming a weaker power level of the faded satellite. On the contrary, if that satellite is used to compute user's position in the conventional approach, it can yield to higher error variances as seen in Figure 5.4. The conventional approach is improved when the WLS algorithm (refer to equation (2.31) for further comments) is considered, with the weighting matrix being computed as in (4.51). However, the conventional approach is still unable to attain the performance of a direct estimation approach. Surprisingly, under a certain C/N_0 threshold, the use of a single antenna based receiver implementing the DPE approach can overcome the results of an antenna array receiver under the conventional positioning approach (in the specific setup in Figure 5.4 this threshold is on the order of 25 dB-Hz).

A more challenging scenario was tested, that accounted for multipath propagation. GNSS receivers are only interested in estimating delays of signals received directly from

the satellites, since they are the ones that carry information of direct propagation time. Hence, reflections distort the received signal in a way that may cause a bias in delay and carrier-phase estimations [Van93]. Multipath is known to be one of the most hazardous effects in GNSS receivers and probably the dominant source of error in high-precision applications. A result given in [Wei95] says that any unbiased time delay estimator based on a single antenna has a variance that approaches to infinity when the relative delay between the LOSS and its replica approach to zero. Relatively short delays are just the case of real-life multipath, where the scatterers use to be close to the receiver and the extra path covered by the wave is shorter than one chip period (about 300 m for a chip rate of 1.023 Mcps), situation referred to as *coherent* multipath in the literature.

For the following test, a multipath signal for satellite ♯9 was introduced whose signal-to-multipath ratio (SMR) was 3 dB. The relative azimuth of the replica with respect to the LOSS was 180^o, with the same elevation angle. All satellites had same power levels, $C/N_0 = 45$ dB-Hz. Figure 5.5 shows the squared root CRBs as a function of the relative delay between the multipath replica and the LOSS of satellite ♯9, normalized to the chip period T_c. The results in Figure 5.5 are in accordance with those published in [Clo07b], in which DPE was seen to provide the receiver with improved multipath mitigation capabilities with respect to the conventional approach. It is important to remark that, even in the single antenna case, the receiver is able to virtually eliminate coherent multipath effects when implementing DPE. Finally, we tested an scenario where the multipath replica had higher power than the LOSS. That is the case of most indoor propagation channels or urban channels. In particular the scenario considered that $C/N_0 = 45$ dB-Hz for all satellites, except for ♯9 that $C/N_0 = 25$ dB-Hz, and the SMR was -20 dB. The results are shown in Figure 5.6 for the single antenna receiver and in Figure 5.7 for the circular antenna array architecture. It can be observed that DPE potentially improves the performance of the conventional approach for the two constellation geometries considered and that it outperforms the latter when both consider antenna array based front-ends. Again, the use of WLS improves the results of LS-based positioning but DPE is more robust to the multipath effect.

5.4 Summary

The need for an accurate knowledge of estimation bounds is present in many (if not all) signal processing applications. Definitely, it is also the case of the GNSS positioning problem which drives the dissertation. The objectives of this chapter are twofold: illustrate the derivation of the variance bounds (particularly the CRB) for a number of interesting signal processing problems found in the GNSS literature; and use these results in the preceding chapters of the dissertation. Namely, we discussed the bounds for:

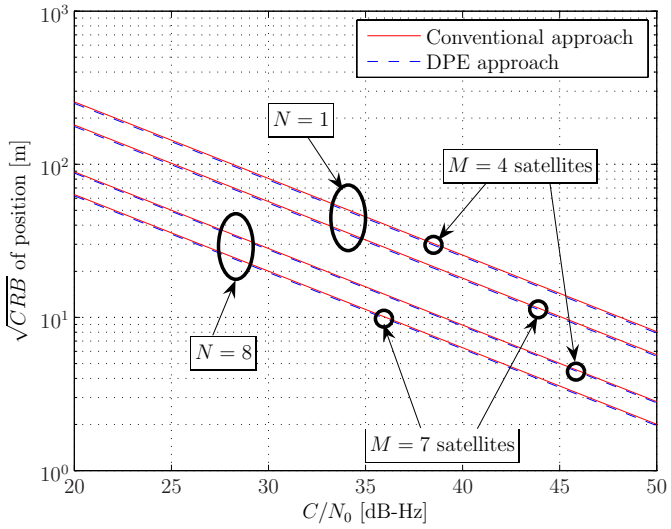

Figure 5.3: CRB versus C/N_0 of the satellites.

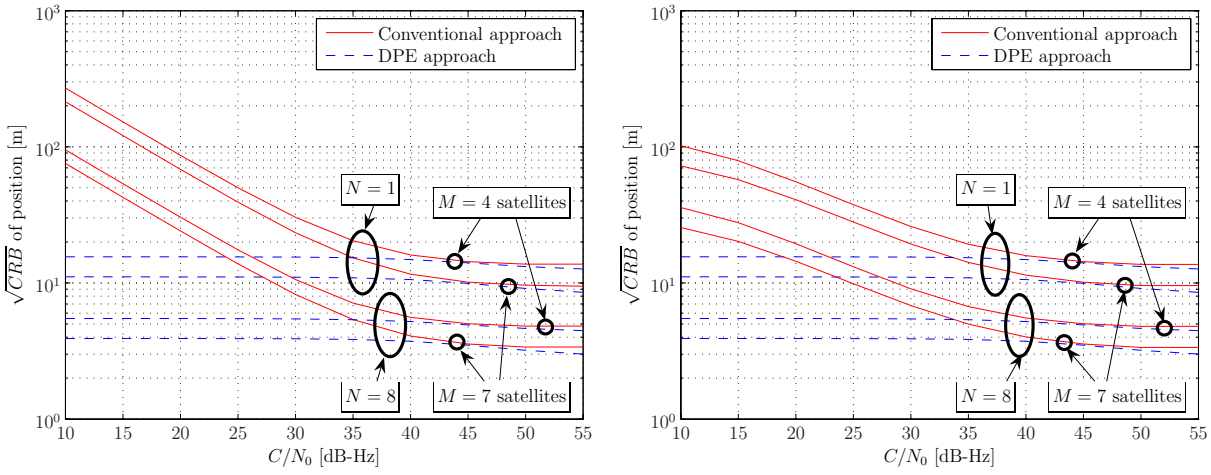

(a) (b)

Figure 5.4: CRB as a function of the C/N_0 of one of the satellites and $C/N_0 = 45$ dB-Hz for the rest. (a) DPE vs. conventional approach with LS and (b) DPE vs. conventional approach with WLS.

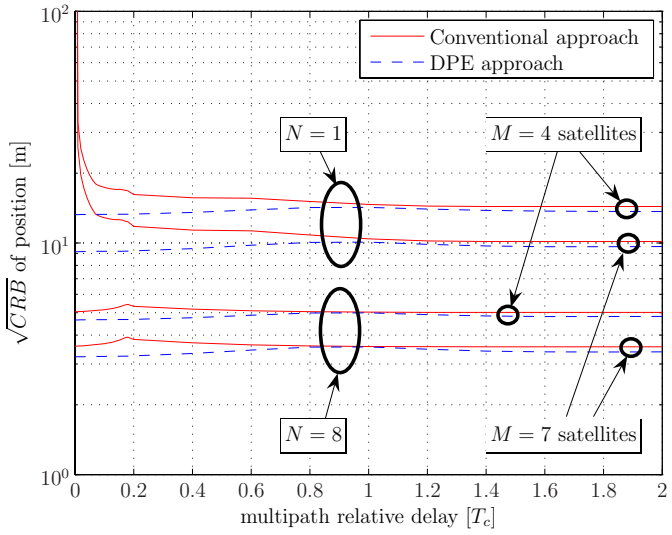

Figure 5.5: CRB as a function of the relative multipath delay.

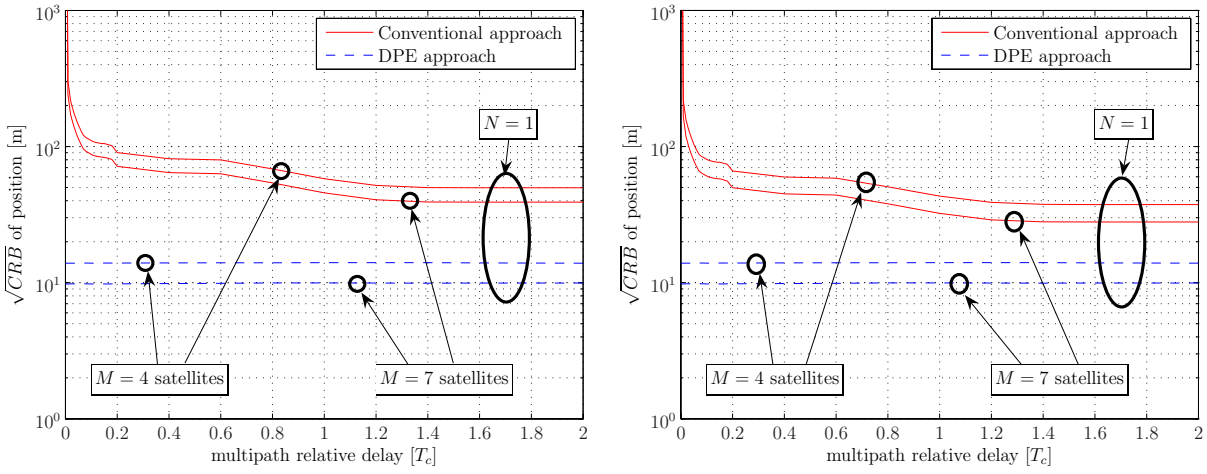

(a) (b)

Figure 5.6: CRB as a function of the relative multipath delay. In this case, the replica has higher power level than the LOSS with $N = 1$. (a) DPE vs. conventional approach with LS and (b) DPE vs. conventional approach with WLS.

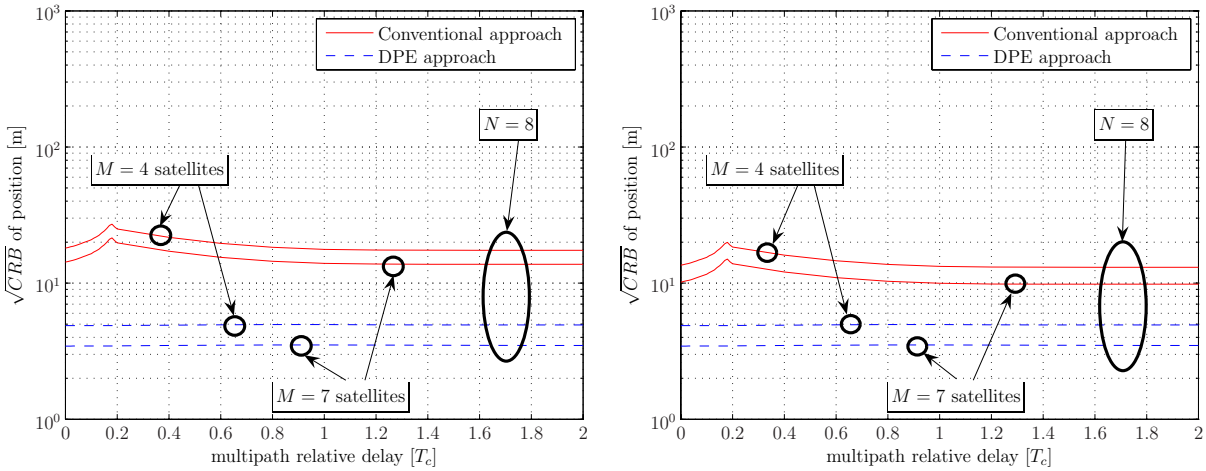

Figure 5.7: CRB as a function of the relative multipath delay. In this case, the replica has higher power level than the LOSS and $N = 8$ antenna elements. (a) DPE vs. conventional approach with LS and (b) DPE vs. conventional approach with WLS.

1. **Conventional two-steps positioning approach.** Although the CRB of synchronization parameters (i.e., the first estimation step) can be found in [SG00] and [FP06], still an accurate link showing the dependency between the estimation of these parameters and the final user position determination was still unavailable. Section 5.1.1 sketched the of derivation the CRB for position coordinates considering the conventional approach.

2. **Direct Position Estimation approach.** DPE is one of the novel contributions of this dissertation, see Chapter 4. Therefore, positioning bounds under DPE's approach were not found in the literature. In Section 5.1.2 the CRB of position under the DPE framework was derived. This bound provides a valuable tool to determine the gain that a GNSS receiver can achieve by implementing DPE, in contrast to the conventional positioning approach.

3. **Tracking of synchronization parameters using a Bayesian filter.** Chapter 3 was devoted to the study of Bayesian filters to mitigate the effect of multipath propagation. In that case, the PCRB is used as the benchmark bound to compare the MSE curves obtained by the tested algorithms. The PCRB and its recursive version were discussed in Section 5.2.

Section 5.3 presented a number of simulation results comparing the CRB of position considering the two positioning approaches. As pointed out in Proposition 4.1, the conventional two-steps approach cannot overcome a direct positioning approach. Simulation results provided quantitative results to assess the performance gain of considering DPE. Tests run showed that the performance improvement comes from the joint processing of satellites that have independent propagation channels. Thus, DPE can deal better with scenarios where certain satellites are jeopardized by independent effects. This is the case of multipath propagation, where the conventional approach was seen to fail, in the sense that it introduces a bias in the final estimation. The robustness exhibited by DPE comes after recognizing that received signals from visible satellites depend on the same user position. In contrast, the two-steps approach does not take into account this constraint. The results comparing the PCRB to the variances achieved by the tested algorithms were showed in Chapter 3.

The research contributions of this chapter were partially published in:

- **Journal:**

  [Clo09c] P. Closas, C. Fernández-Prades, and J. A. Fernández-Rubio, "Cramér-Rao Bound Analysis of Positioning Approaches in GNSS Receivers," *IEEE Trans. Signal Processing*, 2009, accepted.

- **Conference:**

  [Clo09d] P. Closas, C. Fernández-Prades, and J. A. Fernández-Rubio, "Direct Position Estimation Approach: How Good Can it Get?", *Proceedings of the ION GNSS 2009*, Savannah, GA, September 2009.

  [FP09a] C. Fernández-Prades, J. Arribas, and P. Closas, "The Decoupling of DOA/Synchronization Parameters in Colored Noise Environments", *NEWCOM++/ACoRN Joint Workshop*, Barcelona, Spain, March 2009.

Appendix 5.A Time-delays derivative with respect to $\boldsymbol{\gamma}$

To deal with the derivative of $\frac{\partial \tau_i(\boldsymbol{\gamma})}{\partial \boldsymbol{\gamma}}$ we consider

$$\boldsymbol{\gamma} \triangleq \left[\mathbf{p}^T, \mathbf{v}^T, \delta t\right]^T = [x, y, z, v_x, v_y, v_z, \delta t]^T \ , \tag{5.78}$$

and recall from equation (2.21) that

$$\tau_i(\boldsymbol{\gamma}) = \frac{1}{c} \parallel \mathbf{p}_i - \mathbf{p} \parallel + (\delta t - \delta t_i) + \epsilon_i. \tag{5.79}$$

Then, applying basic linear algebra we obtain

$$\frac{\partial \tau_i(\boldsymbol{\gamma})}{\partial \mathbf{p}} = -\frac{\mathbf{u}_i^T}{c} \tag{5.80}$$

$$\frac{\partial \tau_i(\boldsymbol{\gamma})}{\partial \mathbf{v}} = \begin{cases} \mathbf{0}^T & \text{if } \mathbf{a} = \mathbf{0} \\ -\frac{\mathbf{u}_i^T}{c}\left(\mathbf{v} \otimes \tilde{\mathbf{a}}^T\right) & \text{otherwise} \end{cases} \tag{5.81}$$

$$\frac{\partial \tau_i(\boldsymbol{\gamma})}{\partial \delta t} = 1 \ , \tag{5.82}$$

where we take into account that

$$\begin{aligned} \frac{\partial \parallel \mathbf{p}_i - \mathbf{p} \parallel}{\partial \mathbf{p}} &= \frac{1}{2 \parallel \mathbf{p}_i - \mathbf{p} \parallel} \frac{\partial \left((\mathbf{p}_i - \mathbf{p})^T (\mathbf{p}_i - \mathbf{p})\right)}{\partial \mathbf{p}} \\ &= -\frac{(\mathbf{p}_i - \mathbf{p})^T}{\parallel \mathbf{p}_i - \mathbf{p} \parallel} \triangleq -\mathbf{u}_i^T \end{aligned} \tag{5.83}$$

$$\frac{\partial \parallel \mathbf{p}_i - \mathbf{p} \parallel}{\partial \mathbf{v}} = -\frac{(\mathbf{p}_i - \mathbf{p})^T}{\parallel \mathbf{p}_i - \mathbf{p} \parallel} \frac{\partial \mathbf{p}}{\partial \mathbf{v}} = -\mathbf{u}_i^T \frac{\partial \mathbf{p}}{\partial \mathbf{v}} \tag{5.84}$$

and

$$\begin{aligned} \frac{\partial \mathbf{p}}{\partial \mathbf{v}} &= \begin{pmatrix} \frac{\partial x}{\partial v_x} & \frac{\partial x}{\partial v_y} & \frac{\partial x}{\partial v_z} \\ \frac{\partial y}{\partial v_x} & \frac{\partial y}{\partial v_y} & \frac{\partial y}{\partial v_z} \\ \frac{\partial z}{\partial v_x} & \frac{\partial z}{\partial v_y} & \frac{\partial z}{\partial v_z} \end{pmatrix} = \mathbf{v} \otimes \tilde{\mathbf{a}}^T \\ \tilde{\mathbf{a}} &\triangleq \left[\frac{\partial t}{\partial v_x}, \frac{\partial t}{\partial v_y}, \frac{\partial t}{\partial v_z}\right]^T = \left[\frac{1}{a_x}, \frac{1}{a_y}, \frac{1}{a_z}\right]^T \ . \end{aligned} \tag{5.85}$$

Notice that (5.84) is only valid when the components of the acceleration vector ($\mathbf{a} = [a_x, a_y, a_z]^T$) are not null, otherwise the derivative is equal to $\mathbf{0}^T$.

Appendix 5.B Doppler-shifts derivative with respect to $\boldsymbol{\gamma}$

We aim at obtaining $\frac{\partial f_{d_i}(\boldsymbol{\gamma})}{\partial \boldsymbol{\gamma}}$, with $\boldsymbol{\gamma}$ being as defined in (5.78). Recall from equation (2.22) that the Doppler deviation corresponding to the i-th satellite can be expressed as:

$$f_{d_i} = -\left(\mathbf{v}_i - \mathbf{v}\right)^T \mathbf{u}_i \, \frac{f_c}{c} \; , \tag{5.86}$$

then, its derivative with respect to the elements in $\boldsymbol{\gamma}$ are:

$$\frac{\partial f_{d_i}(\boldsymbol{\gamma})}{\partial \mathbf{p}} = \begin{cases} \left(\mathbf{v}_i - \mathbf{v}\right)^T \frac{\mathbf{I}-\mathbf{u}_i\mathbf{u}_i^T}{\|\mathbf{p}_i-\mathbf{p}\|} \frac{f_c}{c} & \text{if } \mathbf{v} = \mathbf{0} \\ -\frac{\mathbf{u}_i^T}{c}\left(\mathbf{a}\otimes\tilde{\mathbf{v}}^T\right)\frac{f_c}{c} + \left(\mathbf{v}_i - \mathbf{v}\right)^T \frac{\mathbf{I}-\mathbf{u}_i\mathbf{u}_i^T}{\|\mathbf{p}_i-\mathbf{p}\|} \frac{f_c}{c} & \text{otherwise} \end{cases} \tag{5.87}$$

$$\frac{\partial f_{d_i}(\boldsymbol{\gamma})}{\partial \mathbf{v}} = \begin{cases} \mathbf{u}_i^T \frac{f_c}{c} & \text{if } \mathbf{a} = \mathbf{0} \\ \mathbf{u}_i^T \frac{f_c}{c} + \frac{\partial f_{d_i}(\boldsymbol{\gamma})}{\partial \mathbf{p}}\left(\mathbf{v}\otimes\tilde{\mathbf{a}}^T\right) & \text{otherwise} \end{cases} \tag{5.88}$$

$$\frac{\partial f_{d_i}(\boldsymbol{\gamma})}{\partial \delta t} = 0 \; , \tag{5.89}$$

where we use the definitions

$$\begin{aligned} \frac{\partial \mathbf{v}}{\partial \mathbf{p}} &= \begin{pmatrix} \frac{\partial v_x}{\partial x} & \frac{\partial v_x}{\partial y} & \frac{\partial v_x}{\partial z} \\ \frac{\partial v_y}{\partial x} & \frac{\partial v_y}{\partial y} & \frac{\partial v_y}{\partial z} \\ \frac{\partial v_z}{\partial x} & \frac{\partial v_z}{\partial y} & \frac{\partial v_z}{\partial z} \end{pmatrix} = \mathbf{a}\otimes\tilde{\mathbf{v}}^T \\ \tilde{\mathbf{v}} &\triangleq \left[\frac{\partial t}{\partial x}, \frac{\partial t}{\partial y}, \frac{\partial t}{\partial z}\right]^T = \left[\frac{1}{v_x}, \frac{1}{v_y}, \frac{1}{v_z}\right]^T \end{aligned} \tag{5.90}$$

and

$$\begin{aligned} \frac{\partial \mathbf{p}}{\partial \mathbf{v}} &= \begin{pmatrix} \frac{\partial x}{\partial v_x} & \frac{\partial x}{\partial v_y} & \frac{\partial x}{\partial v_z} \\ \frac{\partial y}{\partial v_x} & \frac{\partial y}{\partial v_y} & \frac{\partial y}{\partial v_z} \\ \frac{\partial z}{\partial v_x} & \frac{\partial z}{\partial v_y} & \frac{\partial z}{\partial v_z} \end{pmatrix} = \mathbf{v}\otimes\tilde{\mathbf{a}}^T \\ \tilde{\mathbf{a}} &\triangleq \left[\frac{\partial t}{\partial v_x}, \frac{\partial t}{\partial v_y}, \frac{\partial t}{\partial v_z}\right]^T = \left[\frac{1}{a_x}, \frac{1}{a_y}, \frac{1}{a_z}\right]^T \; . \end{aligned} \tag{5.91}$$

with $\mathbf{a} = [a_x, a_y, a_z]^T$ being the acceleration coordinates vector of the receiver.

To compute the derivatives we apply that the derivatives of the direction vector $\mathbf{u}_i$ with respect to $\mathbf{p}$ and $\mathbf{v}$ are

$$\begin{aligned}
\frac{\partial \mathbf{u}_i}{\partial \mathbf{p}} &= \frac{\parallel \mathbf{p}_i - \mathbf{p} \parallel \frac{\partial (\mathbf{p}_i - \mathbf{p})^T}{\partial \mathbf{p}} - (\mathbf{p}_i - \mathbf{p}) \frac{\partial \parallel \mathbf{p}_i - \mathbf{p} \parallel}{\partial \mathbf{p}}}{\parallel \mathbf{p}_i - \mathbf{p} \parallel^2} \\
&= \frac{- \parallel \mathbf{p}_i - \mathbf{p} \parallel + (\mathbf{p}_i - \mathbf{p}) \mathbf{u}_i^T}{\parallel \mathbf{p}_i - \mathbf{p} \parallel^2} \\
&= \frac{\mathbf{u}_i \mathbf{u}_i^T - \mathbf{I}}{\parallel \mathbf{p}_i - \mathbf{p} \parallel} \qquad \text{and} \qquad (5.92) \\
\frac{\partial \mathbf{u}_i}{\partial \mathbf{v}} &= \frac{\partial \mathbf{u}_i}{\partial \mathbf{p}} \frac{\partial \mathbf{p}}{\partial \mathbf{v}} \,, \qquad (5.93)
\end{aligned}$$

respectively.

We have two expressions for $\frac{\partial f_{d_i}(\boldsymbol{\gamma})}{\partial \mathbf{p}}$ depending on whether the receiver is static or it has non-null velocity. Similarly, $\frac{\partial f_{d_i}(\boldsymbol{\gamma})}{\partial \mathbf{v}}$ is computed differently if the receiver has constant velocity or if it has a certain non-null acceleration.

Appendix 5.C Proof of Proposition 5.1

Proceeding as in [Tic98], let us write the joint distribution of measurements and states as

$$\begin{aligned} p(\mathbf{x}_{1:k+1}, \mathbf{z}_{0:k+1}) &= p(\mathbf{x}_{1:k}, \mathbf{z}_{0:k}) p(\mathbf{z}_{k+1}|\mathbf{z}_{0:k}, \mathbf{x}_{1:k}) p(\mathbf{x}_{k+1}|\mathbf{z}_{k+1}, \mathbf{z}_{0:k}, \mathbf{x}_{1:k}) \\ &= p(\mathbf{x}_{1:k}, \mathbf{z}_{0:k}) p(\mathbf{z}_{k+1}|\mathbf{z}_k) p(\mathbf{x}_{k+1}|\mathbf{z}_{k+1}) \ . \end{aligned} \tag{5.94}$$

Using the decomposition of $\mathbf{J}(\mathbf{z}_{0:k})$ made in (5.58), the definitions in (5.61) and the expression for the joint distribution in (5.94), the Trajectory Information Matrix can be written in block form as

$$\mathbf{J}(\mathbf{z}_{0:k+1}) = \begin{pmatrix} \mathbf{A}_k & \mathbf{B}_k & \mathbf{0} \\ \mathbf{B}_k^T & \mathbf{C}_k + \mathbf{D}_k^{11} & \mathbf{D}_k^{12} \\ \mathbf{0} & \mathbf{D}_k^{21} & \mathbf{D}_k^{22} \end{pmatrix} \ . \tag{5.95}$$

The desired BIM can be found as the $n_z \times n_z$ lower-right submatrix of $\mathbf{J}^{-1}(\mathbf{z}_{0:k+1})$:

$$\begin{aligned} \mathbf{J}_{k+1} &= \mathbf{D}_k^{22} - \left(\mathbf{0}, \mathbf{D}_k^{21}\right) \begin{pmatrix} \mathbf{A}_k & \mathbf{B}_k \\ \mathbf{B}_k^T & \mathbf{C}_k + \mathbf{D}_k^{11} \end{pmatrix}^{-1} \begin{pmatrix} \mathbf{0} \\ \mathbf{D}_k^{21} \end{pmatrix} \\ &= \mathbf{D}_k^{22} - \mathbf{D}_k^{21} \left(\mathbf{C}_k + \mathbf{D}_k^{11} - \mathbf{B}_k^T \mathbf{A}_k^{-1} \mathbf{B}_k\right)^{-1} \mathbf{D}_k^{12} \ , \end{aligned} \tag{5.96}$$

which follows from basic algebra [Gol96]. □

6

Conclusions and Directions for Future Research

THIS thesis has dealt with the two probably core signal processing problems of a GNSS receiver: synchronization and positioning. In addition, we studied the fundamental accuracy bounds of those problems. The present is a conclusive chapter that aims at enumerating the conclusions and contributions arose by the research reported in the foregoing chapters. Additionally, a list of topics that may be the subject for future research is also suggested.

The first part of the dissertation dealt with the challenge of tracking the synchronization parameters of one or several replicas of a signal from a given satellite. Notice that the structure of these navigation signals (either LOSS or its replicas) is known. This problem was studied in Chapter 3 making use of Bayesian filtering ideas, thus considering a closed-loop scheme and using prior information about synchronization parameters' evolution. Initially, the chapter started with a review of the Bayesian approach to nonlinear filtering, performing a major revision of concepts and algorithms. Specifically, particle filtering was extensively discussed, constituting one of the main tools along the thesis. The use of a Bayesian Filters, as conceived in this part of the thesis, can be regarded as a substitute of DLL-like algorithms with enhanced multipath mitigation capabilities. A general DSS model was proposed, consisting of a measurement equation and a state

evolution model. The former considered the summation of samples of a direct signal and $M-1$ superimposed multipath replicas, thus taking explicitly into account the contribution of these $M-1$ signals. The state vector was composed of the set of synchronization parameters (i.e., time-delays and complex amplitudes) of the LOSS and its replicas. Since the a priori evolution of these parameters is difficult to model, we adopted a first-order autoregressive prior. This model seems rather simplistic, however this simplicity makes it suitable in a wide range of scenarios, as the obtained performance results told us. Starting from this rather general model, many Bayesian filtering algorithms can be implemented. In particular, three algorithms were proposed and tested: the EKF, the UKF and a PF. The first two algorithms admit few modifications and they were used in its *standard* formulation. Conversely, the design of a PF is typically related to problem to be solved. An initial solution consisted of a Bootstrap Filter with an ad-hoc choice of the importance distribution. Nevertheless, this was seen to require a large number of particles and exhibit some limitations when used for online filtering, whereas for batch processing it could be considered. Therefore, designing a PF was tailored at *i)* obtaining enhanced performance results in multipath environments and *ii)* reducing the computational complexity involved in the implementation of PFs. Both objectives were approached by designing a PF that made an efficient usage of particles, that is to say, decreasing the required number of samples to characterize the posterior distribution with a certain accuracy. Two actions were considered. First, a variance reduction technique was introduced to optimally deal with the linear part of the DSS model. This procedure is referred to as Rao-Blackwellization. Roughly speaking, Rao-Blackwellization tells us that in the presence of linear substructures in the DSS model, the optimal algorithm to deal with them is the KF. This technique had a twofold implication: it reduced the dimension of the state-space that the PF had to account for and the linear states were optimally processed by the KF. Secondly, the design of an importance density function close to the optimal is known to increase the particle efficiency of PFs. In Chapter 3, an approximation of the optimal importance distribution was proposed. This approximation consisted in a local approximation of the likelihood distribution, relying on the Laplace's method. This approximation was implemented by a Newton-Raphson algorithm. The algorithm was completed by a procedure to extract Doppler-shifts of both LOSS and multipath replicas of the signal from their corresponding complex amplitudes estimates. The procedure took into account that Doppler deviation can be seen as a linear term in the formulation of the carrier-phase of the signal.

At the conclusion of this thesis, there remain some research lines related to this topic which might be worth exploring:

- Improve the assumed DSS model by using more sophisticated prior information of synchronization parameters. Additionally, a switching model could be considered to model different dynamics of the receiver or appearance/disappearance of multipath replicas.

- Currently, the number of signals is considered fixed or estimated somehow. A remarkable improvement of the PF algorithm could rely on its ability to estimate this parameter, M. This will enhance the performance of the filter, at the expenses of increasing its computational cost [Dju01]. In any case, an analysis of the sensitivity of the algorithms to model inaccuracies seems appropriate.

- Study the computational complexity of the algorithms.

- One of the main concerns of PFs is their required computational cost. Although the generation of particles can be parallelized, large sample pools yield to impractical algorithms. Thus, major concern should be devoted to design particle filtering algorithms with reduced computational cost.

- Performance comparison with other Bayesian Filters that recently appeared in the literature. For instance, the Cost Reference Particle Filter (CRPF) or the Cubature Kalman Filter [Ara08] are appealing candidates to improve the results of the already proposed PF.

- Implementation of the proposed algorithms (and new ones) in digital platforms such as FPGAs should be a mid-term objective. This would stress the validity of the algorithms in real-time applications.

- Design of similar tracking algorithms for an antenna-array based receiver. In that case, the state-space should be extended to accommodate the spatial parameters (i.e., Angle-Of-Arrivals of the signals) or to the elements of the equivalent channel matrix, depending on the assumed array model (structured or unstructured, respectively).

The second main topic proposed in the thesis was the Direct Position Estimation (DPE) of GNSS receivers. One of the main threads of the thesis was the use of prior information. In Chapter 3 we saw that, though possible, the use of a priori information is not straightforward when dealing with the tracking of synchronization parameters. The reason is the lack of reliable models and devices to provide side information relative to these parameters. Therefore, it seems more convenient to rely on the Bayesian principle when the parameters of interest are the receiver motion parameters. In this case, many sources of prior information can be found and accounted, which was one of the motivations for the study of DPE's approach. DPE proposed to estimate user's position directly from the sampled data stream, in contrast to the conventional two-steps approach consisting of synchronization and positioning. Chapter 4 was delved into the proposal and analysis of the DPE approach. The chapter started highlighting the drawbacks of two-steps' positioning and proving that it cannot outperform a direct position estimation. The rest of the chapter was divided into two parts.

The first was devoted to the analysis of DPE from a ML standpoint, where no prior information was introduced in the process. Due to the novelty of the proposed approach, an analysis of the MLE of position under DPE's framework and a comparison with the conventional positioning approach seemed mandatory before investigating the capabilities of DPE to incorporate prior information. Therefore, it is not surprising that the study of DPE following the ML principle deserved an important space in the dissertation. The signal model was exposed, evidencing the constraint that synchronization parameters of different satellites depend on a common parameter: user's position. The latter was seen to constitute an essential and powerful concept, being the basis of DPE. The MLE of position was derived for the antenna-array case. Besides, the MLE of synchronization parameters was also provided. Either estimators result in the optimization of a cost function, which turns to be the minimization of the generalized variance. Both positioning approaches were compared under several criteria. For instance, we saw that the effect of multipath replicas in the shape of the cost function was different between both approaches. When the optimization was done with respect to the synchronization parameters, an additional local optimum appeared for each multipath replica. This effect is known to degrade the performance of conventional synchronization techniques. Conversely, the effect in the case of optimizing with respect to position coordinates was mitigated: no local optima appeared. This qualitative analysis provided the means to understand the performance improvements of the approach in the presented simulation results. The architecture of a receiver implementing the DPE approach was discussed and compared to the architecture of a conventional GNSS receiver. A possible Acquisition/Tracking procedure was proposed. Position-based Synchronization was introduced, where the receiver took the other way around of the conventional approach by computing satellite's synchronization parameters from the estimated position coordinates. The main impact of considering position-based synchronization is that the receiver could be able to keep track of a satellite even under weak signal conditions or signal blockages, because it is relying on the whole constellation to synchronize each individual satellite. The optimization of the cost function to obtain the ML estimators manifested some challenges, mainly due to its non-convexity and the multivariate nature of the problems. Consequently, optimization algorithms were studied. The Accelerated Random Search (ARS) algorithm was the most appealing candidate because of its simplicity, versatility and performance. The ARS algorithm was then used to implement the MLE of synchronization parameters and the MLE of position, comparing both positioning approaches under realistic scenarios. Either RMSE performances were also compared to the theoretical variance bound give by the Cramér-Rao Bound and derived in Chapter 5. The results were in accordance to Proposition 4.1, hence DPE's performance was outperforming the conventional procedure. Remarkable results were obtained in indoor/outdoor multipath conditions, with bias reductions.

The second part of Chapter 4 studied the inclusion of side information into the position filtering process, based on DPE's philosophy. The framework was termed Bayesian Direct

Position Estimation (BDPE). Since the Bayesian paradigm is the natural framework for this approach, the general DSS model was introduced. The measurements of the DSS model were restricted to the case of a single antenna based receiver, for the sake of simplicity. Whereas the latter admits few modifications, the state evolution model was seen to be adaptable to the nature of the side information and type of application considered. Therefore, we centered our discussion of possible state-spaces to some relevant cases, bearing in mind that the list is almost infinite. The examples proposed covered a wide range of possibilities, ranging from motion models to the use of Inertial Measurement Units, atmospheric models and map matching. Similarly, the list of Bayesian Filters that can be considered to implement BDPE is not closed (Chapter 3 provided an overview). For the sake of simplicity, we considered the Bootstrap Filter in the discussed simulation results. Notice that it was not the aim of the thesis to provide efficient algorithms to carry out BDPE's approach, but to prove the feasibility of the concept. Finally, an interpretation of DPE and BDPE in terms of open and closed loop architectures was given, intended to point possible implementation architectures.

Due to its novelty, this part of the thesis is probably the one which envisages more topics for future work. For instance,

- Introduce the dependency of the AOA of the satellites with respect to $\boldsymbol{\gamma}$. Similarly, the carrier-phase is considered independent of $\boldsymbol{\gamma}$ in this thesis for the sake of simplicity, though it could be related.

- Conceive DPE as a fusion procedure to gather signals from distinct GNSS constellations. That is to say, increase the signal model in (4.4) with the contribution of several navigation signals, e.g. GPS and Galileo.

- Study the relation of the DPE approach and the VDLL, mathematically establishing their relation if possible.

- Design efficient implementation strategies for DPE. One alternative could consist on following the architectures in the vein of those proposed for the VDLL.

- Study efficient algorithms for the implementation of BDPE. CRPF and derivative-free KF solutions such us the UKF, Gaussian Quadrature or Cubature Kalman Filter seem suitable candidates, taking into consideration the nonlinearity of the measurement equation.

- Analyze the antenna-array receiver under the BDPE approach.

- Study the relation between the BDPE using IMU data with the so-called ultra-tight coupling integration of IMU and GNSS data.

- Use Precise Point Positioning concepts to improve the accuracy of the BDPE approach. Basically, one could consider the use of several frequencies and carrier-phases.
- Implementation of DPE/BDPE in a software receiver will indeed constitute and important milestone.

Chapter 5 discussed the fundamental bounds of GNSS synchronization and positioning. Results for the former were already published in the literature. However, the impact of synchronizing each satellite with a given accuracy in the final position estimate was not yet reported. The chapter was divided into two parts. First, the Cramér-Rao Bound of position was derived for either positioning approaches (conventional and DPE) and compared under realistic scenarios. These results were used in Chapter 4 for benchmarking. Secondly, the Posterior Cramér-Rao Bound was introduced, providing an accuracy bound for the tracking problem dealt in Chapter 3.

List of Publications

DURING the elaboration of the dissertation a number of contributions were published. At the end of each chapter, the corresponding contributions were already listed, summarizing the work done. Nevertheless, the hurdle race towards the PhD degree offered the possibility of performing research in collateral topics. Mainly, the research was the fruit of private industry and public administration research projects. In general, the inclusion of this parallel work in the dissertation would have been difficult as it would affect its coherence. A list of all publications by the author (technical reports not included) and advised Master Thesis until the conclusion of the thesis, in chronological order, is provided below.

Book Chapters

2008

[Luc08] O. Lucke, A. Pellón, P. Closas, and J. A. Fernández-Rubio, *Advances in Mobile and Wireless Communications*, vol. 16 of *Lecture Notes in Electrical Engineering*, Chap. 10: Cost-Optimised Active Receive Array Antenna for Mobile Satellite Terminals, pp. 185–204, Springer, 2008, ISBN 978-3-540-79040-2.

[Ber09c] D. Bernal, P. Closas, and J. A. Fernández-Rubio, *Recent Advances in Signal Processing*, Chap. Digital I&Q Demodulation in array processing: Theory and Implementation, I-Tech, 2009, ISBN 978-953-7619-41-1.

Journal Articles

2009

[Clo09b] P. Closas, C. Fernández-Prades, and J. A. Fernández-Rubio, "A Bayesian Approach to Multipath Mitigation in GNSS Receivers," *IEEE J. Select. Topics in Signal Processing*, vol. 3, no. 4, August 2009.

[Clo09c] P. Closas, C. Fernández-Prades, and J. A. Fernández-Rubio, "Cramér-Rao Bound Analysis of Positioning Approaches in GNSS Receivers," *IEEE Trans. Signal Processing*, 2009, accepted.

2007

[Clo07b] P. Closas, C. Fernández-Prades, and J. A. Fernández-Rubio, "Maximum Likelihood Estimation of Position in GNSS," *IEEE Signal Processing Lett.*, vol. 14, no. 5, pp. 359–362, May 2007.

Conference Articles

2009

[Clo09a] P. Closas, M. F. Bugallo, and P. M. Djurić, "Assessing robustness of particle filtering by the Kolmogorov-Smirnov statistics," in *Proceedings of the IEEE International Conference on Acoustics, Speech, and Signal Processing, ICASSP 2009*, Taipei, Taiwan, April 2009.

[Clo09f] P. Closas, A. Pagès-Zamora, and J. A. Fernández-Rubio, "A Game Theoretical algorithm for joint power and topology control in distributed WSN," in *Proceedings of the IEEE International Conference on Acoustics, Speech, and Signal Processing, ICASSP 2009*, Taipei, Taiwan, April 2009.

[Clo09e] P. Closas, C. Fernández-Prades, and J. A. Fernández-Rubio, "Direct Position Estimation approach outperforms conventional two-steps positioning", *Proc. XVII European Signal Processing Conference, EUSIPCO*, Glasgow, Scotland, August 2009, in Special Session.

[Ber09b] D. Bernal, P. Closas, E. Calvo, and J. A. Fernández-Rubio, "Tight GNSS/INS Integration as a Constrained Least-Squares problem", *Proc. XVII European Signal Processing Conference, EUSIPCO*, Glasgow, Scotland, August 2009.

[FP09a] C. Fernández-Prades, J. Arribas, and P. Closas, "The Decoupling of DOA/Synchronization Parameters in Colored Noise Environments", *NEWCOM++/ACoRN Joint Workshop*, Barcelona, Spain, March 2009.

[FP09b] C. Fernández-Prades, and P. Closas, "Synchronization of GNSS Signals with Unstructured Antenna Arrays by a Multivariate Minimization of the Generalized Variance", *16th International Conference on Digital Signal Processing (DSP 2009)*, Santorini, Greece, July 2009.

[Clo09d] P. Closas, C. Fernández-Prades, and J. A. Fernández-Rubio, "Direct Position Estimation Approach: How Good Can it Get?", *Proceedings of the ION GNSS 2009*, Savannah, GA, September 2009.

[FP09c] C. Fernández-Prades, P. Closas, and J. A. Fernández-Rubio, "A Statistical Detector of Multipath and Interferences for Antenna-array based GNSS Receivers," *Proceedings of the ION GNSS 2009*, Savannah, GA, September 2009.

[Ber09a] D. Bernal, P. Closas, E. Calvo, and J. A. Fernández-Rubio, "A Convex Optimization Algorithm for Tight GNSS/INS Integration: An Alternative to Kalman Filtering," *Proceedings of the ION GNSS 2009*, Savannah, GA, September 2009.

[Arr09] J. Arribas, D. Bernal, C. Fernández-Prades, P. Closas, and J. A. Fernández-Rubio, "A Novel Real-time Platform for Digital Beamforming with GNSS Software Defined Receivers," *Proceedings of the ION GNSS 2009*, Savannah, GA, September 2009.

2008

[Clo08a] P. Closas, C. Fernández-Prades, D. Bernal, and J. A. Fernández-Rubio, "Bayesian Direct Position Estimation," *Proceedings of the ION GNSS 2008*, Savannah, GA, September 2008.

[Clo08b] P. Closas, C. Fernández-Prades, and J. A. Fernández-Rubio, "A Particle Filtering Tracking Algorithm for GNSS Synchronization using Laplace's method," in *Proceedings of the IEEE International Conference on Acoustics, Speech, and Signal Processing, ICASSP 2008*, Las Vegas, USA, April 2008.

[Clo08c] P. Closas, C. Fernández-Prades, J. A. Fernández-Rubio, and D. Bernal, "Particle Filtering Strategies for Efficient Multipath Mitigation," *Proceedings of the ION GNSS 2008*, Savannah, GA, September 2008.

[Ber08a] D. Bernal, P. Closas, and J. A. Fernández-Rubio, "Digital I&Q Demodulation in array processing: Theory and Implementation," *Proc. XVI European Signal Processing Conference, EUSIPCO*, Lausanne, Switzerland, August 2008.

[Ber08b] D. Bernal, P. Closas, and J. A. Fernández-Rubio, "Particle Filtering Algorithm for Ultra-tight GNSS/INS Integration," *Proceedings of the ION GNSS 2008*, Savannah, GA, September 2008.

2007

[Clo07a] P. Closas, E. Calvo, J. A. Fernández-Rubio, and A. Pagès-Zamora, "Coupling Noise Effect in Self–Synchronizing Wireless Sensor Networks," in *Proceedings of the* 8^{th} *IEEE International Workshop on Signal Processing Advances for Wireless Communications, SPAWC 2007*, Helsinki, Finland, June 2007.

[Clo07c] P. Closas, C. Fernández-Prades, and J. A. Fernández-Rubio, "ML Estimation of Position in a GNSS Receiver using the SAGE Algorithm," in *Proceedings of the IEEE International Conference on Acoustics, Speech, and Signal Processing, ICASSP 2007*, Hawaii, USA, April 2007.

[FP07] C. Fernández-Prades, P. Closas, and J. A. Fernández-Rubio, "Rao-Blackwellized Variable Rate Particle Filtering for Handset Tracking in Communication and Sensor Networks," in *Proc. XV European Signal Processing Conference, EUSIPCO*, Poznań, Poland, September 2007, in Special Session.

[Pel07a] A. Pellon, N. Carvalho, O. Lücke, P. Closas, J. A. Fernández-Rubio, G. Sims, and L. Salghetti-Drioli, "Design of cost-optimised active receive array antenna for mobile satellite terminals," in *29th ESA Antenna Workshop on Multiple Beams and Reconfigurable Antennas*, ESA/ESTEC, Ed., Noordwijk, The Netherlands, April 2007.

[Pel07b] A. Pellon, N. Carvalho, O. Lücke, P. Closas, J. A. Fernández-Rubio, G. Sims, and L. Salghetti-Drioli, "Design of cost-optimised active receive array antenna for mobile satellite terminals," in *International Conference on Electromagnetics in Advanced Applications, ICEAA*, Pages 719-722, Torino, Italy, September 2007.

[Luc07] O. Lucke, A. Pellon, P. Closas, J. A. Fernández-Rubio, "Cost-optimised active receive array antenna for mobile satellite terminals," in *IST Mobile Communications Summit*, Budapest, Hungary, July 2007.

[Wyl07] C. Wyllie, D. Gould, G. Richards, R. Guy, J. A. Fernández-Rubio, P. Closas, P. Rinous, F. Coromina, "Secured Link TT&C Antennas," in *European Conference on Antennas and Propagation, EuCAP*, Edinburgh, UK, November 2007.

[Cab07a] M. Cabrera, and et al., "Projecte com@web: plataforma web d'aprenentatge intelligent de processament del senyal i comunicacions," *Jornada de Presentació de resultats de projectes de millora a la docència, ICE-UPC 2007* , Barcelona, Spain, June 2007.

[Cab07b] M. Cabrera, and et al., "Proyecto de innovación docente com@web (comunicaciones en la web)," *Simposio Nacional de Tecnologías de la Información y las Comunicaciones en la Educación: CEDI-SINTICE'07* , pp. 113–120, Zaragoza, Spain, September 2007.

2006

[Clo06a] P. Closas, C. Fernández-Prades, and J. A. Fernández-Rubio, "Bayesian DLL for Multipath Mitigation in Navigation Systems using Particle Filters," in *Proceedings of the IEEE International Conference on Acoustics, Speech, and Signal Processing, ICASSP 2006*, Tolouse, France, May 2006.

[Clo06b] P. Closas, C. Fernández-Prades, and J. A. Fernández-Rubio, "Optimizing the Likelihood with Sequential Monte–Carlo methods," in *XXI Simposium Nacional de la Unión Científica Internacional de Radio (URSI)*, Oviedo, Spain, September 2006.

[Clo06c] P. Closas, C. Fernández-Prades, and J. A. Fernández-Rubio, "Particle Filtering applied to Robust Multivariate Likelihood Optimization in the absence of a closed-form solution," in *IEEE Nonlinear Statistical Signal Processing Workshop, NSSPW'06*, Cambridge, UK, September 2006.

[Clo06d] P. Closas, C. Fernández-Prades, and J. A. Fernández-Rubio, "Sequential Monte–Carlo approximation to the ML Time–delay Estimator in a multipath channel," in *Proceedings of the* 7^{th} *IEEE International Workshop on Signal Processing Advances for Wireless Communications, SPAWC 2006*, Cannes, France, July 2006.

[Clo06e] P. Closas, C. Fernández-Prades, J. A. Fernández-Rubio, and A. Ramírez-González, "Multipath Mitigation using Particle Filtering," in *Proceedings of the ION GNSS 2006*, Fort Worth, TX, September 2006.

[Clo06f] P. Closas, C. Fernández-Prades, J. A. Fernández-Rubio, and A. Ramírez-González, "On the Maximum Likelihood Estimation of Position," in *Proceedings of the ION GNSS 2006*, Fort Worth, TX, September 2006.

2005

[FP05b] C. Fernández-Prades, P. Closas, and J. A. Fernández-Rubio, "Time-Frequency Estimation in the COSPAS/SARSAT System Using Antenna Arrays: Variance Bounds and Algorithms," in *Proc. XIII European Signal Processing Conference, EUSIPCO*, Antalya, Turkey, September 2005.

[FP05c] C. Fernández-Prades, P. Closas, J. A. Fernández-Rubio, and A. Ramírez-González, "Advanced Signal Processing Techniques in Local User Terminals for Search

and Rescue Systems Based on MEO Satellites," in *Proceedings of the ION GNSS 2006*, Long Beach, CA, September 2005.

[FP05d] C. Fernández-Prades, P. Closas, and J. Fernández-Rubio, "New Trends In Global Navigation Systems: Implementation of a GPS Antenna Array Receiver," in *ISSPA'05 International Symposium on Signal Processing and Its Applications*, Sydney, Australia, August 2005.

2004

[FP04] C. Fernández-Prades, P. Closas, J. A. Fernández-Rubio, G. Seco-Granados, and I. Stojkovic, "Design of Local User Terminals for Search and Rescue Systems with MEO satellites," in *2nd ESA Workshop on Satellite Navigation User Equipment Technologies, NAVITEC'04*, Noordwijk, The Netherlands, December 2004.

[Clo04a] C. Fernández-Prades, A. Ramírez-González, P. Closas, and J. A. Fernández-Rubio, "Antenna Array Receiver for GNSS," in *Proceedings of the European Navigation Conference GNSS 2004*, Rotterdam, The Netherlands, May 2004.

[Clo04b] P. Closas, C. Fernández-Prades, and J. A. Fernández-Rubio, "Sincronización con arrays de antenas: aplicación al sistema SARSAT," in *XIX Simposium Nacional de la Unión Científica Internacional de Radio (URSI)*, Barcelona, Spain, September 2004.

2003

[Clo03] P. Closas, C. Fernández-Prades, and J. A. Fernández-Rubio, "Estimación de Parametros en Sistemas Search & Rescue Basados en Satelites," in *XIII Simposium Nacional de la Unión Científica Internacional de Radio (URSI)*, A Coruña, Spain, September 2003.

Advised Master Thesis

2008

I. González, "Development of an autonomous field-deployable GPS receiving system for operations in an extreme and remote polar environment," Master Thesis, Escola Tècnica Superior d´Enginyeria de Telecomunicació de Barcelona (ETSETB), Universitat Politècnica de Catalunya (UPC) and CSIC. Barcelona, Spain, January 2008. *Cum Laude qualification.*

2007

D. Bernal, "Digital Beamforming Implementation on an FPGA," Master Thesis, Escola Tècnica Superior d´Enginyeria de Telecomunicació de Barcelona (ETSETB), Universitat Politècnica de Catalunya (UPC). Barcelona, Spain, July 2007. *Cum Laude qualification.*

R. Vilalta, "Integration Platform for real-time GNSS algorithms," Master Thesis, Escola Tècnica Superior d´Enginyeria de Telecomunicació de Barcelona (ETSETB), Universitat Politècnica de Catalunya (UPC) and Institut Cartogràfic de Catalunya (ICC). Barcelona, Spain, September 2007. *Cum Laude qualification.*

Bibliography

[Abe93] J. S. Abel, "A bound on the mean-square-estimate error", *IEEE Trans. Inform. Theory*, vol. 39, no. 5, pp. 1675–1680, September 1993.

[Aka73] H. Akaike, "Information theory and an extension of the maximum likehood principle", B.N. Petrov, F. Csaki (eds.), *2nd International Symposium on Information Theory*, pp. 267–281, Budapest, 1973.

[Ako03] Dennis M. Akos, Alexandru Ene, and Jonas Thor, "A prototyping platform for multi–frequency GNSS receivers", *Proceedings of the ION GPS/GNSS 2003*, pp. 117–128, Portland, OR, September 2003.

[Ama05] A. Amar, and A. J. Weiss, "Direct Position Determination of multiple radio signals", *EURASIP Journal on Applied Signal Processing*, vol. 2005, no. 1, pp. 37–49, January 2005.

[Ama08a] A. Amar, and A. J. Weiss, "Localization of Narrowband Radio Emitters Based on Doppler Frequency Shifts", *IEEE Trans. Signal Processing*, vol. 56, no. 11, pp. 5500–5508, November 2008.

[Ama08b] A. Amar, and A. J. Weiss, "New Asymptotic Results on two Fundamental Approaches to Mobile Terminal Location", *Proc. of the 3rd International Symposium on Communications, Control and Signal Processing (ISCCSP)*, pp. 1320–1323, IEEE, March 2008.

[And79] B. D. O. Anderson, and J. B. Moore, *Optimal Filtering*, Prentice–Hall, 1979.

[Ant05] F. Antreich, O. Esbri-Rodriguez, J.A. Nossek, and W. Utschick, "Estimation of Synchronization Parameters using SAGE in a GNSS-Receiver", *Proceedings of the ION GNSS 2005*, Long Beach, CA, September 2005.

[Ant07] A. Antoniou, and W. Lu, *Practical Optimization: Algorithms and Engineering Applications*, Springer, 2007.

[Ant08] F. Antreich, J. A. Nossek, and W. Utschick, "Maximum likelihood delay estimation in a navigation receiver for aeronautical applications", *Aerospace Science and Technology*, vol. 12, no. 3, pp. 256–267, 2008.

[App04] M. J. Appel, R. LaBarre, and D. Radulovic, "On accelerated random search", *SIAM Journal of Optimization*, vol. 14, no. 3, pp. 708–731, 2004.

[Ara08] I. Arasaratnam, and S. Haykin, "Cubature Kalman Filters", *IEEE Trans. Automat. Contr.*, 2008, under 3rd review.

[Arf01] G. Arfken, and H. Weber, *Mathematical Methods for Physicist*, Elsevier Science, $5^{\underline{\text{th}}}$ ed., 2001.

[Arr09] J. Arribas, D. Bernal, C. Fernández-Prades, P. Closas, and J. A. Fernández-Rubio, "A Novel Real-time Platform for Digital Beamforming with GNSS Software Defined Receivers", *Proceedings of the ION GNSS 2009*, Savannah, GA, September 2009.

[Aru02] S. Arulampalam, S. Maskell, N. Gordon, and T. Clapp, "A Tutorial on Particle Filters for Online Nonlinear/Non-Gaussian Bayesian Tracking", *IEEE Trans. Signal Processing*, vol. 50, no. 2, pp. 174–188, February 2002.

[Aze94] A. Azevedo, and R.D. Shachter, "Laplace's method approximations for probabilistic inference in belief networks with continuous variables", *X Conference in Uncertainty in Artificial Intelligence*, pp. 28–36, San Mateo, CA, July 1994.

[Bab04] R. Babu, and J. Wang, "Ultra-Tight GPS/INS/PL Integration: A System Concept and Performance Analysis", Tech. rep., School of Surveying and Spatial Information Systems, The University of New South Wales, Sydney, Australia, 2004.

[Ban85] S. Bancroft, "An algebraic solution of the GPS equations", *IEEE Transactions on Aerospace and Electronic Systems*, vol. 21, no. 7, pp. 56–69, January 1985.

[Bar49] E. W. Barankin, "Locally best unbiased estimates", *Ann. Math. Stat.*, vol. 20, pp. 477–501, 1949.

[Bar98] R. H. Bartels, J. C. Beatty, and B. A. Barsky, *An Introduction to Splines for Use in Computer Graphics and Geometric Modelling*, Morgan Kaufmann, San Francisco, CA, 1998.

[Bay63] T. Bayes, "An essay towards solving a problem in the doctrine of chances", *The Philosophical Transactions of the Royal Society of London*, vol. 53, pp. 370–418, 1763.

[Bei06] "Submission of the updated information of Compass system to the Fourth Resolution 609 (WRC-03)", RG/036/2006, Radio Regulatory Department. Consultation Meeting. Ministry of Information Industry, China, 2006.

[Ber58] G. Bernard, and T. Bayes, "Studies in the History of Probability and Statistics: IX. Thomas Bayes' Essay towards solving a problem in the doctrine of chances", *Biometrika*, vol. 45, pp. 296–315, December 1958, Bayes' essay in modernized notation.

[Ber97] C. Berzuini, N. Best, W. Gilks, and C. Larizza, "Dynamic conditional independence models and Markov chain Monte Carlo methods", *Journal of American Stat. Assoc.*, vol. 92, pp. 1403–1412, 1997.

[Ber99] N. Bergman, *Recursive Bayesian Estimation: Navigation and Tracking Applications*, PhD Thesis, Linköpings Universitet, Sweden, 1999.

[Ber01] N. Bergman, A. Doucet, and N. Gordon, "Optimal estimation and Cramer-Rao bounds for partial non-Gaussian state space models", *Ann. Inst. Statist. Math.*, vol. 53, no. 1, pp. 97–112, 2001.

[Ber08a] D. Bernal, P. Closas, and J. A. Fernández-Rubio, "Digital I&Q Demodulation in array processing: Theory and Implementation", *Proc. XVI European Signal Processing Conference, EUSIPCO*, Lausanne, Switzerland, August 2008.

[Ber08b] D. Bernal, P. Closas, and J. A. Fernández-Rubio, "Particle Filtering Algorithm for Ultra-tight GNSS/INS Integration", *Proceedings of the ION GNSS 2008*, Savannah, GA, September 2008.

[Ber09a] D. Bernal, P. Closas, E. Calvo, and J. A. Fernández-Rubio, "A Convex Optimization Algorithm for Tight GNSS/INS Integration: An Alternative to Kalman Filtering", *Proceedings of the ION GNSS 2009*, Savannah, GA, September 2009.

[Ber09b] D. Bernal, P. Closas, E. Calvo, and J. A. Fernández-Rubio, "Tight GNSS/INS Integration as a Constrained Least-Squares problem", *Proc. XVII European Signal Processing Conference, EUSIPCO*, Glasgow, Scotland, August 2009.

[Ber09c] D. Bernal, P. Closas, and J. A. Fernández-Rubio, *Recent Advances in Signal Processing*, Chap. Digital I&Q Demodulation in array processing: Theory and Implementation, I-Tech, 2009, ISBN 978-953-7619-41-1.

[Bha46] A. Bhattacharyya, "On some analogues of the amount of information and their use in statistical estimation", *Sankhya Indian J. of Stat.*, vol. 8, pp. 1–14, 201–218, 315–328, 1946.

[Bla47] D. Blackwell, "Conditional expectation and unbiased sequential estimation.", *The Annals of Mathematical Statistics*, vol. 18, no. 1, pp. 105–110, 1947.

[Bob75] B. Z. Bobrovsky, and M. Zakai, "A lower bound on the estimation error for Markov processes", *IEEE Trans. Automat. Contr.*, vol. 20, no. 6, pp. 785–788, December 1975.

[Bob87] B. Z. Bobrovsky, E. Mayer-Wolf, and M. Zakai, "Some classes of global Cramér-Rao bounds", *Ann. of Stat.*, vol. 15, pp. 1421–1438, 1987.

[Bol04] M. Bolić, *Architectures for Efficient Implementation of Particle Filters*, PhD Thesis, Stony Brook University, New York, August 2004.

[Bol05] M. Bolić, P. M. Djurić, and S. Hong, "Resampling Algorithms and Architectures for Distributed Particle Filters", *IEEE Trans. Signal Processing*, vol. 53, no. 7, pp. 2442–2450, July 2005.

[Bor07] K. Borre, D.M. Akos, N. Bertelsen, P. Rinder, and S.H. Jensen, *A Software–Defined GPS and Galileo Receiver. A Single–Frequency Approach*, Applied and Numerical Harmonic Analysis, Birkhäuser, Boston, 2007.

[Boy03] S. Boyd, and L. Vandenberghe, *Convex Optimization*, Cambridge University Press, England, 2003.

[Bra99] Michael S. Braasch, and A. J. Van Dierendonck, "GPS receiver architectures and measurements", *Proceedings of the IEEE*, vol. 87, no. 1, pp. 48–64, January 1999.

[Bro00] A. Brown, M. Marvin, and B. Tanju, "Benefits of Software GPS Receivers for Enhanced Signal Processing", *GPS Solutions*, vol. 4, no. 1, pp. 56–66, July 2000.

[BS01] Y. Bar-Shalom, X. R. Li, and T. Kirubarajan, *Estimation with Applications to Tracking and Navigation: Theory Algorithms and Software*, John Wiley & Sons, 2001.

[Buc71] R. S. Bucy, and K. D. Senne, "Digital synthesis of nonlinear filters", *Automatica*, vol. 7, pp. 287–298, 1971.

[Buc74] R. Bucy, and H. Youssef, "Nonlinear filter representation via spline functions", *In Proceedings of the* 5^{th} *Symposium on Nonlinear Estimation*, pp. 51–60, 1974.

[Cab07a] M. Cabrera, and et al., "Projecte com@web: plataforma web d'aprenentatge intelligent de processament del senyal i comunicacions", *Jornada de Presentació de resultats de projectes de millora a la docència, ICE-UPC 2007*, Barcelona, Spain, June 2007.

[Cab07b] M. Cabrera, and et al., "Proyecto de innovación docente com@web (comunicaciones en la web)", *Simposio Nacional de Tecnologías de la Información y las Comunicaciones en la Educación: CEDI-SINTICE'07*, pp. 113–120, Zaragoza, Spain, September 2007.

[Cap04] Olivier Cappé, Arnaud Guillin, Jean-Michel Marin, and Christian P. Robert, "Population Monte Carlo", *J. Comput. Graph. Statist.*, vol. 13, no. 4, pp. 907–929, 2004.

[Car07] F. Caron, M. Davy, E. Duflos, and P. Vanheeghe, "Particle filtering for multisensor data fusion with switching observation models: Application to land vehicle positioning", *IEEE Trans. Signal Processing*, vol. 55, no. 6, pp. 2703–2719, June 2007.

[Cau47] A. Cauchy, "Methode Generale pour la Resolution des Systemes d'Equations Simultanees", *Comp. Rend. Acad. Sci. Paris*, pp. 536–538, 1847.

[Cev07] V. Cevher, R. Velmurugan, and J. H. McClellan, "Acoustic multitarget tracking using direction-of-arrival batches", *IEEE Trans. Signal Processing*, vol. 55, no. 6, pp. 2810–2825, June 2007.

[Che00] R. Chen, and J. S. Liu, "Mixture kalman filters", *Journal of the Royal Stat. Soc. B*, vol. 62, pp. 493–508, 2000.

[Che03] Z. Chen, "Bayesian filtering: From Kalman filters to particle filters, and beyond", Tech. rep., Adaptive Syst. Lab., McMaster University, Ontario, Canada, 2003.

[Che05] K. W. Cheung, and H. C. So, "A multidimensional scaling framework for mobile location using time of arrival measurements", *IEEE Trans. Signal Processing*, vol. 53, no. 2, pp. 460–470, February 2005.

[Cho04] Nicolas Chopin, "Central limit theorem for sequential monte carlo methods and its application to bayesian inference", *Ann. Statist.*, vol. 32, no. 6, pp. 2385–2411, 2004.

[Clo03] P. Closas, C. Fernández-Prades, and J. A. Fernández-Rubio, "Estimación de Parametros en Sistemas Search & Rescue Basados en Satelites", *XIII Simposium Nacional de la Unión Científica Internacional de Radio (URSI)*, A Corua, Spain, September 2003.

[Clo04a] C. Fernández-Prades P. Closas, J. A. Fernández-Rubio, G. Seco-Granados, and I. Stojkovic, "Design of Local User Terminals for Search and Rescue Systems with MEO satellites", *2nd ESA Workshop on Satellite Navigation User Equipment Technologies, NAVITEC'04*, Noordwijk, The Netherlands, December 2004.

[Clo04b] P. Closas, C. Fernández-Prades, and J. A. Fernández-Rubio, "Sincronizacin con arrays de antenas: aplicacin al sistema SARSAT", *XIX Simposium Nacional de la Unión Científica Internacional de Radio (URSI)*, Barcelona, Spain, September 2004.

[Clo06a] P. Closas, C. Fernández-Prades, and J. A. Fernández-Rubio, "Bayesian DLL for Multipath Mitigation in Navigation Systems using Particle Filters", *Proceedings of the IEEE ICASSP'06*, Toulouse, France, May 2006.

[Clo06b] P. Closas, C. Fernández-Prades, and J. A. Fernández-Rubio, "Optimizing the Likelihood with Sequential Monte–Carlo methods", *XXI Simposium Nacional de la Unión Científica Internacional de Radio (URSI)*, Oviedo, Spain, September 2006.

[Clo06c] P. Closas, C. Fernández-Prades, and J. A. Fernández-Rubio, "Particle Filtering applied to Robust Multivariate Likelihood Optimization in the absence of a closed-form solution", *IEEE Nonlinear Statistical Signal Processing Workshop, NSSPW'06*, Cambridge, UK, September 2006.

[Clo06d] P. Closas, C. Fernández-Prades, and J. A. Fernández-Rubio, "Sequential Monte–Carlo approximation to the ML Time–delay Estimator in a multipath channel", *Proceedings of the* 7^{th} *IEEE International Workshop on Signal Processing Advances for Wireless Communications, SPAWC 2006*, Cannes, France, July 2006.

[Clo06e] P. Closas, C. Fernández-Prades, J. A. Fernández-Rubio, and A. Ramírez-González, "Multipath Mitigation using Particle Filtering", *Proceedings of the ION GNSS 2006*, Fort Worth, TX, September 2006.

[Clo06f] P. Closas, C. Fernández-Prades, J. A. Fernández-Rubio, and A. Ramírez-González, "On the Maximum Likelihood Estimation of Position", *Proceedings of the ION GNSS 2006*, Fort Worth, TX, September 2006.

[Clo07a] P. Closas, E. Calvo, J. A. Fernández-Rubio, and A. Pagès-Zamora, "Coupling Noise Effect in Self–Synchronizing Wireless Sensor Networks", *Proceedings of the* 8^{th} *IEEE International Workshop on Signal Processing Advances for Wireless Communications, SPAWC 2007*, Helsinki, Finland, June 2007, submitted.

[Clo07b] P. Closas, C. Fernández-Prades, and J. A. Fernández-Rubio, "Maximum Likelihood Estimation of Position in GNSS", *IEEE Signal Processing Lett.*, vol. 14, no. 5, pp. 359–362, May 2007.

[Clo07c] P. Closas, C. Fernández-Prades, and J. A. Fernández-Rubio, "ML Estimation of Position in a GNSS Receiver using the SAGE Algorithm", *Proceedings of the*

IEEE International Conference on Acoustics, Speech, and Signal Processing, ICASSP 2007, Hawaii, USA, April 2007.

[Clo08a] P. Closas, C. Fernández-Prades, D. Bernal, and J. A. Fernández-Rubio, "Bayesian Direct Position Estimation", *Proceedings of the ION GNSS 2008*, Savannah, GA, September 2008.

[Clo08b] P. Closas, C. Fernández-Prades, and J. A. Fernández-Rubio, "A Particle Filtering Tracking Algorithm for GNSS Synchronization using Laplace's method", *Proceedings of the IEEE International Conference on Acoustics, Speech, and Signal Processing, ICASSP 2008*, Las Vegas, USA, April 2008.

[Clo08c] P. Closas, C. Fernández-Prades, J. A. Fernández-Rubio, and D. Bernal, "Particle Filtering Strategies for Efficient Multipath Mitigation", *Proceedings of the ION GNSS 2008*, Savannah, GA, September 2008.

[Clo09a] P. Closas, M. F. Bugallo, and P. M. Djurić, "Assessing robustness of particle filtering by the Kolmogorov-Smirnov statistics", *Proceedings of the IEEE International Conference on Acoustics, Speech, and Signal Processing, ICASSP 2009*, Taipei, Taiwan, April 2009.

[Clo09b] P. Closas, C. Fernández-Prades, and J. A. Fernández-Rubio, "A Bayesian Approach to Multipath Mitigation in GNSS Receivers", *IEEE J. Select. Topics in Signal Processing*, vol. 3, no. 4, August 2009, to appear.

[Clo09c] P. Closas, C. Fernández-Prades, and J. A. Fernández-Rubio, "Cramér-Rao Bound Analysis of Positioning Approaches in GNSS Receivers", *IEEE Trans. Signal Processing*, 2009, in review.

[Clo09d] P. Closas, C. Fernández-Prades, and J. A. Fernández-Rubio, "Direct Position Estimation Approach: How Good Can it Get?", *Proceedings of the ION GNSS 2009*, Savannah, GA, September 2009.

[Clo09e] P. Closas, C. Fernández-Prades, and J. A. Fernández-Rubio, "Direct Position Estimation approach outperforms conventional two-steps positioning", *Proc. XVII European Signal Processing Conference, EUSIPCO*, Glasgow, Scotland, August 2009, in Special Session.

[Clo09f] P. Closas, A. Pagès-Zamora, and J. A. Fernández-Rubio, "A Game Theoretical algorithm for joint power and topology control in distributed WSN", *Proceedings of the IEEE International Conference on Acoustics, Speech, and Signal Processing, ICASSP 2009*, Taipei, Taiwan, April 2009.

[Cos04] Cospas-Sarsat Council, "COSPAS–SARSAT 406 MHz MEOSAR implementation plan", C/s r.012, issue 1, COSPAS–SARSAT, October 2004.

[Cra46] H. Cramér, *Mathematical Methods of Statistics*, Princeton University Press, Princeton, NJ, 1946.

[Cri01] D. Crisan, *Sequential Monte Carlo methods in Practice*, Chap. Particle Filters - A theoretical perspective, pp. 17–41, Springer-Verlag, 2001.

[Cri02] D. Crisan, and A. Doucet, "A Survey of Convergence Results on Particle Filtering for Practitioners", *IEEE Trans. Signal Processing*, vol. 50, no. 3, pp. 736–746, March 2002.

[D'A94] Aldo N. D'Andrea, Umberto Mengali, and Ruggero Reggiannini, "The modified Cramer-Rao bound and its applications to synchronization problems", *IEEE Trans. Commun.*, vol. COM–42, no. 2/3/4, pp. 1391–1399, February / March / April 1994.

[Dau03] F. Daum, and J. Huang, "Curse of dimensionality and particle filters", *IEEE Aerospace Conference*, vol. 4, pp. 1979–1993, Big Sky, MT, USA, March 2003.

[Dem77] A. P. Dempster, N. M. Laird, and D. B. Rubin, "Maximum likelihood from incomplete data via the EM algorithm", *Journal of the Royal Statistical Society B*, vol. 39, 1977.

[Die92] A. J. Van Dierendonck, Pat Fenton, and Tom Ford, "Theory and Performance of Narrow Correlator Spacing in a GPS Receiver", *Navigation: Journal of The Institute of Navigation*, vol. 39, no. 3, pp. 265–283, Fall 1992.

[Die97] A. J. Van Dierendonck, and M .S. Braasch, "Evaluation of GNSS Receiver Correlation Processing Techniques for Multipath and Noise Mitigation", *ION National Technical Meeting*, Santa Monica, CA, January 1997.

[Dju01] P. M. Djurić, *Sequential Monte Carlo methods in Practice*, Chap. Sequential Estimation of Signals under Model Uncertainty, pp. 381–400, Springer-Verlag, 2001.

[Dju03] P. M. Djurić, J. H. Kotecha, J. Zhang, Y. Huang, T. Ghirmai, M. F. Bugallo, and J. Míguez, "Particle Filtering", *IEEE Signal Processing Mag.*, vol. 20, no. 5, pp. 19–38, September 2003.

[Dog01] A. Dogandžić, and A. Nehorai, "Cramér-Rao Bounds for estimating range, velocity, and direction with an active array", *IEEE Trans. Signal Processing*, vol. 49, no. 6, pp. 1122–1137, June 2001.

[Dop42] C. Doppler, "Über das farbige Licht der Doppelsterne und einiger anderer Gestirne des Himmels (On the colored light of the double stars and certain other stars of the heavens)", *Abh. Kniglich Bhmischen Ges. Wiss.*, vol. 2, pp. 467–482, 1842.

[Dou98] A. Doucet, "On Sequential Simulation–Based Methods for Bayesian Filtering", Tech. Rep. CUED/F-INFENG/TR.310, University of Cambridge, 1998.

[Dou00] A. Doucet, S. J. Godsill, and C. Andrieu, "On sequential Monte Carlo sampling methods for Bayesian filtering", *Stat. Comput.*, vol. 3, pp. 197–208, 2000.

[Dou01a] A. Doucet, N. de Freitas, and N. Gordon (eds.), *Sequential Monte Carlo Methods in Practice*, Springer, 2001.

[Dou01b] A. Doucet, N. Gordon, and V. Krishnamurthy, "Particle filters for state estimation of jump Markov linear systems", *IEEE Trans. Signal Processing*, vol. 49, pp. 613–624, 2001.

[Dou05] A. Doucet, and X. Wang, "Monte Carlo Methods for Signal Processing: a review in the statistical signal processing context", *IEEE Signal Processing Mag.*, vol. 22, no. 6, pp. 152–170, 2005.

[ESA06] ESA, and GJU, "Galileo open service. Signal in space interface control document (OS SIS ICD)", Tech. Rep. Draft 0, European Space Agency and Galileo Joint Undertaking, May 2006.

[EUR98] EUROCONTROL and the Institute of Geodesy & Navigation, "WGS 84 implementation manual", Tech. rep., World Geodetic System, February 1998.

[Fal06] M. Falcone, P. Erhard, and G. W. Hein, *Understanding GPS: principles and applications*, Chap. Galileo, pp. 559–594, Artech House, Norwood, 2$^{\underline{\text{nd}}}$ ed., 2006.

[Far99] J. A. Farrell, and M. Barth, *The Global Positioning System & Inertial Navigation*, McGraw–Hill, 1999.

[Fea06] S. Feairheller, and R. Clark, *Understanding GPS: principles and applications*, Chap. Other satellite navigation systems, pp. 595–634, Artech House, Norwood, 2$^{\underline{\text{nd}}}$ ed., 2006.

[Fel97] T. Felhauer, "Comparision of EML and DOT discriminator DLL multipath performance in GPS/GLONASS navigation receivers", *Electronics Letters*, vol. 33, no. 3, pp. 179–181, January 1997.

[Fen05] P. Fenton, and J. Jones, "The theory and performance of NovAtel Inc.'s Vision Correlator", *Proceedings of the ION GNSS*, Palm Springs, CA, September 2005.

[Fes94] J. A. Fessler, and A. O. Hero, "Space-Alternating Generalized Expectation-Maximization Algorithm", *IEEE Trans. Signal Processing*, vol. 42, no. 10, pp. 2664–2677, October 1994.

[Fis22] R. A. Fisher, "On the mathematical foundations of theoretical statistics", *Phil. Trans. Roy. Soc. London*, vol. 222, no. 309, 1922.

[Fon01a] F.P. Fontan, M. Vazquez-Castro, C.E. Cabado, J.P. Garcia, and E. Kubista, "Statistical modeling of the LMS channel", *IEEE Trans. Veh. Technol.*, vol. 50, no. 6, pp. 1549–1567, Nov 2001.

[Fon01b] R. D. Fontana, W. Cheung, P. M. Novak, and T. A. Stansell, "The new L2 civil signal", *Proceedings of the International Technical Meeting of the Satellite Division of the Institute Of Navigation, ION GNSS*, Salt Lake City, UT, September 11–14 2001.

[For97] B. Forssell, M. Martin-Neira, and R. A. Harris, "Carrier Phase Ambiguity Resolution in GNSS-2", *Proceedings of the ION GPS*, Kansas City, Missouri, September 1997.

[Foy76] W. Foy, "Position–location solutions by Taylor-series estimation", *IEEE Trans. Aerosp. Electron. Syst.*, vol. 12, pp. 183–193, 1976.

[FP04] C. Fernández-Prades, A. Ramírez-González, P. Closas, and J. A. Fernández-Rubio, "Antenna Array Receiver for GNSS", *Proceedings of the European Navigation Conference GNSS 2004*, Rotterdam, The Netherlands, May 2004.

[FP05a] C. Fernández-Prades, P. Closas, and J. A. Fernández-Rubio, "Advanced Signal Processing Techniques in Local User Terminals for Search & Rescue Systems Based on MEO Satellites", Tech. rep., Universitat Politècnica de Catalunya - European Space Agency, Barcelona, February 2005, eSTEC/Contract no. 17713/03/NL/LvH/jd.

[FP05b] C. Fernández-Prades, P. Closas, and J. A. Fernández-Rubio, "Time-Frequency Estimation in the COSPAS/SARSAT System Using Antenna Arrays: Variance Bounds and Algorithms", *Proc. XIII European Signal Processing Conference, EUSIPCO*, Antalya, Turkey, September 2005.

[FP05c] C. Fernández-Prades, P. Closas, J. A. Fernández-Rubio, and A. Ramírez-González, "Advanced Signal Processing Techniques in Local User Terminals for Search and Rescue Systems Based on MEO Satellites", *Proceedings of the ION GNSS 2006*, Long Beach, CA, September 2005.

[FP05d] C. Fernández-Prades, P. Closas, and J.A. Fernández-Rubio, "New Trends In Global Navigation Systems: Implementation of a GPS Antenna Array Receiver", *ISSPA'05 International Symposium on Signal Processing and Its Applications*, Sydney, Australia, August 2005.

[FP06] C. Fernández-Prades, *Advanced Signal Processing Techniques for GNSS Receivers*, PhD Thesis, Dept. of Signal Theory and Communications, Universitat Politècnica de Catalunya (UPC), Barcelona, Spain, May 2006.

[FP07] C. Fernández-Prades, P. Closas, and J. A. Fernández-Rubio, "Rao-Blackwellized Variable Rate Particle Filtering for Handset Tracking in Communication and Sensor Networks", *Proc. XV European Signal Processing Conference, EUSIPCO*, Poznań, Poland, September 2007, in Special Session.

[FP09a] C. Fernández-Prades, J. Arribas, and P. Closas, "The Decoupling of DOA/Synchronization parameters in Colored Noise Environments", *NEWCOM++ - ACoRN Joint Workshop*, Barcelona, Spain, March 2009.

[FP09b] C. Fernández-Prades, and P. Closas, "Synchronization of GNSS Signals with Unstructured Antenna Arrays by a Multivariate Minimization of the Generalized Variance", *16th International Conference on Digital Signal Processing (DSP 2009)*, Santorini, Greece, July 2009.

[FP09c] C. Fernández-Prades, P. Closas, and J. A. Fernández-Rubio, "A Statistical Detector of Multipath and Interferences for Antenna-array based GNSS Receivers", *Proceedings of the ION GNSS 2009*, Savannah, GA, September 2009.

[Fri02] J. Friedmann, E. Fishler, and H. Messer, "General Asymptotic Analysis of the Generalized Likelihood Ratio Test for a Gaussian Point Source Under Statistical or Spatial Mismodeling", *IEEE Trans. Signal Processing*, vol. 50, no. 11, pp. 2617–2631, November 2002.

[Gar96] L. Garin, F. Van Diggelen, and J. Rousseau, "Strobe and Edge correlator multipath mitigation for code", *Proceedings of the ION GPS*, Kansas City, Missouri, September 1996.

[Gel04] A. Gelman, J. B. Carlin, H. S. Stern, and D. B. Rubin, *Bayesian Data Analysis*, Chapman Hall/CRC, 2004.

[Ger01] A. B. Gershman, M. Pesavento, P. Stoica, and E. G. Larsson, "The stochastic CRB for array processing in unknown noise fields", *Proceedings of the IEEE International Conference on Acoustics, Speech, and Signal Processing, ICASSP 2001*, pp. 2989–2992, Washington, DC, USA, 2001.

[Gew89] J. Geweke, "Bayesian inference in econometric models using Monte Carlo integration", *Econometrica*, vol. 24, pp. 1317–1399, 1989.

[Ghi05] T. Ghirmai, M. F. Bugallo, J. Míguez, and P. M. Djurić, "A sequential monte carlo method for adaptive blind timing estimation and data detection", *IEEE Trans. Signal Processing*, vol. 53, no. 8, pp. 2855–2865, Aug. 2005.

[Gil01] Walter R. Gilks, and Carlo Berzuini, "Following a moving target-monte carlo inference for dynamic bayesian models", *Journal of the Royal Statistical Society. Series B (Statistical Methodology)*, vol. 63, no. 1, pp. 127–146, 2001.

[Gio90] G. Giovanni, and S. M. Radicella, "An analytical model of the electron density profile in the ionosphere", *Advances in Space Research*, vol. 10, no. 11, pp. 27–30, 1990.

[Gir01] A. Giremus, A. Doucet, V. Calmettes, and J. Y. Tourneret, "A Rao-Blackwellized particle filter for INS/GPS integration", *Proceedings of the IEEE International Conference on Acoustics, Speech, and Signal Processing, ICASSP 2001*, Montreal, Canada, April 2001.

[Gir07] A. Giremus, J. Y. Tourneret, and V. Calmettes, "A Particle filter approach for joint detection/estimation of Multipath effects on GPS measurements", *IEEE Trans. Signal Processing*, vol. 55, no. 4, pp. 1275–1285, April 2007.

[GLO02] "Global navigation satellite system - GLONASS - interface control document", Tech. Rep. 5.0, Coordination Scientific Information Center, Moscow, 2002.

[God01] S. Godsill, and T. Clapp, *Sequential Monte Carlo methods in Practice*, Chap. Improvement strategies for Monte Carlo particle filters, pp. 139–158, Springer-Verlag, 2001.

[Gol73] G. Golub, and V. Pereyra, "The differentiation of pseudo-inverses and nonlinear least squares problems whose variables separate", *SIAM J. Numer. Anal.*, vol. 10, pp. 413–432, 1973.

[Gol96] G. H. Golub, and C. F. van Loan, *Matrix Computations*, The John Hopkins University Press, 3$^{\underline{\text{rd}}}$ ed., 1996.

[Gor93] N. Gordon, D. Salmond, and A. Smith, "A novel approach to nonlinear/non-Gaussian Bayesian state estimation", *IEE Proceedings on Radar and Signal Processing*, vol. 140, pp. 107–113, 1993.

[Gre01] M. S. Grewal, L. R. Weill, and A. P. Andrews, *Global Positioning Systems, Inertial Navigation, and Integration*, John Wiley & Sons, 2001.

[Gro08] D. Groves, *Principles of GNSS, inertial and multisensor navigation systems*, Artech House, London, England, 2008.

[Gus02] F. Gustafsson, F. Gunnarsson, N. Bergman, U. Forssell, J. Jansson, R. Karlsson, and P. J. Nordlund, "Particle Filters for Positioning, Navigation and Tracking", *IEEE Trans. Signal Processing*, vol. 50, no. 2, pp. 425–437, February 2002.

[Ham54] J. M. Hammersley, and K. W. Morton, "Poor man's Monte Carlo", *Journal of the Royal Statistical Society*, vol. 16, pp. 23–38, 1954.

[Hen08] G. Hendeby, *Performance and Implementation Aspects of Nonlinear Filtering*, PhD Thesis, Linköpings Universitet, Linköping, Sweden, 2008.

[Hig95] T. Higuchi, "Kitagawa monte carlo filter from the perspective of genetic algorithm", Research memorandum, The Institute of Statistical Mathematics, 1995.

[Hop69] H. S. Hopfield, "Twoquadratic Tropospheric Refractivity Profile for Correction Satellite Data", *Journal of Geophysical Research*, vol. 74(18), pp. 4487–4499, 1969.

[Hub81] Peter J. Huber, *Robust Statistics*, John Wiley & Sons, 2nd ed., 1981.

[HW97] B. Hofmann-Wellenhof, H. Lichtenegger, and J. Collins, *Global Postioning System, Theory and Practice*, Springer-Verlag, New-York, 1997.

[HW08] B. Hofmann-Wellenhof, H. Lichtenegger, and E. Wasle, *GNSS - Global Navigation Satellite Systems: GPS, GLONASS, Galileo & more*, Springer, 2008.

[Ilt90] R. A. Iltis, "Joint Estimation of PN Code Delay and Multipath Using the Extended Kalman Filter", *IEEE Trans. Commun.*, vol. 38, no. 10, pp. 1677–1685, October 1990.

[Ilt94] R.A. Iltis, and L. Mailaender, "An adaptive multiuser detector with joint amplitude and delay estimation", *IEEE J. Select. Areas Commun.*, vol. 12, no. 5, pp. 774–785, June 1994.

[IR97] Recommendation P. 1239 ITU-R, "ITU-R Reference Ionospheric Characteristics", Tech. rep., ITU-R, Geneva, 1997.

[Irs03] M. Irsigler, and B. Eissfeller, "Comparison of Multipath Mitigation Techniques with Consideration of Future Signal Structures", *Proceedings of the ION GPS/GNSS 2003*, Portland, OR, September 2003.

[Irs05] M. Irsigler, J. A. Ávila Rodríguez, and G. W. Hein, "Criteria for GNSS Multipath Performance Assessment", *Proceedings of the ION GPS/GNSS 2005*, Long Beach, CA, September 2005.

[Ito00] K. Ito, and K. Xiong, "Gaussian Filters for Nonlinear Filtering Problems", *IEEE Trans. Automat. Contr.*, vol. 45, no. 5, May 2000.

[Jah96] A. Jahn, H. Bischl, and G. Heiss, "Channel Characterization for Spread Spectrum Satellite Communications", *Proceedings of the* 4^{th} *International Symposium on Spread Spectrum Techniques and Applications, ISSTA 1996*, pp. 1221–1226, Mainz, Germany, September 1996.

[Jak74] W. C. Jakes, *Microwave Mobile Communications*, Wiley, New York, 1974.

[Jan91] H. W. Janes, R. B. Langley, and S. P. Newby, "Analysis of Tropospheric Delay Prediction Models: Comparison with Ray-Tracing and Implications for GPS Relative Positioning", *Bulletin Geodisique*, vol. 65, no. 3, pp. 151–161, 1991.

[Jaz70] A. H. Jazwinski, *Stochastic Processes and Filtering Theory*, vol. 64 of *Mathematics in Science and Engineering*, Academic Press, 1970.

[Joh93] Don H. Johnson, and Dan E. Dudgeon, *Array Signal Processing: Concepts and Techniques*, Prentice–Hall, 1993.

[Jon96] P. de Jonge, and C. Tiberius, "The LAMBDA method for integer ambiguity estimation: implementation aspects", Technical report LGR Series 12, Delft Geodetic Computing Centre, Delft University of Technology, 1996.

[Jon04] Jason Jones, Pat Fenton, and Brian Smith, "Theory and performance of the Pulse Aperture Correlator", September 2004, available at http://www.novatel.com/Documents/Papers/PAC.pdf.

[Jul97] S. Julier, and J. K. Uhlmann, "A new extension of the kalman filter to nonlinear systems", *Int. Symp. Aerospace/Defense Sensing, Simul. and Controls*, vol. 3, 1997.

[Jul00] S. Julier, J. Uhlmann, and H. F. Durrant-White, "A new method for nonlinear transformation of means and covariances in filters and estimators", *IEEE Trans. Automat. Contr.*, vol. 45, pp. 477–482, March 2000.

[Jul02a] S. Julier, "The scaled unscented transformation", *American Control Conference*, vol. 6, pp. 4555–4559, Anchorage, AK, USA, May 2002.

[Jul02b] S. Julier, and J. Uhlmann, "Reduced sigma point filters for the propagation of means and covariances through nonlinear transformations", *American Control Conference*, vol. 6, pp. 887–892, Anchorage, AK, USA, May 2002.

[Jul04] S. Julier, and J. Uhlmann, "Unscented filtering and nonlinear estimation", *Proc. IEEE*, vol. 92, no. 3, pp. 401–422, March 2004.

[Kal60] R. E. Kalman, "A new approach to linear filtering and prediction problems", *Transactions of the ASME-Journal of Basic Engineering*, vol. 82, no. Series D, pp. 35–45, 1960.

[Kan04] R. Kaniuth, A. Pósfay, T. Pany, J. A. Ávila Rodríguez, and B. Eissfeller, "Indoor positioning with the IpexSR software receiver", *2nd ESA Workshop on Satellite Navigation User Equipment Technologies - NAVITEC*, Noordwijk, The Netherlands, December 2004.

[Kap96] E. D. Kaplan, and C. J. Hegarty, *Understanding GPS. Principles and Applications*, Artech House Publishers, 1996.

[Kar05] R. Karlsson, *Particle Filtering for Positioning and Tracking Applications*, PhD Thesis, Linköpings Universitet, Linköping, Sweden, March 2005.

[Kay93] S. M. Kay, *Fundamentals of Statistical Signal Processing. Estimation Theory*, Prentice Hall, 1993.

[Kit87] G. Kitagawa, "Non-gaussian state-space modelling of non-stationary time series", *Journal of the American Statistical Association*, vol. 82, pp. 1032–1063, 1987.

[Kit96] G. Kitakawa, "Monte Carlo filter and smoother for non-Gaussian non-linear state space models", *Journal of Computational and Graphical Statistics*, vol. 5, pp. 1–25, 1996.

[Klo76] J. A. Klobuchar, "Ionospheric Time Delay Corrections for Advanced Satelite Ranging Systems", *Propagation Limitations of Navigation and Positioning Systems*, no. 209, NATO, AGARD, Paris, France, 1976.

[Klo87] J. A. Klobuchar, "Ionospheric time-delay algorithm for single-frequency GPS users", *IEEE Trans. Aerosp. Electron. Syst.*, vol. 23, no. 3, pp. 325–331, May 1987.

[Kon94] A. Kong, J. S. Liu, and W. H. Wong, "Sequential imputations and Bayesian missing data problems", *Journal of the American Stat. Assoc.*, vol. 89, no. 425, pp. 278–288, 1994.

[Kot01] J. H. Kotecha, *Monte Carlo for dynamic state space models with applications to communications*, PhD Thesis, Stony Brook University, New York, December 2001.

[Kot03a] M. Kotecha, and P. M. Djurić, "Gaussian Particle Filtering", *IEEE Trans. Signal Processing*, vol. 51, no. 10, pp. 2592–2601, October 2003.

[Kot03b] M. Kotecha, and P. M. Djurić, "Gaussian Sum Particle Filtering", *IEEE Trans. Signal Processing*, vol. 51, no. 10, pp. 2602–2610, October 2003.

[Kra08] B. Krach, M. Lentmaier, and P. Robertson, "Joint bayesian positioning and multipath mitigation in gnss", *Proceedings of the IEEE ICASSP 2008*, Las Vegas, USA, April 2008.

[Kre06] J. Kreher, "Galileo signals: RF characteristics", *Working paper of the Navigation Systems Panel (NSP)*, vol. ICAO NSP/WGW: WP/36, Montreal, Canada, October 12–22 2006.

[Kru01] K. Krumvieda, C. Cloman, E. Olson, J. Thomas, W. Kober, P. Madhani, and P. Axelrad, "A complete IF software GPS receiver: A tutorial about the details", *Proceedings of the ION GPS/GNSS 2001*, Salt Lake City, UT, September 2001.

[Laa88] P.J.M. van Laarhoven, and E.H.L. Aarts, *Simulated annealing: theory and applications*, D. Reidel, Dordrecht, 1988.

[Lac07] G. Lachapelle, and M. Petovello, "Weighting GNSS Observations and Variations of GNSS/INS Integration", *Inside GNSS*, vol. 2, no. 1, pp. 26–33, January/February 2007.

[Las07] M. Lashley, and D. M. Bevly, "Comparison of Traditional Tracking Loops and Vector Based Tracking Loops for Weak GPS Signals", *Proceedings of the ION GNSS 2007*, Fort Worth, TX, September 2007.

[Leh83] E. Lehmann, *Theory of Point Estimation. Probability and Mathematical Statistics*, John Wiley & Sons, Ltd, 1983.

[Len08] M. Lentmaier, B. Krach, and P. Robertson, "Bayesian time delay estimation of GNSS signals in dynamic multipath environments", *International Journal of Navigation and Observation*, March 2008.

[Li08] Y. Li, and P. Djurić, "Target Tracking with Mobile Sensors using Cost-Reference Particle Filtering", *Proceedings of the IEEE International Conference on Acoustics, Speech, and Signal Processing, ICASSP 2008*, Las Vegas, USA, April 2008.

[Liu95] J. S. Liu, and R. Chen, "Blind deconvolution via sequential imputations", *Journal of the American Stat. Assoc.*, vol. 90, pp. 567–576, 1995.

[Liu98] J. S. Liu, and R. Chen, "Sequential Monte Carlo methods for dynamical problems", *Journal of the American Stat. Assoc.*, vol. 93, pp. 1032–1044, 1998.

[Lu08] T. Lu, M. Bugallo, and P. Djurić, "RLS-Assisted Cost-Reference Particle Filtering", *Proceedings of the IEEE International Conference on Acoustics, Speech, and Signal Processing, ICASSP 2008*, Las Vegas, USA, April 2008.

[Luc07] O. Lucke, A. Pellon, P. Closas, and J. A. Fernández-Rubio, "Cost-optimised active receive array antenna for mobile satellite terminals", *IST Mobile Communications Summit 2007*, Budapest, Hungary, July 2007.

[Luc08] O. Lucke, A. Pellón, P. Closas, and J. A. Fernández-Rubio, *Advances in Mobile and Wireless Communications*, vol. 16 of *Lecture Notes in Electrical Engineering*, Chap. 10: Cost-Optimised Active Receive Array Antenna for Mobile Satellite Terminals, pp. 185–204, Springer, 2008, ISBN 978-3-540-79040-2.

[MÓ4] J. Míguez, M. F. Bugallo, and P. M. Djurić, "A new class of particle filters for random dynamic systems with unknown statistics", *EURASIP Journal on Advances in Signal Processing*, vol. 2004, no. 15, pp. 2278–2294, 2004.

[MÓ7a] J. Míguez, "Analysis of parallelizable resampling algorithms for particle filtering", *ELSEVIER Signal Processing*, vol. 87, no. 12, pp. 3155–3174, December 2007.

[MÓ7b] J. Míguez, "Analysis of selection methods for cost-reference particle filtering with applications to maneuvering target tracking and dynamic optimization", *ELSEVIER Digital Signal Processing*, vol. 17, pp. 787–807, 2007.

[Mar06] R. Maronna, D. Martin, and V. Yohai, *Robust Statistics - Theory and Methods*, John Wiley & Sons, $1^{\underline{\text{st}}}$ ed., 2006.

[McG99] G.A. McGraw, and M.S. Braash, "GNSS Multipath Mitigation Using Gated and High Resolution Correlator Concepts", *Proceedings of the ION GPS/GNSS 1999*, pp. 333–342, 1999.

[McG00] S. McGinnity, and G. W. Irwin, "Multiple Model Bootstrap Filter for maneuvering target tracking", *IEEE Trans. Aerosp. Electron. Syst.*, vol. 36, pp. 1006–1012, 2000.

[Mer00] R. Van der Merwe, A. Doucet, N. Freitas, and E. Wan, "The unscented particle fitler", Tech. Rep. CUED/F-INFENG/TR 380, University of Cambridge, August 2000.

[Mic96] B. Michalewicz, *How to solve it: Modern Heuristics*, Springer, 1996.

[Mit00] J. Mitola, *Software Radio Architecture: Object-Oriented Approaches to Wireless Systems Engineering*, Wiley Interscience, 2000.

[Mon80] Robert A. Monzingo, and Thomas W. Miller, *Introduction to Adaptive Arrays*, John Wiley & Sons, 1980.

[Mus00] C. Musso, N. Oudjane, and F. Le Gland, *Sequential Monte Carlo methods in Practice*, Chap. Improving Regularised Particle Filters, pp. 247–272, Springer-Verlag, 2000.

[Nee95] R. D. J. Van Nee, *Multipath and Multi–Transmitter Interference in Spread–Spectrum Communication and Navigation Systems*, PhD Thesis, Delft University, The Netherlands, 1995.

[Nie87] F. Nietzsche, *Zur Genealogie der Moral: Eine Streitschrift*, Leipzig, Germany, 1887.

[Ott89] R.H.J.M. Otten, and L.P.P.P. van Ginneken, *The Annealing Algorithm*, The Kluwer international series in engineering and computer science ; SECS72. VLSI, computer architecture, and digital signal processing, Kluwer Academic Publishers, Boston, 1989.

[Ott93] B. Ottersten, M. Viberg, P. Stoica, and A. Nehorai, *Radar Array Processing*, Chap. 4: Exact and Large Sample ML Techniques for Parameter Estimation and Detection in Array Processing, pp. 99–151, Springer-Verlag, Berlin, 1993.

[Pan06] T. Pany, and B. Eissfeller, "Use of a Vector Delay Lock Loop Receiver for GNSS Signal Power Analysis in Bad Signal Conditions", *Proceedings of ION Annual Meeting/IEEE PLANS*, pp. 893–902, San Diego, California, April 2006.

[Pap01] A. Papoulis, and S. U. Pillai, *Probability, Random Variables and Stochastic Processes*, McGraw-Hill, $4^{\underline{\text{th}}}$ ed., 2001.

[Par96] B.W. Parkinson, and J.J. Spilker (eds.), *Global Positioning System: Theory and Applications*, Progress in Astronautics and Aeronautics, AIAA, Washington DC, 1996.

[Pel07a] A. Pellon, N. Carvalho, O. Lücke, P. Closas, J. A. Fernández-Rubio, G. Sims, and L. Salghetti-Drioli, "Design of cost-optimised active receive array antenna for mobile satellite terminals", ESA/ESTEC (ed.), *29th ESA Antenna Workshop on Multiple Beams and Reconfigurable Antennas*, Noordwijk, The Netherlands, April 2007.

[Pel07b] A. Pellon, N. Carvalho, O. Lücke, P. Closas, J. A. Fernández-Rubio, G. Sims, and L. Salghetti-Drioli, "Design of cost-optimised active receive array antenna for mobile satellite terminals", *International Conference on Electromagnetics in Advanced Applications, ICEAA'07*, pp. 719–722, Torino, Italy, September 2007.

[Pit99] M. Pitt, and N. Shephard, "Filtering via simulation: Auxiliary particle filters", *Journal of American Stat. Assoc.*, vol. 94, no. 446, pp. 590–599, 1999.

[Pit01] M. Pitt, and N. Shephard, *Sequential Monte Carlo methods in Practice*, Chap. Auxiliary variable based particle filters, pp. 273–294, Springer-Verlag, 2001.

[Pla50] R. Plackett, "Some Theorems in Least Squares", *Biometrika*, vol. 37, no. 1/2, pp. 149–157, 1950.

[Pro94] J.G. Proakis, and M. Salehi, *Communciation Systems Engineering*, Prentice–Hall, 1994.

[Pro95] J.G. Proakis, *Digital Communciations*, McGraw-Hill, New York, 3$^{\underline{\text{rd}}}$ ed., 1995.

[Pun03] E. Punskaya, *Sequential Monte Carlo Methods for digital communications*, PhD Thesis, University of Cambridge, UK, July 2003.

[Rai72] H. Raiffa, and R. Schlaifer, *Applied Statistical Decision Theory*, MIT Press, Cambridge, MA, 1972.

[Rao45] C. Rao, "Information and the accuracy attainable in the estimation of statistical parameters", *Bull. Calcutta Math. Soc.*, vol. 37, pp. 81–91, 1945.

[Rap96] T. S. Rappaport, *Wireless communications: principles and practice*, Prentice-Hall, 1996.

[Ree02] Jeffrey H. Reed, *Software Radio: A Modern Approach to Radio Engineering*, Prentice Hall, 2002.

[Reu97] I. Reuven, and H. Messer, "A Barankin-type lower bound on the estimation error of a hybrid parameter vector", *IEEE Trans. Inform. Theory*, vol. May, no. 3, pp. 1084–1093, May 1997.

[Rho05] H. Rho, and R. B. Langley, "SBAS Ionospheric Modeling with Quadratic Approach: Reducing the risks", *Proceedings of the ION GNSS 2005*, Long Beach, CA, September 2005.

[Ris85] J. Rissanen, "Minimum Description Length principle", *Encyclopedia of Statistical Sciences*, vol. V, pp. 523–527, 1985.

[Ris04] B. Ristic, S. Arulampalam, and N. Gordon, *Beyond the Kalman Filter: Particle Filters for tracking applications*, Artech House, Boston, 2004.

[Rub88] D. B. Rubin, J. M. Bernardo, M. H. De Groot, D. V. Lindley, and A. F. M. Smith, *Bayesian Statistics 3*, Oxford: University Press, 1988.

[Saa73] J. Saastamoinen, "Contribution to the theory of atmospheric refraction", *Bulletin Geodesique*, vol. 107, pp. 13–34, 1973.

[Sah06] M. Sahmoudi, and M. G. Amin, "Fast iterative maximum-likelihood algorithm (fimla) for multipath mitigation in next generation of gnss receivers", *Signals, Systems and Computers, 2006. ACSSC '06. Fortieth Asilomar Conference on*, pp. 579–584, 2006.

[Sca84] W. C. Scales, and R. Swanson, "Air and sea rescue via satellite systems", *IEEE Spectrum*, vol. 21, pp. 48–52, March 1984.

[Sch91] Louis l. Scharf, *Statistical Signal Processing. Detection, Estimation and Time series analysis*, Addison–Wesley, 1991.

[Sch03] T. Schön, *On Computational Methods for Nonlinear Estimation*, PhD Thesis, Linköpings Universitet, Linköping, Sweden, October 2003.

[Sch05] T. Schön, F. Gustafsson, and P.J. Nordlund, " Marginalized particle filters for mixed linear/nonlinear state-space models", *IEEE Trans. Signal Processing*, vol. 53, no. 7, pp. 2279–2289, July 2005.

[Sel03] J. Selva, *Efficient Multipath Mitigation in Navigation Systems*, PhD Thesis, Dept. of Signal Theory and Communications, Universitat Politècnica de Catalunya (UPC), Barcelona, Spain, December 2003.

[Ser05] ARINC Engineering Services, "NAVSTAR GPS space segment/navigation user L5 interfaces. Interface specification, IS-GPS-705, IRN-705-003", Tech. rep., GPS NAVSTAR, 2005.

[Ser06a] ARINC Engineering Services, "NAVSTAR GPS space segment/navigation user interfaces. Interface specification, IS-GPS-200, revision D, IRN-200D-001", Tech. rep., GPS NAVSTAR, 2006.

[Ser06b] ARINC Engineering Services, "NAVSTAR GPS space segment/navigation user L1C interfaces. Interface specification, Draft IS-GPS-800", Tech. rep., GPS NAVSTAR, 2006.

[SG00] G. Seco-Granados, *Antenna Arrays for Multipath and Interference Mitigation in GNSS Receivers*, PhD Thesis, Dept. of Signal Theory and Communications, Universitat Politècnica de Catalunya (UPC), Barcelona, Spain, July 2000.

[SG05] G. Seco-Granados, J. A. Fernández-Rubio, and C. Fernández-Prades, "ML estimator and Hybrid Beamformer for multipath and interference mitigation in GNSS receivers", *IEEE Trans. Signal Processing*, vol. 53, no. 3, pp. 1194–1208, March 2005.

[Sha05] M. E. Shaw, "Global Positioning System: a policy and modernization review", *Presented at United Nations, International Comittee on GNSS*, December 1–2 2005.

[Shu57] M. P. Shutzenberg, "A generalization of the Fréchet-Cramér inequality to the case of Bayes estimation", *Bull. Amer. Math. Soc.*, vol. 63, 1957.

[Sim01] M. Simandl, J. Královec, and P. Tichavsky, "Filtering, predictive, and smoothing Cramér-Rao bounds for discrete-time nonlinear dynamic systems", *Automatica*, vol. 37, pp. 1703–1716, 2001.

[Smi05] S.T. Smith, "Covariance, subspace, and intrinsic Cramér-Rao bounds", *IEEE Trans. Signal Processing*, vol. 53, no. 5, pp. 1610–1630, May 2005.

[Sor88] H. Sorenson, *Recursive estimation for nonlinear dynamic systems*, New York: Marcel Dekker, 1988.

[Sou02] J. Soubielle, I. Fijalkow, P. Duvaut, and A. Bibaut, "GPS Positioning in a Multipath Environment", *IEEE Trans. Signal Processing*, vol. 50, no. 1, pp. 141–150, January 2002.

[Spa07] M. Spangenberg, A. Giremus, P. Poiré, and J. Y. Tourneret, "Multipath estimation in the global positioning system for multicorrelator receivers", *Proceedings of the IEEE International Conference on Acoustics, Speech, and Signal Processing, ICASSP 2007*, Hawaii, USA, April 2007.

[Spe02] "Special Issue on Monte Carlo methods for Statistical Signal Processing", *IEEE Trans. Signal Processing*, vol. 50, no. 2, February 2002.

[Ste03] A. Steingass, and A. Lehner, "Measuring Galileo's Multipath Channel", *Proceedings of the European Navigation Conference, ENC-GNSS 2003*, Graz, Austria, April 2003.

[Ste04] A. Steingass, and A. Lehner, "Measuring the Navigation Multipath Channel - A Statistical Analysis", *Proceedings of the ION GPS/GNSS 2004*, Long Beach, CA, September 2004.

[Ste05] A. Steingass, and A. Lehner, "A Channel Model for land mobile satellite navigation", *Proceedings of the European Navigation Conference, ENC-GNSS 2005*, Munich, Germany, July 2005.

[Sto96] Petre Stoica, and Mats Viberg, "Maximum likelihood parameter and rank estimation in reduced–rank multivariate linear regressions", *IEEE Transactions on Signal Processing*, vol. 44, no. 12, pp. 3069–3078, December 1996.

[Sto97] P. Stoica, and R. Moses, *Introduction to Spectral Analysis*, Prentice Hall, Upper Saddler River, NJ, 1997.

[Sto98] P. Stoica, and B. C. Ng, "On the Cramér-Rao bound under parametric constraints", *IEEE Signal Processing Lett.*, vol. 5, no. 7, pp. 177–179, July 1998.

[Sto01] P. Stoica, E. G. Larsson, and A. B. Gershman, "The stochastic CRB for array processing: a textbook derivation", *IEEE Signal Processing Lett.*, vol. 8, no. 5, pp. 148–150, May 2001.

[Sto04] P. Stoica, Y. Selén, and J. Li, "On Information Criteria and the Generalized Likelihood Ratio Test of Model Order Selection", *IEEE Signal Processing Lett.*, vol. 11, no. 10, pp. 794–797, October 2004.

[Str97] Gilbert Strang, and Kai Borre, *Linear Algebra, Geodesy, and GPS*, Wellesley–Cambridge Press, 1997.

[Swi98] A. Lee Swindlehurst, and Petre Stoica, "Maximum Likelihood Methods in Radar Array Signal Processing", *Proc. IEEE*, vol. 86, no. 2, pp. 419–420, February 1998.

[Teu93] P.J.G. Teunissen, "Least squares estimation of the integer GPS ambiguities", *IAG General Meeting, Invited Lecture, Section IV: Theory and methodology*, Beijing, China, 1993.

[Tic98] P. Tichavsky, C. .H. Muravchik, and A. Nehorai, "Posterior Cramér-Rao Bounds for Discrete-Time Nonlinear Filtering", *IEEE Trans. Signal Processing*, vol. 46, no. 5, pp. 1386–1396, May 1998.

[Tip78] Paul A. Tipler, *Physics For Scientists And Engineers*, Worth Publishers Inc., 1978.

[Tor84] D. J. Torrieri, "Statistical theory of passive location systems", *IEEE Trans. Aerosp. Electron. Syst.*, vol. 20, no. 2, pp. 183–198, Mar. 1984.

[Tow94] B. Townsend, and P. Fenton, "A practical approach to the reduction of pseudorange multipath errors in a L1 GPS receiver", *Proceedings of the ION GPS*, pag. 143148, Salt Lake City, UT, September 1994.

[Tre68] Harry L. Van Trees, *Part I of Detection, Estimation and Modulation Theory*, Wiley Interscience, New York, 1968.

[Tre02] Harry L. Van Trees, *Optimum Array Processing: Part IV of Detection, Estimation and Modulation Theory*, Wiley Interscience, 2002.

[Tre07] Harry L. Van Trees, and Kristine L. Bell (eds.), *Bayesian Bounds for Parameter Estimation and Nonlinear Filtering/Tracking*, Wiley Interscience, 2007.

[Tsu00] James Bao-Yen Tsui, *Fundamentals of Global Positioning System Receivers. A Software Approach*, John Willey & Sons, Inc., 2000.

[Tsu01] J. Tsui, *Digital Techniques for Wideband Receivers*, Artech House, Norwood, $2^{\underline{\text{nd}}}$ ed., 2001.

[Tut02] Walter H. W. Tuttlebee (ed.), *Software Defined Radio: Enabling Technologies*, John Wiley & Sons, Chichester, England, 2002.

[Van91] R. D. J. Van Nee, and A. Coenen, "New Fast GPS code-acquisition technique using FFT", *Electronics Letters*, vol. 27, pp. 158–160, Jan. 1991.

[Van93] R. D. J. Van Nee, "Spread–Spectrum Code and Carrier Synchronization Errors Caused by Multipath and Interference", *IEEE Trans. Aerosp. Electron. Syst.*, vol. 29, no. 4, pp. 1359–1365, October 1993.

[Van94] R. D. J. Van Nee, J. Siereveld, P. C. Fenton, and B. R. Townsend, "The multipath estimating delay lock loop: approaching theoretical accuracy limits", *Position Location and Navigation Symposium*, pp. 246–251, April 1994.

[Vee88] Barry D. Van Veen, and Kevin M Buckley, "Beamforming: A versatile approach to spatial filtering", *IEEE Signal Processing Magazine*, vol. 5, no. 2, pp. 4–24, April 1988.

[Vit95] Andrew J. Viterbi, *CDMA. Principles of Spread Spectrum Communication*, Addison–Wesley Wireless Communication Series, Addison–Wesley, 1995.

[Wal99] R. H. Walden, "Analog-to-Digital Converter Survey and Analysis", *IEEE J. Select. Areas Commun.*, vol. 17, no. 4, pp. 539–550, April 1999.

[Wan00] E. Wan, and R. Van der Merwe, "The unscented kalman filter for nonlinear estimation", *IEEE Symp. Adaptive Systems for Signal Proc., Comm. and Control*, pp. 153–158, Alberta, Canada, 2000.

[War96] P.W. Ward, "GPS receiver search techniques", *Position Location and Navigation Symposium, 1996., IEEE 1996*, pp. 604–611, Apr 1996.

[Wax96] M. Wax, and Y. Anu, "Performance analysis of the minimum variance beamformer in the presence of steering vector errors", *Signal Processing, IEEE Transactions on*, vol. 44, no. 4, pp. 938–947, Apr 1996.

[Wei85] A. J. Weiss, and E. Weinstein, "A lower bound on the mean square error in random parameter estimation", *IEEE Trans. Inform. Theory*, vol. 31, no. 5, pp. 680–682, September 1985.

[Wei94] L. R. Weill, "C/A Code Pseudoranging Accuracy - How good can it get?", *Proceedings of the ION GPS/GNSS 1994*, pp. 133–141, Salt Lake City, UT, 1994.

[Wei95] L. R. Weill, "Achieving Theoretical Accuracy Limits for Pseudoranging in Presence of Multipath", *Proceedings of the ION GPS/GNSS 1995*, pp. 1521–1530, Palm Springs, CA, 1995.

[Wei02] L. R. Weill, "Multipath mitigation using modernized GPS signals: How good can it get?", pp. 24–27, September 2002.

[Wei04] A. J. Weiss, "Direct Position Determination of Narrowband Radio Frequency Transmitters", *IEEE Signal Processing Lett.*, vol. 11, no. 5, pp. 513–516, May 2004.

[Wer03] W. Werner, and J. Winkel, "TCAR and MCAR options with Galileo and GPS", *Proceedings of the ION GNSS*, Portland, OR, September 2003.

[Wid67] B. Widrow, P.E. Mantey, L.J. Griffiths, and B.B. Goode, "Adaptive antenna systems", vol. 55, pp. 2143–2159, Dec. 1967.

[Wil32] S. S. Wilks, "Certain Generalizations in the Analysis of Variance", *Biometrika*, vol. 24, no. 3/4, pp. 471–494, 1932.

[Wit00] B. Witchayangkoon, *Elements of GPS precise point positioning*, PhD Thesis, University of Maine, Orono, Maine, 2000.

[Woo56] R. Wooding, "The multivariate distribution of complex normal variables", *Biometrika*, vol. 43, pp. 212–215, 1956.

[Wyl07] C. Wyllie, D. Gould, G. Richards, R. Guy, J. A. Fernández-Rubio, P. Closas, P. Rinous, and F. Coromina, "Secured link tt&c antennas", *European Conference on Antennas and Propagation, EuCAP*, Edinburgh, UK, November 2007.

[Xav05] J. Xavier, and V. Barroso, "Intrinsic Variance Lower Bound (IVLB): an extension of the Cramér-Rao Bound to Riemannian manifolds", *Proceedings of the IEEE International Conference on Acoustics, Speech, and Signal Processing, ICASSP 2005*, Philadelphia, USA, May 2005.

[Yan04] N. Yang, W. F. Tian, Z. H. Jin, and C. B. Zhang, "Particle filter for sensor fusion in a land vehicle navigation system", *Measurement science and technology*, vol. 16, pp. 677–681, 2004.

[Ziv69] J. Ziv, and M. Zakai, "Some lower bounds on signal processing estimation", *IEEE Trans. Inform. Theory*, vol. IT-15, no. 3, pp. 386–391, May 1969.

Index